Novel Phosphasalen Ligands for the Ring-Opening Polymerisation of Lactones

Charlotte Alice Coleman

Department of Inorganic Chemistry

New College

University of Oxford

December 2017

A thesis submitted in partial fulfilment of the requirements for the degree of Doctor of Philosophy in Chemistry.

For Grandpa John

Always and Forever

Declaration

All work, unless stated otherwise, was carried out by the author between October 2014 and December 2017 at Imperial College London and the University of Oxford.

Abstract

Bio-derived polymers offer a sustainable alternative to petroleum-derived polymers. One such polymer, polylactide (PLA) is synthesised from the ring-opening polymerisation (ROP) of *rac*-lactide (*rac*-LA). The monomer contains two stereocentres which gives a range of tacticities. The isotactic ROP of *rac*-LA yields the most desirable polymer properties (physical and mechanical properties) and is quantified using a P_i (probability of isotactic enchainment) value. This thesis investigates tri- and tetradentate ligands coordinated to zinc(II), aluminium(III) and indium(III) to understand the ligand effects on both rate and isoselectivity.

The first results chapter, Chapter 3, outlines the synthesis of a tetradentate salen ligand, its analogous phosphasalen ligand, where the imine bonds are replaced with iminophosphorane bonds and a hybrid ligand containing a mixture of both imine and iminophosphorane bonds. The salen, phosphasalen and hybrid ligands are coordinated to both aluminium and indium and used as initiators for the ROP. The indium hybrid initiator yields the highest isoselectivity (P_i = 0.71) which is significantly higher than its salen and phosphasalen analogues (P_i = 0.51 - 0.52)

Chapter 4 investigates structure-activity relationships of the indium hybrid initiator, by modification of the ligand scaffold. Bulkier *ortho*-phenolate substituents do not affect rate or isoselectivity. Electron-withdrawing chloride substituents increase rate but decrease isoselectivity (P_i = 0.61). Modification of the phosphorus substituents yields the highest isoselectivity value (P_i = 0.75). It may be hypothesised that isoselectivity depends upon steric hindrance at both *ortho*-substituents and at phosphorus. Furthermore, the synthesis of a ferrocene containing indium hybrid complex is developed for future use in redox-switch catalysis.

Chapter 5 describes the synthesis of two tridentate half-phosphasalen ligands and their coordination chemistry with zinc(II) and indium(III). Zinc initiators are active but display poor polymerisation control and low isoselectivity values (P_i = 0.67). Zinc complexes, with a less sterically encumbered ligand, preferentially form a homoleptic complex, which cannot be used in ROP. Indium initiators are slower than analogous half Schiff base initiators reported in the literature but show an improved isoselectivity value (P_i = 0.72).

Acknowledgements

Firstly, I would like to express my deepest gratitude to my two supervisors, Charlotte and Nick. Your passion, intelligence and drive have constantly inspired and motivated me, further than I ever thought possible. Thank you for your unfaltering confidence in me.

To the Long and Williams groups, you have all stood by me through the highs and lows and I am forever grateful. This journey has really taught me who I am, what I can achieve, and that I am nothing without the love and support of my friends. Especially to the "Long Slaggys", Emma, Samantha, Lucy, Beth and Adam, thank you for the holidays (Are you ready to bike the bridge?), the unrelenting support and the memories. Also to Dom, Jenni, PJ, Anish, Guun and Arnaud for your incredible knowledge and support on my project. Moving to Oxford was an experience I will now happily admit that I will never regret, but to Gemma, Alice, Arron, Arnaud, Andrés, Tim, Tom, Giulia, Ni and Sumesh, thank you. To all past and present members of both groups, there are too many to name but I hope I get to celebrate the achievement with you over a drink.

I would also like to thank all the experts in: NMR, Peter Haycock and Nick Rees, X-ray crystallography, Dr Andrew White and Dr Christopher Durr, elemental analysis, Stephen Boyer and electrochemistry, Dr Lucy Wilson.

A special thank you goes to Tim, I know you don't think you deserve a shout out here but you have kept me sane in this final year, at times, where I honestly didn't think I had it in me to keep going. You have made Oxford a very special place for me, but not the CRL…never the CRL.

Finally to my family. To my Mum and Dad who have never doubted my ability and have constantly supported me. I am forever in your debt (literally), and I have eternal gratitude for making me into the person I am today. You are both the most hard-working and determined people I know and I hope I continue you to make you proud. And to my Grandpa, who gets to join me on the end of this journey in my heart and memories only, this is for you.

List of abbreviations

Ad	Adamantyl
amu	Atomic mass unit
CEC	Chain-end control
COSY	Correlation spectroscopy
CyHex	Cyclohexyl
CV	Cyclic Voltammetry
d	Deuterium
D	Diffusion coefficient
1D	One-dimensional
2D	Two-dimensional
D	Diffusion coefficient
Đ	Dispersity
DCM	Dichloromethane
dn/dc	Refractive index increment
DOSY	Diffusion-ordered spectroscopy
Δ*E*	Difference in oxidation and reduction potentials
$E_{1/2}$	Half-cell potential
EA	Elemental analysis
Equiv.	Equivalents
E_{ox}	Oxidation potential
E_{red}	Reduction potential
ESC	Enantiomorphic site control

Et	Ethyl
EtOH	Ethanol
η	Viscosity
exp	Exponential
Fc	Ferrocene
GPC	Gel permeation chromatography
G_z	Field gradient
HMBC	Heteronuclear multiple-bond coherence
HSQC	Heteronuclear single quantum coherence
i	Iso dyad
i_p	Current potential
i_{pa}	Aniodic potential
i_{pc}	Cathiodic potential
v_s	Scan rate
I	Nuclear spin
*i*Pr	*Iso*-propyl
IPA	*Iso*-propanol
IR	Infrared
k_{app}	Apparent rate constant
k_i	Initiation rate constant
k_{obs}	Observed rate constant
k_p	Propagation rate constant
k_t	Termination rate constant

k_{te}	Transesterification rate constant
LA	Lactide
M	Metal
MALDI-ToF	Matrix assisted laser desorption/ionisation – time of flight
MALLS	Multi-angle laser light scattering
Me	Methyl
MeCN	Acetonitrile
MeOH	Methanol
M_n	Number average molecular weight
M_n^{calc}	Theoretical number average molecular weight
M_w	Weight average molecular weight
M_r	Molar mass
MS	Mass spectrometry
m/*z*	Mass-to-charge ratio
NMR	Nuclear magnetic resonance
Ph	Phenyl
P_i	Probability of isotactic enchainment
ppm	Parts per million
P_s	Probability of heterotactic enchainment
PE	Polyethylene
PET	Polyethylene terephthalate
PLA	Polylactide
rac	Racemic

r_H	Hydrodynamic radii
ROP	Ring opening polymerisation
s	Hetero dyad
SEC	Size exclusion chromatography
t	Time
T	Temperature
τ	Structural parameter
*t*Bu	*tert*-butyl
tert	Tertiary
THF	Tetrahydrofuran
T_m	Melting temperature
TOF	Turnover frequency

List of figures, schemes and tables

Chapter 1

Chapter 5

Contents

Chapter 1

Introduction

1.1. Bio-derived Polymers

The large-scale manufacturing of plastics and their integration into modern society has made them an invaluable asset. Their ease of manufacture, low cost, versatility and resistance to water allow applications in an extensive range of commercial products.[1] In 2014, 99% of all polymers were derived from fossil fuels (4-6% of European oil and gas), which, despite being a cheap and facile resource, is also finite.[2] There are environmental concerns about the end-of-life options of petroleum-derived polymers, as they are not biodegradable and accumulate in landfills and oceans.[3] It has been estimated that 12.7 million metric tonnes entered the oceans in 2010, with this number expected to grow. Despite a social and economic drive for recycling of plastics, the high-energy processes required further increase the environmental costs (CO_2 emissions). There is a need for polymers to be bio-derived, to relive pressure on finite fossil fuels and biodegradable, to reduce the environmental harm from plastic accumulation.

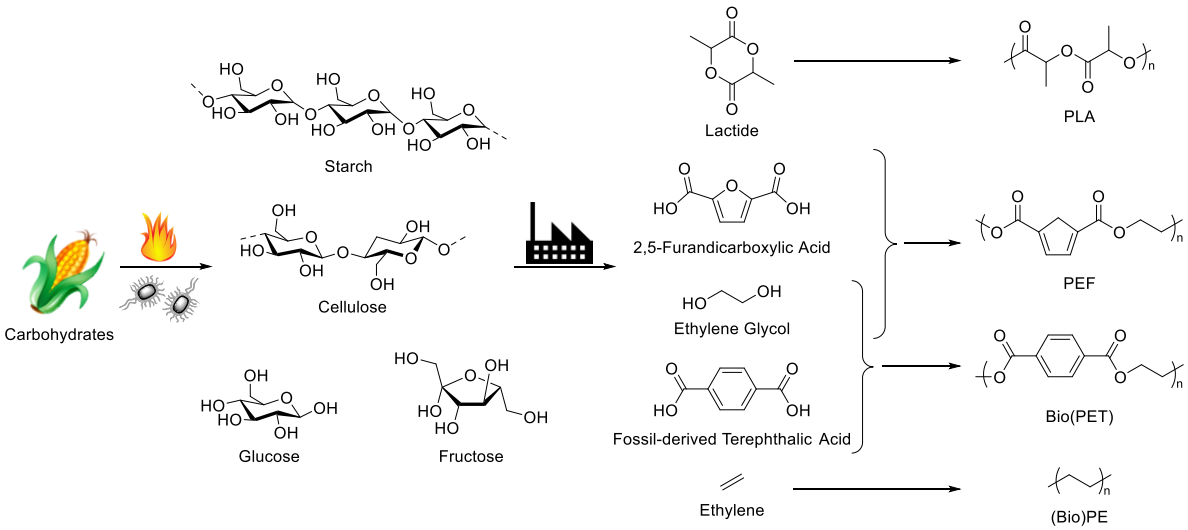

Figure 1.1. Monomers derived from carbohydrate sources and their resultant polymers.[2]

Polymer sustainability may be improved by replacing fossil fuels with biomass and designing polymer backbone chemistries that are suitable for recycling or biodegradation. In 2014, the three most manufactured bio-derived polymers were polyethylene

terephthalate (PET), polyethylene (PE) and polylactide (PLA), the starting materials of which can be acquired from carbohydrate sources (Figure 1.1).[2] Unfortunately, bio-PET and bio-PE are still not biodegradable and despite their potential, bioplastics only represent less than 1% of the planets plastic production. Furthermore, their physical and mechanical properties are not yet comparable with petroleum-derived polymers, and therefore is a key focus in the field. Hence, there is still a drive for further research into polymers, such as PLA, that are both bio-derived and biodegradable.[4]

1.2. Polylactide

Polylactide (PLA) is an aliphatic polyester comprised of repeat units of lactide (LA). It is derived from starch-rich crops such as corn, beet-sugar and cane sugar. The lactic acid is acquired through fermentation using microorganisms e.g. *Bacillus acidilacti* before being converted into lactide. It is advantageous to use crops as the monomer feedstock as CO_2, a greenhouse gas, is absorbed from the atmosphere in the process (Figure 1.2).

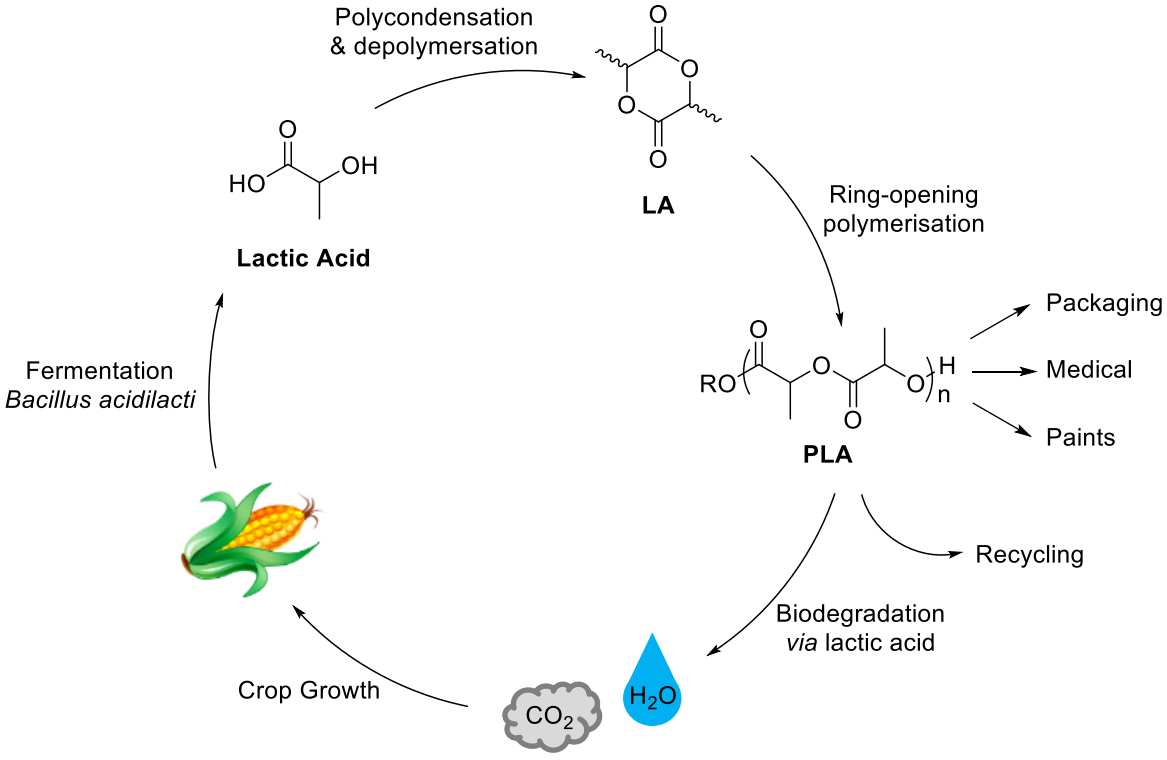

Figure 1.2. The simplified lifecycle of PLA.[7,8]

PLA is biodegradable in typical compost conditions *via*, first, hydrolysis or oxidative processes to fragment the polymer chains into oligomers. Then, by microorganisms, using biodegradative pathways, to form lactic acid, and eventually CO_2, water and other minerals. Despite these pathways, complete disappearance in a natural environment can take several years and with improvements to its mechanical and physical properties, this process may become more challenging and an increased environmental concern.[5]

PLA has numerous excellent physical and mechanical properties compared to other aliphatic polyesters, which are summarised in Table 1.1. It has properties most suitable to replace polystyrene (PS), a commonly used material in protective and food packaging. The melt temperatures can be further improved using certain tacticities of PLA, discussed below, which is a key target in the field.

Table 1.1. Physical and mechanical properties of PLA (M_w = 66,000, 96:4 *L*:*D*) and PS.[6]

Property	PLA	PS
Glass transition temperature (T_g)	55 °C	100 °C
Melt temperature (T_m)	165 °C	210-249 °C
Tensile Strength	59 MPa	36 MPa
Elongation at break	7%	1.6%
Young's Modulus	1280 MPa	2280 MPa

PLA already has a range of applications in both durable and non-durable materials. These applications include packaging, 3D printing, paints and medical.[7] Its medical uses (e.g. sutures) are of interest because of PLAs compatibility with the metabolism of the human body on a suitable timescale (weeks).

The largest producer of PLA is NatureWorks LLC, which manufacture Inego™ PLA polymers specifically using corn feedstocks.[7] They have demonstrated that by frequent analysis of the eco-profile of their production process, they can reduce greenhouse gas emissions of their technologies, which are consistently lower than for the production of petroleum-derived polymers (e.g. polypropylene (PP), PE and PS). Their life-cycle analysis has also shown that the final recovery or disposal method for any polymer is extremely important and polymers which can be recycled or biodegradable are more sustainable.[8]

1.2.1. Synthesis of PLA

PLA can be prepared by either the ring-opening polymerisation (ROP) of lactide or condensation of lactic acid (Figure 1.3). The latter is a step polymerisation process which requires high conversions to afford polymers with sufficient molecular weights (M_n), as defined by the Carothers equation (i.e. the degree of polymerisation is limited by the extent of the reaction).[9] Since esterification is an equilibrium process, the removal of water is essential to drive the reaction towards polymer formation.[10]

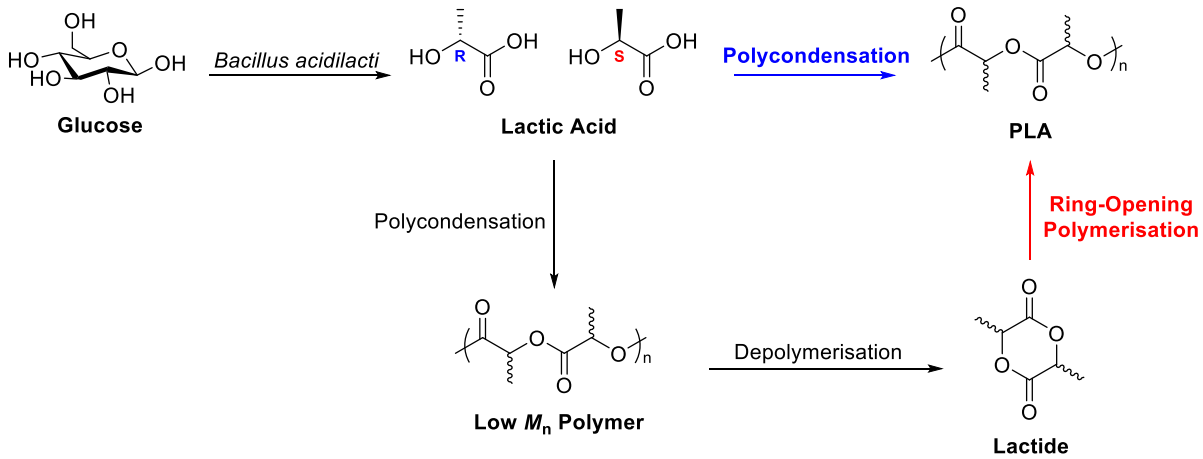

Figure 1.3. The two main synthetic routes to PLA *via* polycondensation or ring-opening polymerisation.

The ROP of lactide is the industrially preferred route as it allows access to high M_n PLA. Lactide is synthesised by polycondensation to oligomers, which are then depolymerised.

The purification of the lactide feedstock is achieved by cycles of recrystallisation and sublimation. The ROP typically requires an initiator and is a thermodynamically driven process, due to the relief of ring strain (ΔH = 22.1 kJ mol^{-1} for *L*-LA) which overrides the entropic cost (ΔS = -41.1 J mol^{-1} K^{-1}, for *L*-LA).[11]

The ROP of lactide operates using two potential mechanisms, an activated monomer mechanism or a coordination-insertion mechanism (Figure 1.4). Generally, the initiator dictates the type of mechanism that occurs, whereby organocatalytic and cationic initiators operate by the activated monomer mechanism whereas neutral Lewis acidic metal alkoxides or amides operate by the coordination-insertion mechanism.[12,13] This preference for metal complexes to use coordination-insertion has been confirmed through experimental and computational studies.[14–20] A wide variety of metal complexes are active as initiators for the ROP of lactide, some of which will be discussed in more detail below.[21–23]

The activated monomer mechanism proceeds by nucleophilic attack of an activated lactide unit. The reaction uses Brønsted acids (CF_3SO_3H), nucleophiles (N-heterocyclic carbenes) or substances containing hydrogen-bonding moieties (thiourea).[24–26] Ring-opening of a lactide monomer occurs through attack by the nucleophile (e.g., a carbene in Figure 1.4), through acyl cleavage. The alcohol end-group of a polymer chain then replaces the nucleophile, freeing it for further attack and adding the ring-opened monomer to the growing polymer chain.

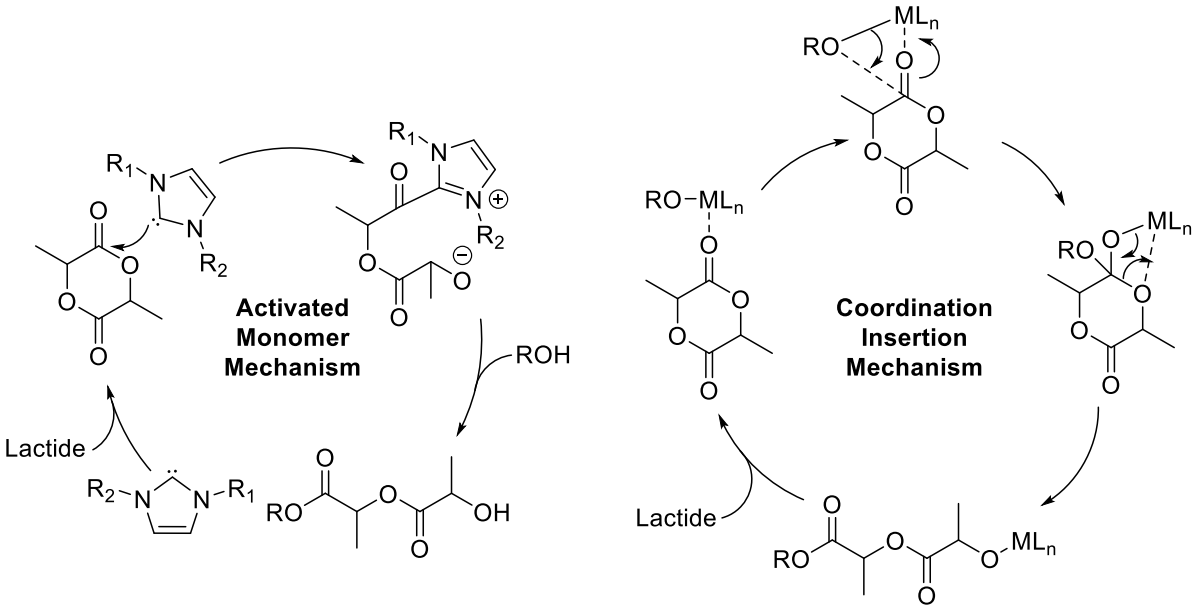

Figure 1.4. Mechanisms for the ROP of lactide (M = metal, OR = alkoxide group, L_n = ligands).

The coordination-insertion mechanism initially proceeds by coordination and activation of the lactide monomer to the metal centre *via* the carbonyl oxygen atom. After this, the metal-alkoxide group attacks the carbonyl bond of lactide creating a four centre intermediate (never isolated) which undergoes ring-opening to form a new metal-alkoxide bond. Repetition of the cycle enables growth of the polymer chain.[19,20] Effective initiators for the coordination-insertion mechanism need to be suitably Lewis acidic to ensure LA binding and yet have a labile metal alkoxide bond to allow for lactide insertion. In this thesis, the focus will be on initiators that operate by the coordination-insertion mechanism.

1.2.2. Polymerisation Kinetics

The key characteristics by which initiators are compared are polymerisation rate, polymerisation control and stereocontrol. Other important characteristics are low toxicity, commercial availability, high tolerance and processability. For many initiators the metal is not removed from the resultant polymer and forms the oxide upon degradation,

therefore the oxides need to be non-toxic. Fortunately, many of them are non-toxic, including Al_2O_3, Fe_2O_3, ZnO, TiO_2 and many lanthanide oxides.

The overall rate law for the ROP of lactide can be written according to Equation 1.1. The rate is defined by the propagation rate constant, k_p, only when the polymerisation is living (see below). This omits the rate of initiation because it is sufficiently fast ($k_i > k_p$) and rate of termination because it is essentially absent ($k_p >> k_t$) for a truly living polymerisation.

$$-\frac{d[LA]}{dt} = k_p[LA]_0^n[I]_0^m$$

Equation 1.1. Overall rate law for ROP of LA. *k_p = propagation rate constant, $[LA]_0$ = lactide concentration, $[I]_0$ = initial concentration of the initiator, n = order in lactide and m = order in initiator.*

To calculate k_p, the order dependence in [LA] must be determined. Experiments are carried out in which $[LA]_0$ remains constant and $[I]_0$ is varied, this means a pseudo first-order kinetics rate law can be written (Equation 1.2). The observed rate constant (k_{obs}), for a given $[I]_0$ concentration, is determined if a linear fit to a plot of $\ln([LA]_0/[LA]_t)$ vs. time is achieved, confirming that the order in [LA] is 1. First order dependence in [LA] is typical but zero or fractional order are not uncommon and typically occur when the initiator suffers from aggregation effects.

$$-\frac{d[LA]}{dt} = k_{obs}[LA]_0^n$$

Equation 1.2. Pseudo first-order rate law for ROP of lactide. *k_{obs} = observed rate constant, $[LA]_0$ = initial lactide concentration and $k_{obs} = k_p[I]_0^m$.*

By plotting k_{obs} against $[I]_0$ (for a range of concentrations), the order dependence in [I] can be determined. If a linear fit is observed in the plot, then the order is 1 and the

overall rate-law can be defined as second-order, first order in both $[LA]_0$ and $[I]_0$. The determination of these two rate constants from experimental data is outlined in Section 2.1.

1.2.3. Polymerisation Control

For the ROP to be considered a controlled, living polymerisation, which is a type of chain-growth polymerisation, then a number of conditions must be met: [27–29]

1. Large difference in rate of initiation over propagation ($k_i > k_p$).
2. Narrow distribution of molecular weights, i.e. Dispersity (Đ).
3. Linear increase in M_n with % conversion and $1/[\text{initiator}]_0$.
4. Ability of control the synthesis of block copolymers by sequential monomer addition.
5. Limited transesterification reactions ($k_p >> k_{te}$, k_{te} = rate of transesterification).

To meet all these requirements using one initiator can be challenging, as transesterification is a common side reaction. There are two mechanisms by which transesterification occurs, intermolecularly (between chains) and intramolecularly (within chains), resulting in chain scrambling for the former and creation of cyclic oligomeric species for the latter (Figure 1.5).[30] Transesterification can be indicated by an increase in Đ and by no change in M_n. The presence of transesterification can also be determined using $^{13}C\{^1H\}$ NMR spectroscopy or MALDI-ToF spectrometry.[31]

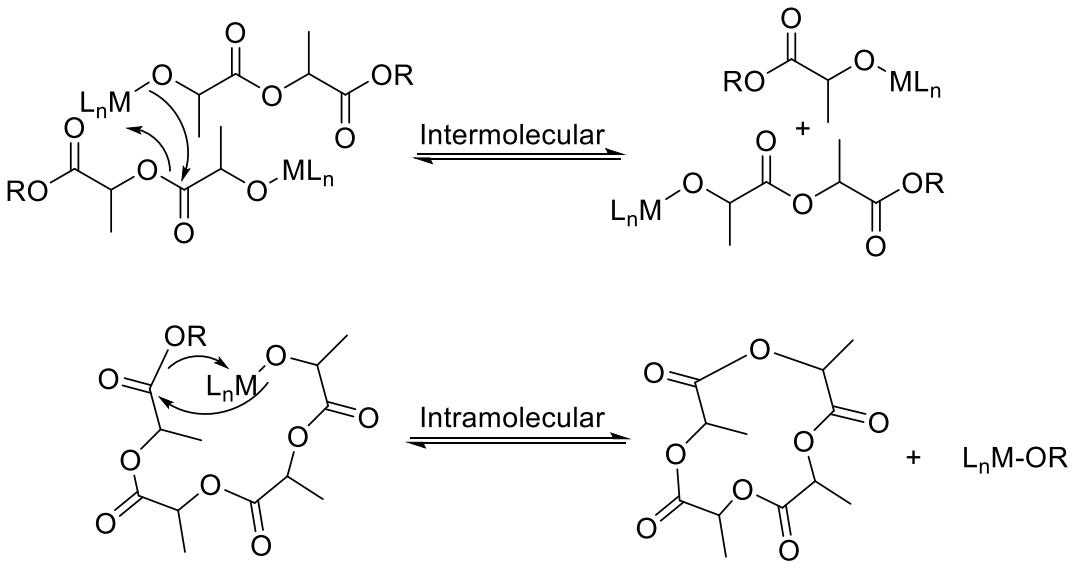

Figure 1.5. Mechanisms for the two routes of transesterification of PLA during polymerisation reactions.

Using a number of analytical techniques, the degree of polymerisation control can be determined: gel permeation chromatography (GPC) for M_n and Đ, matrix-assisted laser desorption ionization (MALDI-ToF) mass spectrometry and nuclear magnetic resonance spectroscopy (NMR) for transesterification identification. These techniques will be described in more detail in Chapter 2.

1.2.4. PLA Tacticity

The lactide monomer contains two stereocentres, which gives rise to *SS*-LA, *RR*-LA and *SR*- or *meso*-LA. Tacticity is used to describe the relative stereochemistry of adjacent chiral centres in the polymer chain and is important since tacticity dictates the overall physical and thermal properties of the final polymer.

The polymerisation of enantiopure and racemic (*rac*) lactide generates a number of different tacticities of PLA, which possess differing individual physical properties (Table 1.1).[32] Polymerisation of one enantiomer (e.g. *SS*-LA) produces isotactic PLA, which is semi-crystalline.[33] There are two isotactic arrangements possible from *rac*-LA, stereocomplex (individual polymer chains of the two different enantiomers) and

stereoblock (bound chains of the two different enantiomers). Stereoblock gives higher melt temperatures (T_m) than isotactic PLA; due to intermolecular co-crystallisation, but stereocomplex typically gives even higher values.[34,35] The higher T_m values associated with stereoblock PLA can make it a competitive replacement for polymers such as PS and PET. The materials composed of atactic (random incorporation of either enantiomer) or heterotactic (alternating incorporation of the two enantiomers) PLA do not have the thermal resistance necessary for being used as an engineering polymer.[36,37]

Table 1.2. Tacticities of PLA and their glass transition and melting temperatures.[32–36]

PLA tacticity	Glass transition temperature (°C, T_g)	Melting temperature (°C, T_m)
Atactic	50-60	N/A
Heterotactic	50-60	N/A
Syndiotactic	~ 34	≤ 152
Isotactic	~ 60	~ 175
Stereocomplex	60-70	170-230
Stereoblock	60-70	170-230

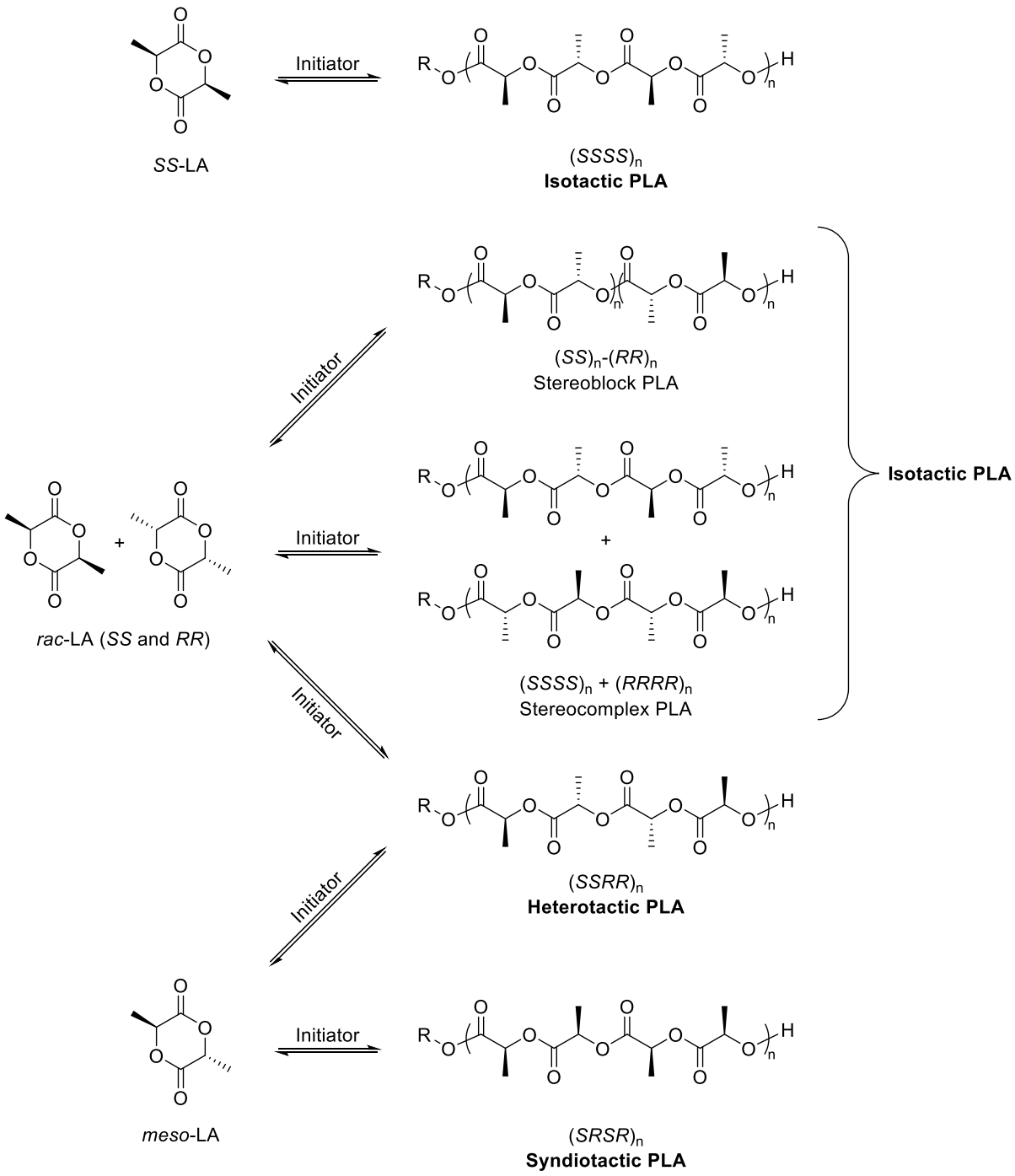

Figure 1.6. The tacticities of PLA possible from different enantiomeric feedstocks.[38]

Polymerisations with *rac*-LA can also result in heterotactic PLA and atactic and polymerisations with *meso*-LA may yield either heterotactic or syndiotactic PLA (sequential stereocentres of opposite relative configuration - *SRSR*) but atactic PLA is also possible.[39]

1.2.5. Stereocontrol Mechanisms

The tacticity of PLA is mediated by two mechanisms: chain-end-control (CEC) or enantiomorphic site-control (ESC) (Figure 1.7).[38] In the CEC mechanism, the stereochemistry of the previously enchained monomer determines the stereochemistry of the subsequent one and is typical in achiral initiators. The ESC mechanism controls the stereochemistry of the newly enchained monomer by chirality at metal. It has the ability to "autocorrect" errors whereas during CEC mechanisms errors initiate a change in stereochemistry within the polymer chain. The determination of which stereocontrol mechanism is present, using NMR, is outlined in Section 2.1. It is also possible to distinguish between the two because for an ESC mechanism, there will be an inherent preference for one enantiomer, therefore a difference in rate constants. These can be determined by carrying out the polymerisations with each enantiomer under the same set of reaction conditions.

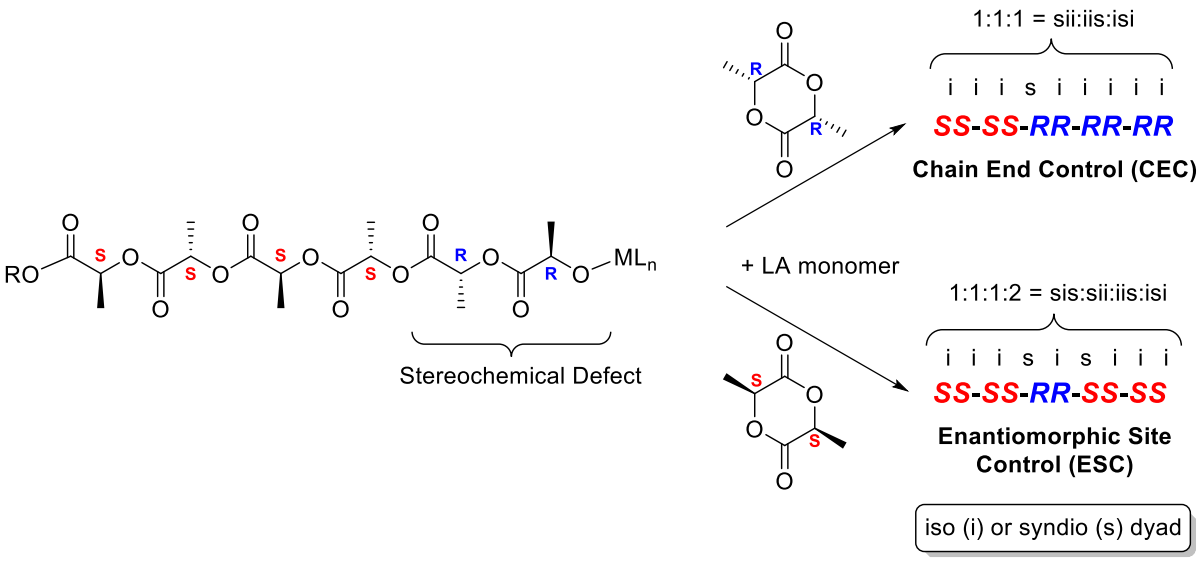

Figure 1.7. The two mechanisms of stereocontrol: chain end control (CEC) and enantiomorphic site control (ESC) with the relative integrals of their defect tetrads.

It is possible to define the level of stereocontrol, exhibited by an initiator, as a probability of a certain stereosequence, P_i = the probability of isotactic enchainment and P_s = the probability of hetero/syndiotactic enchainment.[40] A perfectly isotactic PLA polymer yields

P_i = 1 or P_s = 0, and the inverse is true for a perfectly heterotactic PLA polymer. For an atactic PLA polymer, and P_i = P_s = 0.5, therefore when targeting an isotactic initiator, values of 0.5 < P_i ≤ 1 are desirable. The probabilities of a particular stereochemistry are calculated using Bernoullian statistics. The experimental determination, using NMR spectroscopy, of these values is outlined in Section 2.1.

1.3. Initiators

There are metal centres from all across the periodic table, with a wide range of ligands, which are active as initiators for the ROP of LA. This section will focus on (i) aluminium(III) for its precedence for high levels of isoselectivity, (ii) indium(III) for improved rates vs. aluminium, whilst maintaining good isoselectivity and (iii) zinc(II) for its good activity and compatibility with a range of ligands. Furthermore, these metals are all abundant, colourless and suitable for facile characterisation (diamagnetic). This section will also discuss the recent field of redox-switchable initiators in the ROP of *rac*-LA and the interesting behaviour they demonstrate.

1.3.1. Aluminium

Aluminium complexes are the most extensively reported initiators for the ROP of lactide.[30,41,42] The first isotactic initiator, reported by Spassky and co-workers, was a chiral, binaphthyl aluminium salen complex (Figure 1.8, **A**).[43] The major weakness of **A** was long reaction times, taking up to 5 days to reach 90% conversion ([I]:[LA] 1:75, toluene, 353 K).

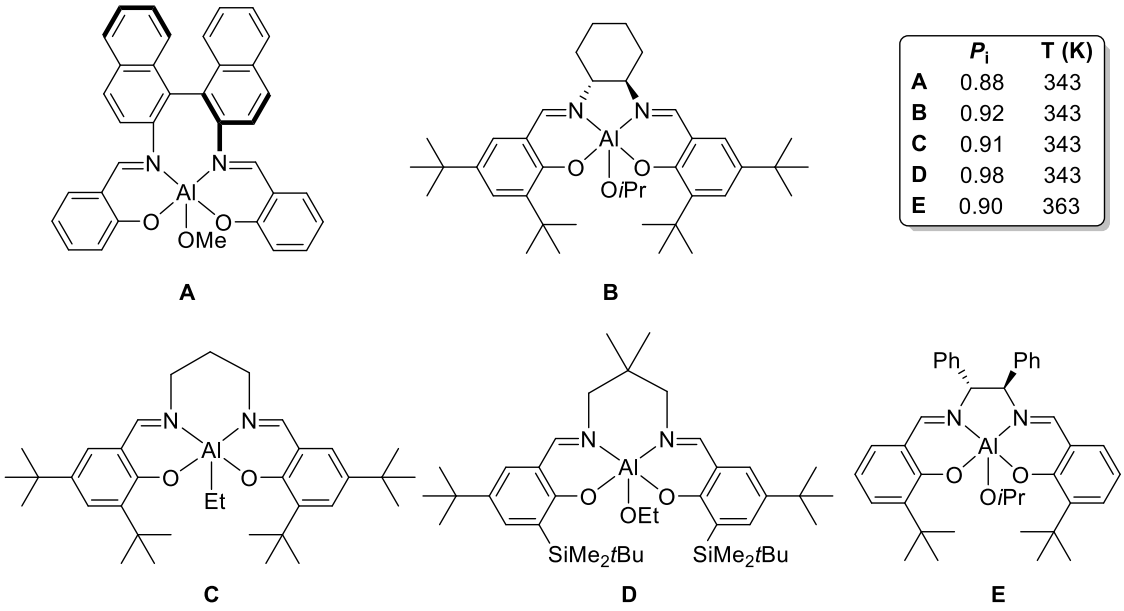

	P_i	T (K)
A	0.88	343
B	0.92	343
C	0.91	343
D	0.98	343
E	0.90	363

Figure 1.8. A selection of key isotactic aluminium salen initiators and their P_i values.[43–47]

Feijen and co-workers applied the inexpensive and widely used Jacobsen ligand in both its racemic and enantiomeric (*R*,*R*) form (**B**) to prepare new aluminium initiators.[44,48] Whilst the rates were still modest (5 days for 93% conversion, [I]:[LA] 1:68, toluene, 353 K), high degrees of isotacticity and melt temperatures were reported: P_i = 0.92 and T_m = 184 °C respectively. Nomura and co-workers were the first to develop achiral aluminium initiators that preserved high *iso*-selectivity (P_i = 0.91, 353 K, **C**) as well as faster rates of polymerisation, reaching full conversion in hours rather than days (14 hours for 95% conversion, [I]:[Benzyl alcohol(BnOH)]:[LA] 1:1:100, toluene, 353 K). Further investigation revealed that the mechanism for stereocontrol was instigated by a flexible ligand backbone through CEC.[45] Modification of the initiator, by increasing the steric bulk of substituents in the *ortho*-position of the phenolate groups, resulted in higher degrees of isotacticity (P_i = 0.98, 353 K, **D**), albeit with slower rates of polymerisation.[46]

Carpentier and co-workers synthesised a range of monometallic chiral salen aluminium initiators and achieved P_i values of 0.80-0.90 (**E**).[47] Interestingly, despite the initiators

being chiral, a CEC mechanism was found to dominate, demonstrating that chirality is not a prerequisite for an ESC mechanism. Furthermore, electron-withdrawing substituents (*para*-position of phenolate) led to increased rates of polymerisation, which was consistent with reports by Hillmyer, Tolman, Gibson and Nomura.[46,49,50] A complete study of the Schiff base/salen ligand substituent effects, on both rate and stereoselectivity was conducted by Gibson and co-workers.[50] The key findings were:

1. Electron withdrawing substituents in the *para*-phenolate site increase rates.
2. Flexible, three-carbon backbones also increase rates and isoselectivity.
3. Rates are supressed but isoselectivity is increased by bulky *ortho*-phenoxy groups.

Modifications beyond varying steric bulk or the ligand backbone have focused on changing the donor groups. Fully saturating the imine bonds to amine groups yields the salan ligand, whereas saturating just one, yields the salalen ligand. Both ligands and their complexes have a range of applications beyond lactide ROP.[51–53]

Gibson and co-workers were the first to report aluminium salan initiators for the ROP of *rac*-lactide.[54] The rates of polymerisation were similar to aluminium salen initiators, taking 24 hours to reach full conversion ([I]:[LA] 1:100, toluene, 343 K). By varying the substituents of the ligand, either isotactic (P_i = 0.86, **F**, R = Cl, Figure 1.9) or heterotactic (P_s = 0.79, **F**, R = H) PLA could be obtained. The initiators were chiral at the aluminium centre, due to the N donors becoming stereogenic upon metal coordination, therefore yielding isotactic PLA *via* an ESC mechanism. Similar degrees of isotacticity have been achieved with other aluminium salan initiators, as well as changes between tacticities upon varying the ligand substituents.[55]

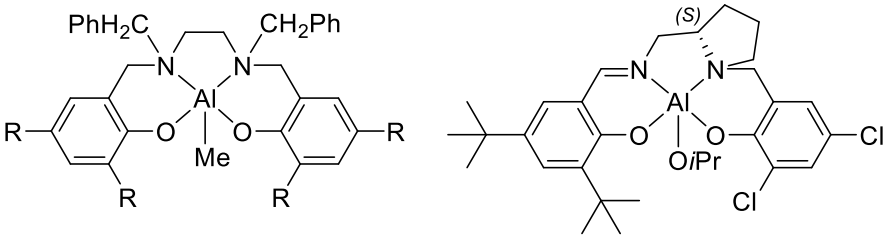

F **G**

Figure 1.9. Isotactic aluminium salan and salalen initiators.[54,56]

Kol and co-workers reported a series of chiral salalen aluminium initiators and also found that substituents played a major role in tacticity control.[56] The highest isotacticity reported (P_i = 0.82, 353 K, **G**) was obtained with sterically bulky substituents at the *ortho*-phenolate adjacent to the imine (e.g. Adamantyl or *t*Bu) and electron-withdrawing groups (e.g. Cl) at the *ortho*-phenolate adjacent to the amine. Increased steric hindrance from the amine phenolate gave rise to heterotactic PLA and larger halides (e.g. Br/I) at this site decreased isotacticity.[56] Studies comparing both salan and salalen ligands have demonstrated that large differences in both isoselectivites and rates can be obtained simply from the change in donor groups in the ligand backbone.[57]

1.3.2. Indium

Due to the slow polymerisation rates but excellent isoselectivites observed by aluminium initiators, heavier Group 13 analogues were explored. The first example of a discrete indium initiator, published by Mehrkhodavandi and co-workers, was an asymmetrically bridged, chiral dinuclear complex which gave modest isoselectivity (P_i = 0.62, 273 K, **H**, Figure 1.10).[58] Despite the moderate stereoselectivity, its activity was significantly higher than aluminium initiators, reaching complete conversion in 30 minutes ([I]:[LA] 1:200, CD_2Cl_2, 298 K). This highlighted the potential of indium initiators to be both active at room temperature and demonstrate isotactic bias.[59]

Okuda, Arnold and co-workers reported similar P_i values using chiral indium alkoxide initiator (**I**), but the nature of the initiating group is uncertain because of its configurational instability.[60] Nevertheless, isotactic PLA was produced by an ESC mechanism.

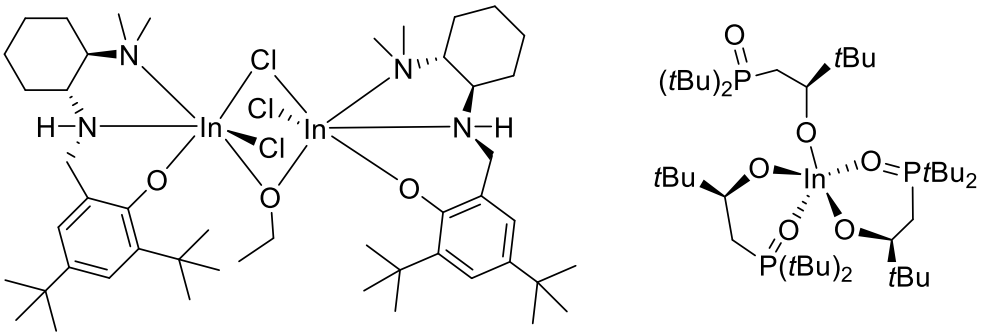

Figure 1.10. Isoselective indium initiators by Mehrkhodavandi (**H**, P_i = 0.62, 273 K) and Okuda/Arnold (**I**, P_i = 0.63, 298 K).[58,60]

A chiral, salen indium initiator, also reported by Mehrkhodavandi and co-workers, demonstrated good rates, converting 1000 equivalents of *rac*-LA in under four hours ([I]:[LA] 1:200, CH_2Cl_2, 298 K, **J**, Figure 1.11). These initiators operated by an ESC mechanism and yielded P_i = 0.77 (298 K).[61] Upon changing to racemic 2,2'-bis(diphenylphosphino)-1,1'-binaphthyl (BINAP), analogous to the aluminium system pioneered by Spassky and co-workers, stereocontrol was lost and rates were slower by several orders of magnitude (**K**).[62] This was rationalised by an increase in the number of coordination modes, most likely due to the ligand flexibility and the larger ionic radius of indium. Further studies using initiator **J**, which was targeted to decrease aggregation by using a coordinating alkoxide, pyridine-2-ylmethoxide, enabled a series of monomeric initiators to be isolated but neither an increase in rate nor stereoselectivity was observed.[63]

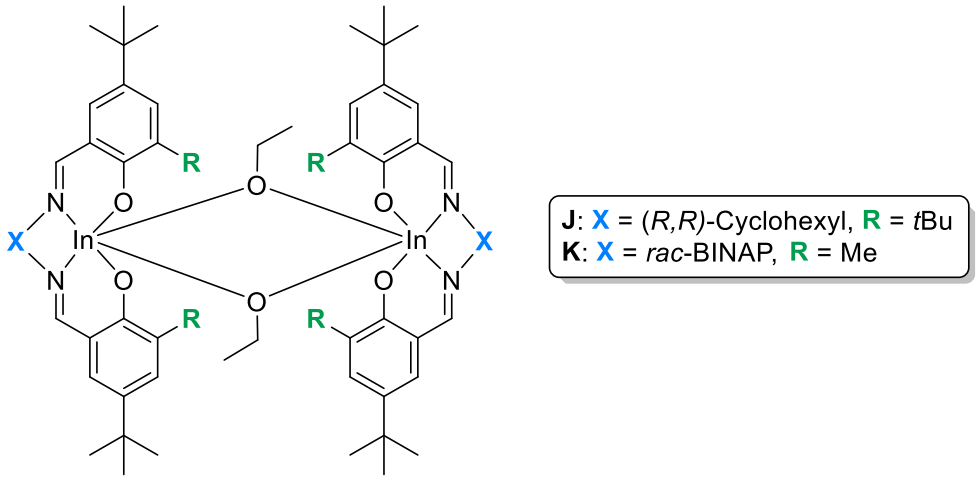

Figure 1.11. Dinuclear indium salen initiators with different backbones and *ortho*-phenolate substituents reported by Mehrkhodavandi.[61,62]

In a recent report, by Mehrkhodavandi and co-workers, indium and gallium initiators were compared and the Lewis acidity of Group 13 metals was investigated.[64] Gallium initiators were poorly active with *rac*-LA and unreactive with ε-caprolactone. Whilst Lewis acidity investigations were inconclusive, it was postulated that the smaller ionic radii of gallium might create a stabilised first monomer insertion product, thereby slowing the polymerisation rate.

Beyond discrete ligand systems, Tolman and co-workers developed a robust catalyst system, which was stable to air and water, from the combination of $InCl_3$, NEt_3 and BnOH.[65] Controlled polymerisation was observed under a range of conditions and the system displayed a strong heterotactic bias (P_s = 0.86 [333 K] - 0.97 [273 K]). The polymerisation mechanism was proposed to initiate by BnOH insertion to the indium chloride bond, at rates such that $k_i > k_p$, which is essential for a living polymerisation. The role of the halide atom was also important: rates decreased in the order Cl > Br > I. The system operated by a coordination-insertion mechanism and a CEC stereocontrol mechanism.[66]

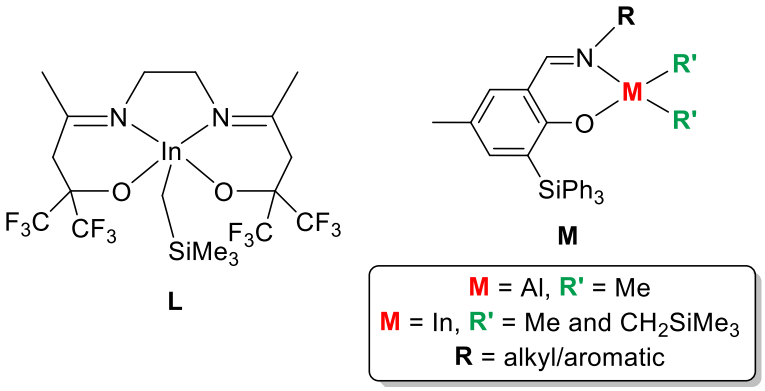

Figure 1.12. Examples of other Schiff base initiators with both aluminium and indium.[67,68]

Carpentier and co-workers compared aluminium and indium salen and half-salen Schiff base ligands, some of which produced isotactic PLA.[67] Tetradentate fluorinated indium initiators yielded P_i = 0.69, at 353 K (**L**, Figure 1.12) which was lower than the analogous aluminium complexes (P_i = 0.87). There was an uncertainty in the initiation mechanisms between the two metal centres, which was further investigated using a series of aluminium and indium phenoxy-imine complexes (**M**).[68] Kinetic studies revealed different rate laws for the two metal systems, specifically in the order in [ROH], and it was proposed that aluminium operated through a coordination-insertion mechanism and indium through an activated monomer mechanism. The independent reaction between the dialkylindium complexes with an equivalent of alcohol did not form any alkoxide product, which provided further evidence for the activated monomer mechanism.

Gallium initiators have so far demonstrated limited polymerisation rates, control and stereoselectivity.[64] Recently, Chakraborty and co-workers reported a gallium initiator which yielded isotactic PLA (P_i < 0.84, 298 K), which interestingly, was higher than the analogous indium initiators (P_i < 0.76, **N**, Figure 1.13).[69]

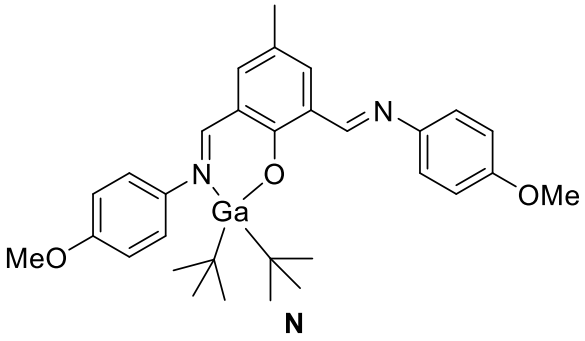

Figure 1.13. An isotactic gallium initiator reported by Chakraborty (P_i = 0.84, 298 K).[69]

1.3.3. Zinc

Zinc initiators have been of interest for the ROP of lactide for several decades as they yield excellent rates and contain a cheap metal centre. There is a strong track record of heteroleptic zinc initiators with showing high activities and stereoselectivities, some ligands include: *β*-diketiminates (BDI), *tris*(pyrazolyl)borates (an early example) and phenoxy-amines.[70]

Coates and co-workers applied the BDI ligand to prevent aggregation of the zinc centres and were also able to achieve target stereoselective polymerisations *via* CEC (Figure 1.14).[37] Initiator **O** polymerised *rac*-lactide, yielding heterotactic PLA (P_s = 0.90, 293 K) with excellent rates (97% conversion in 20 minutes, [I]:[LA] 1:200, CH_2Cl_2, 298 K) and polymerisation control.[71] The BDI aromatic ring substituents are important and reducing the steric bulk (Me and *n*Pr) at these positions decreased heteroselectivity.

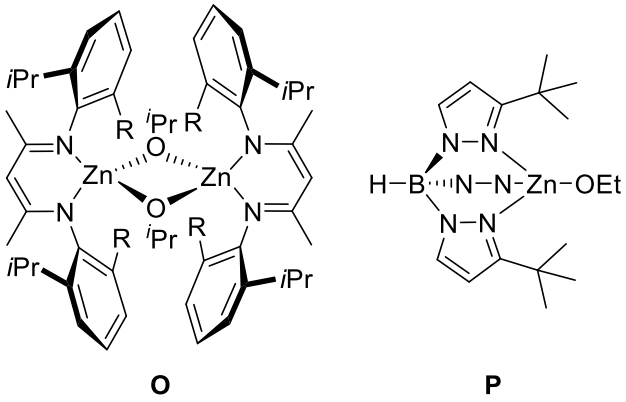

O **P**

Figure 1.14. Examples of a *β*-diketiminate zinc initiator (**O**, R = Me or *n*Pr) and a tris(pyrazolyl)borate zinc initiator (**P**).

Chisholm and co-workers reported the *tris*(pyrazolyl)borate zinc initiator, **P**.[72] Their aim was also to prevent aggregation and ligand scrambling *via* the Schlenk equilibrium (the equilibrium process between two heteroleptic complexes and their respective homoleptic complexes – Equation 1.3).[73] The rate of the initiator was attributed to the polarity of the alkoxide bond activating the carbonyl of lactide to nucleophilic attack.[74] When electron withdrawing groups (CF_3) were present on the pyrazolyl ring the polymerisation rate was reduced, highlighting that decreased Lewis acidity at zinc and, therefore, an increased polarity of the alkoxide bond, that was rate determining.

$$L_1ZnOR + L_2ZnOR \rightleftharpoons L_1L_2Zn + Zn(OR)_2$$

Equation 1.3. An example of the Schlenk equilibrium. *L_1 and L_2 = ligands, OR = alkoxide group.*

Phenoxy-amines have demonstrated some of the best rates with zinc by also preventing aggregation of zinc centres. Initiator **Q**, which has zinc coordinated by a Schiff base ligand, has long been one of the fastest initiators, for LA ROP (Figure 1.15).[70] It showed good molecular weight control and narrow dispersities and operated at low catalyst loadings of <0.1%. The highest TOF (turnover frequency) achieved was 4430 h^{-1} ([I]:[LA] 1:1000, $[LA]_0$ = 1M, CH_2Cl_2, 298 K). The high activity was attributed to the monomeric structure, as

dimers typically displayed lower rates; therefore, ligands that favoured lower coordination numbers and a monomeric zinc centre were proposed to induce greater polymerisation activity.

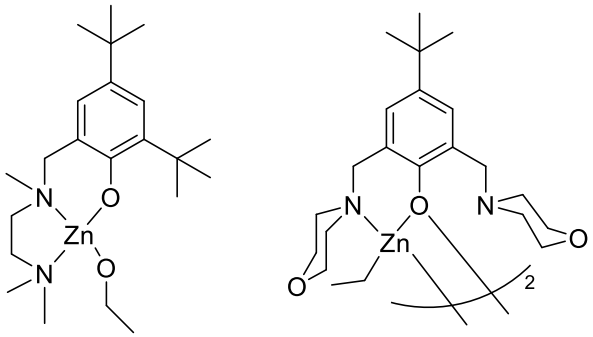

Q **R**

Figure 1.15. Highly active zinc Schiff base initiators.[70,75]

Carpentier and co-workers later reported initiator **R**, also with the goal of low coordination number complexes by using bulkier ligands.[75] The complex was stable even when excess alcohol was added (for immortal ROP). To date, the fastest zinc initiators are di-zinc complexes coordinated by bis(imino)diphenylamido ligands, which show TOFs of 12,500 h^{-1} ([I]:[LA] 1:1000, $[LA]_0$ = 1M, THF, 298 K, N.B. different solvent to **A**).[76] This excellent activity was attributed to metal-metal cooperativity with further enhancement by the conformation of the ancillary ligand. Typically, zinc initiators display little/no stereoselectivity and there are only a handful of isoselective initiators, this will be discussed in Chapter 5.

1.3.4. Redox Active

Redox-active initiators are a category of switchable catalysts, which are unique catalysts for gaining more control during a chemical transformation.[77] Switchable catalysis is an atom-economical method that generates multiple, catalytically active species with different reactivity. These catalysts have already been reported in olefin polymerisation,

metathesis reactions, cyclic esters ROP and co-polymerisations with cyclic esters/CO_2/epoxides.[78–82] The use of ferrocene-based switches, or redox-switchable metal centres has also been most widely studied for cyclic esters (Figure 1.16).[83–88]

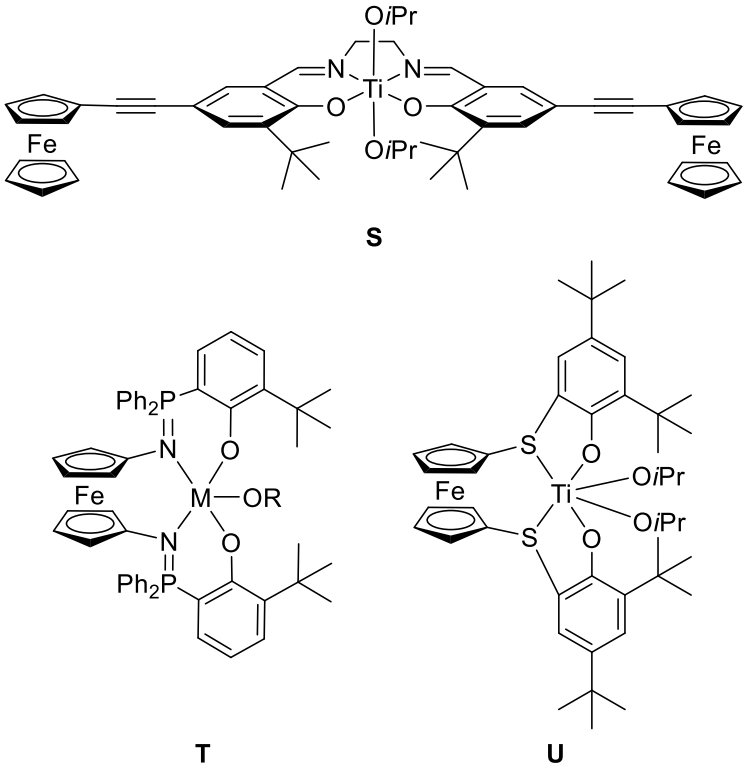

Figure 1.16. Ferrocene-containing redox-active initiators for lactone ROP (M = Y, In; R = *t*Bu, Ph).[79,80,83]

Gibson, Long and co-workers were the first to report a redox-switchable initiator for LA polymerisation (**S**).[83] A titanium salen initiator achieved a significant reduction in rate upon oxidation of the conjugated ferrocene moieties (k_{app}[reduced]/k_{app}[oxidised] = 30). Diaconescu and co-workers were able to "switch off" the polymerisation of *L*-LA upon oxidation of the ferrocene moiety, retaining the same polymerisation rate after reduction of the system and consecutive redox-switches (**T**).[80] The ferrocene was incorporated as the backbone of the ligand, therefore changing the proximity of the redox-site to the metal centre, which was found to positively influence the characteristics of the two-redox states.[79,80,89] Modification of the ligand scaffold to utilise a "thiolfan" ligand led to a

change in monomer preference between the two-redox states (**U**). The titanium thiolfan initiator in its reduced state polymerised LA, with minor incorporation of ε-caprolactone, and vice versa in its oxidised state.[80]

1.4. The Phosphasalen Ligand

The iminophosphorane bond is defined as a formal phosphorus=nitrogen double bond. First synthesised by Staudinger and Meyer in 1919, these bonds and subsequent compounds feature in biochemical applications such as drug design and delivery, as well as ligands for a variety of catalytic processes.[90–94] The phosphasalen ligand is the direct analogue of the salen ligand whereby the imine bonds have been replaced by iminophosphorane bonds. It was first synthesised by Auffrant and co-workers and further developed in collaboration with our group (Figure 1.17).[23,95,96] For metal complexes, the P=N bonds are better σ- and π-donors than the salen analogue and the addition of phosphorus substituents offer steric protection at metal. There are a range of sites for structure-activity studies: (i) phosphorus (R), (ii) the backbone (R_1) or (iii) phenolate (R_n) substituents.

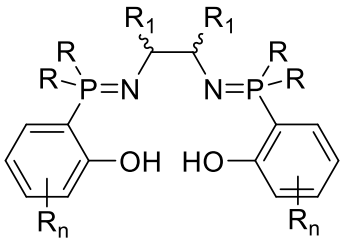

Figure 1.17. General structure of the phosphasalen ligand (R_n substituents typically present on the *ortho*- and *para*-positions).[95]

Phosphasalens are generally synthesised using the Kirsanov reaction, starting from the phosphinophenol and reacting with one equivalent of bromine (Br_2), to generate "PR_3Br_2" *in situ*, which then undergoes nucleophilic substitution with a diamine, in the presence of base, to generate the aminophosphonium bromide salt.[97–99] These salts are typically air and moisture stable, therefore can be to isolated and purified. A stronger base is then

required (MeLi or $KN(SiMe_3)_2$) to fully deprotonate the salts before coordination to a metal centre. This synthetic methodology will be utilised throughout this thesis.

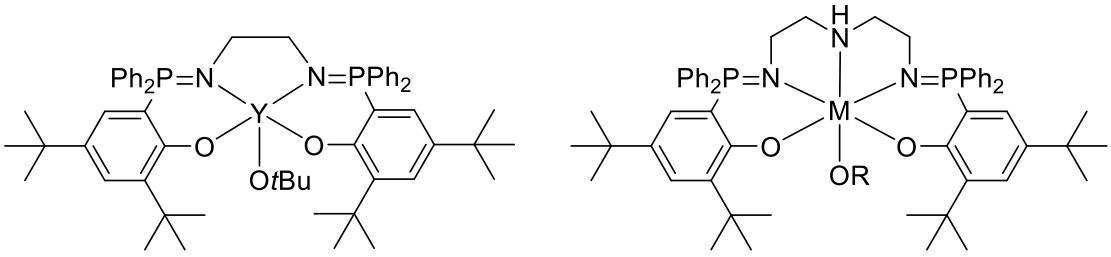

V **W**

Figure 1.18. Lanthanide phosphasalen initiators reported in our group (M = Y, Lu or La; R = Et or *t*Bu).[23,96,100]

The Williams and Long groups synthesised phosphasalen yttrium and lanthanide complexes for the ROP of *rac*-LA (Figure 1.18).[23,96,100] The yttrium initiator was highly active, demonstrated excellent polymerisation control and depending on the structure of the backbone, achieved highly heterotactic (P_s = 0.87, 298 K, **V**) or isotactic (P_i = 0.84, 298 K, **W**, M = Y, R = Et or *t*Bu) PLA.[23] The additional NH donor in the ligand backbone was postulated to limit the fluxionality of the initiator and was important in isoselectivity. Upon changing the metal centre in initiator **W**, it was found that rates and isoselectivites were closely linked to metallic covalent radii. The larger metal centre, lanthanum, achieved excellent rates (98% conversion in 20 seconds, [I]:[IPA]:[LA] 1:1:500, THF, 298 K) but low isoselectivites (P_i = 0.28) whereas the smaller lutetium centre had slower rates (84% conversion in 9 hours, same conditions) but high isoselectivites (P_i = 0.84). As observed in the yttrium initiator, using rotating-frame nuclear Overhauser effect spectroscopy (ROESY), limiting the fluxionality of the complex led to higher P_i values, which was also observed in the lutetium initiator.[100]

1.5. Aims

The first aim of this thesis is to synthesise a novel tetradentate ligand, based on the salen motif containing one imine and one iminophosphorane bond. This hybrid ligand will be analogous to salalen ligands, already reported in the literature, which demonstrate good polymerisation activity (rate and isoselectivity) for *rac*-LA. It is of interest to incorporate an iminophosphorane bond, because phosphasalen ligands, when coordinated to a number of metals, yield good rates and high isoselectivites. The initiators synthesised with this ligand will be focus on coordination to Group 13 metals, due to their precedence for high isoselectivites (aluminium) and good rates (indium).

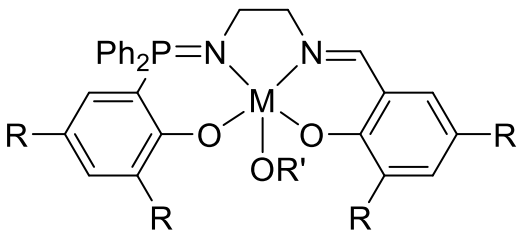

Figure 1.19. Structure of the proposed hybrid initiators and sites of potential modifications (R) for investigation of structure-activity relationships.

The second aim is to investigate structure-activity relationships with the novel hybrid ligand by modification (steric and electronic) of the ligand scaffold. In previously reported initiators, higher isoselectivites can be achieved through modification, as well as highlighting the sites which may be important in rate determination or stereocontrol (Figure 1.19).

The third aim is to incorporate ferrocene into the hybrid ligand and to synthesise an initiator for redox-switchable catalysis. The target with these initiators will be to instigate a change in stereocontrol with a redox-switch.

Finally, the fourth aim is to broaden the scope of phosphasalen ligands to target M(II) centres by using "half-phosphasalen" ligands. As discussed in this chapter, zinc has demonstrated good rates and isoselective capabilities.

For all new initiators, their properties in the ROP of *rac*-LA will investigated and compared. Therefore, it will be desirable to fulfil the following requirements:

1. High activity (full conversion of monomer on appropriate timescales e.g. minutes to an hour) under appropriate testing conditions (1M in LA, THF, 298 K).
2. High polymerisation control and operating by a living polymerisation mechanism (predictable molecular weights, narrow dispersities and limited transesterification reactions).
3. High isoselectivites ($0.5 < P_i < 1$), targeting values of $P_i > 0.9$.

1.6. References

1 PlasticsEurope, *PlasticsEurope*, 2016, 1–38.

2 Y. Zhu, C. Romain and C. K. Williams, *Nature*, 2016, **540**, 354–362.

3 J. R. Jambeck, R. Geyer, C. Wilcox, T. R. Siegler, M. Perryman, A. Andrady, R. Narayan and K. L. Law, *Science*, 2015, **347**, 768–771.

4 F. Aeschelmann and M. Carus, *Ind. Biotechnol.*, 2015, **11**, 154–160.

5 X. Qi, Y. Ren and Z. Wang, *Int. Biodeterior. Biodegrad.*, 2017, **117**, 215–223.

6 S. Farah and D. G. Anderson, *Adv. Drug Deliv. Rev.*, 2016, **107**, 367–392.

7 E. T. H. Vink and S. Davies, *Ind. Biotechnol.*, 2015, **11**, 167–182.

8 E. T. H. Vink, S. Davies and J. J. Kolstad, *Ind. Biotechnol.*, 2010, **6**, 212–224.

9 W. H. Carothers, G. L. Dorough and F. J. van Natta, *J. Am. Chem. Soc.*, 1932, **54**, 761–772.

10 S. Mecking, *Angew. Chem. Int. Ed.*, 2004, **43**, 1078–1085.

11 A. Duda and S. Penczek, *Macromolecules*, 1990, **23**, 1636–1639.

12 M. K. Kiesewetter, E. J. Shin, J. L. Hedrick and R. M. Waymouth, *Macromolecules*, 2010, **43**, 2093–2107.

13 N. E. Kamber, W. Jeong, R. M. Waymouth, R. C. Pratt, B. G. G. Lohmeijer and J. L. Hedrick, *Chem. Rev.*, 2007, **107**, 5813–5840.

14 I. Barakat, P. Dubois, R. Jérôme and P. Teyssié, *J. Polym. Sci. Part A Polym. Chem.*, 1993, **31**, 505–514.

15 A. Kowalski, A. Duda and S. Penczek, *Macromolecules*, 2000, **33**, 689–695.

16 J. L. Eguiburu and M. J. Fernandez-Berridi, *Macromolecules*, 1999, **32**, 8252–8258.

17 H. R. Kricheldorf, M. Berl and N. Scharnagl, *Macromolecules*, 1988, **21**, 286–293.

18 P. Dubois, C. Jacobs, R. Jerome and P. Teyssie, *Macromolecules*, 1991, **24**, 2266–2270.

19 M. Ryner, K. Stridsberg, A.-C. Albertsson, H. von Schenck and M. Svensson, *Macromolecules*, 2001, **34**, 3877–3881.

20 E. L. Marshall, V. C. Gibson and H. S. Rzepa, *J. Am. Chem. Soc.*, 2005, **127**, 6048–6051.

21 A. Pilone, M. Lamberti, M. Mazzeo, S. Milione and C. Pellecchia, *Dalton Trans.*, 2013, **42**, 13036–13047.

22 S. Dagorne, M. Normand, E. Kirillov and J.-F. Carpentier, *Coord. Chem. Rev.*, 2013, **257**, 1869–1886.

23 C. Bakewell, T.-P.-A. Cao, N. Long, X. F. Le Goff, A. Auffrant and C. K. Williams, *J. Am. Chem. Soc.*, 2012, **134**, 20577–20580.

24 D. Bourissou, B. Martin-Vaca, A. Dumitrescu, M. Graullier, F. Lacombe, B. Didier,

M.-V. Blanca, A. Dumitrescu, G. Magalie and F. Lacombe, *Macromolecules*, 2005, **38**, 9993–9998.

25 E. F. Connor, G. W. Nyce, M. Myers, A. Möck and J. L. Hedrick, *J. Am. Chem. Soc.*, 2002, **124**, 914–915.

26 A. P. Dove, R. C. Pratt, B. G. G. Lohmeijer, R. M. Waymouth and J. L. Hendrick, *J. Am. Chem. Soc.*, 2005, **127**, 13798–13799.

27 P. J. Flory, *J. Am. Chem. Soc.*, 1940, **62**, 1561–1565.

28 M. Szwarc, M. Levy and R. Milkovich, *J. Am. Chem. Soc.*, 1956, **78**, 2656–2657.

29 M. Szwarc, *Nature*, 1956, **178**, 1168–1169.

30 R. Platel, L. Hodgson and C. K. Williams, *Polym. Rev.*, 2008, **48**, 11–63.

31 M. Bero, J. Kasperczyk and Z. J. Jedlinski, *Die Makromol. Chemie*, 1990, **191**, 2287–2296.

32 L.-E. Chile, P. Mehrkhodavandi and S. G. Hatzikiriakos, *Macromolecules*, 2016, **49**, 909–919.

33 H. Tsuji, *Macromol. Biosci.*, 2005, **5**, 569–597.

34 P. De Santis and A. J. Kovacs, *Biopolymers*, 1968, **6**, 299–306.

35 H. Tsuji, *Adv. Drug Deliv. Rev.*, 2016, **107**, 97–135.

36 H. Tsuji and I. Fukui, *Polymer*, 2003, **44**, 2891–2896.

37 M. Cheng, A. B. Attygalle, E. B. Lobkovsky and G. W. Coates, *J. Am. Chem. Soc.*, 1999, **121**, 11583–11584.

38 M. J. Stanford and A. P. Dove, *Chem. Soc. Rev.*, 2010, **39**, 486–494.

39 T. M. Ovitt and G. W. Coates, *J. Am. Chem. Soc.*, 1999, **121**, 4072–4073.

40 J. Coudane, C. Ustariz-Peyret, G. Schwach and M. Vert, *J. Polym. Sci. Part A Polym. Chem.*, 1997, **35**, 1651–1658.

41 C. K. Williams and M. Hillmyer, *Polym. Rev.*, 2008, **48**, 1–10.

42 P. J. Dijkstra, H. Du and J. Feijen, *Polym. Chem.*, 2011, **2**, 520–527.

43 N. Spassky, M. Wisniewski, C. Pluta and A. Le Borgne, *Macromol. Chem. Phys.*, 1996, **197**, 2627–2637.

44 Z. Zhong, P. J. Dijkstra and J. Feijen, *Angew. Chem. Int. Ed.*, 2002, **41**, 4510–4513.

45 N. Nomura, R. Ishii, M. Akakura and K. Aoi, *J. Am. Chem. Soc.*, 2002, **124**, 5938–5939.

46 N. Nomura, R. Ishii, Y. Yamamoto and T. Kondo, *Chem. Eur. J.*, 2007, **13**, 4433–4451.

47 N. Maudoux, T. Roisnel, V. Dorcet, J.-F. Carpentier and Y. Sarazin, *Chem. Eur. J.*, 2014, **20**, 6131–6147.

48 Z. Zhong, P. J. Dijkstra and J. Feijen, *J. Am. Chem. Soc.*, 2003, **125**, 12291–11298.

49 M. O. Miranda, Y. DePorre, H. Vazquez-Lima, M. A. Johnson, D. J. Marell, C. J. Cramer and W. B. Tolman, *Inorg. Chem.*, 2013, **52**, 13692–13701.

50 P. Hormnirun, E. L. Marshall, V. C. Gibson, R. I. Pugh and A. J. P. White, *Proc. Natl. Acad. Sci.*, 2006, **103**, 15343–15348.

51 D. A. Atwood, *Coord. Chem. Rev.*, 1997, **165**, 267–296.

52 K. Press, A. Cohen, I. Goldberg, V. Venditto, M. Mazzeo and M. Kol, *Angew. Chem. Int. Ed.*, 2011, **50**, 3529–3532.

53 J. Fujisaki, K. Matsumoto, K. Matsumoto and T. Katsuki, *J. Am. Chem. Soc.*, 2011, **133**, 56–61.

54 P. Hormnirun, E. L. Marshall, V. C. Gibson, A. J. P. White and D. J. Williams, *J. Am. Chem. Soc.*, 2004, 2688–2689.

55 K. Press, I. Goldberg and M. Kol, *Angew. Chem. Int. Ed.*, 2015, **54**, 14858–14861.

56 A. Pilone, K. Press, I. Goldberg, M. Kol, M. Mazzeo and M. Lamberti, *J. Am. Chem. Soc.*, 2014, **136**, 2940–2943.

57 P. McKeown, M. G. Davidson, G. Kociok-Köhn and M. D. Jones, *Chem. Commun.*, 2016, **52**, 10431–10434.

58 A. F. Douglas, B. O. Patrick and P. Mehrkhodavandi, *Angew. Chem. Int. Ed.*, 2008, **47**, 2290–2293.

59 I. Peckermann, A. Kapelski, T. P. Spaniol and J. Okuda, *Inorg. Chem.*, 2009, **48**, 5526–5534.

60 J.-C. Buffet, J. Okuda and P. L. Arnold, *Inorg. Chem.*, 2010, **49**, 419–426.

61 D. C. Aluthge, B. O. Patrick and P. Mehrkhodavandi, *Chem. Commun.*, 2013, **49**, 4295–4297.

62 D. C. Aluthge, E. X. Yan, J. M. Ahn and P. Mehrkhodavandi, *Inorg. Chem.*, 2014, **53**, 6828–6836.

63 D. C. Aluthge, J. M. Ahn and P. Mehrkhodavandi, *Chem. Sci.*, 2015, **6**, 5284–5292.

64 A. B. Kremer, R. J. Andrews, M. J. Milner, X. R. Zhang, T. Ebrahimi, B. O. Patrick, P. L. Diaconescu and P. Mehrkhodavandi, *Inorg. Chem.*, 2017, **56**, 1375–1385.

65 A. Pietrangelo, M. A. Hillmyer and W. B. Tolman, *Chem. Commun.* , 2009, 2736–2737.

66 A. Pietrangelo, S. C. Knight, A. K. Gupta, L. J. Yao, M. A. Hillmyer and W. B. Tolman, *J. Am. Chem. Soc.*, 2010, **132**, 11649–11657.

67 M. Normand, E. Kirillov, T. Roisnel and J.-F. Carpentier, *Organometallics*, 2012, **31**, 1448–1457.

68 M. Normand, V. Dorcet, E. Kirillov and J.-F. Carpentier, *Organometallics*, 2013, **32**, 1694–1709.

69 S. Ghosh, R. R. Gowda, R. Jagan, D. Chakraborty, A. Garcés, A. Lara-Sánchez, A. M. Rodríguez, J. P. Lowea, P. L. Diaconescu and C. M. Thomas, *Dalton Trans.*, 2015, **44**,

10410–10422.

70 C. K. Williams, L. E. Breyfogle, S. K. Choi, W. Nam, V. G. Young, M. A. Hillmyer and W. B. Tolman, *J. Am. Chem. Soc.*, 2003, **125**, 11350–11359.

71 B. M. Chamberlain, M. Cheng, D. R. Moore, T. M. Ovitt, E. B. Lobkovsky and G. W. Coates, *J. Am. Chem. Soc.*, 2001, **123**, 3229–3238.

72 M. H. Chisholm and N. W. Eilerts, *Chem. Commun.*, 1996, 853–854.

73 W. Schlenk and W. Schlenk, *Eur. J. Inorg. Chem.*, 1929, **62**, 920–924.

74 M. H. Chisholm, N. W. Eilerts, J. C. Huffman, S. S. Iyer, M. Pacold and K. Phomphrai, *J. Am. Chem. Soc.*, 2000, **122**, 11845–11854.

75 V. Poirier, T. Roisnel, J.-F. Carpentier, Y. Sarazin, C. Giacovazzo, A. Guagliardi, A. G. G. Moliterni, G. Polidori and R. Spagna, *Dalton Trans.*, 2009, **32**, 9820–9827.

76 A. Thevenon, C. Romain, M. S. Bennington, A. J. P. White, H. J. Davidson, S. Brooker and C. K. Williams, *Angew. Chem. Int. Ed.*, 2016, **55**, 8680–8685.

77 S. M. Guillaume, E. Kirillov, Y. Sarazin and J.-F. Carpentier, *Chem. Eur. J.*, 2015, **21**, 7988–8003.

78 L. H. Peeck, S. Leuthäusser and H. Plenio, *Organometallics*, 2010, **29**, 4339–4345.

79 E. M. Broderick, N. Guo, C. S. Vogel, C. Xu, J. Sutter, J. T. Miller, K. Meyer, P. Mehrkhodavandi and P. L. Diaconescu, *J. Am. Chem. Soc.*, 2011, **133**, 9278–9281.

80 X. Wang, A. Thevenon, J. L. Brosmer, I. Yu, S. I. Khan, P. Mehrkhodavandi and P. L. Diaconescu, *J. Am. Chem. Soc.*, 2014, **136**, 11264–11267.

81 C. Romain and C. K. Williams, *Angew. Chemie Int. Ed.*, 2014, **53**, 1607–1610.

82 M. Chen, B. Yang and C. Chen, *Angew. Chemie Int. Ed.*, 2015, **54**, 15520–15524.

83 C. K. A. Gregson, V. C. Gibson, N. J. Long, E. L. Marshall, P. J. Oxford and A. J. P. White, *J. Am. Chem. Soc.*, 2006, **128**, 7410–7411.

84 A. B. Biernesser, B. Li and J. A. Byers, *J. Am. Chem. Soc.*, 2013, **135**, 16553–16560.

85 C. M. Manna, A. Kaur, L. M. Yablon, F. Haeffner, B. Li and J. A. Byers, *J. Am. Chem. Soc.*, 2015, **137**, 14232–14235.

86 A. B. Biernesser, K. R. Delle Chiaie, J. B. Curley and J. A. Byers, *Angew. Chem. Int. Ed.*, 2016, **55**, 5251–5254.

87 K. R. Delle Chiaie, A. B. Biernesser, M. A. Ortuño, B. Dereli, D. A. Iovan, M. J. T. Wilding, B. Li, C. J. Cramer and J. A. Byers, *Dalton Trans.*, 2017, **46**, 12971–12980.

88 A. Sauer, J.-C. Buffet, T. P. Spaniol, H. Nagae, K. Mashima and J. Okuda, *ChemCatChem*, 2013, **5**, 1088–1091.

89 X. Wang, J. L. Brosmer, A. Thevenon and P. L. Diaconescu, *Organometallics*, 2015, **34**, 4700–4706.

90 H. Staudinger and J. Meyer, *Helv. Chim. Acta*, 1919, **2**, 635–646.

91 P. Potin and R. Dejaeger, *Eur. Polym. J.*, 1991, **27**, 341–348.

92 C. T. Laurencin, H. J. Koh, T. X. Neenan, H. R. Allcock and R. Langer, *J. Biomed. Mater. Res.*, 1987, **21**, 1231–1246.

93 H. R. Allcock and N. L. Morozowich, *Polym. Chem.*, 2012, **3**, 578–590.

94 N. L. Morozowich, J. L. Nichol, R. J. Mondschein and H. R. Allcock, *Polym. Chem.*, 2012, **3**, 778–786.

95 T.-P.-A. Cao, S. Labouille, A. Auffrant, Y. Jean, X. F. Le Goff and P. Le Floch, *Dalton Trans.*, 2011, **40**, 10029–10037.

96 C. Bakewell, T.-P.-A. Cao, X. F. Le Goff, N. J. Long, A. Auffrant and C. K. Williams, *Organometallics*, 2013, **32**, 1475–1483.

97 A. V. Kirsanov, *Izv. Akad. Nauk Sssr-Ser. Khim.*, 1950, 426–437.

98 H. Zimmer and G. Singh, *J. Org. Chem.*, 1963, **28**, 483–486.

99 L. Horner and H. Oediger, *Justus Liebigs Ann. Chem.*, 1959, **627**, 142–162.

100 C. Bakewell, A. J. P. White, N. J. Long and C. K. Williams, *Angew. Chem. Int. Ed.*, 2014, **53**, 9226–9230.

Chapter 2

Characterisation Techniques

This chapter describes the characterisation techniques used throughout this thesis and how they are applied for characterisation of compounds and polymers, data collection and data analysis. The techniques discussed are nuclear magnetic spectroscopy (NMR), single crystal X-ray diffraction (SCXRD), mass spectrometry (MS), size exclusion chromatography (SEC) and cyclic voltammetry (CV).

2.1. NMR

Nuclear Magnetic Resonance (NMR) spectroscopy is used for the characterisation of ligands, complexes, initiators and polymers using ^{1}H, ^{31}P and ^{13}C nuclei.

2.1.1. Characterisation of polymers

Throughout this thesis, the conversion of *rac*-lactide (*rac*-LA) is monitored using ^{1}H NMR spectroscopy. For polylactide (PLA) samples, the relative integration of the methine proton in the monomer (5.00 - 5.07 ppm, $CDCl_3$, 400 MHz, 298 K) and polymer (5.10 – 5.24 ppm, same conditions) was selected due to the absence of overlapping peaks (Figure 2.1).

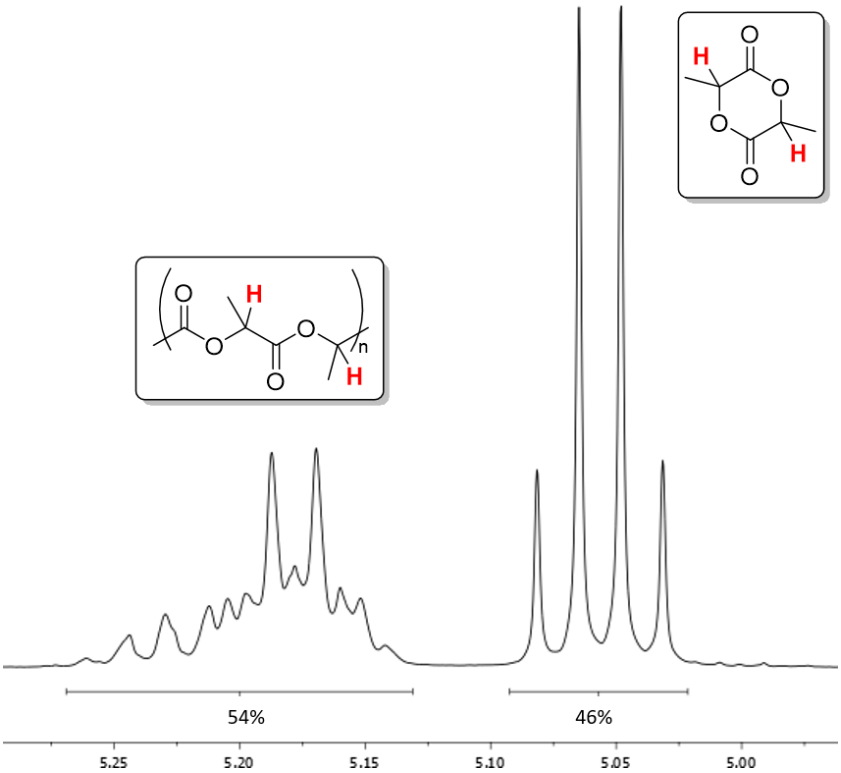

Figure 2.1. ^{1}H NMR spectrum of crude PLA sample. (Conversion = 54%, $CDCl_3$, 400 MHz, 298 K).

PLA tacticity is reported as a probability of enchainment of a diad, P_i = isotactic or P_s = heterotactic. It is generally reported at the tetrad level and there are five tetrads expected in the absence of transesterification. The ^{1}H NMR spectrum of PLA yields five

overlapping quartet signals (Figure 2.2), but using homonuclear decoupled $^1H\{^1H\}$ NMR spectroscopy, five singlet resonances due to the different tetrads are yielded (Figure 2.3). The $^1H\{^1H\}$ spectrum often still shows some overlapping resonances, therefore, all spectra were deconvoluted using the MestReNova software package (fit is assessed by residual error, if < 2%, then the fit is acceptable). From the normalised integrals of each tetrad resonance, P_i was calculated by comparison against values determined using Bernoullian statistics. The average P_i was reported using values for all five tetrads.

Possible Tetrads:

sis **sii** **iis** **iii** **isi**

Dyad (i or s): i ii ii si ii ii si si ii

PLA stereoconfiguration: SS-SS-SS-RR-RR-RR-SS-RR-RR

Tetrad	Probability
sis	$\frac{P_s^2}{2}$
sii	$\frac{P_s P_i}{2}$
iis	$\frac{P_s P_i}{2}$
iii	$P_i^2 + \frac{P_s P_i}{2}$
isi	$\frac{P_s^2 + P_s P_i}{2}$
$P_s + P_i = 1$	

Figure 2.2. Description of the possible dyads and tetrads and how they arise for the ROP of *rac*-LA (left). Tetrad probabilities predicted from Bernoullian statistics (right).

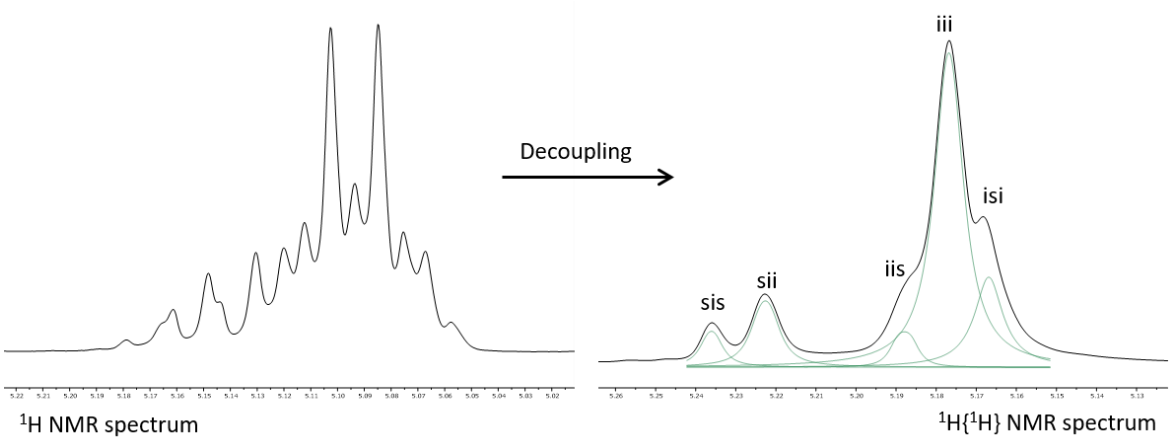

Figure 2.3. Before (^1H - left) and after ($^1H\{^1H\}$ right) decoupling of methine proton to methyl group of PLA, using a sample concentration of ~15 mg mL^{-1} ($CDCl_3$, 400 MHz, 298 K).

The mechanism of stereocontrol can be determined from the relative integrals of the five tetrads. For a enantiomorphic site control mechanism the ratio is [sis]:[sii]:[iis]:[isi] = 1:1:1:2 whereas for chain-end control the ratio is [sii]:[iis]:[isi] = 1:1:1.

Transesterification reactions are side reactions in which the metal initiates exchange of ester groups through reactions with the carbonyl groups of adjacent chains either within the propagating chain or between propagating chains. The presence of transesterification is observed through either an increase in dispersity (using GPC – see Section 2.4), using MALDI-ToF to identify cyclic structures and/or odd number of repeat units (see Section 2.3) or using $^{13}C\{^{1}H\}$ NMR spectroscopy.

In the $^{13}C\{^{1}H\}$ NMR spectrum for PLA ($CDCl_3$), the tetrads for the methine carbon atom occur at 69.0 (iii, iis, sii and sis) and 69.2 ppm (isi).[1] After intermolecular transesterification new resonances are observed at 69.1 and 69.4 ppm, due to the ssi and iss tetrads, respectively (Figure 2.4). Multiple intermolecular transesterification reactions enable observation of a resonance at 69.3 ppm, from the sss tetrad. The three new tetrads can only occur after transesterification; therefore, their presence is indicative of its presence.

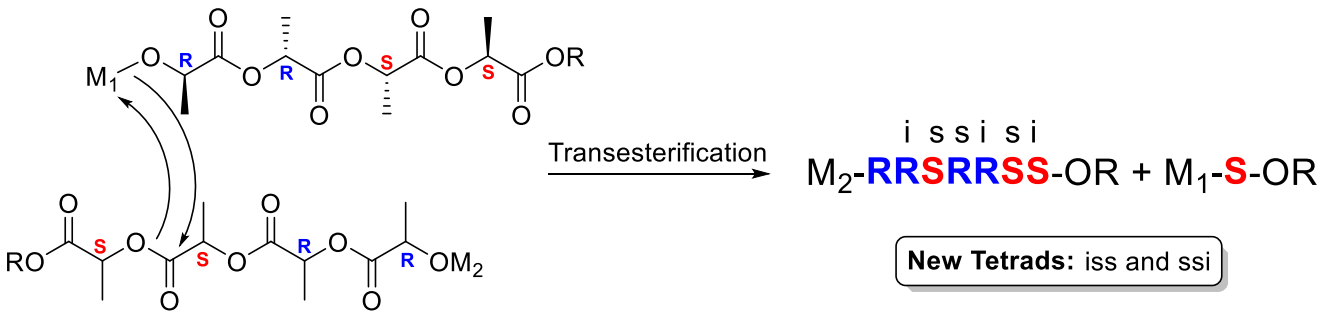

Figure 2.4. New tetrads that occur after transesterification reactions.

2.1.2. Determination of rate constants: k_{obs} and k_p

To compare rates between initiators, two different rate constants can be used: k_{obs} (for polymerisations carried out under a specific set of conditions: loading, solvent and temperature) or k_p (for polymerisations carried out in the same solvent and temperature, independent of monomer or initiator concentration). To determine k_{obs}, pseudo first-order fits to experimental data are applied, often leading to a linear fit under semi-logarithmic conditions, due to a first order in monomer concentration (Equation 2.1).

$$\ln\left(\frac{[LA]_0}{[LA]_t}\right) = k_{obs} \times t$$

Equation 2.1. Integrated and rearranged pseudo first order rate law. *$[LA]_0$ = initial monomer concentration, $[LA]_t$ = monomer concentration at a specific time, k_{obs} = observed rate constant ($k_{obs} = k_p[I]$), t = time.*

By plotting $\ln([LA]_0/[LA]_t)$ against time, a linear fit indicates a first order in [LA] and the gradient is k_{obs} (Figure 2.5). In order to collect the data, aliquots are collected at specific time intervals (t) throughout the polymerisation and each aliquot is analysed using ^{1}H NMR spectroscopy to obtain the % monomer conversion (see Section 2.1.1.). To convert conversion into the lactide concentration at a specific time interval ($[LA]_t$), the initial lactide concentration ($[LA]_0$) must be known, which in this thesis is always 1 M (Equation 2.2).

$$[LA]_t = 1 - \left(\frac{conversion}{100} \times [LA]_0\right)$$

Equation 2.2. Calculation of lactide concentration at a specific time.

To determine k_p, the k_{obs} value is typically obtained over at least four different initiator concentrations, and plots of k_{obs} vs. [I] enable k_p to be determined. Linear fits to the data indicate a first order in [I] and k_p is the gradient. The error of k_{obs} is determined by

carrying out the polymerisation three times, then, using the regression analysis tool on Microsoft Excel.

Conversion (%)	t (secs)	$[LA]_t$ (M)	$\ln([LA]_0/[LA]_t)$
0	0	1	0
25	150	0.75	0.288
42	300	0.58	0.545
65	600	0.35	1.045
78	900	0.22	1.514
85	1200	0.15	1.897

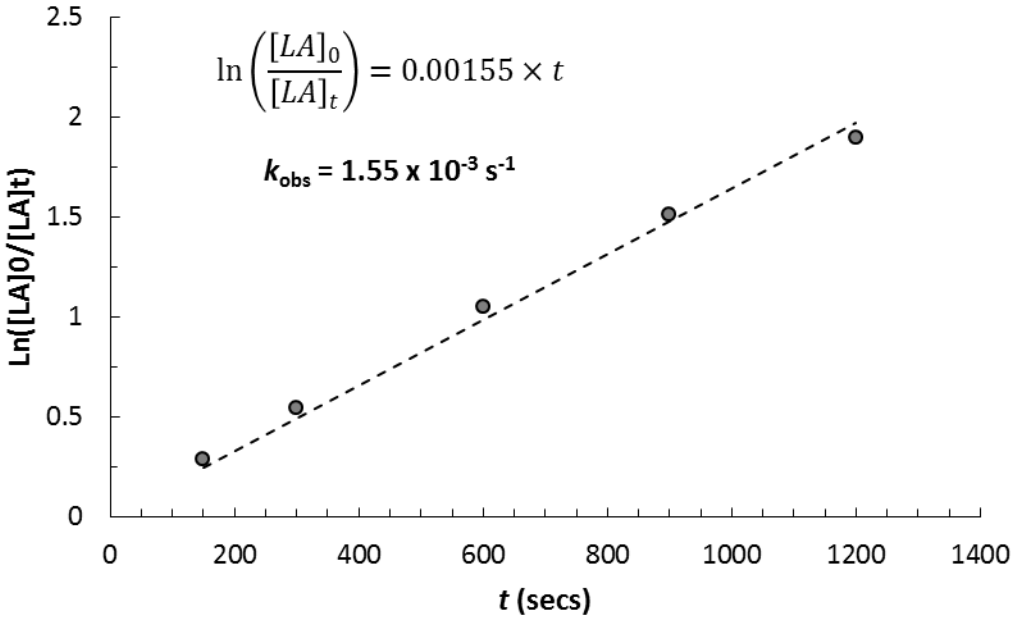

Figure 2.5. Polymerisation data, kinetic plot and determination of k_{obs} for initiator **4.5**. Conditions: [I]:[LA] 1:100, THF, 298 K.

2.1.3. $^{31}P\{^{1}H\}$ NMR

$^{31}P\{^{1}H\}$ NMR spectroscopy is an invaluable characterisation method since ^{31}P nuclei have I = ½ and are ~100% naturally abundant. In this thesis, most ligands and, therefore, complexes contain phosphorus, are characterised using $^{31}P\{^{1}H\}$ NMR spectroscopy. This technique was useful in elucidating structural information and in confirming purity (combined with elemental analysis). During complexation reactions, intermediates were not isolated but reactions could be using $^{31}P\{^{1}H\}$ NMR spectroscopy to confirm the completion of each synthetic step (Figure 2.6).

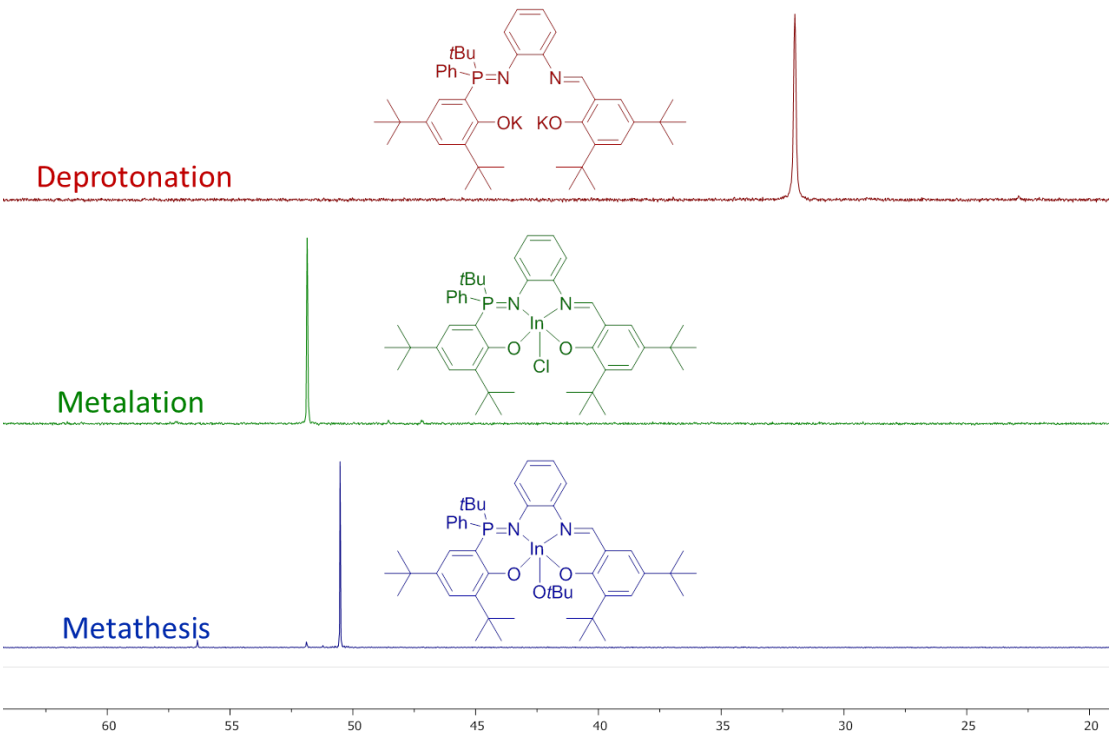

Figure 2.6. Stacked $^{31}P\{^{1}H\}$ NMR spectra (C_6D_6, 400 MHz, 298 K) for the synthesis of initiator **4.8**.

2.1.4. Two-dimensional NMR spectroscopy

Two-dimensional (2D) NMR spectroscopic techniques was used throughout this thesis to provide extra structural data and to assign ligand, complex and initiator spectra. The "through-bond" methods used were COSY, HSQC and HMBC. "Through-space" methods used were NOESY experiments (Table 2.1).

Table 2.1. Comparison of 2D NMR spectroscopic techniques used in this thesis.

	Homonuclear	Heteronuclear	Correlation	Range
COSY	✓		Through-bond	2-4 bonds
HSQC		✓	Through-bond	1 bond
HMBC		✓	Through-bond	2-4 bonds
NOSEY	✓		Through-space	Up to ~ 5 Å

All techniques were used simultaneously for assigning multiple couplings or second order ^{1}H and $^{13}C\{^{1}H\}$ resonances. For example, in assigning the novel un-symmetrical hybrid initiators (e.g. **3.8**), an NOE experiment was used to selectively excite the imine proton, therefore to identify the aromatic phenolate protons adjacent to the imine (Figure 2.7). By then using a COSY NMR experiment, the second aromatic proton was identified. Subsequently, by elimination, the iminophosphorane phenolate protons were identified.

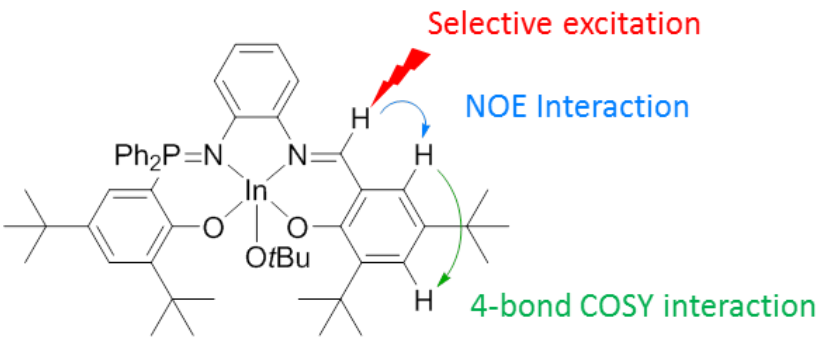

Figure 2.7. Types of 2D experiments used in assigning novel compounds in this thesis.

2.1.5. Diffusion ordered NMR spectroscopy

Diffusion Ordered Spectroscopy (DOSY) can be used to resolve compounds according to hydrodynamic radius. It is based on the measurement of translational diffusion coefficients, which depend on a molecule's shape and size. The technique uses a pulsed magnetic field gradient as a way of spatially labelling the spins of different nuclei, from which, the spatial displacement of these spins can be measured as a function of time. The diffusion profile is obtained by a series of 1D experiments that vary the magnitude of the field gradient (G_z). The rate of molecular diffusion then correlates with the attenuation of the NMR signal as a function of G_z (i.e. faster diffusion gives faster signal attenuation) and depends upon a rage of parameters. The intensity change is defined in Equation 2.3 and rearranged for the purpose of data plotting in Equation 2.4.

$$I = I_0 \exp\left(-D\gamma^2\delta^2G^2\left(\Delta - \frac{\delta}{3}\right)\right)$$

Equation 2.3. Intensity change using molecular diffusion. *I = observed peak intensity, I_0 = reference peak intensity (unattenuated signal intensity), D = diffusion coefficient, γ = gyromagnetic radio of the observed nucleus, δ = length of gradient pulse, G = gradient strength, Δ = diffusion time.*

$$\ln\left(\frac{I}{I_0}\right) = -D\gamma^2\delta^2G^2\left(\Delta - \frac{\delta}{3}\right)$$

Equation 2.4. Rearranged Equation 2.1 for data plotting purposes.

Then, from the Stokes-Einstein equation, it is possible to relate the diffusion coefficient for a particular species to its hydrodynamic radius (r_H) (Equation 2.5).

$$D = \frac{k_B T}{6\pi\eta r_H}$$

Equation 2.5. Stokes-Einstein equation. *D = diffusion coefficient, k_B = Boltzmann constant, T = temperature, η = viscosity of the solution, r_H = hydrodynamic radius.*

Therefore, using DOSY, it is possible to study the nuclearity of a particular species, as well as any relevant aggregation phenomena. One method involves the use of a range of standard compounds of known molecular weight and nuclearity, from which, it is possible to generate a pseudo-calibration of molecular weight against diffusion coefficient.[2] From the diffusion coefficient of a new species it is then possible to estimate its molecular weight and hence, the approximate nuclearity in solution. However, this method is limited by assumptions that the molecular weight will always correlate well with molecular size and that all species behave the same way in solution.

Alternatively, if the hydrodynamic radius for a particular species is known (either theoretically or from a solid-state structure), it is possible to compare the hydrodynamic radius obtained through the Stokes-Einstein equation to the value obtained from its theoretical/solid-state structure and hence determine a compound's size. This method also suffers limitations, for example, from the Stokes-Einstein equation, which treats all particles as completely spherical. However, this method generally works well for a semi-quantitative analysis, and is preferentially used in this thesis.

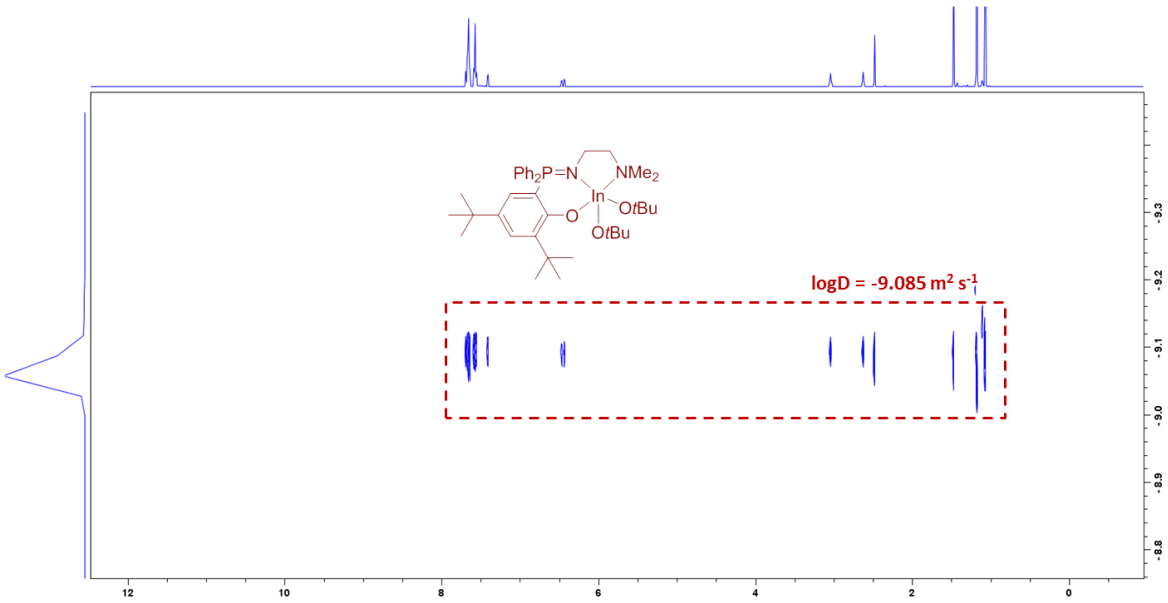

Figure 2.8. ^{1}H DOSY NMR spectrum of indium half-phosphasalen initiator **5.12** in d_8-THF.

Using the diffusion coefficient from DOSY NMR experiments, it is possible to obtain the hydrodynamic radii for a given complex. For example for initiator **5.12** in Figure 2.8:

$$D = 10^{y} \text{ (y = log(D), obtained from DOSY spectrum)}$$

$$D = 10^{-9.085}$$

$$D = 8.22 \times 10^{-10}\ m^2\ s^{-1}$$

The hydrodynamic radius can then be determined using a rearranged format of the Stokes-Einstein equation (Equation 2.3):

$$r_H = \frac{k_B T}{6\pi\eta D} = \frac{1.38 \times 10^{-23}\ m^2\ kg\ s^{-2} K^{-1} \times 298\ K}{6 \times \pi \times 4.80 \times 10^{-4}\ kg\ m^{-1}\ s^{-1} \times 8.22 \times 10^{-10}\ m^2\ s^{-1}}$$

$$r_H = 5.53 \times 10^{-10}\ m$$

$$r_H = 5.53\ \text{Å}$$

It is also possible to estimate the hydrodynamic radius from the X-ray crystallographic data, assuming a spherical shape, and compare this with the value obtained from DOSY

analysis. Using an arranged format of the volume of a sphere and calculating the volume from the crystallographic data, the radius of the solid-state structure of **5.12** can be calculated (Equation 2.6 and 2.7).

$$r = \sqrt[3]{\frac{3V}{4\pi}}$$

Equation 2.6. Rearranged volume of sphere. *V = volume of the sphere, r = radius.*

$$V = \frac{V_{uc} \times PE}{z}$$

Equation 2.7. Molecular volume calculation. *V_{uc} = volume of unit cell, PE = packing efficiency*, z = number of formula units in the unit cell.*

Therefore:

$$r = \sqrt[3]{\frac{3 \times 624.21\ \text{Å}^3}{4\pi}}$$

$$r = 5.30\ \text{Å}$$

In this case, there is close agreement between solution-state (5.53 Å) and solid-state (5.30 Å) values which suggests that the initiator adopts a mononuclear structure in solution because a mononuclear structure is observed in the solid-state.

2.2. Single Crystal X-ray Diffraction

Single crystal X-ray diffraction (SCXRD) eludes information about the internal lattice of a crystalline solid. It provides bond lengths and angles, as well as an accurate description of the molecular structure in the solid state.

* Determined from the PLATON suite of programs.[8]

Monochromatic X-rays are diffracted by solids that possess long-range order. X-rays are used because their wavelength is on the same order of magnitude as the spacing between diffraction planes in the crystal. Upon interaction of incident waves with the sample, the scattered rays will interfere constructively and destructively produce intense peaks (Bragg peak), if Bragg's law is satisfied (Equation 2.8).

$$n\lambda = 2dsin\theta$$

Equation 2.8. Bragg's Law. *n = positive integer, λ = wavelength of incident ray, d = interplanar spacing of the crystal, ϑ = angle between the incident ray and the surface of the crystal.*

These peaks appear as reflection spots in the diffraction pattern and from each reflection, it is possible to obtain information about atomic position and intensity. By acquiring the relative intensities of thousands of unique reflections at multiple crystal orientations, it is possible to determine the distribution of electron density throughout the crystal.

In this thesis, SCXRD was used to determine the solid-state molecular structures of ligands and metal complexes where possible. From the metal complexes obtained, tetracoordinate and pentacoordinate structures were observed, with certain geometries (Figure 2.9).

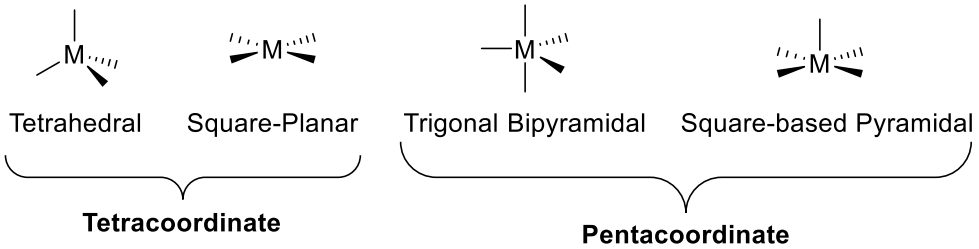

Figure 2.9. Representation of the coordination geometries of tetracoordinate and pentacoordinate metal complexes.

For tetracoordinate complexes, a structural parameter (τ_4) was used to determine whether a particular geometry was tetrahedral or square-planar (Equation 2.9). For a perfect tetrahedral geometry, $\tau_4 = 1$ and for a perfect square-planar geometry, $\tau_4 = 0$. [3]

$$\tau_4 = -0.00709\alpha - 0.00709\beta + 2.55$$

Equation 2.9. Calculation of τ_4. *β > α and are the two largest valence angles at the coordination centre.*

For pentacoordinate complexes, another structural parameter (τ) was used to determine whether a particular geometry was trigonal bipyramidal or square-based pyramidal (Equation 2.10). For a perfect trigonal bipyramidal geometry, $\tau = 1$ and for a perfect square-based pyramidal $\tau = 0$.[4]

$$\tau = \left[\frac{(\beta - \alpha)}{60}\right]$$

Equation 2.10. Calculation of τ. *β > α and are the two largest valence angles at the coordination centre.*

2.3. Mass Spectrometry

Mass spectrometry is used to determine the atomic constitution and charge state of a molecule; therefore, it can be used to elucidate molecular structure, molar mass and chemical purity.

A mass spectrometry generally comprises of an ionisation source to ionise the sample, usually through the formation of a cationic species; a mass analyser that sorts ions based on their mass/charge (*m*/*z*) ratio, usually with electromagnetic fields; and a detector, which measures the abundance of resolved ions in the form of an electronically converted digital output.

2.3.1 Matrix assisted laser desorption/ionisation

Matrix assisted laser desorption/ionisation time of flight (MALDI-ToF) analysis is a soft ionisation technique that is useful for the analysis of large molecules such as polymers. MALDI samples are prepared by uniform mixing of a sample into a matrix excess. Then, a laser is applied onto the sample, which causes sample vaporisation. For polymer samples, the mass spectrum will display an array of peaks corresponding to a polymer chain with a particular mass (Figure 2.10). The difference between each peak within a particular series should be equivalent of the mass of the polymer repeat unit (e.g. 144 for PLA).

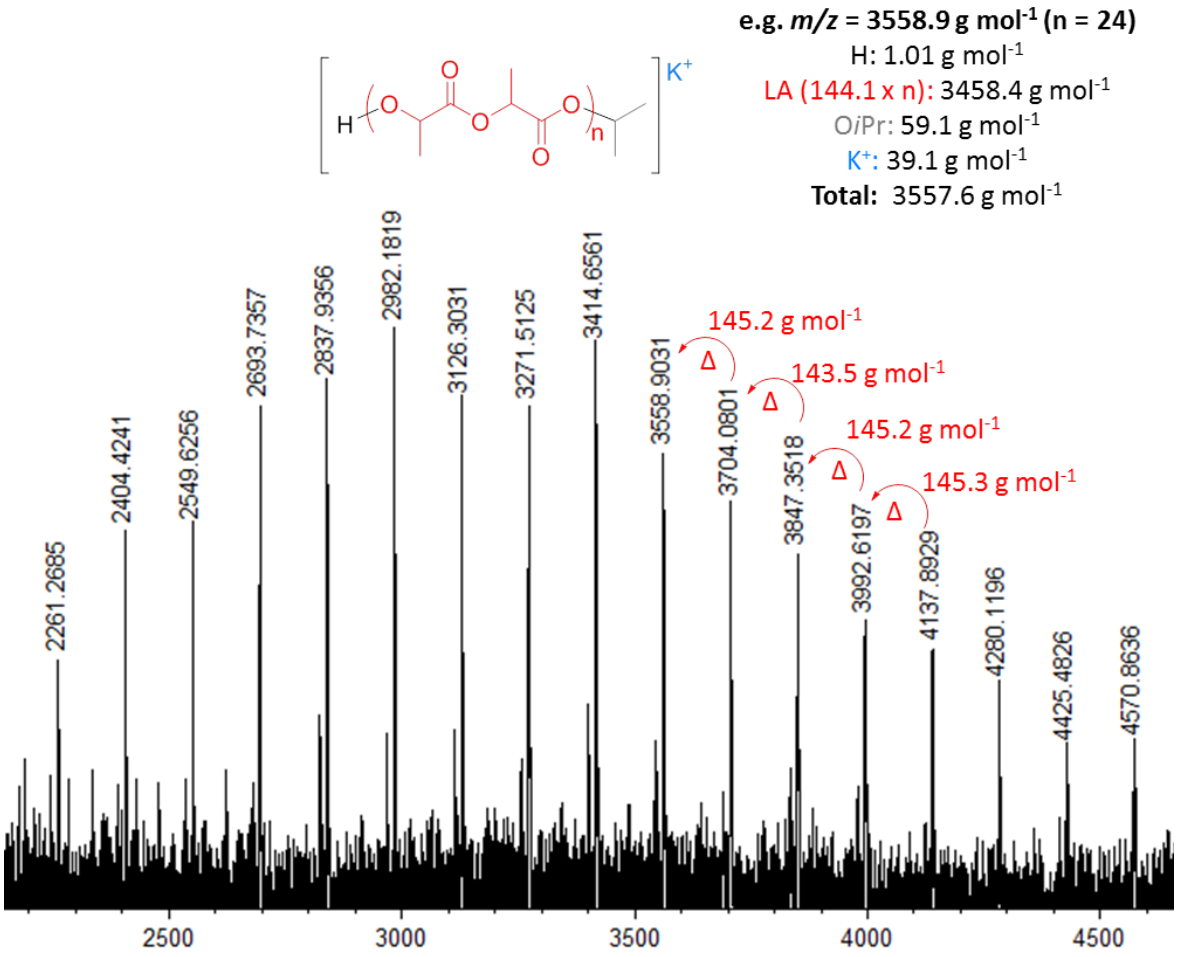

Figure 2.10. MALDI-ToF spectrum of a PLA sample.

For a typical linear polymer chain, the series will correspond to the repeat unit, two end groups (the alkoxide initiating group and H) and the cation (Na^+ or K^+). For polymers with different initiating groups or in the presence of transesterification, additional series will be observed. For example during an intramolecular transesterification reaction, cyclic species are produced, yielding a series corresponding to a polymer and cation but with no apparent end-groups.

2.4. Size Exclusion Chromatography

Size exclusion chromatography (SEC) is a technique that separates larger molecules based on size. It is useful in polymer chemistry as a way of determining molecular weights (M_n or M_w) and dispersity ($Đ = M_w/M_n$). From the M_n, the degree of polymerisation can be obtained, which is important in determining the polymerisation mechanism. The step-growth polymerisation mechanism (present in the condensation of lactic acid route to PLA) requires high conversions to reach high M_n values, whereas the chain-growth polymerisation mechanism (present in the ROP of lactide) observes a linear increase in M_n with conversion.

SEC columns are filled with a porous medium, which in this thesis, comprises a highly cross-linked polystyrene (PS)-divinylbenzene copolymer matrix. When dissolved, molecules of various sizes enter the column; smaller species will penetrate further into pores, whilst larger molecules will flow quickly with minimal interactions, as they are unable to enter the pores. Overall, larger molecules elute from the column first, followed by progressively smaller molecules, therefore, sorting the molecules based on hydrodynamic volume (Figure 2.11). In this thesis, SEC is used for organic polymers, therefore using a hydrophobic column and a non-aqueous mobile phase (THF).

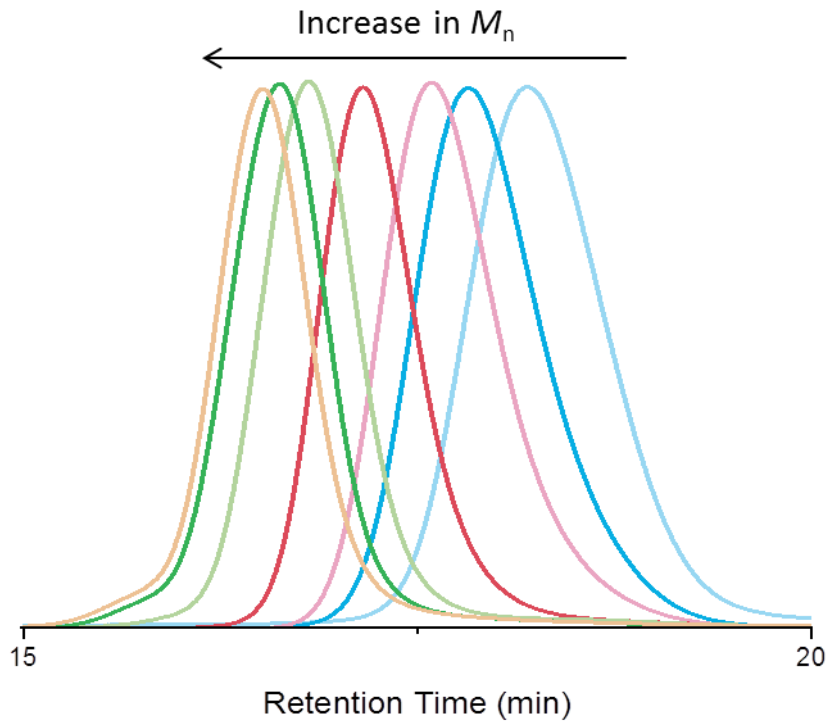

Figure 2.11. GPC graph demonstrating decrease in M_n with increased retention time.

The retention time on the column for the different sized molecules directly correlates to hydrodynamic radius, therefore it is possible to calibrate against a known standard in order to obtain molecular weight information. Ideally, the polymer should interact with the solvent and behave in the same manner as the standard. In this thesis, polylactide samples are measured against PS standards with a correction factor of 0.58 applied or using triple detection (multi-angle laser light scattering) to determine absolute M_n.[5]

Light scattering detectors operate by irradiating a sample, typically using a laser beam and collecting the resultant scattered light. The intensity of scattered light relates to its molecular weight. It is vital that the refractive index increment (dn/dc) is known; it is a measure of the degree by which the refractive index of a solution varies as a function of solute concentration. For PLA in THF, the dn/dc is 0.042 mL g^{-1}.[6] In this thesis, light scattering detection was used as it eliminates the use of standards, as absolute M_n values are determined.

2.5. Cyclic Voltammetry

Voltammetry is a type of electroanalytical method that investigates the half-cell reactivity of an analyte. It is the study of current as a function of applied potential. Cyclic voltammetry (CV) is a particular type of potentiodynamic electrochemical measurement, which determines the reversibility of a redox event, therefore eluding information about redox potentials.[7]

A cyclic voltammogram analyses the change in current as the potential is increased and decreased linearly over a set range. The oxidation event is indicated by an increase in aniodic current, and conversely, a decrease in anionic current for the reduction event. This achieves the characteristic line shape observed in Figure 2.12. The potentials are referenced to a ferrocene Fe^{2+}/Fe^{3+} redox couple, which in this thesis, is internally referenced to a decamethyl ferrocene Fe^{2+}/Fe^{3+} redox couple.

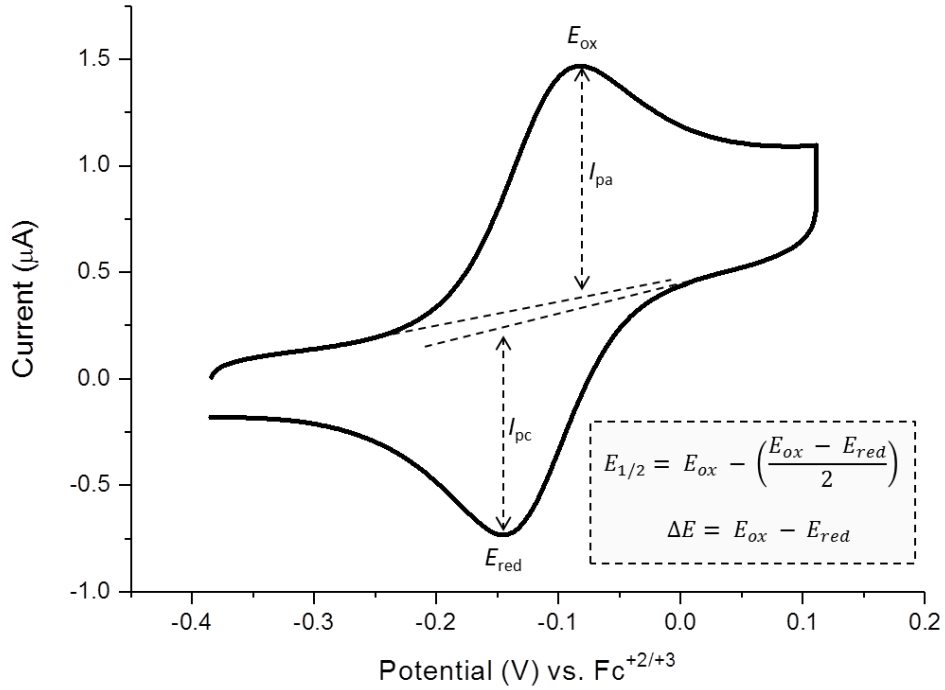

Figure 2.12. Example of a cyclic voltammogram, referenced to ferrocene, and the calculation of $E_{1/2}$ and ΔE.

The half-cell potential ($E_{1/2}$) is the mid-point between the oxidation (E_{ox}) and reduction (E_{red}) potentials and eludes information about the energy required to oxidise a molecule. The difference between the oxidation and reduction potentials (ΔE) indicates the number of electrons involved in the redox-event as well as its reversibility. In this thesis, these values are used to discuss stability, reversibility and indicate which chemical oxidants and reductants that would be suitable.

2.6. References

1 M. Bero, J. Kasperczyk and Z. J. Jedlinski, *Die Makromol. Chemie*, 1990, **191**, 2287–2296.

2 J. A. Garden, P. K. Saini and C. K. Williams, *J. Am. Chem. Soc.*, 2015, **137**, 15078–15081.

3 L. Yang, D. R. Powell and R. P. Houser, *Dalton Trans.*, 2007, 955–964.

4 A. W. Addison, T. N. Rao, J. Reedijk, J. van Rijn and G. C. Verschoor, *J. Chem. Soc., Dalton Trans.*, 1984, 1349–1356.

5 J. Baran, A. Duda, A. Kowalski, R. Szymanski and S. Penczek, *Macromol. Symp.*, 1997, **123**, 93–101.

6 J. R. Dorgan, J. Janzen, D. M. Knauss, S. B. Hait, B. R. Limoges and M. H. Hutchinson, *J. Polym. Sci. Part B Polym. Phys.*, 2005, **43**, 3100–3111.

7 A. J. Bard and L. Y. Faulkner, *Electrochemical Methods*, Wiley, 2nd edn., 2004.

8 A. L. Spek, *PLATON, A Multipurpose Crystallographic Tool*, 2009.

Chapter 3

A Hybrid Salen/Phosphasalen Ligand: Coordination Chemistry with Group 13 Metals and Activity in ROP of *rac*-lactide

In this chapter, the synthesis of a novel hybrid salen/phosphasalen ligand and its coordination to aluminium and indium is discussed. The aim was to combine the excellent rates of indium phosphasalen initiators with the high isoselectivites of aluminium salen initiators to create a new class of highly active and isoselective initiators. This new class of ligand was compared to its salen and phosphasalen derivatives in the solution state (multinuclear and DOSY NMR spectroscopy), solid state (X-ray diffraction) and tested in the ring-opening polymerisation of rac-lactide.

3.1. Introduction

Group 13 metal complexes, most notably aluminium and indium, are a widely studied class of initiators for the ROP of *rac*-LA. The salen ligand when coordinated to aluminium can reach excellent degrees of isoselectivity (P_i > 0.98) but only with moderate rates, and typically requiring high temperatures (< 353 K). Indium salen initiators show improved rates and operate efficiently at 298 K, but the P_i values are modest (P_i > 0.77, 298 K).[1–9]

The phosphasalen ligand, as discussed earlier, has enabled initiators demonstrating excellent rates and high P_i values, when coordinated to yttrium and lutetium (P_i = 0.81–0.84, 298 K).[10,11] Recently, our group reported the first indium phosphasalen initiator, which yielded higher rates over other indium systems and a marked increase in P_i (Figure 3.1). Both initiators (**A** and **B**) induced high levels of stereocontrol (P_i = 0.85-0.87, 298 K) and analysis of the stereocontrol mechanism indicated chain-end control (CEC) rather than enantiomorphic site control (ESC). Low temperature polymerisations, with **A**, yielded PLA with P_i of 0.92 (258 K) and a T_m of 179 ^oC, confirming the formation of stereo-block PLA. It was clear that the bulky *ortho*-substituents mediated stereocontrol, by acting as both steric protection and direction of the monomer to the metal centre. A feature also observed in aluminium salen initiators.[9]

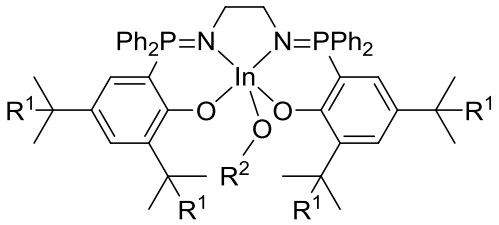

A: R^1 = Ph, R^2 = Et
B: R^1 = Me, R^2 = *t*Bu

Figure 3.1. Indium phosphasalen initiators.[12]

Unsymmetrical Schiff base initiators can be arranged into two key groups: one where their lack of symmetry arises from differing steric bulk on the two sides of the ligand and one where they contain different imine/amine moieties, e.g. salalen ligands.[13] The latter is most widely reported for Group 13 initiators.[14–17] In an example by Kol and co-workers, a P_i value of 0.82 (353 K) was observed for a chiral salalen ligand coordinated to aluminium (Figure 3.2, **C**).[14] It also contained unsymmetrical groups on the two sides of the ligand, which aided in increasing isoselectivity. Conversely, increasingly bulky groups or the introduction of larger halides produced heterotactic PLA.

Beyond the Group 13 metals, unsymmetrical ligands whilst coordinated to Group 4 metals, including hafnium and zirconium, have also achieved excellent rates and isoselectivity (**D**, P_i = 0.91, 323 K).[18] The mechanism for stereocontrol was not determined, therefore rationalisation of the high stereocontrol was not discussed, but symmetrical ligands gave much lower isoselectivites (P_i = 0.50-0.64), compared to the unsymmetrical ligands (P_i = 0.76-0.91) across a range of substituents.

The use of unsymmetrical ligands is not limited to the ROP of LA. A report by Lu and co-workers utilised a chiral-unsymmetrical salen ligand to catalyse the asymmetric alternating copolymerisation of CO_2 and *meso*-epoxides (**E**, Figure 3.2).[19] They obtained highly isotactic poly(cyclohexene carbonate)s from a *meso*-cyclohexane oxide starting material, with up to 98:2, RR:SS enantiomeric bias. Reducing the steric bulk of the adamantyl group to a cumyl (CMe_2Ph) or *t*Bu group gave a reduction in the RR:SS ratio.

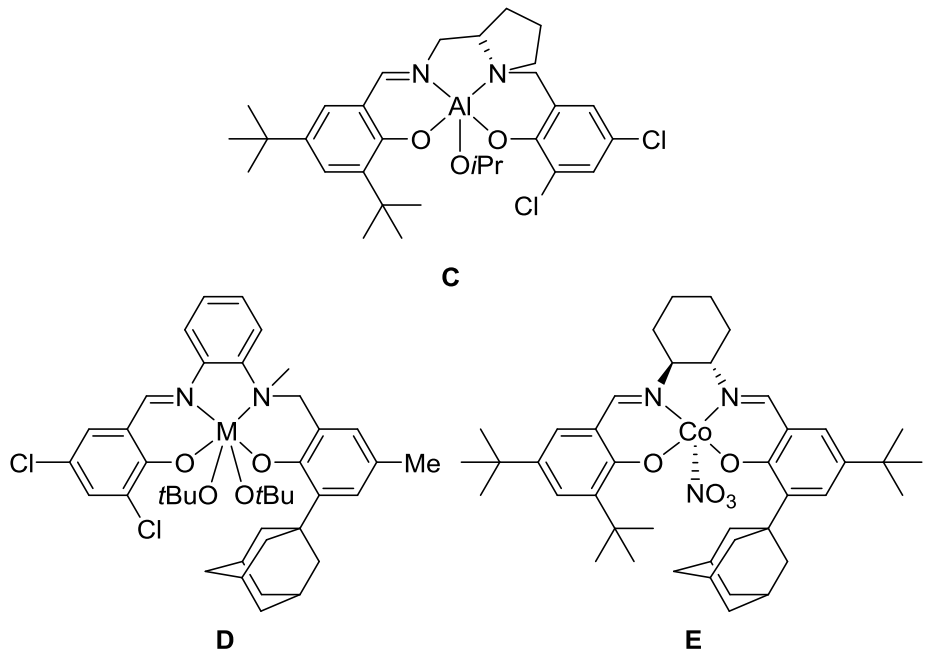

Figure 3.2. Other unsymmetrical initiators (M = Zr and Hf).[14,19]

It is well known from the literature that the choice of metal is crucial for rate and isoselectivity but that the ligand has great control over the characteristics of the initiating ability. The phosphasalen ligand, to date, has not been modified to be unsymmetrical, in terms of steric bulk or a mixture of donating groups.[10–12] The ultimate goal is to develop initiators showing the high isotacticity control displayed by symmetrical non-chiral aluminium initiators and combine this with the fast rates of indium initiators.

3.1.1. Aims

To investigate the modification of the phosphasalen ligand and target excellent rate and isoselectivity, a mixed salen/phosphasalen ligand is proposed. The generic structure of this type of ligand class is illustrated in Figure 3.3. Similar to successful salen and phosphasalen initiators, *tert*-butyl groups are maintained at the *ortho*- and *para*-phenolate substituents to prevent aggregation and aid solubility. The new ligand is

targeted for coordination to both aluminium and indium to understand its effect on rate and isoselectivity.

The synthesis of unsymmetrical salen ligands has been previously achieved by sequential incorporation of phenolate groups by two separate imine-bond formation steps. Two potential synthetic routes are envisaged to the target ligand; either construction of an iminophosphorane bond or an imine bond (Figure 3.3). Formation of the imine bond requires the new intermediate, **H** and commercially available aldehyde, **I**. Iminophosphorane bonds are typically synthesised by a modified Kirsanov reaction (See Section 1.4), where the necessary phosphinophenol (for example, **F**), is reacted with an equivalent of bromine, to form an *in situ* phosphonium bromide, which is directly reacted with a diamine, in the presence of base, to form the phosphasalen ligand. In these reactions, all free amine moieties are reactive; therefore, isolation of product **H** is foreseen to be difficult.

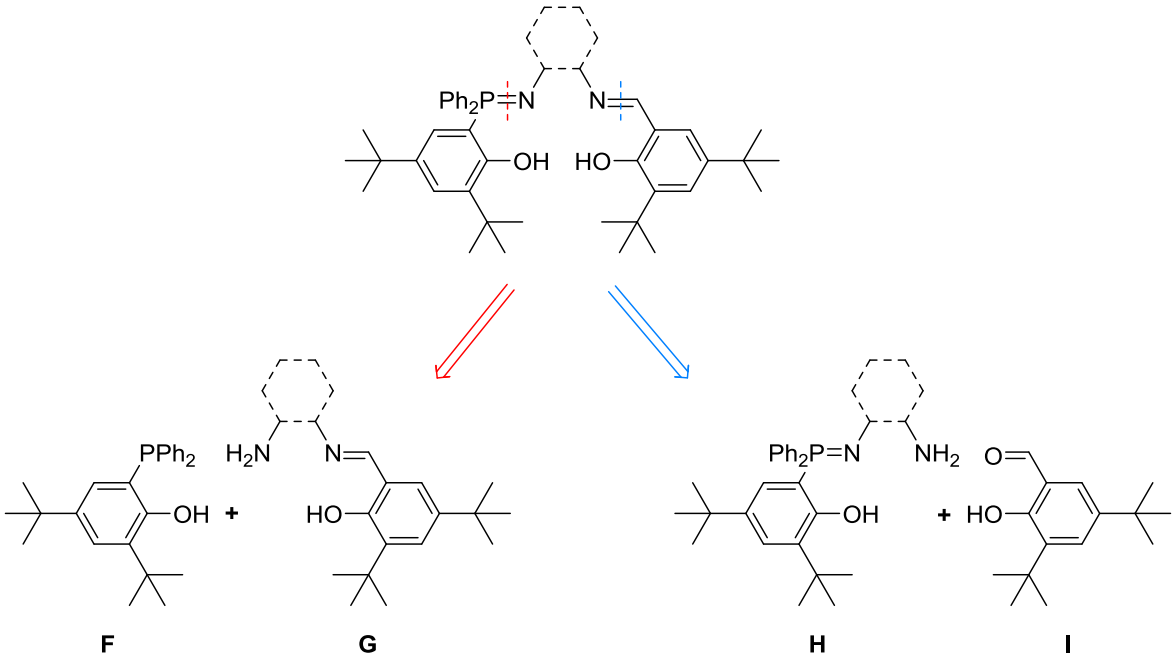

Figure 3.3. Proposed hybrid ligand structure and potential synthetic routes.

The iminophosphorane route requires the phosphinophenol, **F**, which is a known intermediate, and a half-salen species, **G**.[10] The free amine group, present in **G**, is essential for the Kirsanov reaction to form the iminophosphorane bond. The synthesis of asymmetric salen ligands also utilises similar half-salens are intermediates, exploiting two protecting group routes:

1. Alternating protection and deprotection of amine functionalities, to introduce different substituents in separate steps, without risk of forming the symmetrical salen (using Boc and Fmoc groups).[13,19]
2. HCl protection of one amine group of a diamine, which allows functionalisation of the unprotected amine before deprotonation and functionalisation of the originally protected amine.[20–23]

These two synthetic routes are successful because the amine moieties are generated and reacted *in situ*, sequentially forming the second imine bond. Nonetheless, both routes suffer from significant rearrangement reactions to form the diamine and symmetric salen ligand, due to the susceptibility of the imine bond to hydrolysis. This reactivity is most prevalent and widely studied with cyclohexyl diamine backbones. Further investigation revealed that a half-salen intermediate was, however, easily isolated by using a phenylene diamine backbone instead.[24]

Thus, returning to the two potential routes to the target hybrid phosphasalen/salen ligand. It was proposed to focus primarily on the synthesis from precursors **F** and **G**, and to use a phenylene diamine backbone.

3.2. Ligand Synthesis

The synthesis of hybrid ligand, **3.2**, started from the condensation of *o*-phenylenediamine and half an equivalent of 3,5-di-*tert*-butyl-2-hydroxybenzaldehyde to yield 2-((2-aminophenylimino)methyl)-4,6-di-tert-butylphenol) in a 35% yield.[24] The reaction was carried out using a minimal amount of dry ethanol as solvent, which led to the precipitation of the product after 18 hours; low yields can be attributed to the partial solubility of the product in methanol. The preferential formation of the half-salen, over the full salen, can be attributed to the deactivation of the amine substituent after the first imine bond formation. Furthermore, use of the correct stoichiometry and the precipitation of the intermediate half-salen facilitated in the isolation of the pure product.

Synthesis of the phosphinophenol proceeded through known routes.[10] Firstly, bromination of 2,4-di-*tert*-butylphenol, using *N*-bromosuccinamide (NBS), followed by a phosphorylation reaction with *n*-butyllithium and, then, addition of chlorodiphenylphosphine. Next, 2,4-di-*tert*-butyl-6-phosphinophenol was reacted with an equivalent of bromine, followed by addition of an equivalent 2-((2-aminophenylimino)methyl)-4,6-di-tert-butylphenol),) and using 1,4-diazabicyclo[2.2.2]octane (DABCO) as a base in the modified Kirsanov reaction. The ligand, **3.2**, was isolated as a yellow solid after precipitation from *n*-hexane, in a 54% yield (Scheme 3.1).[10]

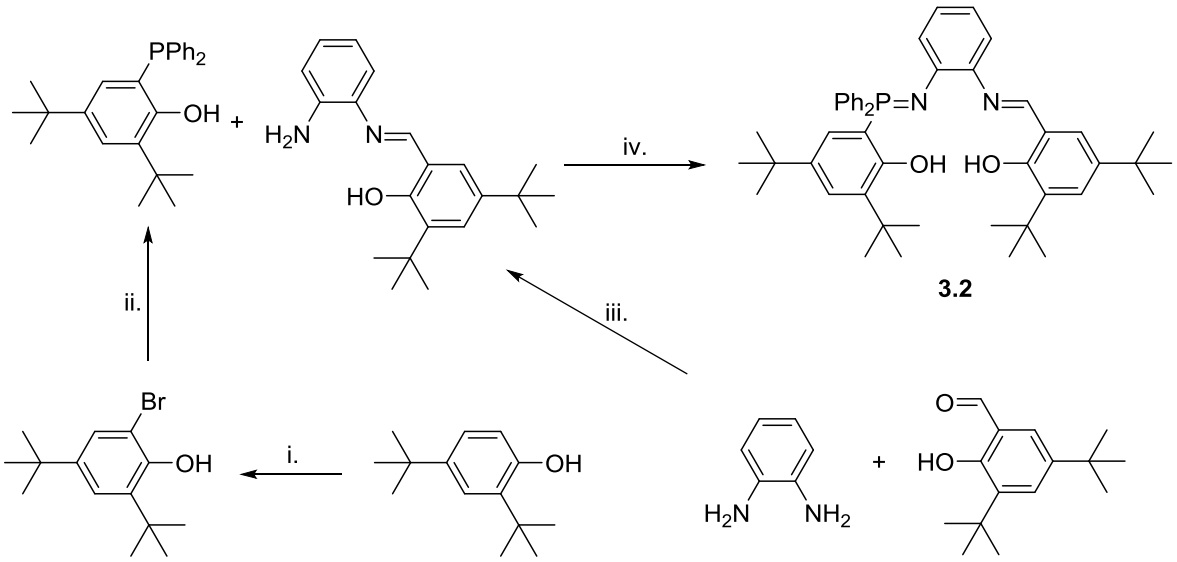

Scheme 3.1. Synthetic route to hybrid ligand, **3.2**. Reagents and conditions: i. NBS (1 equiv.), MeCN; ii. (a) *n*-Butyllithium (2.1 equiv.), Et_2O, 195 K, (b) Chlorodiphenylphospine (1 equiv.), 195 K; iii. EtOH; iv. (a) Br_2 (1 equiv.), DCM, 195 K, (b) DABCO (1 equiv.) 195 K.

Kirsanov reactions typically yield the phosphonium bromide salt product (**I**) which shows chemical shifts of between 40-45 ppm in the $^{31}P\{^1H\}$ NMR spectrum (Figure 3.4). The hybrid ligand, **3.2**, showed a $^{31}P\{^1H\}$ NMR signal at 20.7 ppm (C_6D_6). It is known from previous $^{31}P\{^1H\}$ NMR analysis of deprotonated phosphasalen ligands, that the observed chemical shift resonances lie between 15-20 ppm.[10] Therefore, it would imply that the species achieved after the attempted synthesis of the hybrid ligand was not a phosphonium bromide salt, but a deprotonated ligand, **3.2**. Using elemental analysis, this was confirmed.

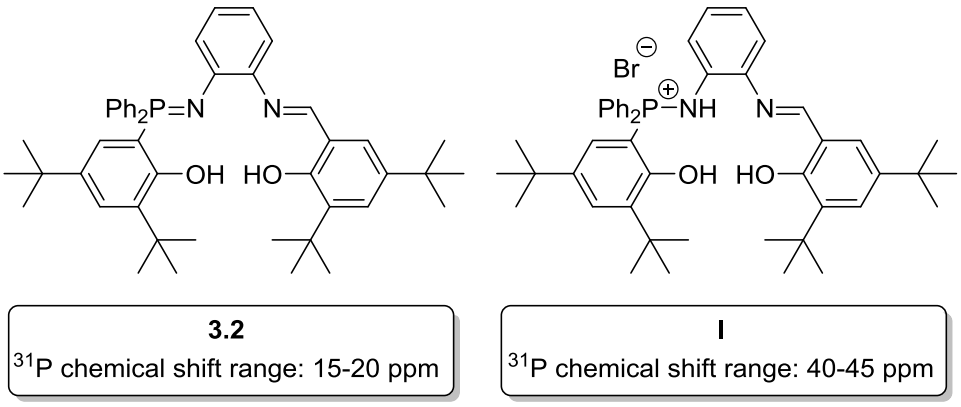

Figure 3.4. Potential products from the Kirsanov reaction and their respective $^{31}P\{^1H\}$ chemical shift resonances.

The analogous salen ligand, **3.1**, was synthesised according to previously reported methods *via* a stoichiometric reaction between *o*-phenylenediamine and 3,5-di-*tert*-butyl-2-hydroxybenzaldehyde and was isolated in 90% yield.[25] The analogous phosphasalen ligand, **3.3**, was synthesised by a Kirsanov reaction between 2,4-di-*tert*-butyl-6-phosphinophenol and *o*-phenylenediamine using DABCO as the base. The phosphonium bromide salt was initially isolated and was further purified, to remove residual DABCO salts and to neutralise the ligand, by column chromatography (alumina, DCM:EtOH 40:1). The pure product was collected in 39% yield. This purification was unfortunately unsuited to the hybrid ligand due to the propensity to hydrolysis of imine bonds during column chromatography. All ligands were fully characterised using multinuclear NMR spectroscopy and their purity was confirmed by elemental analysis.

3.3. Initiator Synthesis

3.3.1. Aluminium Initiators

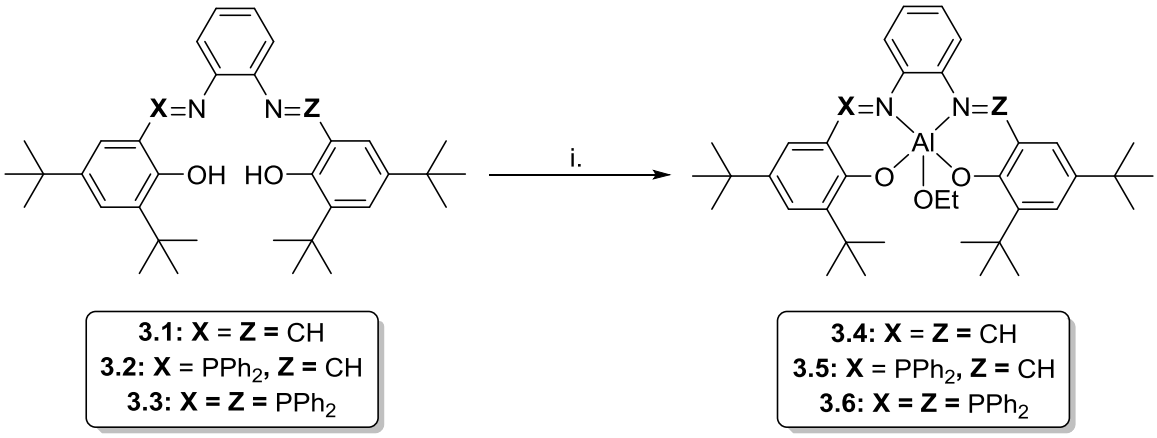

Scheme 3.2. Synthesis of initiators **3.4**-**3.6**. Conditions: i. (a) $AlEt_2Cl$ (1 equiv.), THF, 298 K, (b) KOEt (1 equiv.) 298 K.

Initiators **3.4**-**3.6** were synthesised from the corresponding salen, hybrid and phosphasalen ligands respectively. The proteo-ligands were each reacted with an equivalent of diethylaluminium chloride ($AlEt_2Cl$) in THF, to form *in situ* the aluminium chloride complexes. Next, potassium ethoxide (KOEt) was added to the solution and the aluminium ethoxide initiators were isolated by centrifugation to remove the KCl salt and recrystallisation from THF/*n*-hexane at 243 K. (Scheme 3.2). For initiator **3.4**, the reaction progress was monitored by ^{1}H NMR spectroscopy: after addition of $AlEt_2Cl$; the resonance corresponding to the phenol protons, at 13.5 ppm, disappeared. After addition of KOEt, new quartet and triplet resonances were observed at 3.34 and 0.64 ppm respectively, which were found to correlate in a COSY NMR experiment. Furthermore, the ethoxide signals were clearly shifted from those of potassium ethoxide.

The formation of initiators **3.5** and **3.6** were monitored by $^{31}P\{^{1}H\}$ NMR spectroscopy. The addition of $AlEt_2Cl$ to phosphasalen ligand, **3.3**, resulted in a change in the chemical shift

from 17.7 ppm to 32.2 ppm. Minor impurities at this step were not problematic to the synthesis of the final product. After addition of KOEt, a singlet at 29.2 ppm was observed, corresponding to the alkoxide. The ^{1}H NMR spectrum of **3.6** also confirmed by presence of the ethoxide co-ligand (3.62 and 0.61 ppm) and the pure product, **3.6**, was isolated, by recrystallisation to remove any impurities, in 26% yield.

The hybrid ligand, **3.2**, displayed a resonance of 20.7 ppm in the ^{31}P{^{1}H} NMR spectrum, which shifted to the major peak of 31.8 ppm after addition of $AlEt_2Cl$. Next, KOEt was added and a single, sharp peak at 31.6 ppm was observed. Quartet and triplet resonances were observed at 3.45 ppm and 0.69 ppm, respectively, in the ^{1}H NMR spectrum and 2D correlation spectroscopy confirmed the presence of the ethoxide co-ligand. Due to the asymmetry of the hybrid ligand, a greater degree of complexity was observed in the ^{1}H and ^{13}C NMR spectra. Nonetheless, the spectra were fully characterised using COSY, HSQC and NOE NMR spectroscopy experiments (Figure 3.5). All aluminium initiators were found to be pure as confirmed by elemental analysis.

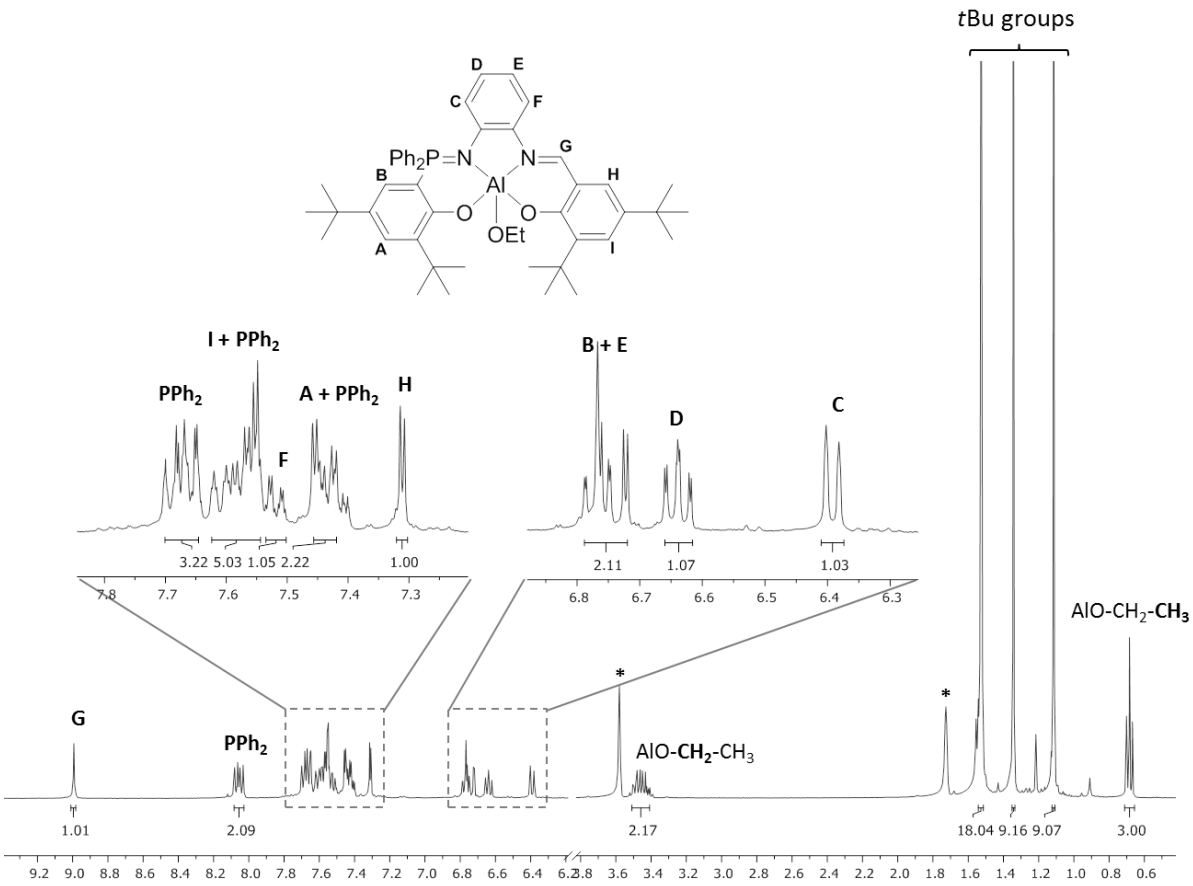

Figure 3.5. ^{1}H NMR spectrum of aluminium hybrid initiator **3.5** (d_8-THF*, 400 MHz, 298 K).

3.3.2. Indium Initiators

Initiators **3.7**-**3.9** were synthesised from the salen, hybrid and phosphasalen ligands respectively using the same synthetic procedure for each ligand. Firstly, the proteo-ligand was dissolved in THF, followed by addition of two equivalents of base, potassium bis(trimethylsilyl)amide ($K(N(SiMe)_2)_2$), next, indium(III) chloride ($InCl_3$) was added and finally potassium *tert*-butoxide (KO*t*Bu) (Scheme 3.3). The ethoxide co-ligand was initially targeted to maintain continuity between all initiators but a pure product could not be isolated due to the presence of multiple side products. Multiple attempts to recrystallise the solution did not yield the desired product. The indium chloride derivative, compounds **3.10-3.12**, of the three ligand classes were isolated and *in situ* monitoring was used to investigate routes to other alkoxide species. $^{31}P\{^{1}H\}$ NMR spectroscopy reactions in d_8-THF demonstrated that **3.11** and **3.12** formed multiple peaks/products after reaction with

KOEt. The same reactions using KO*t*Bu revealed a single *tert*-butoxide species for all complexes. The synthesis of initiators **3.7**-**3.9** was then repeated, on a larger scale, using KO*t*Bu to form the alkoxide product.

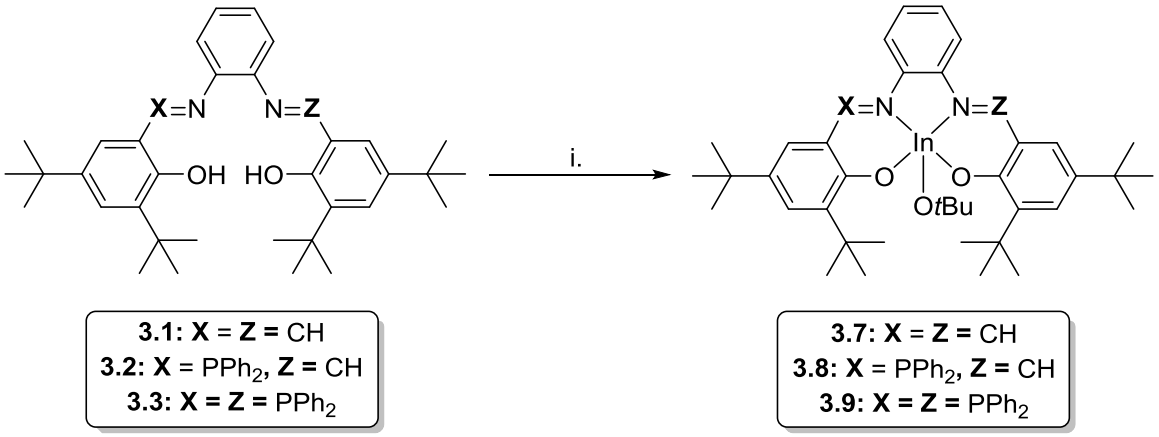

Scheme 3.3. Synthesis of initiators **3.7**-**3.9**. Conditions: i. (a) $K(N(SiMe)_2)_2$ (2 equiv.), THF, 298 K, (b) $InCl_3$ (1 equiv.), 298 K (c) KO*t*Bu (1 eq.), 298 K.

The synthesis of initiator **3.7** was monitored by ^1H NMR spectroscopy and resonances corresponding to the phenol protons at 13.6 ppm disappeared, indicating successful deprotonation. $InCl_3$ was added and changes to all resonances were observed, e.g. the imine proton shifted from 8.46 ppm to 8.20 ppm (C_6D_6). Finally KO*t*Bu was added, a new resonance at 1.05 ppm in the ^1H NMR spectrum was observed and corresponded to the *tert*-butoxide co-ligand. The pure product was isolated in moderate yields (58%).

The synthesis of initiators **3.8** and **3.9** were monitored by $^{31}P\{^1H\}$ NMR spectroscopy. For the synthesis of initiator **3.9**, the $^{31}P\{^1H\}$ NMR spectra observed a shift in the resonance for the phosphasalen ligand, **3.3**, ($^{31}P\{^1H\}$ = 18.1 ppm) to the deprotonated ligand ($^{31}P\{^1H\}$ = 13.1 ppm) after addition of $K(N(SiMe)_2)_2$. The final product was isolated after addition of $InCl_3$ ($^{31}P\{^1H\}$ = 34.7 ppm) and KO*t*Bu ($^{31}P\{^1H\}$ = 34.4 ppm) followed by recrystallisation from THF/*n*-hexane at 243 K. Addition of $K(N(SiMe)_2)_2$ to hybrid ligand, **3.2**, in THF gave a

change in the $^{31}P\{^{1}H\}$ resonance (in C_6D_6) from 20.7 to 13.4 ppm. The single resonance moved to 32.9 ppm after addition of $InCl_3$ and to 33.4 ppm after addition of KO*t*Bu. The pure product was isolated using the same method as for initiator **3.9** above, in low yields (35%). The purity of initiators **3.7**-**3.9** were confirmed by elemental analysis.

All initiators were fully characterised by multinuclear NMR spectroscopy. It was observed that each *tert*-butyl group on hybrid initiator **3.8** yielded a distinct chemical shift environment before and after coordination to indium, with an additional environment for the *tert*-butoxide co-ligand. The protons present in the two-phenyl rings on phosphorus in ligand **3.2** are chemically and magnetically equivalent, with the *ortho*, *para* and *meta* protons being found at 7.74, 7.52 and 7.42 ppm respectively. Upon coordination to indium, the ligand becomes restricted to free rotation and the two phenyl rings become magnetically inequivalent. This was reflected in the ^{1}H NMR spectrum of **3.8** where there was increased complexity in the aromatic region and in the $^{13}C\{^{1}H\}$ NMR spectrum, two chemical shift environments were present for each *ortho*, *meta* and *para* proton (Figure 3.6).

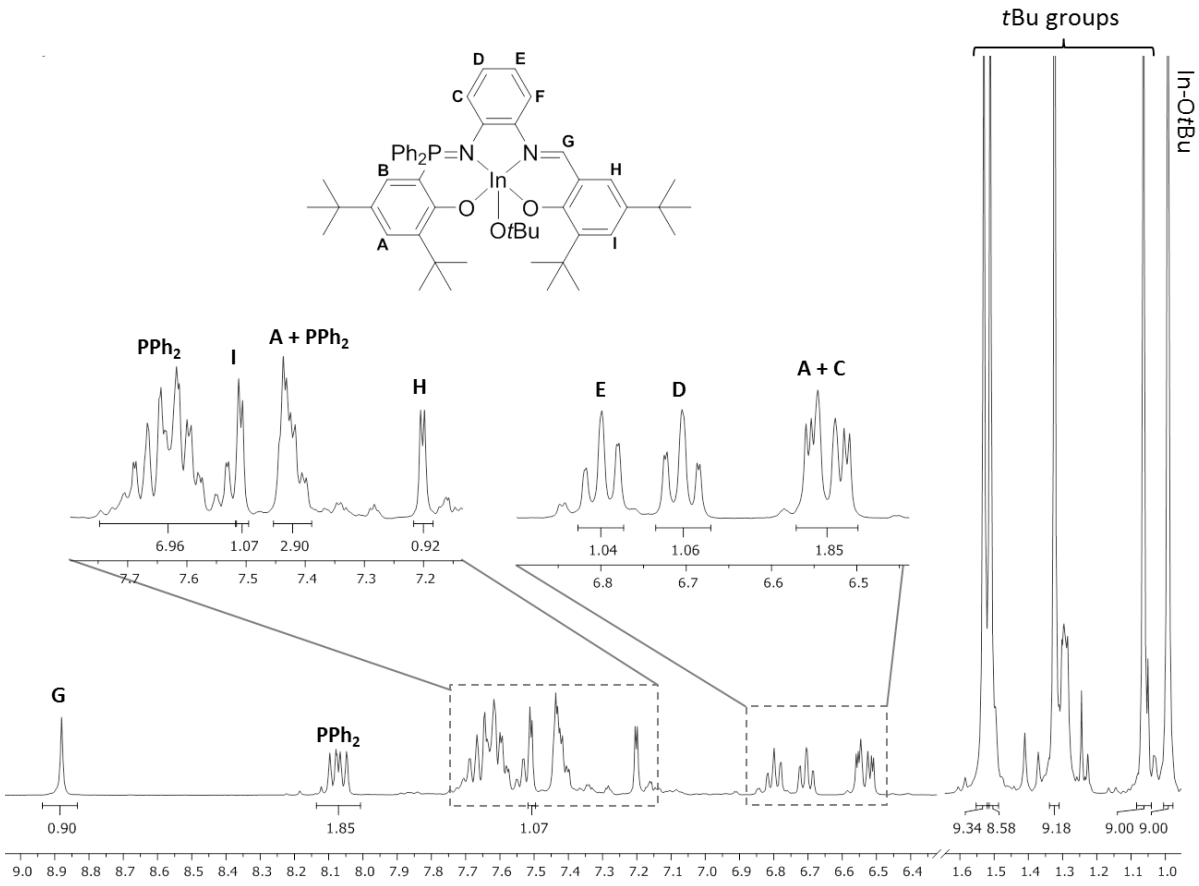

Figure 3.6. ^{1}H NMR spectrum of indium hybrid initiator **3.8** (d_8-THF, 400 MHz, 298 K).

3.3.3. X-ray crystal structures of Initiators 3.6 and 3.8

A single crystal suitable for X-ray diffraction experiments were grown of initiators **3.6** and **3.8** from saturated THF/*n*-hexane solutions at 243 K. Initiator **3.6** crystallised in a monoclinic space group ($P2_1/n$) (Figure 3.7) whereas initiator **3.8** crystallised in a triclinic space group (P-1) (Figure 3.8).

The aluminium complex has a pentacoordinate aluminium centre with trigonal bipyramidal geometry (τ = 0.86). In the equatorial positions is one nitrogen, from one iminophosphorane bond (N8), one phenolate oxygen (O22) and the oxygen from the ethoxide co-ligand (O70). The axial positions are occupied by the remaining iminophosphorane nitrogen (N15) and phenolate oxygen (O1). The indium complex has a penta-coordinate indium centre with a square-based pyramidal geometry (τ = 0.18). The phenolate oxygens (O1 and O22) and two nitrogen atoms (N8 and N15) on the ligand backbone make up the base of the square based pyramid geometry, with the *tert*-butoxide group (O60) occupying the apex of the pyramid.

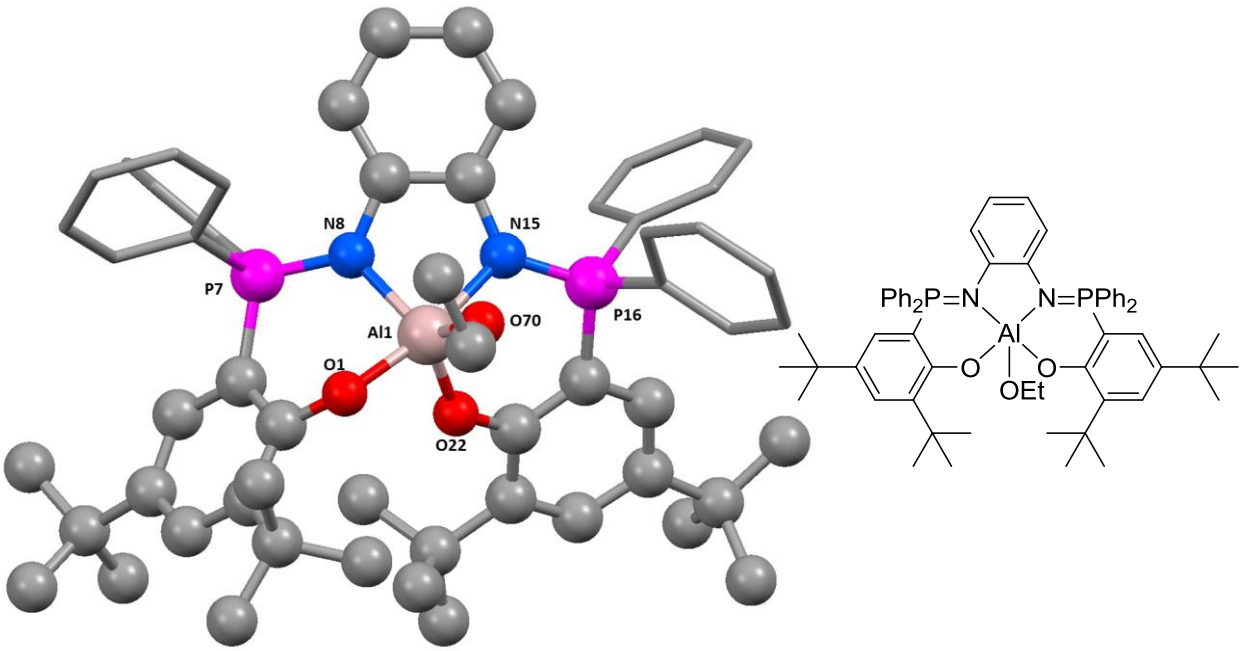

Figure 3.7. Ball and stick representation of initiator **3.6** (H-atoms omitted for clarity. See Appendix for complete bond lengths and angles).

The N-Al-N bite angle is 78.86(7)^{o,} which indicates that the phenyl backbone restricts the ability of the ligand to reside in a fully trigonal bipyramidal geometry. Furthermore, the P=N bond lengths are shorter than those found in phosphasalen ligands when coordinated to yttrium or indium, likely due to the smaller ionic radii of Al(III).[10,11] This also results in a shorter metal alkoxide bond for the aluminium initiator, 1.741(2) Å compared to the indium initiator, 2.016(2) Å, due to increased Lewis acidity of the smaller metal centre.

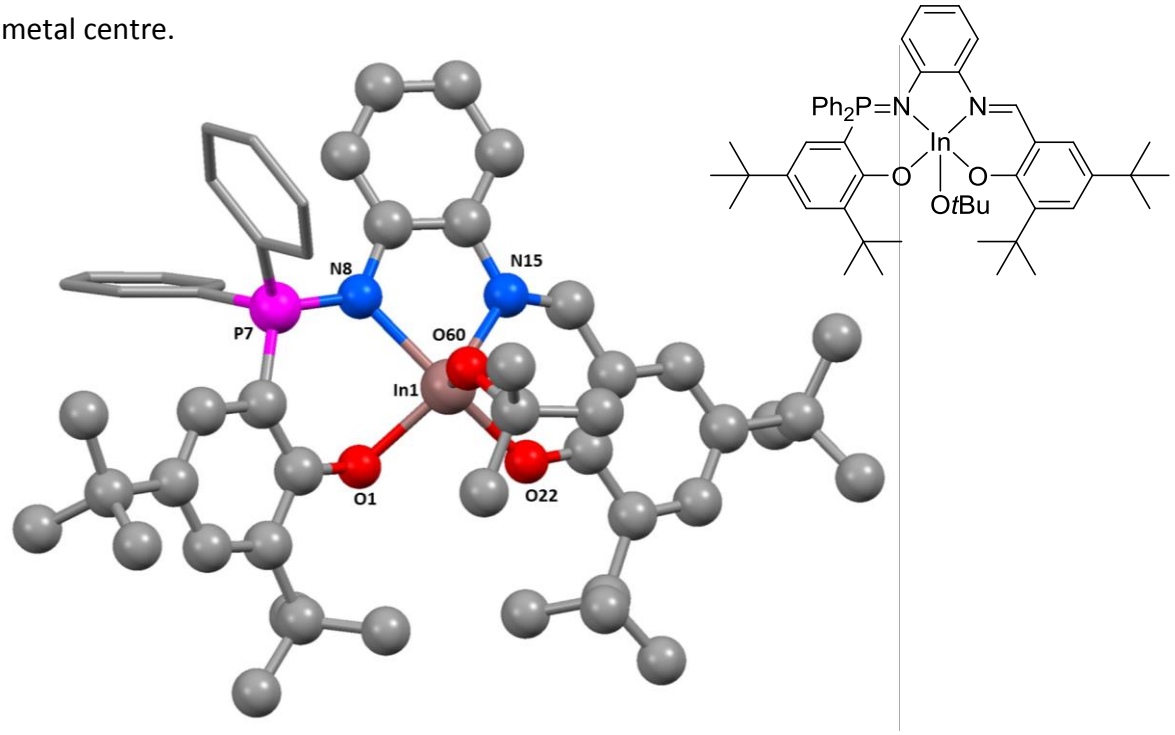

Figure 3.8. Ball and stick representation of initiator **3.8** (H-atoms omitted for clarity. See Appendix for complete bond lengths and angles).

3.3.4. DOSY NMR Analysis

To verify the aggregation state of each initiator in solution, especially in solvents relevant to polymerisation catalysis, each initiator was analysed by DOSY NMR. All aluminium initiators were analysed in toluene-d_8 and indium initiators in THF-d_8. In the cases where X-ray structures were obtained (initiators **3.6** and **3.8**) comparisons between the hydrodynamic radii could be made (For calculations). For initiator **3.6**, the two values were found to be in good agreement (r_H $^{\text{Toluene-}d8}$ = 6.05 Å and r_H $^{\text{solid-state}}$ = 5.99 Å),

similarly for **3.8** (r_H $^{THF\text{-}d8}$ = 6.04 Å and r_H $^{solid\text{-}state}$ = 5.69 Å). From the diffusion coefficients, an estimation of the molecular weight was feasible by comparison to initiators **3.6** and **3.8** and in all cases; initiators were monomeric (Table 3.1). Interestingly, indium salen initiators, reported by Mehrkhodavandi and co-workers, with a chiral cyclohexyl diamine bridge, are dimeric in the solid and solution state, whereas initiator **3.8**, with a phenylene diamine bridge, is monomeric in the solution state.[26,27] In the initiator reported by Mehrkhodavandi, rates were increased by breaking the aggregation state of the dimer but had little effect on isoselectivity.

Table 3.1. Calculation of the molecular weight values obtained using DOSY NMR (298 K, 500 MHz).

Initiator	NMR Solvent (d_8)	Diffusion Coefficient (x 10^{-10})	Estimation of Molecular Weight[a]	Calculated Molecular Weight
3.4	Toluene	7.78	488	610.8
3.5	Toluene	6.19	724	782.9
3.6	Toluene	6.44	677	970.2
3.7	THF	7.33	789	726.7
3.8	THF	7.53	752	898.9
3.9	THF	6.81	900	1071.0

[a]See Section 2.1 for calculations.

3.4. Polymerisation Catalysis

Initiators **3.4**-**3.9** were tested as catalysts in the ring-opening polymerisation (ROP) of *rac*-LA. The polymerisations were carried out under standard conditions: 1 M solution of *rac*-LA and with a catalyst loading of 1 mol%. The room temperature polymerisation kinetics were obtained by collecting aliquots at regular intervals. For high temperature polymerisations, each aliquot was taken by quenching individual vials at the allotted time. The individual aliquots were analysed by ^{1}H NMR spectroscopy to determine conversion (%). For aluminium initiators **3.4**-**3.6**, the polymerisations were carried out in toluene at 373 K and for indium initiators **3.7**-**3.9**, in THF at 298 K. Attempts were made to use the aluminium initiators, in both THF at 298 K and toluene at 353 K, but no polymer was produced after several days. The key results are summarised in Table 3.2.

Table 3.2. Polymerisation data using initiators **3.4**-**3.9**.

Entry	Initiator	Conv. (%)[c]	Time	k_{obs} (x 10^{-6} s^{-1})[d]	M_n (g mol^{-1})[e]	M_n^{calc} (g mol^{-1})	Đ[e]	P_i[f]
1	**3.4**[a]	77	7 days	1.76 ± 0.11	9110	11100	1.06	0.65 ± 0.05
2	**3.5**[a]	84	7 days	4.26 ± 0.17	9300	12100	1.31	0.65 ± 0.02
3	**3.6**[a]	71	8 days	1.73 ± 0.06	7200	10000	1.28	0.64 ± 0.03
4	**3.7**[b]	99	10 min	6480 ± 60	13800	13800	1.02	0.51 ± 0.05
5	**3.8**[b]	99	20 min	2720 ± 19	15600	13800	1.02	0.71 ± 0.02
6	**3.9**[b]	99	60 min	1000 ± 60	16200	12800	1.05	0.52 ± 0.03

[a]Polymerisation conditions: [Initiator]:[LA] = 1:100, [LA] = 1 M, Toluene, 373 K [b]Polymerisation conditions: [Initiator]:[LA] = 1:100, [LA] = 1 M, THF, 298 K [c]Determined by integration of the methine region of the ^{1}H NMR spectrum (LA, 5.00 - 5.07 ppm; PLA, 5.10 – 5.24 ppm). [d]Measured by determining the gradients of the plots of $\ln\{[LA]_0/[LA]_t\}$ vs. time. [e]Determined by gel-permeation chromatography in THF, using multiangle laser light scattering (GPC-MALLS). [f]Determined by integrating the average P_i values obtained for each tetrad signal in the methine region of the homonuclear-decoupled ^{1}H NMR spectrum.

3.4.1. Polymerisation Kinetics

Pseudo first-order rate kinetics were apparent from linear fits to plots of $\ln([LA]_0/[LA]_t)$ vs. time. All initiators obeyed pseudo first-order kinetics, as indicated from linear semi-logarithmic plots (Figure 3.9 and Figure 3.10). Initiators, **3.4**-**3.6** were active but displayed slow rates, taking 7 days to reach 84% conversion even for the best initiator, **3.5** (Table 3.2, entry 2). Faster rates were demonstrated by all indium analogues due to the increased lability of their metal-alkoxide bonds, despite the fact that slow initiation is expected from the *tert*-butoxide co-ligand vs. an ethoxide co-ligand.[10]

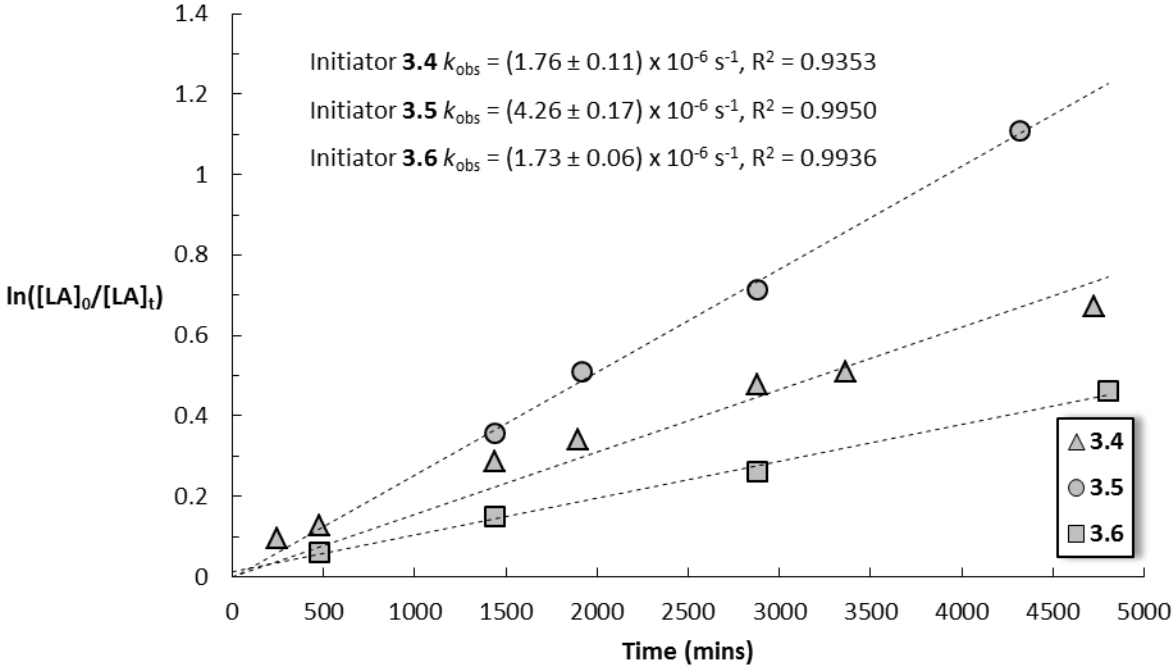

Figure 3.9. Plot of $\ln([LA]_0/[LA]_t)$ vs time of initiators **3.4**-**3.6**. Conditions: [I]:[LA] = 1:100, [LA] = 1M, Toluene, 373 K.

A comparison of the k_{obs} values, as displayed in Figure 3.8, demonstrates a slight difference in rate, the hybrid coordinated initiator **3.5** demonstrates a two-fold increase in rate, k_{obs} = 4.26 x 10^{-6} s^{-1}, over its salen (**3.4**), k_{obs} = 1.76 x 10^{-6} s^{-1}, analogue and a three-fold, over the phosphasalen derivative (**3.6**), k_{obs} = 1.73 x 10^{-6} s^{-1}.

For the indium initiators, **3.7**-**3.9**, different reactivity as a result of the ligand scaffold is also observed, the salen initiator demonstrates the best rate, reaching full conversion of

the lactide monomer in 10 minutes, k_{obs} = 6.48 x 10^{-3} s^{-1} (Table 3.2, Entry 4). For the indium initiators coordinated by the hybrid and phosphasalen ligands, **3.8** and **3.9**, the rates were four times and six times slower, k_{obs} = 2.72 and 1.00 x 10^{-3} s^{-1} respectively.

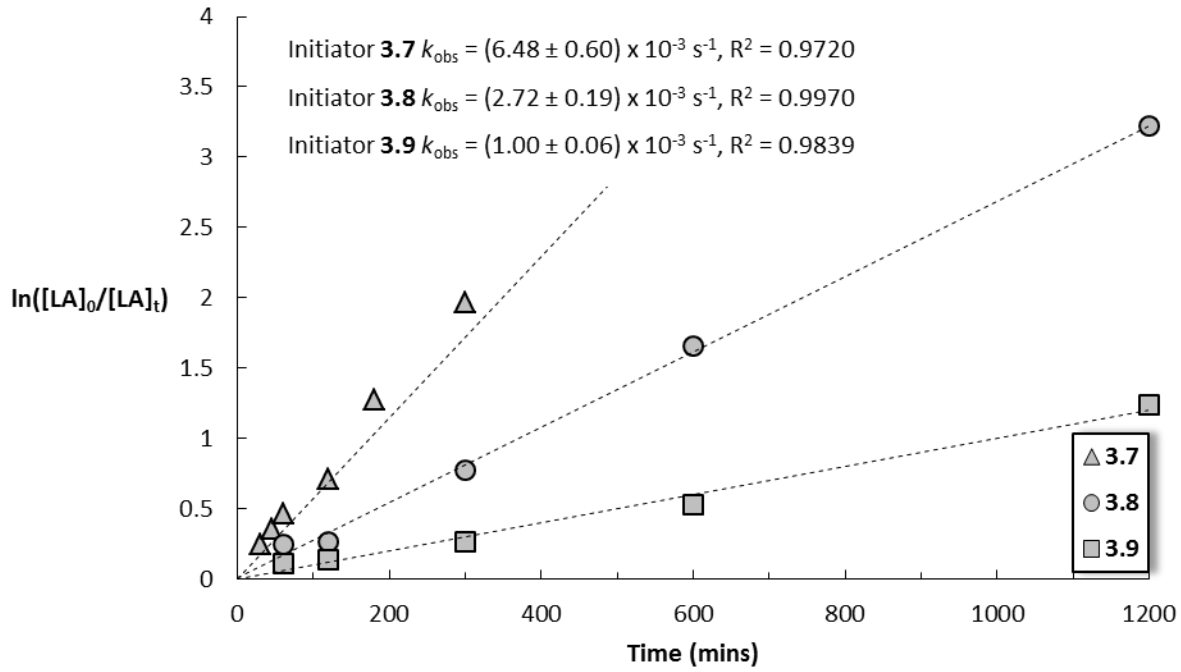

Figure 3.10. Plot of $\ln([LA]_0/[LA]_t)$ vs time of initiators **3.7**-**3.9**. Conditions: [I]:[LA] = 1:100, [LA] = 1M, THF, 298 K.

3.4.2. Polymerisation Control

Gel permeation chromatography (GPC) analysis was carried out to determine the molecular weight (M_n) and dispersities of each aliquot taken during the polymerisation. Initiators **3.4-3.6** demonstrated good polymerisation control as indicated by linear fits to kinetics plots and linear increase in M_n with % conversion. For initiators **3.5** and **3.6**, slightly higher molecular weights than predicted and broader dispersities were displayed. This could be an artefact of slow initiation, but this was not observed for initiator **3.4** despite the similar reaction times (Figure 3.11). Long polymerisation times and high temperatures may also allow transesterification reactions to take place, which only result in a change of dispersity, not molecular weight.

Initiators **3.6**-**3.8** all displayed excellent polymerisation control, with the experimental M_n corresponding well with predicted M_n, evolving linearly with % conversion and maintaining narrow dispersities throughout each polymerisation. This is somewhat unexpected as more hindered initiating groups, such as *tert*-butoxide, can cause initiation problems, manifesting as broader dispersities and less predictable molecular weights.[10] For the indium initiators, broadening of the dispersities only occur near to complete conversion, this is likely due to transesterification rates becoming competitive.

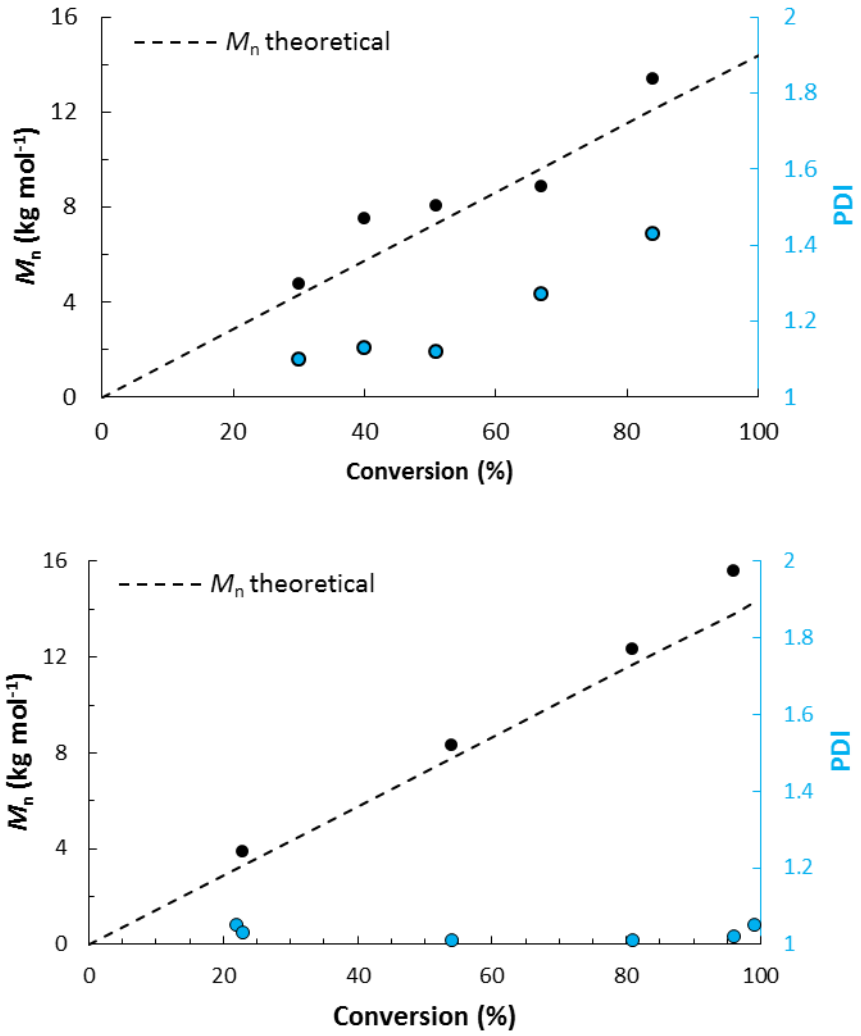

Figure 3.11. Plots of the molecular weight and polydispersity vs. conversion for the polymerisation of *rac*-LA mediated by initiator **3.5** (top) and **3.7** (bottom). Conditions: [**3.5**]:[LA] = 1:100, [LA] = 1M, Toluene, 373 K; [**3.7**]:[LA] = 1:100, [LA] = 1M, THF, 298 K.

Matrix assisted laser desorption ionization-time of flight (MALDI-ToF) mass spectrometry was used to analyse the low molecular weight polymers produced by all initiators. For initiators **3.3**-**3.6**, the only polymer series present showed ethoxide end-groups, proving the absence of detectable transesterification reactions. Similarly, for initiators **3.7**-**3.9**, a single polymer series with *tert*-butoxide capped was observed (Figure 3.12). The peak separation was always 144 amu which ruled out significant transesterification reactions (a series separated by 72 amu would be observed in the presence of transesterification). The technique is unsuited for analysis of polymers of high M_n, so it is difficult to determine the extent of transesterification at the later stages of polymerisation.

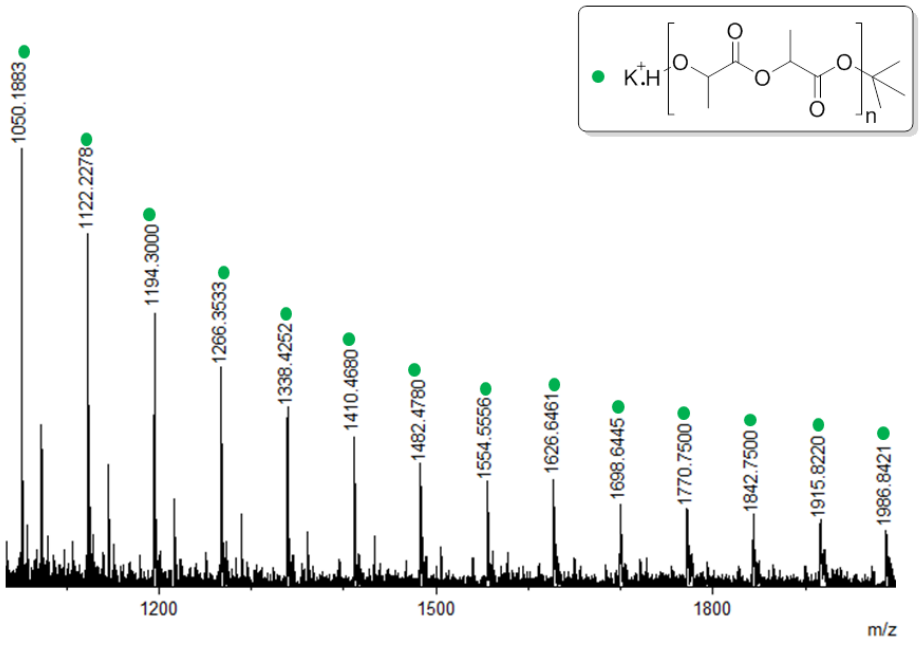

Figure 3.12. MALDI-ToF spectrum obtained from the polymerisation with initiator **3.8**. Conditions: [**3.8**]:[LA] = 1:100, [LA] = 1M, THF, 298 K.

3.4.3. Isoselectivity

The isoselectivity of the polymers was determined by analysis of the tetrad resonances, of the methine proton, in the deconvoluted homonuclear decoupled $^1H\{^1H\}$ NMR spectrum. Initiators **3.4** and **3.5** were found to achieve P_i = 0.65 and for initiator **3.6**, P_i = 0.64. An isotactic bias is typically observed for aluminium initiators and comparatively,

these values are low.[2–4,8,9,28] An increase in the isotactic bias may be demonstrated by carrying out polymerisations at lower temperatures but attempts did not produce sufficient polymer to analyse.

Further analysis of the methine region of the stereoerrors allows determination of the mechanism of stereocontrol as either ESC or CEC. Depending on the mechanism present, different ratios of the tetrads will arise, for ESC the ratio = [sis]:[sii]:[iis]:[isi] = 1:1:1:2 whereas for CEC the ratio = [sii]:[iis]:[isi] = 1:1:1. For initiators **3.4**-**3.6**, the stereoerrors suggest a CEC mechanism, which is in line with the initiators being coordinated by achiral ligands.

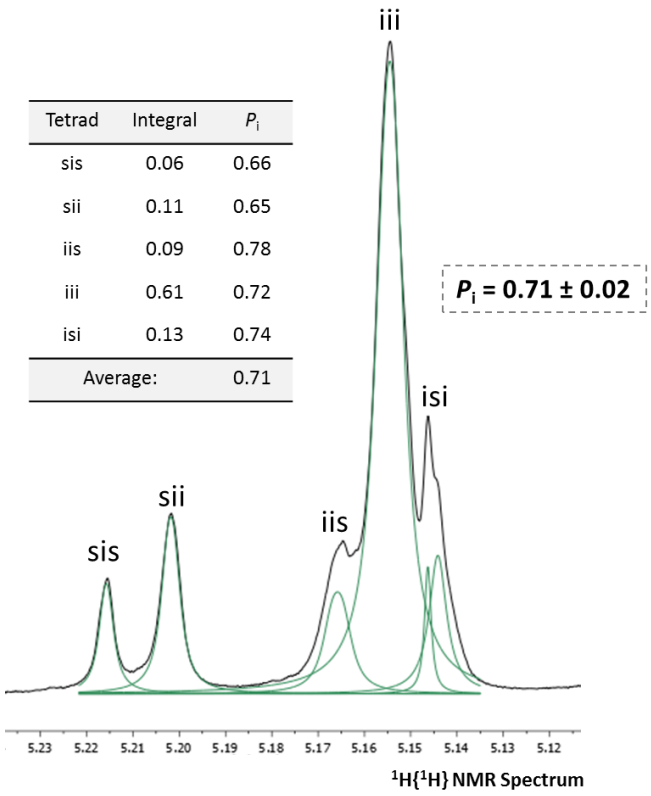

Figure 3.13. ^{1}H NMR spectra ($CDCl_3$, 400 MHz, 298 K) and calculation of P_i value for PLA sample yielded from initiator **3.8**. Conditions: [**3.8**]:[LA] = 1:100, [LA] = 1M, THF, 298 K.

Initiators **3.7** and **3.9** yielded atactic PLA with P_i values of 0.51 and 0.52, respectively. This differs greatly to previously reported indium salen and phosphasalen initiators which

yield P_i values of between 0.77-0.87.[12,26] Unlike the literature initiators, these initiators lack either chiral or a flexible diamine linker group, which appears to be implicated in isoselectivity. Interestingly, initiator **3.8**, P_i = 0.71 was achieved, and analysis of stereoerrors, implicates a CEC mechanism (Figure 3.13).

3.4.4. Discussion

Whilst the origin of the increased isoselectivity of the indium hybrid initiator is unclear, and will be the subject of investigation in the next chapter, the differences in rate can be rationalised by considering the steric and electronic properties of the ligands and metal centres. Aluminium, a smaller and therefore more Lewis acidic metal centre features a stronger metal alkoxide bond, as evident from the solid-state structures obtained of initiator **3.6**, 1.741(2) Å, and indium initiator **3.8**, 2.016(2) Å. Therefore the slower rate observed for aluminium initiators **3.4**-**3.6** can be attributed to a strong aluminium-alkoxide bond; requiring higher activation temperatures to undergo the nucleophilic attack of the newly coordinated monomer, necessary for polymerisation. The converse argument, a larger and less Lewis acidic indium metal centre, justifies the increased rate displayed for initiators **3.7**-**3.9**, which correlates with similar reports in the literature.[29,30]

For indium initiators, the difference in rates for the three ligands is phosphasalen < hybrid < salen. The key differences between the salen and phosphasalen are that the iminophosphorane bond is a stronger σ- and π-donor which overall reduces the Lewis acidity of the metal centre (Figure 3.14). This electronic effect might be expected to result in an increase in polymerisation rate due to a weakening of the metal-alkoxide bond, but this was not observed experimentally. It could be that the steric influence of the phenyl groups on phosphorus hinders the rates of coordination or insertion of the lactide

monomer. The electron-donating ability of the hybrid ligand is assumed to lay between the salen and phosphasalen ligands, with a greater reduction in metal Lewis acidity than the salen ligand. Sterically, the hybrid ligand is less encumbered than the phosphasalen ligand, which may play a role in facilitating the approach of the lactide monomer and may account for the increase in rate. Experimentally, the rate of the hybrid ligand lays in-between the salen and phosphasalen ligands, which implies that the steric effect, is a factor in rate determination.

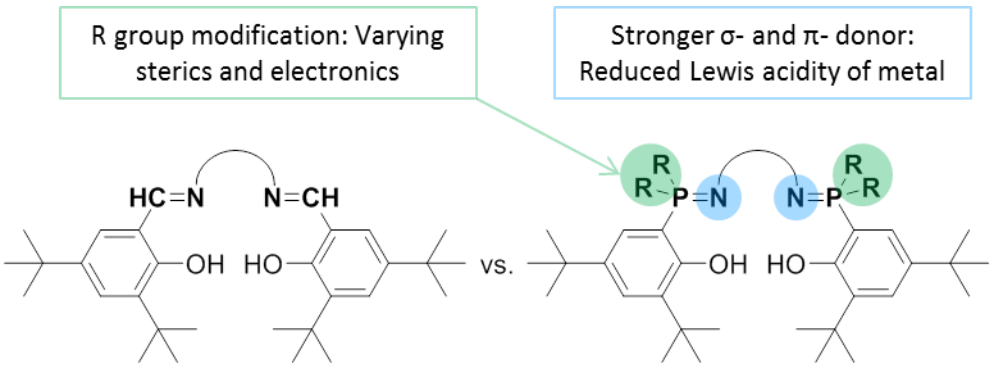

Figure 3.14. Key differences between salen and phosphasalen ligands.

Initiator **3.8** showed first-order rate dependence on initiator concentration, as observed by linear fit of k_{obs} vs. [Initiator] (Figure 3.15). Therefore, the overall rate law was second-order and the propagation rate constant was k_p = 13 ± 0.6 M^{-1} min^{-1}, which is approximately two times slower than previously reported indium phosphasalen initiators.[12] The rate law correlates with the rate-limiting step being the nucleophilic attack of the indium-alkoxide bond on the carbonyl bond of the lactide monomer.[31] It is suggested that the differences between the three ligand classes arises from differences in steric hindrance. On the other hand, a more subtle electronic influence cannot be ruled out.

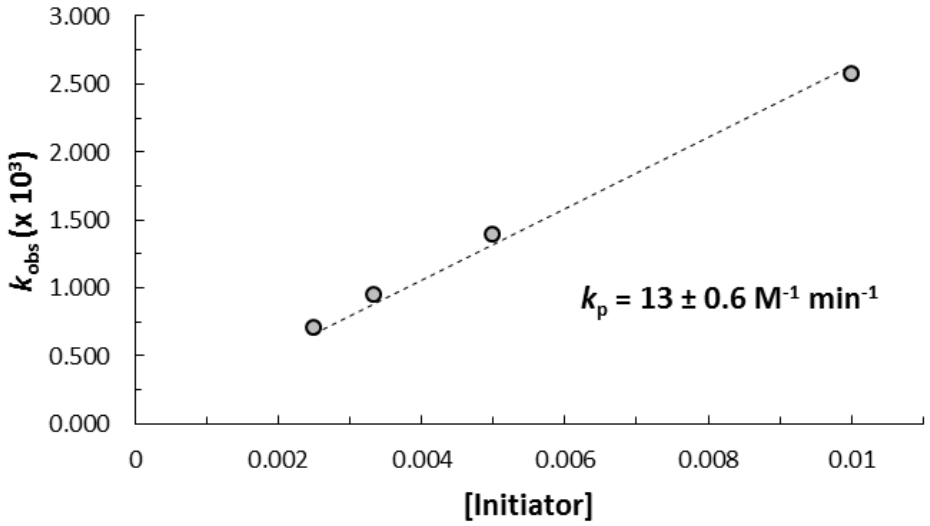

Figure 3.15. Plot of k_{obs} against initiator concentration for calculation of the propagation rate constant, k_p.

3.5. Summary and Outlook

3.5.1. Summary

The design and synthesis of a hybrid ligand containing one imine and one iminophosphorane bond is described. A series of aluminium and indium initiators, coordinated by the novel hybrid ligand (**3.5**, **3.8**) and the comparative salen (**3.4**, **3.7**) and phosphasalen initiators (**3.6**, **3.9**), were synthesised. All compounds were fully characterised by NMR spectroscopy, elemental analysis and in some cases, X-ray diffraction. All initiators were analysed by DOSY NMR and found to be monomeric under polymerisation conditions.

Aluminium initiators demonstrated slow rates with the order: hybrid > salen > phosphasalen. In the case of the indium initiators, the rates of the ligands were salen > hybrid > phosphasalen. For the indium hybrid initiator, further investigation of the rate law found that the nucleophilic attack of the alkoxide bond on the monomer was the

rate-limiting step. This correlated with the behaviour observed with other indium and phosphasalen initiators.[10,12]

All initiators demonstrated good polymerisation control, with the presence broadening of dispersities in the aluminium systems due to long polymerisation times and high temperatures. A linear evolution of molecular weight with conversion and narrow dispersities throughout were observed with the indium initiators. The aluminium initiators demonstrated a slight isotactic stereocontrol with all ligand classes giving a P_i of 0.64-0.65. The salen and phosphasalen indium initiators gave atactic PLA but the hybrid indium initiator gave a P_i of 0.71. In all cases where tacticity control was demonstrated, a chain-end control mechanism prevailed.

3.5.2. Outlook

The results in this chapter have demonstrated that the hybrid ligand when coordinated to aluminium has limited scope, as it is unable to match the rates or isoselectivity values achieved previously using aluminium initiators in the literature.[9,12] Conversely, when coordinated to indium, good rates of polymerisation are achieved as well as an interesting isoselective bias, especially when compared to the salen and phosphasalen analogues. The origin of the isoselectivity demonstrated by the indium hybrid initiator is currently unclear. Further modification of the hybrid ligand is needed to understand the stereocontrol. Figure 3.16 illustrates the range of potential modifications that could be made at the imine phenolate, iminophosphorane phenolate or phosphorus substituents.

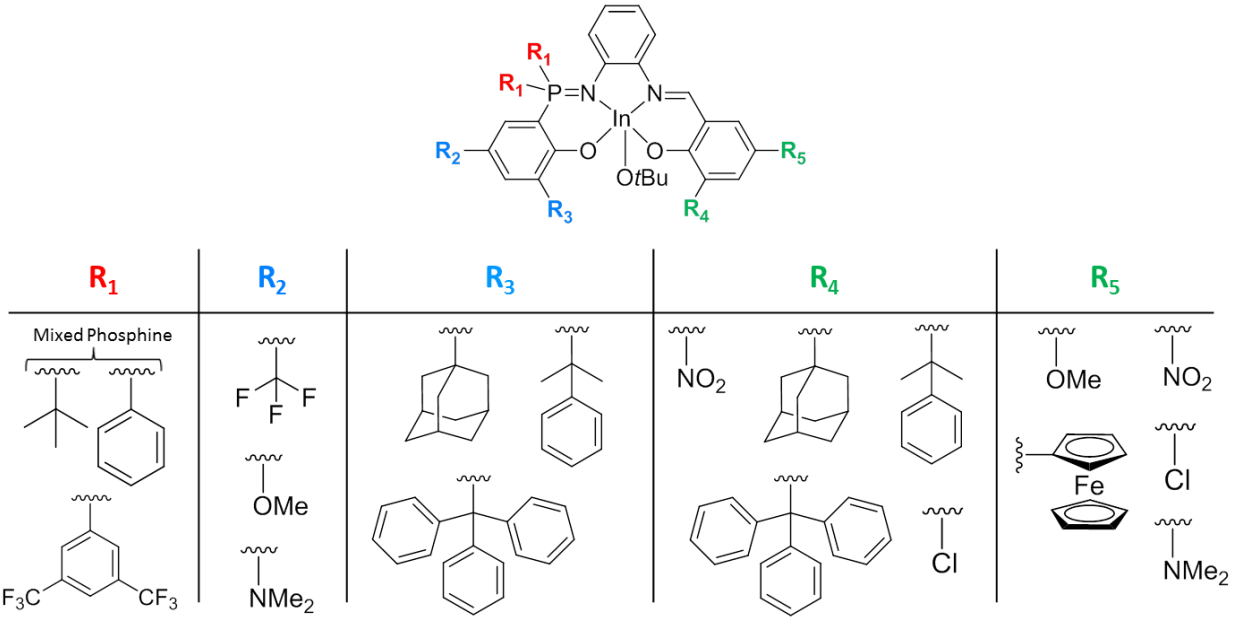

Figure 3.16. Overview of potential modifications of indium hybrid initiator system.

The modifications proposed aim to vary both the steric and electronic features of the hybrid ligand. It has already been shown that isoselectivity can increase by changing the steric bulk in the *ortho*-phenolate positions for aluminium and indium initiators.[9,12] Therefore, ligands featuring adamantyl, cumyl and trityl should be used to investigate the steric effect. In particular, targeting increased steric hindrance at just one side of the initiator would allow more investigation of the role of unsymmetrical ligands on isoselectivity.

The hybrid ligand can also be substituted with: (i) electron withdrawing groups (EWG) such as chloride, nitro and -CF_3 and (ii) electron-donating groups (EDG), including the bulkier analogues mentioned above, and methoxy and tertiary amine groups. For aluminium salen initiators, it is known that EWGs increase rate but may reduce isoselectivity; it is interesting to investigate whether this behaviour extends to the hybrid ligand and whether EDGs increase the P_i.[9] Modifications at phosphorus could introduce chirality (e.g. mixture of Ph and *t*Bu), and allow an ESC mechanism to be targeted.

Increased bulk at this site may also have implications in rate and even the potential to change the rate-limiting step to lactide coordination.

Finally, redox-active initiators have recently been shown to control rate and monomer selectivity upon changing the oxidation state of the metal or ligand.[32–34] Initiators featuring a ferrocene moiety may allow such activity to be investigated within the hybrid system. The key target would be to switch stereoselectivity by changing oxidation state, a feature that has yet to be exploited in redox-switch catalysis. Ferrocene used as the backbone of the ligand has been previously reported; therefore, the target of this work will be to incorporate it at the *ortho*- or *para*-phenolate positions.[33]

The modification of hybrid ligands according to some of these suggestions will be the focus of the next chapter.

3.6. References

1 N. Spassky, M. Wisniewski, C. Pluta and A. Le Borgne, *Macromol. Chem. Phys.*, 1996, **197**, 2627–2637.

2 Z. Zhong, P. J. Dijkstra and J. Feijen, *Angew. Chem. Int. Ed.*, 2002, **41**, 4510–4513.

3 Z. Zhong, P. J. Dijkstra and J. Feijen, *J. Am. Chem. Soc.*, 2003, **125**, 12291–11298.

4 H. Du, A. H. Velders, P. J. Dijkstra, J. Sun, Z. Zhong, X. Chen and J. Feijen, *Chem. Eur. J.*, 2009, **15**, 9836–9845.

5 P. J. Dijkstra, H. Du and J. Feijen, *Polym. Chem.*, 2011, **2**, 520–527.

6 N. Nomura, R. Ishii, M. Akakura and K. Aoi, *J. Am. Chem. Soc.*, 2002, **124**, 5938–5939.

7 N. Nomura, R. Ishii, Y. Yamamoto and T. Kondo, *Chem. Eur. J.*, 2007, **13**, 4433–4451.

8 N. Maudoux, T. Roisnel, V. Dorcet, J.-F. Carpentier and Y. Sarazin, *Chem. Eur. J.*, 2014, **20**, 6131–6147.

9 P. Hormnirun, E. L. Marshall, V. C. Gibson, R. I. Pugh and A. J. P. White, *Proc. Natl. Acad. Sci. U. S. A.*, 2006, **103**, 15343–15348.

10 C. Bakewell, T.-P.-A. Cao, N. Long, X. F. Le Goff, A. Auffrant and C. K. Williams, *J. Am. Chem. Soc.*, 2012, **134**, 20577–20580.

11 C. Bakewell, A. J. P. White, N. J. Long and C. K. Williams, *Angew. Chem. Int. Ed.*, 2014, **53**, 9226–9230.

12 D. Myers, A. J. P. White, C. M. Forsyth, M. Bown and C. K. Williams, *Angew. Chem. Int. Ed.*, 2017, **56**, 5277–5282.

13 K. Matsumoto, B. Saito, H. Watanabe, T. Ozawa, K. Suzuki, T. Katsuki, A. S. Peregudov, G. I. Timofeeva, M. Tasinazzo, G. I. Timofeeva and L. V. Yashkina, *Chem. Commun.*, 2007, **45**, 3619–3627.

14 A. Pilone, K. Press, I. Goldberg, M. Kol, M. Mazzeo and M. Lamberti, *J. Am. Chem. Soc.*, 2014, **136**, 2940–2943.

15 P. McKeown, M. G. Davidson, G. Kociok-Köhn and M. D. Jones, *Chem. Commun.*, 2016, **52**, 10431–10434.

16 S. M. Kirk, G. Kociok-Köhn and M. D. Jones, *Organometallics*, 2016, **35**, 3837–3843.

17 P. McKeown, M. G. Davidson, J. P. Lowe, M. F. Mahon, L. H. Thomas, T. J. Woodman, M. D. Jones, K. Wieghardt, C. Wade, R. M. Waymouth and J. L. Hedrick, *Dalton Trans.*, 2016, **45**, 5374–5387.

18 A. Stopper, T. Rosen, V. Venditto, I. Goldberg and M. Kol, *Chem. Eur. J.*, 2017, **23**, 11540–11548.

19 G.-P. Wu, W.-M. Ren, Y. Luo, B. Li, W.-Z. Zhang and X.-B. Lu, *J. Am. Chem. Soc.*, 2012, **134**, 5682–5688.

20 A. Alaaeddine, C. M. Thomas, T. Roisnel and J.-F. Carpentier, *Organometallics*, 2009, **28**, 1469–1475.

21 M. F. Renehan, H.-J. Schanz, E. M. McGarrigle, C. T. Dalton, A. M. Daly and D. G. Gilheany, *J. Mol. Catal. A Chem.*, 2005, **231**, 205–220.

22 M. Holbach, X. Zheng, C. Burd, C. W. Jones and M. Weck, *J. Org. Chem.*, 2006, 2903–2906.

23 E. J. Campbell and S. T. Nguyen, *Tetrahedron Lett.*, 2001, **42**, 1221–1225.

24 L. Ding, S. Liang, J. Zhang, C. Ding, Y. Chen and X. Lu, *Inorg. Chem. Commun.*, 2014, **44**, 173–176.

25 Y. Wang, Y. Qin, X. Wang and F. Wang, *Catal. Sci. Technol.*, 2014, **4**, 3964–3972.

26 D. C. Aluthge, B. O. Patrick and P. Mehrkhodavandi, *Chem. Commun.*, 2013, **49**, 4295–4297.

27 D. C. Aluthge, E. X. Yan, J. M. Ahn and P. Mehrkhodavandi, *Inorg. Chem.*, 2014, **53**, 6828–6836.

28 M. O. Miranda, Y. DePorre, H. Vazquez-Lima, M. A. Johnson, D. J. Marell, C. J. Cramer and W. B. Tolman, *Inorg. Chem.*, 2013, **52**, 13692–13701.

29 A. F. Douglas, B. O. Patrick and P. Mehrkhodavandi, *Angew. Chem. Int. Ed.*, 2008, **47**, 2290–2293.

30 A. B. Kremer, R. J. Andrews, M. J. Milner, X. R. Zhang, T. Ebrahimi, B. O. Patrick, P. L. Diaconescu and P. Mehrkhodavandi, *Inorg. Chem.*, 2017, **56**, 1375–1385.

31 R. Platel, L. Hodgson and C. K. Williams, *Polym. Rev.*, 2008, **48**, 11–63.

32 C. K. A. Gregson, V. C. Gibson, N. J. Long, E. L. Marshall, P. J. Oxford and A. J. P. White, *J. Am. Chem. Soc.*, 2006, **128**, 7410–7411.

33 X. Wang, A. Thevenon, J. L. Brosmer, I. Yu, S. I. Khan, P. Mehrkhodavandi and P. L. Diaconescu, *J. Am. Chem. Soc.*, 2014, **136**, 11264–11267.

34 A. B. Biernesser, B. Li and J. A. Byers, *J. Am. Chem. Soc.*, 2013, **135**, 16553–16560.

Chapter 4

Further investigation of the indium hybrid initiator by modification of the ligand scaffold

In this chapter, the indium hybrid initiator, described in Chapter 3, was subject to further investigation. The aim was to understand the origin of stereocontrol and reach higher degrees of isoselectivity (P_i > 0.71). This was carried out by modification of the ligand scaffold. The redox behaviour was also investigated using cyclic voltammetry, by introduction of a ferrocene moiety, to target a change in stereoselectivity upon redox switching.

4.1. Introduction

In Chapter 3, the synthesis of a novel Schiff base-type ligand containing one imine and one iminophosphorane was described. It was defined as a hybrid ligand due to its mixed donor groups and whilst coordinated to indium, good rates of polymerisation with *rac*-lactide (*rac*-LA) and moderate isoselectivites (99% conversion in 20 minutes, [I]:[LA] 1:100, 298 K, THF, P_i = 0.71) were observed. The isotactic bias for the indium hybrid initiator was notably higher than its salen and phosphasalen analogues which produced atactic PLA (P_i = 0.51 - 0.52). The origin of this isoselectivity was unclear and so one of the aims of this chapter is to acquire further data by modification of the ligand scaffold.

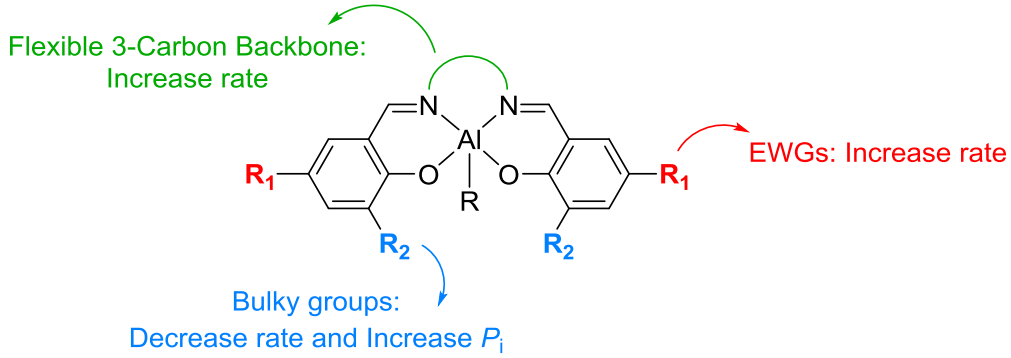

Figure 4.1. Summary of the key modifications on aluminium salen initiators and their effect on rate and isoselectivity.[1]

Ligand structure-activity studies have previously been used with other initiators to understand the effects that govern rate and isoselectivity. The indium hybrid initiator contains a mixture of donor groups, imine and iminophosphorane bonds and is perhaps somewhat similar to the aluminium salalen (mixture of imine and amine bonds) initiators discussed in Section 1.3.[2] Lamberti and co-workers found that EWGs resulted in higher rates, and that the unsymmetrical *ortho*-phenolate groups were important in both rate and P_i determination (Figure 4.2).[3] Initiator **A1**, with an adamantyl group on the amine phenolate, the rate was higher than **A2** which features the same group on the imine phenolate (75% vs. 42% conversion, 24 hours, [I]:[LA] 1:100, toluene, 353 K). Despite the

increased rate, **A1** yielded heterotactic PLA (P_s = 0.76), but **A2** produced isotactic PLA (P_i = 0.82).

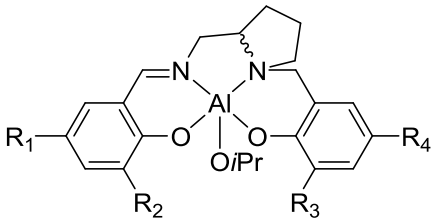

A

	R_1	R_2	R_3	R_4	*S*/*R*?
A1:	Cl	Cl	Ad	Me	*S*
A2:	Me	Ad	Cl	Cl	*S*
A3:	*t*Bu	*t*Bu	Cl	Cl	*S*/*R*/*rac*
A4:	*t*Bu	*t*Bu	I	I	*R*

Figure 4.2. Modifications to the aluminium salalen initiators (Ad = adamantyl).[3]

The size of the substituent at the *ortho*-position on the imine phenolate was reduced (adamantyl to *tert*-butyl), **A3**, the P_i values and rates were improved (78% conversion, P_i = 0.82). Changing the *para*-phenolate substituent from chloride to iodide, **A4**, achieved the highest rate but a significant drop in isoselectivity (91% conversion, P_i = 0.59). Furthermore, either enantiomer (*S* or *R*) gave better P_i values than the racemic mixture. Overall, it was established that EWGs were significant in producing high rates, as observed previously for aluminium salen initiators, and that the size and asymmetric steric shielding at *ortho*-phenolate sites is important.

In the literature of indium Schiff base initiators, the original ligand scaffolds have not been significantly modified. An indium salen initiator, reported by Mehrkhodavandi and co-workers, showed a significant drop in rate and P_i upon changing the ligand backbone from a chiral cyclohexyl to a racemic 2,2'-binaphthyl (BINAP).[4,5] In our group, an indium phosphasalen initiator showed an increase in both rate and P_i upon increasing the size (*tert*-butyl to cumyl (CMe_2Ph)) of the *ortho*-/*para*-phenolate substituents. This was rather different to aluminium salen initiators, which show much lower rates with bulky *ortho*-

substituents.[1] Incorporating EWGs or changing the backbone of indium phosphasalen initiators has not yet been investigated.

4.1.1. Aims

In line with the literature, the two modifications to the hybrid ligand that appear to offer the most significant insights into rate/stereocontrol are increasing the size of *ortho*-phenolate substituents and changing the electronic properties, most notably by introducing EWGs. The *ortho*-phenolate substitution offers understanding of the coordination environment at metal whereas the latter reveals information about its Lewis acidity and alkoxide bond lability, which intrinsically govern rate.

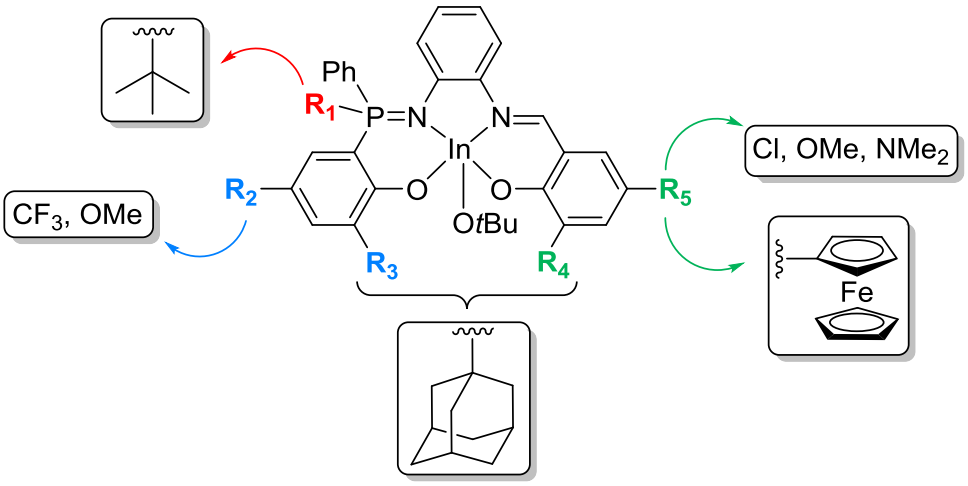

Figure 4.3. Proposed modifications of the indium hybrid initiator at the phosphorus and phenolate substituents.

The proposed modifications for the indium hybrid initiator are summarised in Figure 4.3. First, the *tert*-butyl groups in the *ortho*-phenolate substituent will be replaced by bulkier analogues such as adamantyl groups. Replacement will be targeted at each phenolate, to investigate whether a particular site is preferable and the role (if any) of asymmetry. Next, the substitution of one of the phenyl groups on phosphorus with a *tert*-butyl group will be targeted. The commercial availability of the necessary phosphine makes it a facile

target. Then, EWGs (Cl, CF_3) and electron donating groups (EDGs – OMe, NMe_2) will be incorporated. These substitutions are targeted primarily at positions R_2 and R_5, but depending on the ease of synthetic route, they may also be incorporated at R_3 and R_4.

The switch in monomer selection represents an important step-forward in the ROP of *rac*-LA field. One of the great challenges is the selection between monomers and even enantiomeric forms of monomers. There is not yet any report of a redox-switchable initiator, which produces a change in stereoselectivity upon oxidation/reduction. Incorporation of ferrocene into known highly isoselective initiators, indium phosphasalens, is targeted to accomplish this switching, but the reactivity of ferrocene with the reagents used in the phosphasalen ligand synthesis (*n*-butyl lithium and bromine) may be problematic. Therefore, its incorporation into the hybrid ligand at the R_5 position was targeted as a more viable synthesis.[6–10]

4.2. Ligand Synthesis

4.2.1. Introduction of *ortho*-Adamantyl Substituents

4.2.1.1. Imine Phenolate

The first aim of this chapter was to change the *ortho*-phenolate substituents from *tert*-butyl to bulkier analogues such as adamantyl, cumyl or trityl. All derivatives were attempted but only the adamantyl substitutions will be discussed here. To introduce the adamantyl group in the *ortho*-substituent on the imine phenolate of the ligand, an electrophilic substitution between 4-*tert*-butylphenol and 1-adamantanol under acidic conditions was carried out (Scheme 4.1).[11] The product, 2-adamantyl-4-*tert*-butylphenol was isolated after purification by column chromatography (silica, 25:1 petroleum ether:ethyl acetate) in good yields (64%).

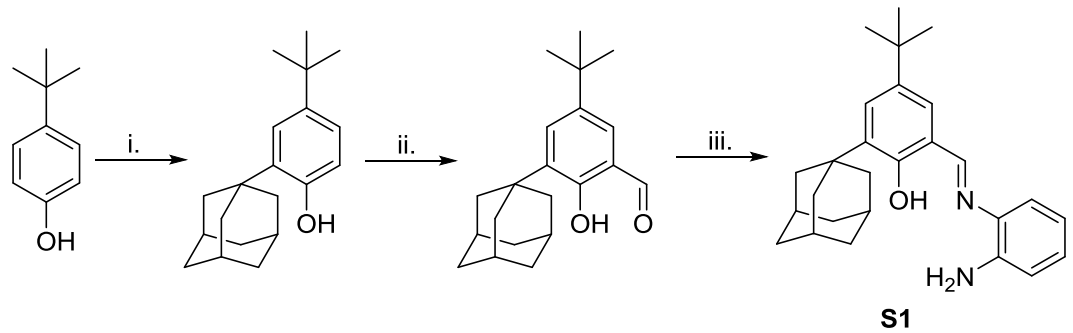

Scheme 4.1. Synthesis of adamantyl precursors on the imine phenolate. Conditions: i. 1-adamantanol (1 equiv.), H_2SO_4, DCM, 273 K; ii. $MgCl_2$ (1.5 equiv), Et_3N (2 equiv.), paraformaldehyde (2 equiv.), THF, 348 K; iii. *o*-phenylenediamine (2 equiv.), EtOH, 298 K.

The reaction between 2-adamantyl-4-*tert*-butylphenol, magnesium chloride ($MgCl_2$), triethylamine (Et_3N) and paraformaldehyde was used to prepare 3-adamantyl-5-*tert*-butyl-2-hydroxybenzaldehyde.[12] The product was purified by column chromatography (silica, 20:1 *n*-pentane:EtOAc) and isolated as a white solid (45%). The synthesis of the half-salen species was carried out using the procedure discussed in Section 3.2, whereby the aldehyde was reacted with two equivalents of *o*-phenylenediamine in dry EtOH.[13] The

product, **S1**, precipitated from solution as a yellow solid and was collected in moderate yields (47%). These yields were obtained due to the partial solubility of the product in EtOH, but isolation in this way ensured high product purity (confirmed by elemental analysis).

Half-amine **S1** was reacted in a Kirsanov reaction with 2-(diphenylphosphino)-4,6-di-*tert*-butylphenol, in DCM at 195 K, and using DABCO as a base (Scheme 4.2). Ligand **4.1**, was isolated after precipitation from *n*-hexane in low yields (22%) but with purity as determined by elemental analysis. It was characterised using multinuclear 1D and 2D NMR spectroscopy.

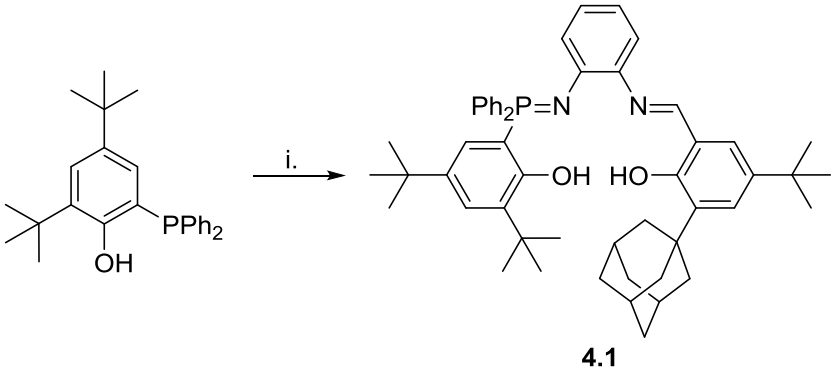

4.1

Scheme 4.2. Synthesis of ligand **4.1**. Conditions: i. (a) Br_2 (1 equiv.), DCM, 195 K, (b) **S1** (1 equiv.), DABCO (1 equiv.), 195 K.

4.2.1.2. Iminophosphorane Phenolate

Introduction of an adamantyl group on the iminophosphorane phenolate of the hybrid ligand began with the addition of a bromide group to 2-adamantyl-4-*tert*-butylphenol (Scheme 4.3). This was carried out by addition of one equivalent of Br_2 to the phenol, the product, **S2**, was then isolated after washing with water in good yields (77%). The phosphorylation reaction, to give product **S3**, was carried out by, first, dehalogenation, using 2.1 equivalents of *n*-BuLi (1.6 M) at 195 K, followed by addition of one equivalent of chlorodiphenylphosphine ($ClPPh_2$), also at 195 K. The $^{31}P\{^1H\}$ NMR spectrum ($CDCl_3$) of

the crude reaction mixture showed a major species with two doublets at 116.7 and -20.8 ppm and a minor species with a singlet at -30.1 ppm, corresponding to the product. The species corresponding to the two doublets was the phosphinite product, whereby a PPh_2 group was covalently bound to the phenolate oxygen (hence the J_{PP} = 136.2 Hz being observed). The O-PPh_2 bond of this side product was cleaved, by reaction with excess acetic acid, for three hours, at room temperature and crystallisation from MeOH to give **S3**, albeit in low overall yields (21%).

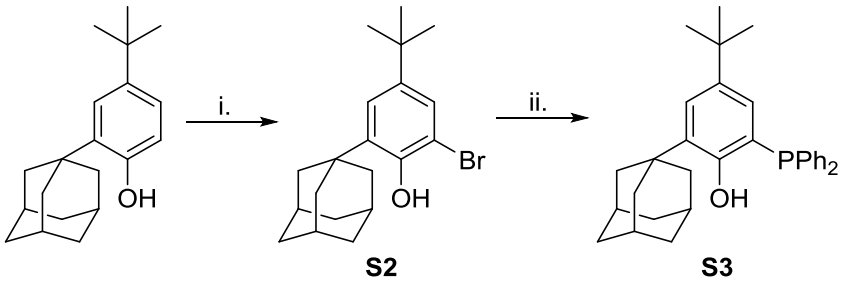

Scheme 4.3. Synthesis of adamantyl precursors on the iminophosphorane phenolate. Conditions: i. Br_2 (1 equiv.), DCM, 298 K; ii. (a) *n*-BuLi (2.1 equiv), Et_2O, 195 K, (b) $ClPPh_2$, 195 K.

A Kirsanov reaction between **S3** and 2-((2-aminophenylimino)methyl)-4,6-di-*tert*-butylphenol was carried out, at 195 K, using DABCO as a base. A solid product was precipitated from *n*-hexane and the $^{31}P\{^1H\}$ NMR spectrum ($CDCl_3$) showed two signals at 40.8 ppm and 20.4 ppm, corresponding to the phosphonium bromide and deprotonated ligand (Figure 4.4). The addition of HCl, in Et_2O (2M), to a small amount of the collected solid, in C_6D_6, resulted in a single resonance at 40.8 ppm which was due to the quantitative conversion to the phosphonium halide product. Attempts to repeat this acidification on a larger scale were not successful due to the acidic reactant being sensitive to trace water in the collected product. Instead, $K(N(SiMe_3)_2)_2$ was added to fully deprotonate both derivatives of the ligand, yielding the potassium salt of the ligand, **4.2** (Scheme 4.4) The ratio of the two ligands was calculated from the $^{31}P\{^1H\}$ NMR spectrum,

then by accounting for the different equivalents of base required for each derivative (three equiv. for the phosphonium bromide and two for the deprotonated neutral) an accurate amount of the base was used.

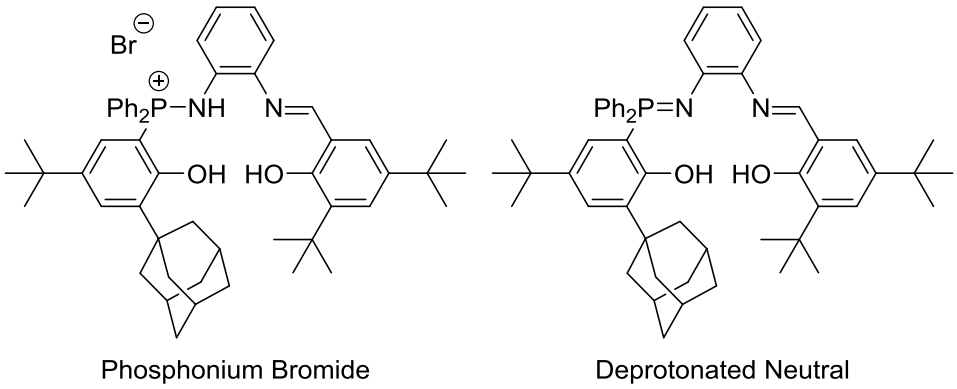

Figure 4.4. The two ligand derivatives formed during the Kirsanov reaction with **S3**.

The full deprotonation of both derivatives of the ligand was confirmed by a single resonance in the $^{31}P\{^{1}H\}$ NMR spectrum at 12.2 ppm (d_8-THF). The salts were removed by centrifugation and ligand **4.2** was isolated by precipitation from a THF/*n*-hexane solution at 243 K. It was characterised by multinuclear NMR spectroscopy and elemental analysis.

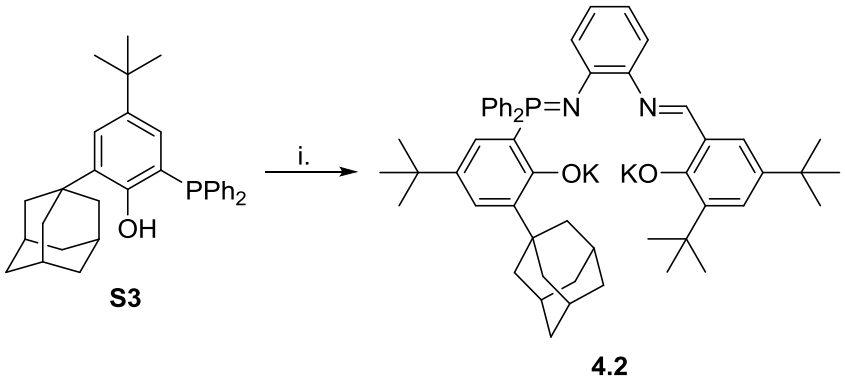

Scheme 4.4. Synthesis of ligand **4.2**. Conditions: i. (a) Br_2 (1 equiv.), DCM, 195 K, (b) **S1** (1 equiv.), DABCO (1 equiv.), 195 K, (c) $KN(SiMe_3)_2$ (1.2 equiv.), THF, 298 K.

A Kirsanov reaction with **S1** and **S3** was attempted to synthesise the ligand containing adamantyl substituents at both *ortho*-phenolate positions. As observed during the synthesis of **4.2**, two products formed after the Kirsanov reaction ($^{31}P\{^{1}H\}$ ($CDCl_3$): 19.4

and 40.9 ppm), therefore the mixture was deprotonated using $KN(SiMe_3)_2$, in THF. A single product was not obtained (as evident from the $^{31}P\{^1H\}$ NMR spectrum of the reaction mixture) and attempts to isolate a single species by crystallisation were not successful. Some crystals were isolated and single crystal X-ray diffraction showed a dimer of the deprotonated salen ligand, with adamantyl groups at both *ortho*-phenolate substituents, coordinated through two potassium atoms and with two bound THF molecules at each one of the potassium atoms (Figure 4.5). The presence of the salen derivative of the ligand implies that hydrolysis of **S1** occurred in the Kirsanov reaction.

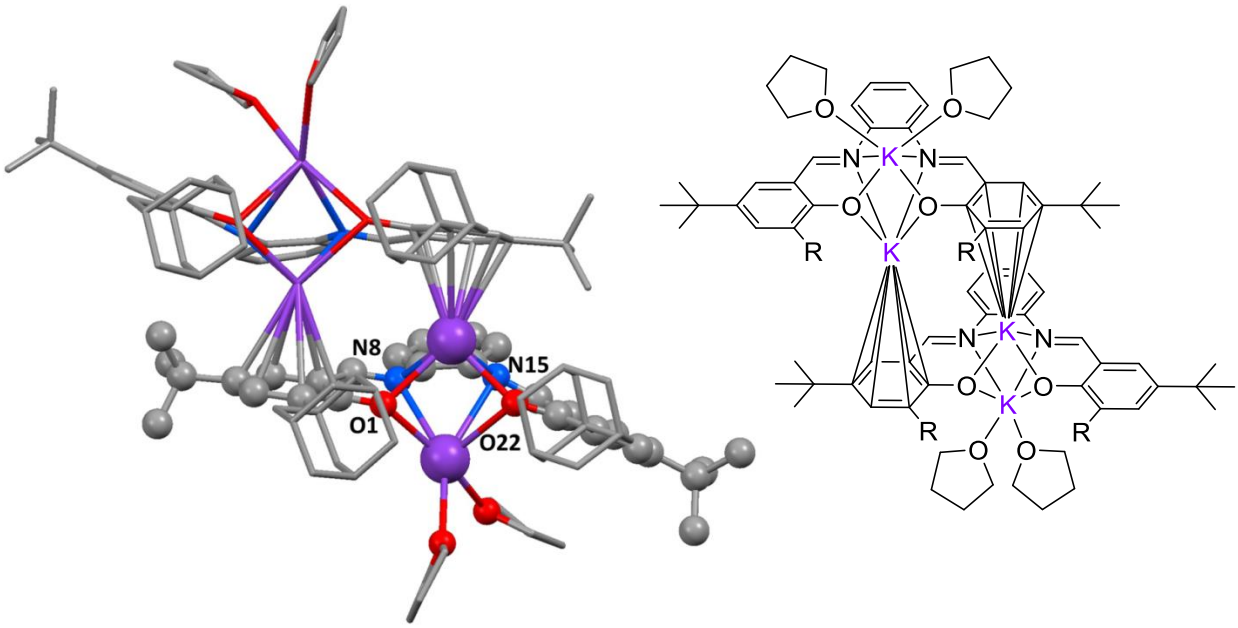

Figure 4.5. Ball and stick representation of the side product obtained in the attempted synthesis of doubly *ortho*-adamantyl-substituted hybrid ligand (H-atoms omitted for clarity, R = Adamantyl).

4.2.2. Varying the Substituent at Phosphorus

Using commercially available chloro(*tert*-butyl)phenylphosphine, **S4** was synthesised in a phosphorylation reaction from 2-bromo-4,6-di-*tert*-butylphenol (Scheme 4.5). The product was collected as clear crystals, after crystallisation, from MeOH, in moderate yields (41%). **S4** was reacted in a Kirsanov reaction with 2-((2-aminophenylimino)methyl)-4,6-di-*tert*-butylphenol to synthesise hybrid ligand, **4.3**, with two different phosphine substituents. Ligand **4.3** was isolated in its deprotonated neutral form by precipitation from *n*-pentane in a yield of 35%. It was characterised by multinuclear NMR spectroscopy and elemental analysis.

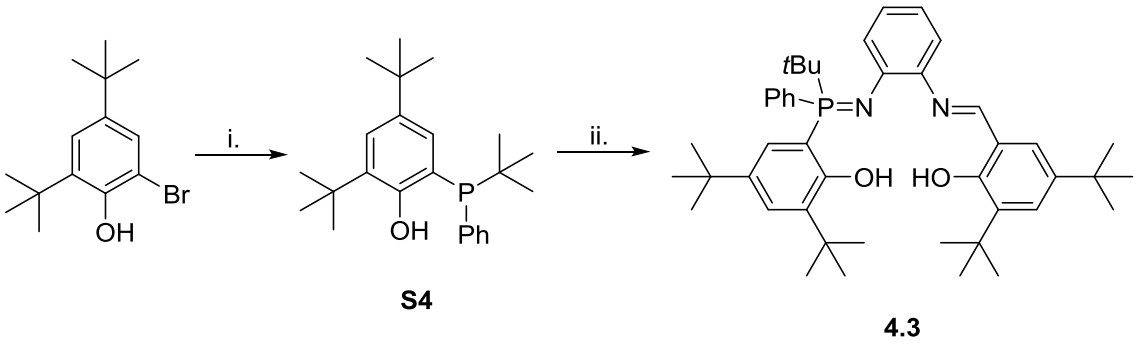

Scheme 4.5. Synthesis of precursor **S4** and ligand **4.3**. Conditions: i. (a) *n*-BuLi (2.1 equiv), Et_2O, 195 K, (b) ClP(*t*Bu)Ph (1 equiv), 195 K; ii. (a) Br_2 (1 equiv.), DCM, 195 K, (b) 2-((2-aminophenylimino)methyl)-4,6-di-*tert*-butylphenol (1 equiv.), DABCO (1 equiv), 195 K.

4.2.3. Introduction of Electron-Withdrawing Substituents

4.2.3.1. Imine Phenolate

The introduction of electron-withdrawing substituents on the hybrid scaffold was targeted at a number of sites: on the imine phenolate, iminophosphorane phenolate or a combination of both. As a starting point, commercially available 3, 5-dichloro-2-hydroxybenzaldehyde was reacted with two equivalents of *o*-phenylenediamine, in dry EtOH, to form the half-salen **S5** (Scheme 4.6). The reaction was complete within seconds, with the immediate precipitation of the product, as a red solid, in excellent yields (88%).

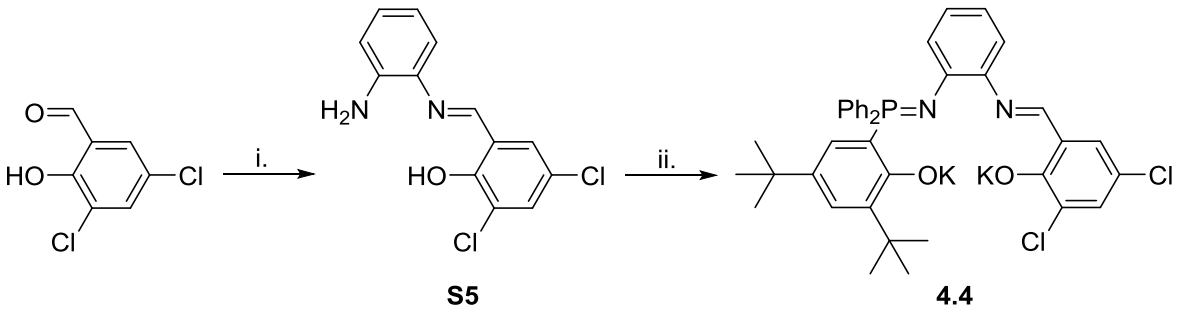

Scheme 4.6. Synthesis of half-salen **S5** and ligand **4.4**. Conditions: i. *o*-phenylenediamine (2 equiv.), EtOH, 298 K; ii. (a) 2-(diphenylphosphino)-4,6-di-*tert*-butylphenol (1 equiv.), Br_2 (1 equiv.), DCM, 195 K (b) **S5** (1 equiv.), DABCO (1 equiv.), 195 K, (c) $KN(SiMe_3)_2$ (0.81 equiv.), THF, 298 K.

2-(Diphenylphosphino)-4,6-di-*tert*-butylphenol was used in the Kirsanov reaction with **S5** as the amine and DABCO as the base. As observed with ligand **4.2**, a mixture of the phosphonium bromide and deprotonated neutral ligand derivatives was obtained, as evident from the $^{31}P\{^1H\}$ NMR spectrum of the solid precipitated from *n*-hexane. The mixture was deprotonated to achieve ligand **4.4** as a potassium salt, by adding $K(N(SiMe_3)_2)_2$ to a solution of the mixture, in THF. Successful deprotonation was confirmed by a single resonance the $^{31}P\{^1H\}$ NMR spectrum at 12.6 ppm (d_8-THF). The product was isolated as a yellow solid, in a low overall yield across the two steps of 26%. Ligand **4.4** was characterised by multinuclear NMR spectroscopy and elemental analysis.

4.2.3.2. Iminophosphorane Phenolate

Introduction of an EW-trifluoromethyl (CF_3) group, on the iminophosphorane phenolate was attempted. Starting from 4-(trifluoromethyl)phenol, the first step was to install a *tert*-butyl group in one of the *ortho*-positions.[14] This was carried out by an electrophilic aromatic substitution using *tert*-butanol and H_2SO_4, in MeOH. After purification of the product by column chromatography (silica, 1:1 DCM:*n*-pentane), the obtained product was not pure by NMR spectroscopy, with a large mixture of side-products still present and the highest possible yield for the product being ~5%. Despite carrying out the

reaction on a large scale, it clearly not a viable synthetic route for introduction of EWGs on the iminophosphorane phenolate.

4.2.4. Introduction of Electron-Donating Substituents

To understand the ligand electronic effects, the introduction of EDGs were also targeted. The synthesis of 5-methoxy-3-*tert*-butyl-2-hydroxybenzaldehyde is reported in the literature.[15] The oxidation/formylation reaction conditions were the same as those described above (Section 4.2.1.), but the solvent was replaced with MeCN to allow for higher reflux temperatures (Scheme 4.7). The product was isolated as a yellow oil, after column chromatography (silica, 5% diethylether in hexanes), in good yields (61%). The half-salen, **S6**, was synthesised by reaction of the product with two equivalents of *o*-phenylenediamine, in dry EtOH, to yield yellow crystals in moderate yields (49%).

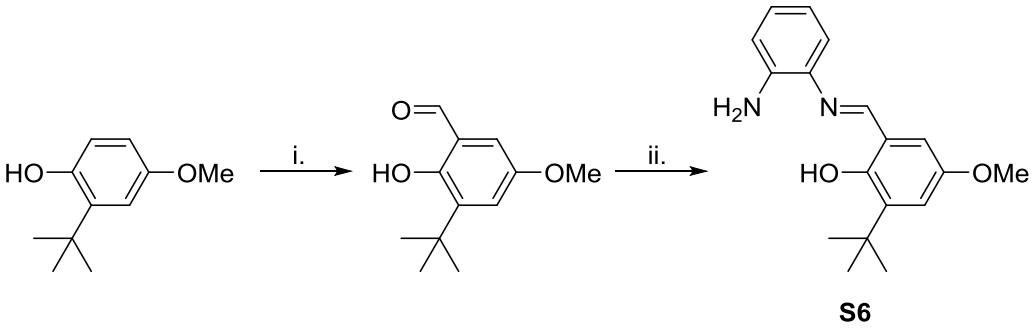

Scheme 4.7. Synthesis of half-salen **S6**. Conditions: i. $MgCl_2$ (1.5 equiv), Et_3N (2 equiv.), paraformaldehyde (2 equiv.), MeCN, 363 K; iii. *o*-phenylenediamine (2 equiv.), EtOH, 298 K.

A Kirsanov reaction with 2-(diphenylphosphino)-4,6-di-*tert*-butylphenol, using **S6** as the amine and DABCO as the base, was carried out but multiple attempts at this reaction did not yield the desired hybrid ligand. Analysis of the isolated products from these reactions showed side products **E**-**G**, as well as the starting material, **S6** (Figure 4.6). Side products **F** and **G** were confirmed by mass spectrometry and ^{1}H NMR spectroscopy, respectively. In one attempt, the starting material, **S6**, was quantitatively re-isolated and the $^{31}P\{^{1}H\}$ NMR spectrum showed a single resonance at 40.8 ppm. This did not correspond to the

phosphinophenol starting material but was likely a phosphonium bromide species, e.g. **E**. The reaction of 2-(diphenylphosphino)-4,6-di-*tert*-butylphenol with one equivalent of Br_2, also formed a product with a single resonance in the $^{31}P\{^1H\}$ NMR spectrum at 40.8 ppm. Analysis by elemental analysis confirmed the presence of **E**.

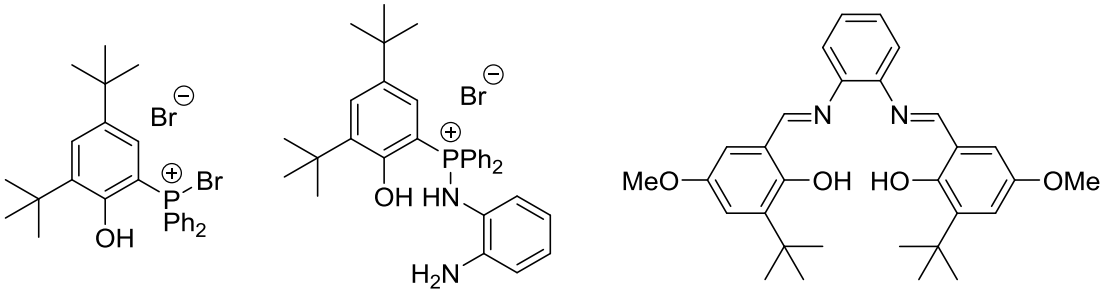

E **F** **G**

Figure 4.6. Structures of observed side products of the Kirsanov reaction using half-salen, **S6**, as the amine.

The presence of side products **F** and **G** may have arisen due to increased imine bond sensitivity to hydrolysis. Despite using dry solvents and reagents, a single equivalent of water may be able to initiate various hydrolysis reactions. The origin of this heightened sensitivity is less obvious, as the electron-donating methoxy group does not activate the imine bond.

To investigate if this reactivity was unique to the methoxy substituent, the dimethylamino derivative was also synthesised (Scheme 4.8). The dimethylamino group was introduced, by reaction of 3-*tert*-butyl-2-hydroxybenzaldehyde with nitric acid, in acetic acid, at 273 K.[16] The product, 5-nitro-3-*tert*-butyl-2-hydroxybenzaldehyde, was isolated by precipitation from water and crystallised from EtOH in good yields (59%). It was then hydrogenated with a palladium on carbon (Pd/C) catalyst in the presence of formaldehyde, to methylate the amine group; enabling isolation of 5-dimethylamino-3-*tert*-butyl-2-hydroxybenzaldehyde in low yields (16%), after purification by column

chromatography (silica, 5:1 *n*-hexane:ethyl acetate). The half-salen, **S7**, was synthesised using the same procedure described above to yield the product in low yields (26%).

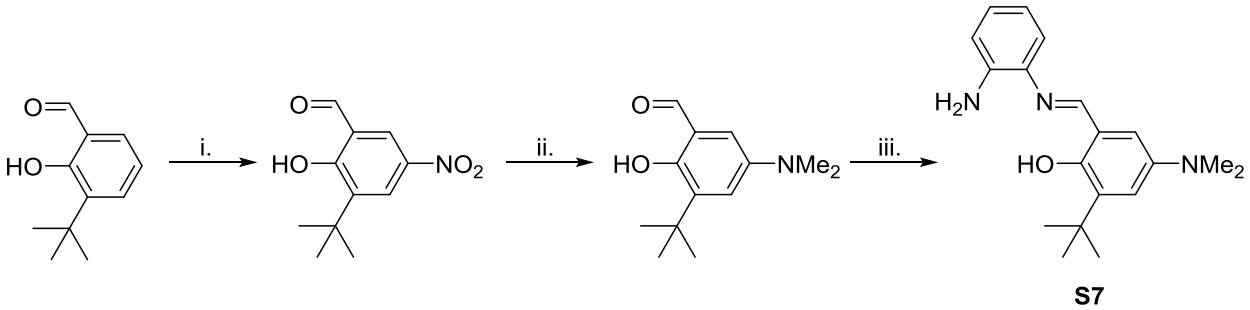

Scheme 4.8. Synthesis of half-salen **S7**. Conditions: i. HNO_3, AcOH, 273 K; ii. H_2 (1 atm.), Pd/C (10%, 0.1 equiv.), formaldehyde (aqueous solution, 37%), EtOH, 298 K; iii. *o*-phenylenediamine (2 equiv.), EtOH.

The Kirsanov reaction using **S7** with 2-(diphenylphosphino)-4,6-di-*tert*-butylphenol and DABCO as a base yielded a single product in the crude $^{31}P\{^1H\}$ NMR spectrum, at 40.8 ppm, which corresponded to side-product, **E**. The product was further analysed using ^1H NMR spectroscopy and it was found that **S7** had fully hydrolysed to yield the full salen ligand. Therefore, it can be concluded that the imine sensitivity is not a characteristic unique to the methoxy substituent and that substitution with EDGs appears to be more challenging.

4.2.5. Introduction of a Redox-Switchable Substituent

There are a number of routes to covalently bond ferrocene to phenol rings, such as Sonogashira and Suzuki cross-coupling reactions, but a Negishi cross coupling was chosen in this instance.[10] A Negishi reaction couples halides with organozinc compounds.[7] 3-*tert*-Butyl-2-hydroxybenzaldehyde was reacted with iodine monochloride, in acetic acid (1 M) to form 3-*tert*-butyl-5-iodosalicyaldehyde (Scheme 4.9).[17] Yields were low (18%), but the reaction could be carried out on large scales, therefore, sufficient product was obtained (~5-6 g) for subsequent reactions. The organozinc reagent for the cross-coupling was prepared by first, isolation of monolithioferrocene.[9] This was carried out by reaction of

ferrocene with two equivalents of *t*-butyllithium (1.7 M in *n*-pentane) in THF at 195 K, the monolithioferrocene was then precipitated using *n*-hexane and collected by filtration.[9] Despite its high moisture sensitivity, it was stored for months in the glovebox freezer and was collected in a good yield (7.80 g, 65 %).

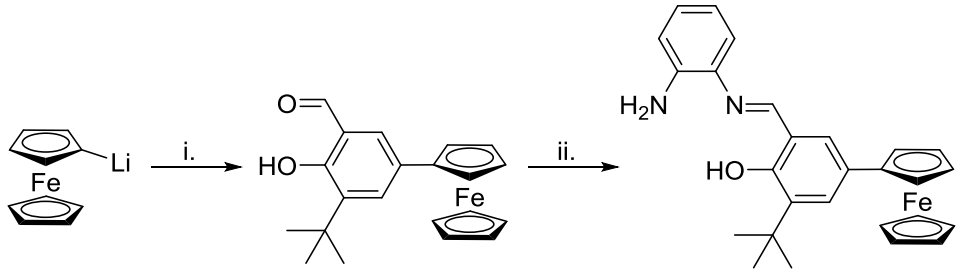

S8 **S9**

Scheme 4.9. Synthesis of ferrocene half-salen **S9**. Conditions: i. (a) Monolithioferrocene (1 equiv.), $ZnCl_2$ (1 equiv.), THF, 195 K, (b) 3-*tert*-butyl-5-iodosalicyaldehyde (0.5 equiv.), $Pd(PPh_3)_4$ (0.1 equiv.), THF, 333 K; ii. *o*-phenylenediamine (2 equiv.), EtOH, 298 K.

Ferrocenyl zinc chloride was then prepared *in situ* by reaction of one equivalent of monolithioferrocene with one equivalent of zinc chloride ($ZnCl_2$), in THF, at 195 K. This reaction yielded the ferrocenyl zinc chloride species, which was immediately added to a THF solution of 3-*tert*-butyl-5-iodosalicyaldehyde with the catalyst, palladium tetrakis(triphenylphosphine) [$Pd(PPh_3)_4$]. The reaction was then heated to reflux, for 24 hours, and the product, **S8**, was isolated by column chromatography (silica 3:7 DCM:*n*-hexane) in moderate yields (48%).[10] Half-salen, **S9**, was prepared using the same procedure outlined above and obtained in low yields (22%).

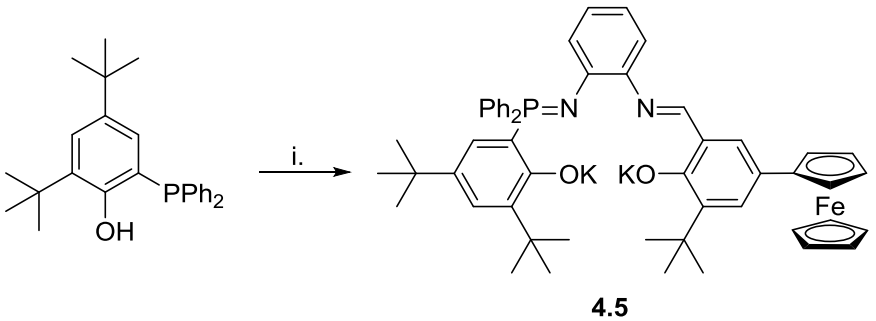

4.5

Scheme 4.10. Synthesis of ligand **4.5**. Conditions: i. (a) 2-(diphenylphosphino)-4,6-di-*tert*-butylphenol (1 equiv.), Br_2 (1 equiv.), DCM, 195 K (b) **S9** (1 equiv.), DABCO (1 equiv.), 195 K, (c) $KN(SiMe_3)_2$ (0.60 equiv.), THF, 298 K.

A Kirsanov reaction with 2-(diphenylphosphino)-4,6-di-*tert*-butylphenol, using **S9** as the amine and DABCO as the base, resulted in two products, the phosphonium bromide ligand and the deprotonated neutral ligand. This was evident from two resonances in the $^{31}P\{^{1}H\}$ NMR spectrum at 20.9 and 40.8 ppm (Scheme 4.10). Initial attempts to crystallise this mixture, from *n*-hexane at 243 K, gave crystals suitable for X-ray diffraction. The structure was the deprotonated neutral ligand (Figure 4.7). These crystals were also analysed by ^{1}H and $^{31}P\{^{1}H\}$ NMR spectroscopy and (as expected) showed a singlet 20.9 ppm. The original ligand mixture was deprotonated, using $KN(SiMe_3)_2$, to yield **4.5** as the potassium salt. It was characterised by multinuclear NMR spectroscopy and elemental analysis.

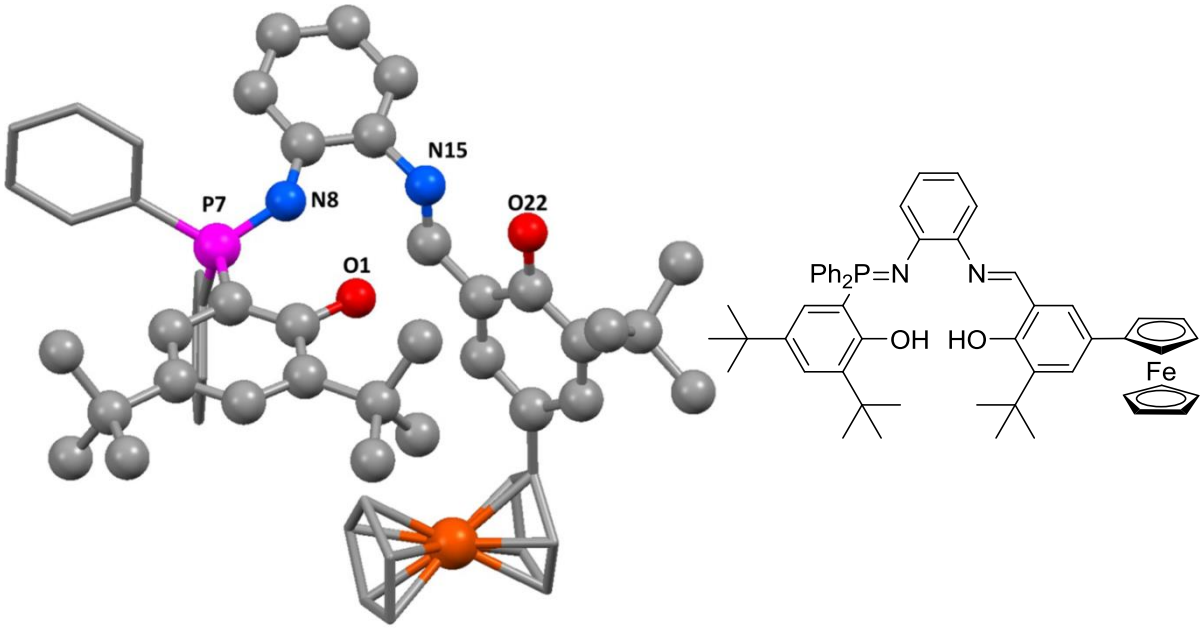

Figure 4.7. Ball and stick representation of deprotonated neutral derivative of ligand **4.5** (H-atoms omitted for clarity. See Appendix for complete bond lengths and angles).

4.3. Initiator Synthesis

4.3.1. Ligands 4.1-4.4

The coordination of protic ligands **4.1** and **4.3** to indium (III) followed the same procedure described in Chapter 3. Deprontation was carried out using two equivalents of $KN(SiMe_3)_2$, followed by addition of one equivalent of indium(III) chloride ($InCl_3$). Finally, addition of one equivalent of potassium *tert*-butoxide (KO*t*Bu) yielded the indium *tert*-butoxide initiators, **4.6** and **4.8**. The potassium ligands, **4.2** and **4.4**, did not require a deprotonation step; and rather were reacted with one equivalent of $InCl_3$, followed by one equivalent of potassium *tert*-butoxide to yield initiators **4.7** and **4.9**. All initiators, **4.6**-**4.9** were purified by crystallisation from THF/*n*-hexane solutions, at 343 K, and the purity was confirmed using elemental analysis (Scheme 4.11).

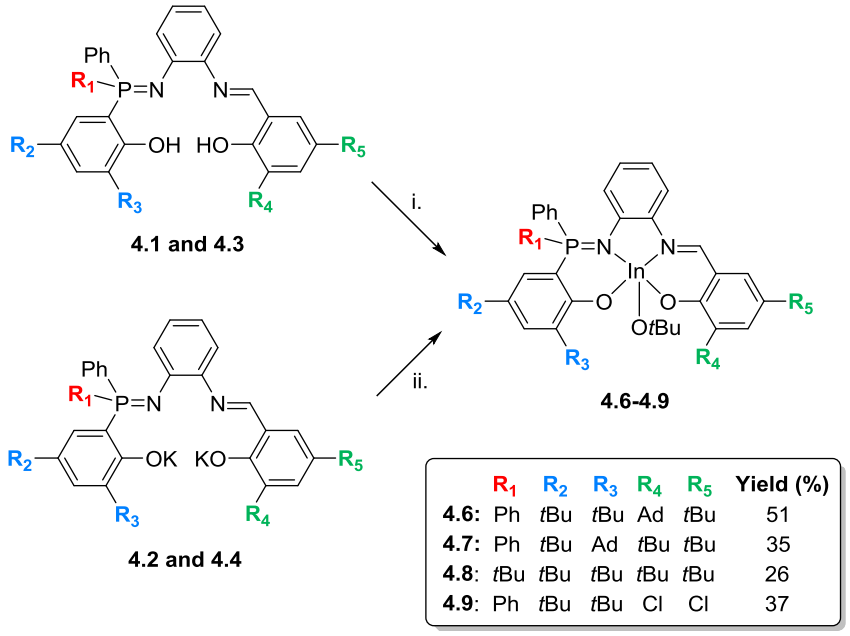

	R_1	R_2	R_3	R_4	R_5	Yield (%)
4.6:	Ph	*t*Bu	*t*Bu	Ad	*t*Bu	51
4.7:	Ph	*t*Bu	Ad	*t*Bu	*t*Bu	35
4.8:	*t*Bu	*t*Bu	*t*Bu	*t*Bu	*t*Bu	26
4.9:	Ph	*t*Bu	*t*Bu	Cl	Cl	37

Scheme 4.11. Synthesis of initiators **4.6**-**4.9**. Conditions: i. (a) $KN(SiMe_3)_2$ (2 equiv,), THF, 298 K, (b) $InCl_3$ (1 equiv.), THF, 298 K, (c) KO*t*Bu (1 equiv.), THF, 298 K; ii. (a) $InCl_3$ (1 equiv.), THF, 298 K, (b) KO*t*Bu (1 equiv.), THF, 298 K.

All initiators were characterised using multinuclear NMR spectroscopy. For initiators **4.6** and **4.7**, featuring adamantly groups, differences in the ^1H chemical shifts were observed

at the phenolate (**A**, **B**, **H** and **I**), imine (**G**) and *ortho*-phenyl phosphorus protons in the ^{1}H NMR spectra (Figure 4.8). The differences were likely a result of distortions to accommodate the increased steric hindrance at metal and increased electron donation of the adamantyl group.

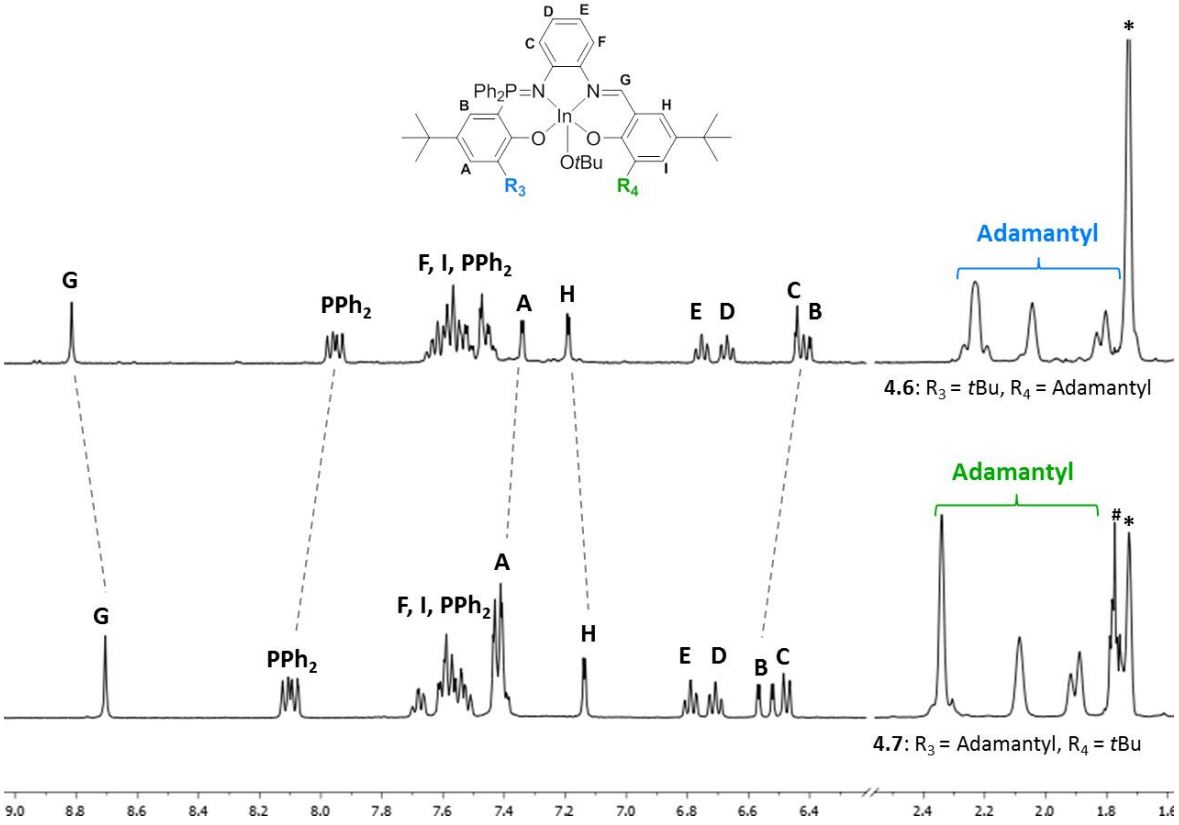

Figure 4.8. ^{1}H NMR spectra of initiators **4.6** (top) and **4.7** (bottom) (d_8-THF*, 400 MHz, 298 K, residual solvent#. *tert*-Butyl region omitted for clarity.)

All initiators were monomeric, in THF, as observed by DOSY NMR, where a correlation of the calculated molecular weight and observed molecular weight was found. For initiator **4.7**, crystals suitable for X-ray diffraction experiments were grown from a saturated solution of **4.7** in THF/*n*-hexane at 243 K (Figure 4.9). The hydrodynamic radius from the solid-state structure was compared with the value determined by DOSY NMR and there was good agreement between the two (r_H $^{THF\text{-}d8}$ = 5.86 Å and r_H $^{solid\text{-}state}$ = 7.04 Å). Small errors in these calculations arise from assuming a spherical shape in the solution state. Initiator **4.7** shows a pentacoordinate indium centre with a τ = 0.25, i.e. with a square-

based pyramidal geometry. There is a some ligand distortion, with the angle between the two phenolate groups being 71.7 °, which may be responsible for the differences observed in the ^{1}H NMR spectra between initiators **4.6** and **4.7**.

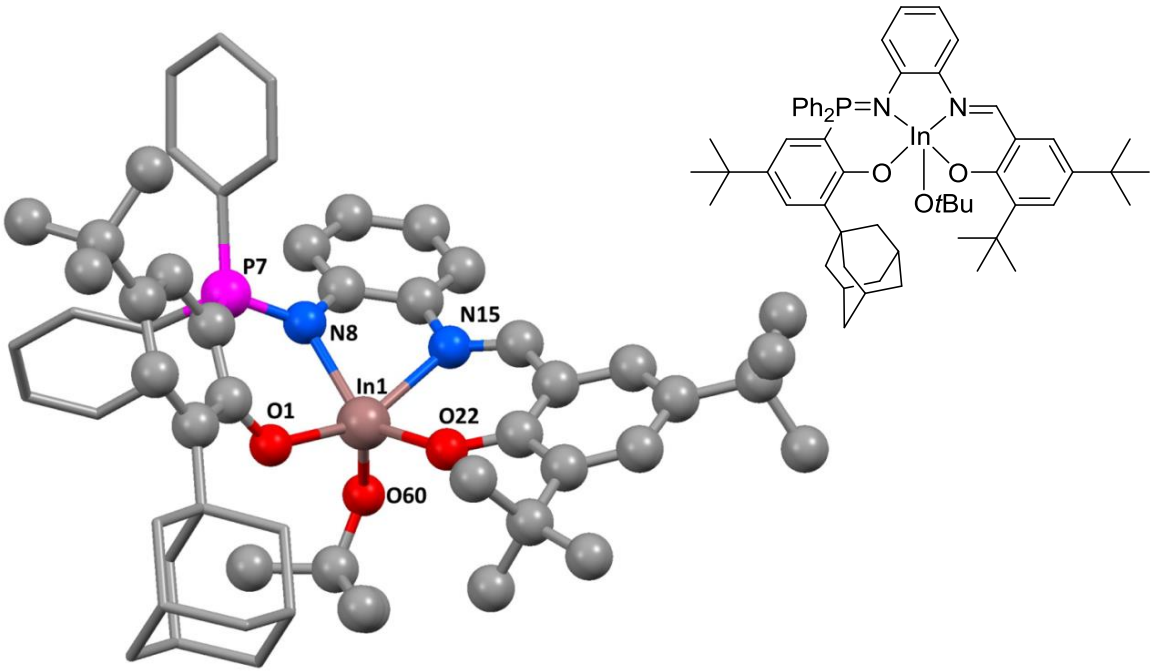

Figure 4.9. Ball and stick representation of initiator **4.7** (H-atoms omitted for clarity. See Appendix for full bond lengths and angles).

The ^{1}H NMR spectrum of Initiator **4.8** shows less complexity in the aromatic region and featured a diagnostic doublet at 1.37 ppm, with a $^{3}J_{PH}$ = 15.4 Hz, corresponding to the *tert*-butyl group attached to phosphorus (Figure 4.10). Further evidence for the successful synthesis of **4.8** was the resonance at 0.96 ppm, corresponding to the *tert*-butoxide co-ligand.

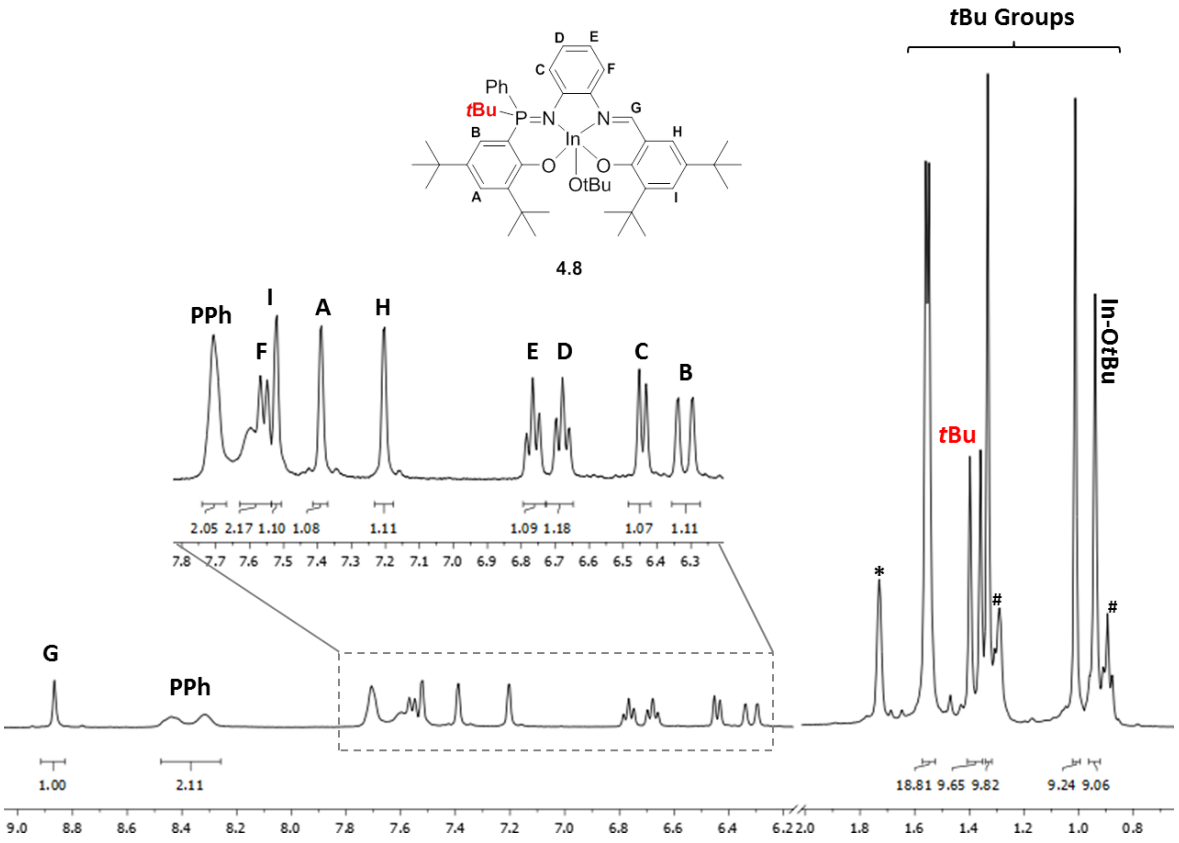

Figure 4.10. ^{1}H NMR spectrum of initiator **4.8** (d_8-THF*, 400 MHz, 298 K, residual solvent$^{\#}$).

Similarly, for initiator **4.9**, the *tert*-butoxide co-ligand resonance was observed at 1.10 ppm (Figure 4.11). The presence of electron-withdrawing chloride substituents does not give rise to any particular changes to ligand, imine or phenolate resonances (**G**, **H** and **I**). Unfortunately, initiator **4.9** was not sufficiently soluble in d_8-THF for NMR analysis, but a spectrum was collected in $CDCl_3$ due to increased solubility. Initiator **4.9** was sufficiently soluble for polymerisation studies in THF.

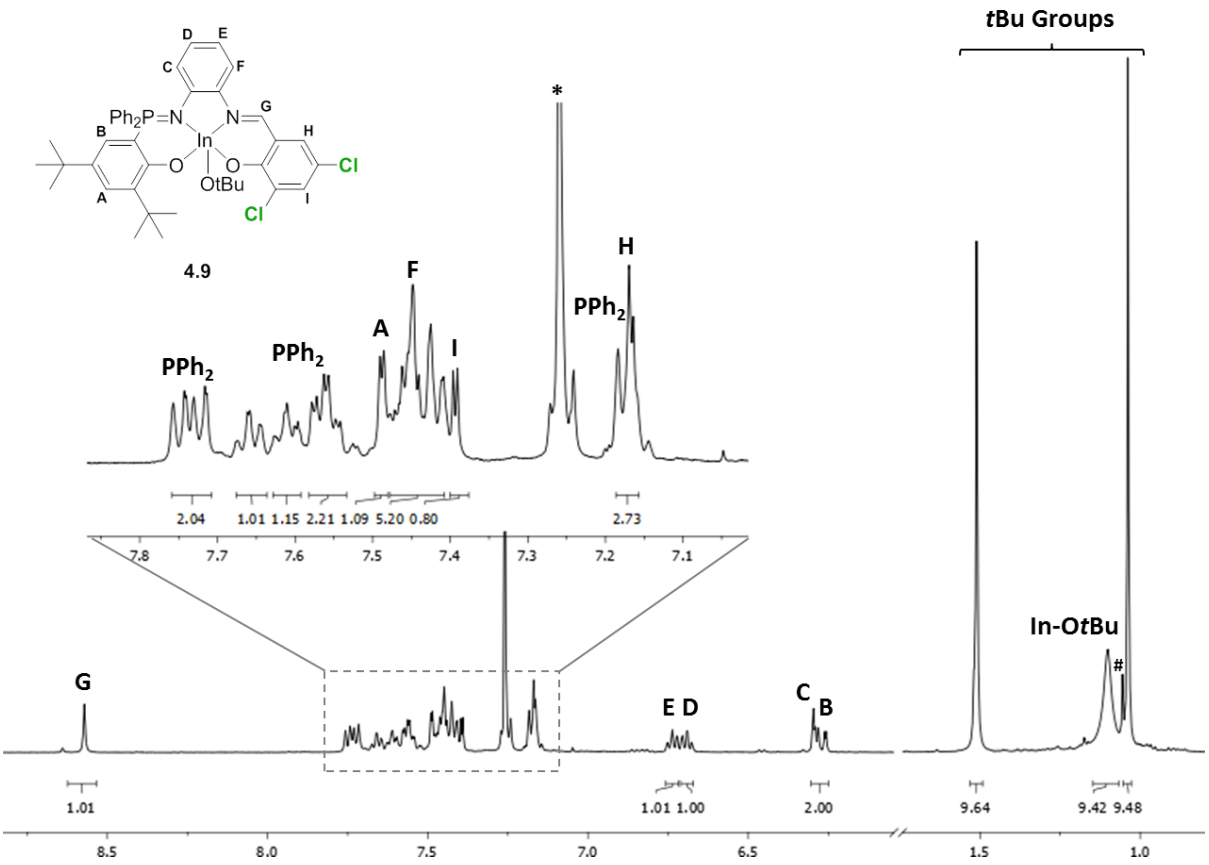

Figure 4.11. ^{1}H NMR spectrum of initiator **4.9** ($CDCl_3$*, 400 MHz, 298 K, residual solvent$^{\#}$).

4.3.2. Ligand 4.5

Ligand **4.5** was reacted with one equivalent of $InCl_3$, in THF (Scheme 4.12). The reaction was carried on a small scale (50 mg of **4.5**), due to the low yields obtained in previous steps. For electrochemical studies, the indium chloride complex, **4.10**, was preferentially isolated over the indium *tert*-butoxide complex, due to its higher stability to hydrolysis. A small quantity of product was isolated from the complexation step (25 mg, 50% yield), which was subsequently used in electrochemical studies, for characterisation and purity testing (elemental analysis).

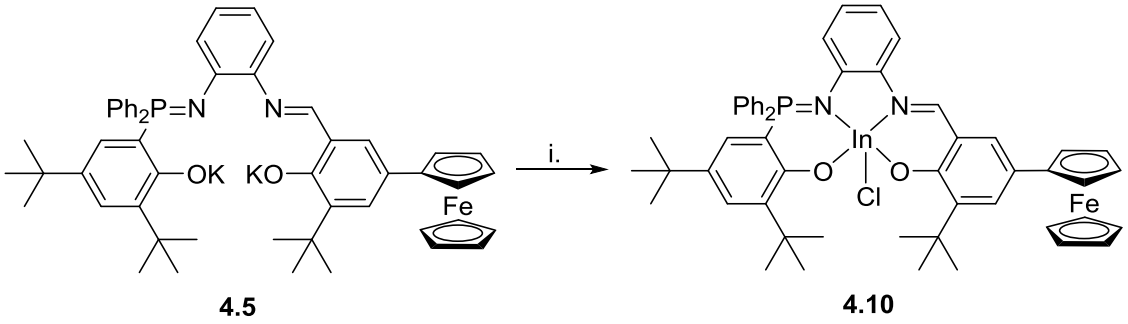

4.5 **4.10**

Scheme 4.12. Synthesis of complex **4.10** using ligand **4.5**. Conditions: i. $InCl_3$ (1 equiv), THF, 298 K.

Complex **4.10** was characterised by multinuclear NMR spectroscopy and elemental analysis. (Figure 4.12). Crystals suitable for single X-ray diffraction were grown from a saturated solution of complex **4.10** in THF/*n*-hexane at 253 K. They crystallised in a triclinic P-1 space group in an octahedral geometry, with the tetradentate ligand in a *trans*-configuration and the chloride and THF ligands being mutually *trans* to one another (Figure 4.13).

The ligand **4.5** has an angle between the two-phenolate rings of 85.61 ^{o} and between the imine phenolate ring and bonded cyclopentadienyl (Cp) ring of ferrocene of 32.72 ^{o}. The distortion between the phenolate rings is greatly reduced upon coordination to indium to 18.08 ^{o}, whereas the imine phenolate and Cp ring angle remains similar (30.67 ^{o}).

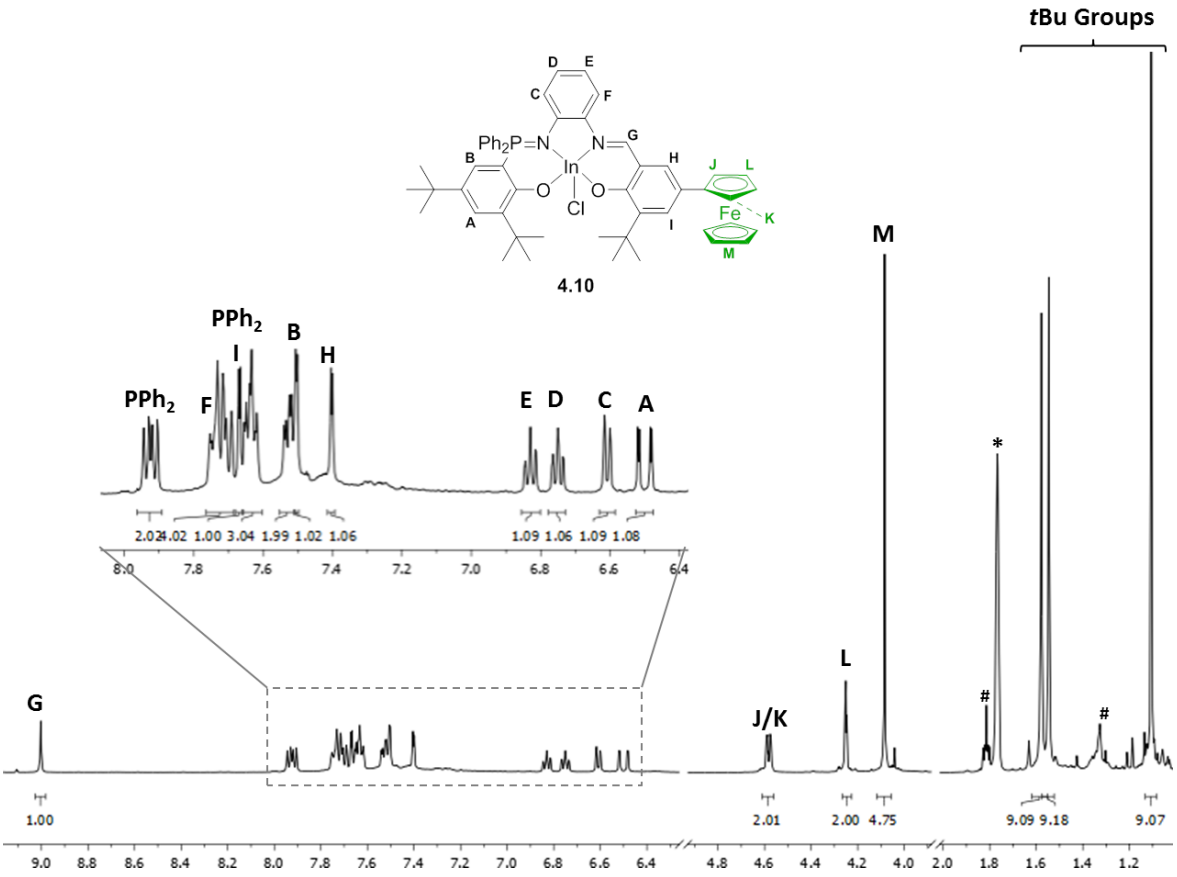

Figure 4.12. ^{1}H NMR spectrum of complex **4.10** (d_8-THF*. 400 MHz. 298 K. residual solvent$^{\#}$).

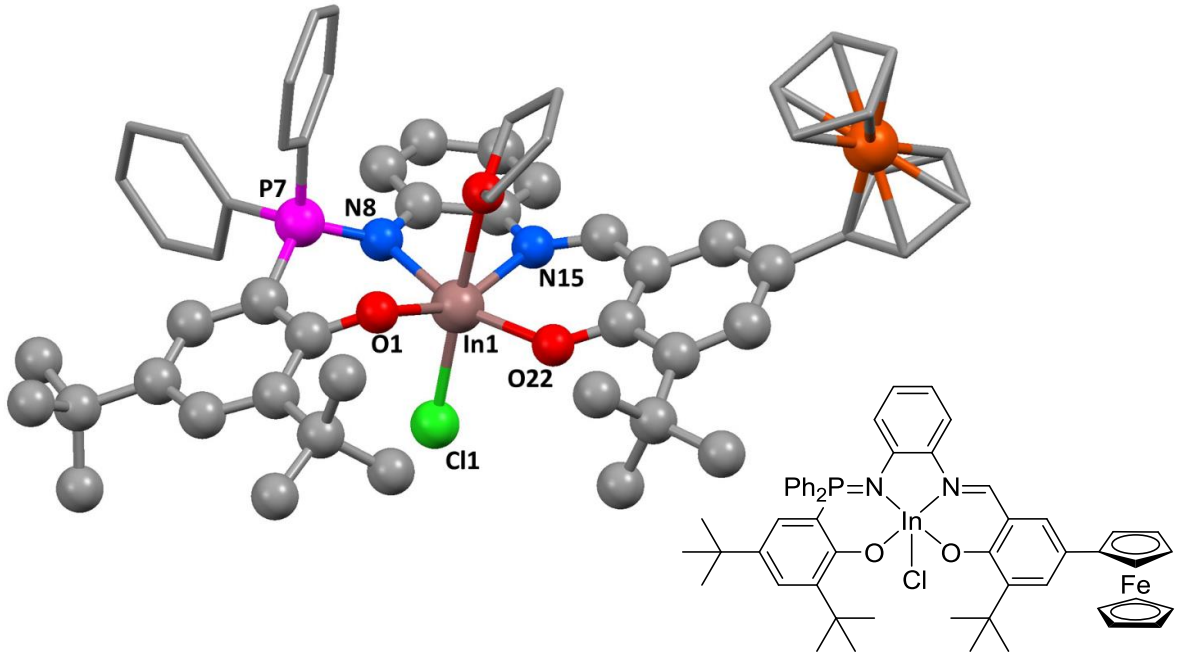

Figure 4.13. Ball and stick representation of complex **4.10** (H-atoms omitted for clarity. See Appendix for full bond lengths and angles).

4.4. Polymerisation Catalysis

Complexes **4.6**-**4.9** were tested as initiators in the ROP of *rac*-LA. The polymerisations were carried out under standard conditions: 298 K, 1 M solution of *rac*-LA in THF and with a catalyst loading of 1 mol %. Reactions were monitored by regular collection of aliquots at regular time intervals. The aliquots were analysed by ^{1}H NMR spectroscopy to determine conversion (%) and by GPC to determine M_n. The key results are summarised in Table 4.1 and compared with the data of the original hybrid initiator **3.8**.

Table 4.1. Polymerisation data using initiators **4.6**-**4.9**.

Entry[a]	Initiator	Conv. (%)[b]	*t* (mins)	k_{obs} (x 10^{-3} s^{-1})[c]	M_n (g mol^{-1})[d]	M_n^{calc} (g mol^{-1})	Đ[d]	P_i[e]
1	**4.6**	95	45	1.55 ± 0.05	12900	13700	1.04	0.73 ± 0.04
2	**4.7**	98	45	0.87 ± 0.02	12100	14100	1.08	0.70 ± 0.05
3	**4.8**	93	15	4.89 ± 0.58	16400	13400	1.03	0.75 ± 0.04
4	**4.9**	93	2	19.2 ± 0.24	14900	13400	1.02	0.61 ± 0.04
5	**3.8**	99	20	2.72 ± 0.19	15600	13800	1.02	0.71 ± 0.02

[a]Polymerisation conditions: [Initiator]:[LA] = 1:100, [LA] = 1 M, THF, 298 K [b]Determined by integration of the methine region of the ^{1}H NMR spectrum (LA, 5.00 - 5.07 ppm; PLA, 5.10 – 5.24 ppm). [c]Measured by determining the gradients of the plots of ln{$[LA]_0/[LA]_t$} vs. time. [d]Determined by gel-permeation chromatography in THF, using multiangle laser light scattering (GPC-MALLS). [e]Determined by integrating the average P_i values obtained for each tetrad signal in the methine region of the homonuclear-decoupled ^{1}H NMR spectrum.

4.4.1. Polymerisation Kinetics

All initiators **4.6**-**4.9** displayed pseudo first-order kinetics, as evident from linear fits to plots of ln($[LA]_0/[LA]_t$) vs. time (Figure 4.14). Initiator **4.9** exhibited the fastest rate, reaching high conversions within 2 minutes (Entry 4, Table 4.1). Initiator **4.8**, with a *tert*-butyl group replacing one of the phenyl groups at phosphorus, was the next fastest, reaching high conversions in 15 minutes (Entry 3). The adamantyl-containing initiators, **4.6** (Entry 1) and **4.7** (Entry 2), were slower than the original hybrid initiator, **3.8**, taking

45 minutes to reach high conversions. Overall, comparing all initiators, the differences in rate were **4.7** < **4.6** < **3.8** < **4.8** < **4.9**.

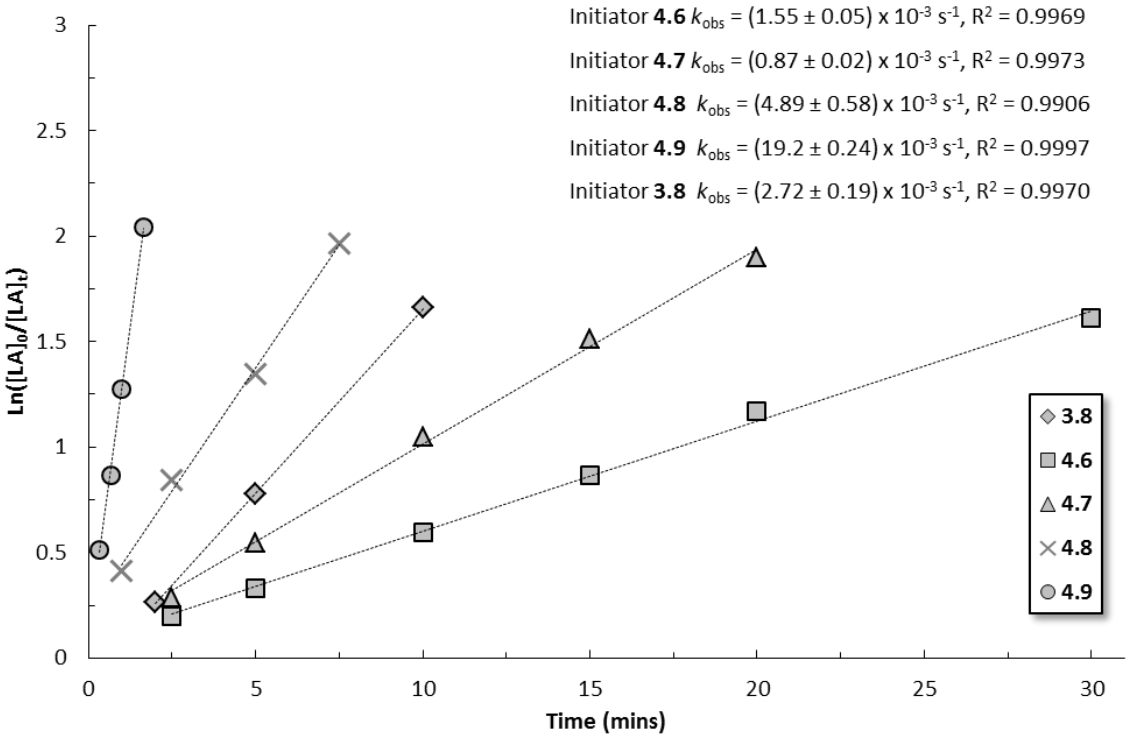

Figure 4.14. Plot of $\ln([LA]_0/[LA]_t)$ vs time of initiators **4.6**-**4.9**. Conditions: [I]:[LA] = 1:100, [LA] = 1M, THF, 298 K.

4.4.2. Polymerisation Control

All initiators **4.6**-**4.9** displayed excellent polymerisation control with linear increase of M_n against % conversion, good correlation between calculated and experimental M_n values and narrow dispersities throughout. It is assumed from the degree of control that there are little/no transesterification reactions taking place. Especially for initiator **4.9**, where the rate was very fast, the control was excellent (Figure 4.15).

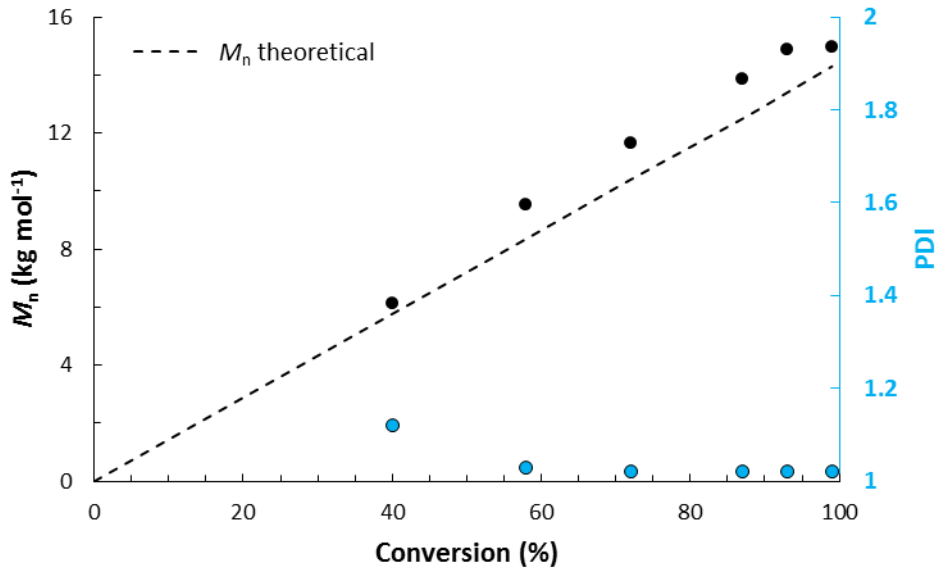

Figure 4.15. Plot of the molecular weight and polydispersity vs. conversion for the polymerisation of *rac*-LA mediated by initiator **4.9**. Conditions: [**4.9**]:[LA] = 1:100, [LA] = 1M, THF, 298 K.

4.4.3. Isoselectivity

The isoselectivity for initiators **4.6**-**4.9** was determined by analysis of the tetrad resonances, of the methine proton, in the deconvoluted homonuclear decoupled $^{1}H\{^{1}H\}$ NMR spectrum. Adamantyl containing initiators **4.6** and **4.7** achieved P_i values = 0.73 and 0.70, respectively. Initiator **4.8**, with *tert*-butyl/phenyl substituents at phosphorus, yielded the highest P_i value of 0.75. Chloride-substituted, initiator **4.9**, obtained a P_i = 0.61, a significant decrease from the other initiators and compared to the original hybrid at P_i = 0.71.

Further analysis of the stereoerrors to determine the mechanism of stereocontrol was challenging. For all initiators, the ratio between tetrads [sis]:[sii]:[iis]:[isi] was approximately 1:2:1:2, which could be due to either CEC or ESC. A CEC mechanism seems more probable as it is the same stereocontrol mechanism observed in the original hybrid initiator.

Table 4.2. Tetrad integrals and corresponding P_i values for initiators **4.6**-**4.8** from their $^1H\{^1H\}$ NMR spectra.

	4.6		**4.7**		**4.8**		**4.8**	
Tetrad	**Integral**	P_i	**Integral**	P_i	**Integral**	P_i	**Integral**	P_i
sis	0.05	0.68	0.06	0.65	0.04	0.70	0.12	0.53
sii	0.11	0.63	0.12	0.61	0.12	0.65	0.12	0.64
iis	0.06	0.84	0.07	0.83	0.05	0.89	0.09	0.76
iii	0.67	0.74	0.60	0.70	0.66	0.75	0.45	0.57
isi	0.11	0.74	0.15	0.69	0.13	0.74	0.22	0.56
Average		**0.73**		**0.70**		**0.75**		**0.61**

4.4.4. Discussion

In Chapter 3, the hybrid ligand when coordinated to indium gave intermediate rates compared to its salen and phosphasalen analogues, but yielded increased isoselectivity (P_i = 0.71 vs. P_i = 0.51 – 0.52). The origin of this stereocontrol was not understood. The aim of this chapter was to modify the hybrid system to target faster rates and higher P_i values (Figure 4.16).

Considering the ROP by rate, increasing the size of the *ortho*-phenolate substituent, the rate was decreased by two- or three-fold (for substitutions at imine or iminophosphorane phenolates, respectively). This behaviour is similar to that exhibited by aluminium salen initiators, but differs from indium phosphasalen initiators, where the rate is increased.[1] For initiator **4.7**, where the adamantyl group is present on the iminophosphorane phenolate, the solid-state structure indicates a distorted ligand environment with the phenolate rings at an angle of 71.7 ^{o}. It may be that steric hindrance at this site restricts or slows the coordination of lactide binding or may hinder access to the insertion transition states.

When replacing one phenyl group on phosphorus with a *tert*-butyl group in initiator **4.8**, a two-fold increase in rate was observed. This might be due to increased electron donation from the *tert*-butyl group perhaps leading to an increased alkoxide bond lability.[18] An electronic rationale seems more likely since there is also an increased steric hindrance with a *tert*-butyl group vs. a phenyl ring which may be expected to reduce the rate.[19]

The addition of electron-withdrawing chloride groups on the imine phenolate in initiator, **4.9**, yielded a seven-fold increase in rate compared to the original hybrid. Aluminium salen initiators also showed similar behaviour with rates increasing as the Lewis acidity of the metal decreased, but these characteristics had not been previously investigated with indium initiators. It therefore shows that, for indium, the same rule applies.

Considering the isoselectivity displayed by each initiator, increasing the steric bulk on the imine phenolate resulted in a small increase in isoselectivity (P_i = 0.73) but on the iminophosphorane phenolate, resulted in a small decrease in isoselectivity (P_i = 0.70). This finding was somewhat unexpected since the indium phosphasalen initiators showed a clear increase in P_i with increasing the size *ortho*-phenolate substituents.[20]

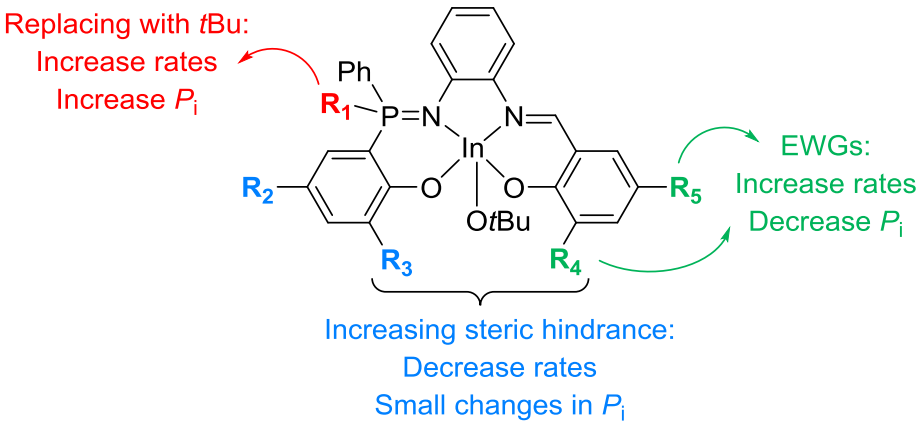

Figure 4.16. Summary of the effects on rate and isoselectivity upon modification of the indium hybrid initiator.

When replacing both imine phenolate substituents with chloride groups, a significant reduction in isoselectivity was observed (P_i = 0.61). Aluminium salen initiators substituted with EWGs showed no change in isoselectivity.[1] It appears that the size of the *ortho*-substituents are, indeed, important in isoselectivity. In the case of initiators **4.6** and **4.7**, ligand distortion may orientate the bulky groups away from the metal centre and limit influence over isoselectivity. Synthesis of an initiator with a *tert*-butyl group in the imine *ortho*-phenolate position and a chloride group in respective *para*-phenolate position would clarify this hypothesis.

Finally, replacing one phosphorus substituent with a *tert*-butyl group resulted in the highest isoselectivity value achieved by an indium hybrid initiator (P_i = 0.75). It is not yet clear how the *tert*-butyl group is located relative to the growing polymer chain and monomer coordination site. Further study of both other unsymmetrical phosphines and attempts to isolate intermediates are recommended.

In conclusion, it was found that EWG groups on the imine phenolate significantly increased polymerisation rates, but also decreases in isoselectivity. Increasing the size of the *ortho*-phenolate substituents did not yield notable changes in either rate or isoselectivity, which was rationalised by ligand distortion orientating these groups away from the active site. The best isoselectivity value (P_i = 0.75) and a small increase in rate was yielded by initiator **4.8**, where the phosphorus substituents featured one phenyl and one *tert*-butyl group.

4.5. Electrochemical Studies*

The electrochemical properties of ferrocene-containing complex **4.10** were investigated to inform its use as as a redox-active initiator. The cyclic voltammetry of complex **4.10** was studied, in THF, using a 0.1 M [nBu$_4$N]PF$_6$ as the supporting electrolyte (Figure 4.17). It displayed a single reversible oxidation [Fe(II)/Fe(III)] at a half-cell potential ($E_{1/2}$) of -0.115 V vs. Fc/Fc$^+$.[21] Thus, complex **4.10** is oxidised at a lower potential than ferrocene, which is to be expected due to the electron-donating properties of the hybrid ligand.

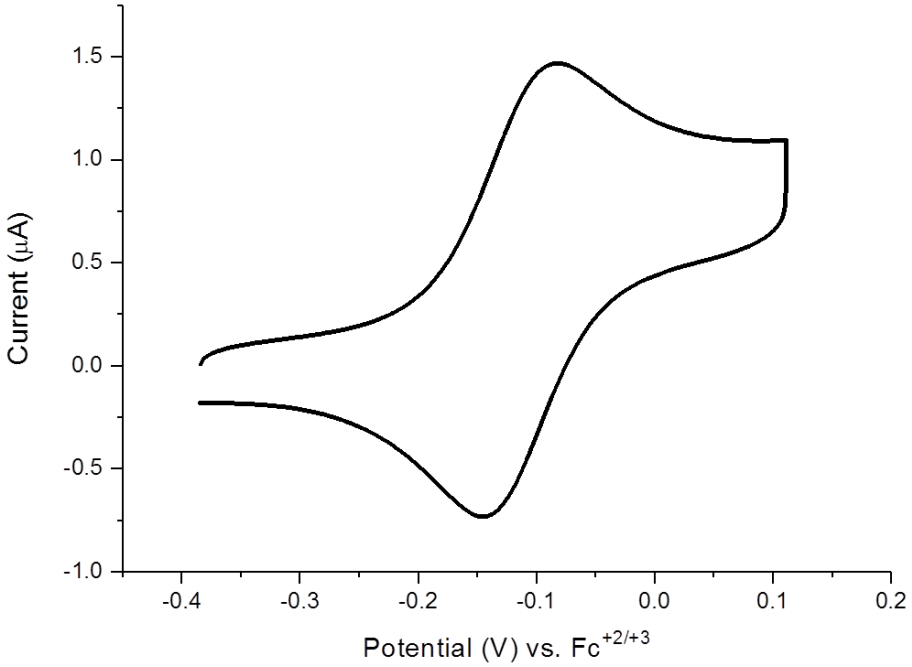

Figure 4.17. Cyclic voltammogram for complex **4.10**. Conditions: 0.1 M [nBu$_4$N]PF$_6$/THF, E vs. [Cp$_2$Fe]/[Cp$_2$Fe]$^+$, corrected for iRs, scan rate 0.01 V s^{-1}.

For a perfect reversible, one-electron exchange in solution, a ΔE value of 59 mV at 298 K is expected, here, ΔE was 61 mV at 0.01 V s^{-1}. Thus, complex **4.10** appears to undergo a reversible one-electron exchange. The reversibility of a system is also indicated by $i_{pc}/i_{pa} \approx 1$; here i_{pc}/i_{pa} = -1.07 at 0.01 V s^{-1}.[22]

* A special thanks goes to Dr Lucy Wilson for her practical and theoretical support in this section.

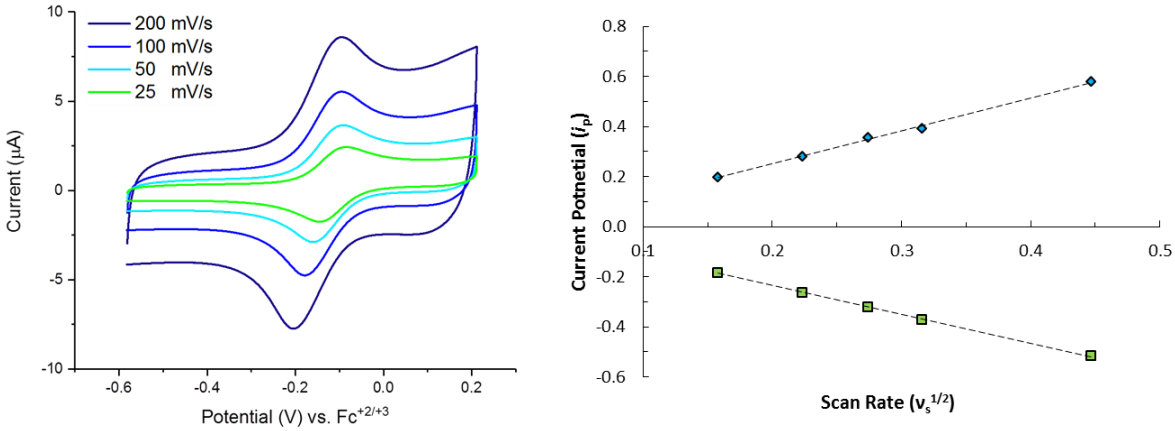

Figure 4.18. Overlay of cyclic voltammograms at different scan rates and plot of scan rate vs. current potential (right) for complex **4.10**. Conditions: 0.1 M [*n*Bu_4N]PF_6/THF, E vs. [Cp_2Fe]/[Cp_2Fe]$^+$, corrected for iRs, scan rate range: 0.025-0.200 V s^{-1}.

The reversibility of the oxidation was reproducible over a range of scan rates, which demonstrated the stability of complex **4.10** (Figure 4.18). At each scan rate, (v_s) the relationship with the current potential (i_p) was analysed and shown to be $i_p \propto v_s^{1/2}$ (Figure 4.18). When i_p vs. $v_s^{1/2}$ is linear, the redox event is diffusion controlled. This is advantageous for future electrochemical switches of ferrocene-containing initiators, as the complex is oxidised in solution (not decomposing at the electrode).

By determining the half-cell potential ($E_{1/2}$), it was possible to also to identify a suitable chemical oxidant/reductant for an *in situ* redox switch. Suitable oxidants and reductants are ferroceniumtetrakis(3,5-bis(trifluoromethyl)phenyl) borate ($FcBAr^F$) and cobaltocene ($CoCp_2$), respectively. It is assumed that these would be suitable for use with a putative indium alkoxide complex, as the alkoxide co-ligand should not greatly change the redox potential.

4.6. Summary and Outlook

4.6.1. Summary

The synthesis of five new hybrid ligands and their precursors were described. Ligands **4.1** and **4.2** featured adamantyl groups in the *ortho*-positions on the imine and iminophosphorane phenolates of the hybrid ligand, respectively. Ligand **4.3** had one phenyl group on phosphorus replaced with a *tert*-butyl group. Ligand **4.4** featured chloride groups in the *ortho*- and *para*- positions on phosphorus on the imine phenolate and ligand **4.5** introduced a ferrocene group in the *para*-position, also on the imine phenolate. The ligand formation step proceeded by two routes: (i) synthesis of the hybrid ligand as described in Chapter 3 *via* a Kirsanov reaction; (ii) further reaction of the Kirsanov reaction mixture to yield the potassium salt of the ligand. Ligands **4.1** and **4.3** were isolated in the deprotonated neutral form and ligands **4.2**, **4.4** and **4.5** were isolated as potassium salts. All ligands were characterised using multi-nuclear NMR spectroscopy and elemental analysis.

Ligands **4.1**-**4.4** were coordinated to indium and the *tert*-butoxide initiators, **4.6**-**4.9** were synthesised. Ligand **4.5**, containing a ferrocene group, was also coordinated to indium, but the indium-chloride complex was preferentially isolated for use in electrochemical studies. All complexes were characterised using multi-nuclear NMR spectroscopy, elemental analysis and X-ray crystallography, where possible.

Initiators **4.6**-**4.9** were tested as initiators in the ROP of *rac*-LA and compared to the original indium hybrid initiator (**3.8**) from Chapter 3. The differences in rate were **4.7** < **4.6** < **3.8** < **4.7** < **4.8**. All initiators displayed excellent polymerisation control with

predictable M_n values, linear increase in M_n with % conversion and narrow dispersities throughout.

Initiators **4.6**-**4.8** produced isotactic PLA, with the highest value (P_i = 0.75) achieved by initiator **4.8**, containing different phosphorus substituents. Interestingly, increasing the size of *ortho*-substituents on either the imine or iminophosphorane phenolates did not have a significant effect on isoselectivity. This is quite different to what was observed using indium phosphasalen initiators and may be associated with ligand distortion. The fastest initiator, **4.9**, yielded a low isoselectivity value (P_i = 0.61), which was attributed to the decreased size of the *ortho*-phenolate substituent.

The electrochemical studies with complex **4.10**, showed a reversible one-electron transfer ($E_{1/2}$ = -0.115 V). As such, chemical oxidants and reductants are recommended for future use with an indium *tert*-butoxide analogue.

4.6.2. Outlook

In this chapter, the hybrid ligand has demonstrated that subtle changes in substituents results in variations of rate and isoselectivity. The most notable increase in rate arose from EWGs on the imine phenolate, but this also gave reduced isoselectivity values. Therefore, a future target would feature a *tert*-butyl group in the *ortho*-phenolate position and a chloride group in the *para*-position on the imine phenolate. Further modifications whereby the electronic properties are changed at the *para*-position on either phenolate and steric bulk is maintained at the *ortho*-position might be expected to allow for high and increased isoselectivity. Unfortunately, due to synthetic issues, the effect of EDGs on either phenolate, or any electronic effects on the iminophosphorane phenolate, could not be investigated. Furthermore, as discussed in the introduction,

changing the backbone to either cyclohexyl or ethylene could also increase isoselectivity, as observed in yttrium phosphasalen initiators.[23] Development of reliable synthetic routes to the half-salen intermediates in the future is suggested as a strategy to improve performance.

There are no reports of modifications on the original indium phosphasalen system other than increasing the size of phenolate substituents.[20] Nonetheless, substitution at this site has resulted in both higher rates and isoselectivites than the hybrid initiators reported in this chapter. Although beyond the scope of this thesis, an investigation into modifying: the electronic properties (incorporation of EWGs and EDGs), the ligand backbone and the phosphorus substituents on indium phosphasalen initiators is clearly an important target.

It is apparent that when using indium(III) as the active site, the phosphasalen ligand is superior to the hybrid ligand, therefore, there is scope to expand its use to other metals. A recent report, by Kol and co-workers, demonstrated phenylene-salalen Group 4 complexes (zirconium(IV) and hafnium(IV)), featuring a phenylene backbone, which showed high isoselectivites (**E**, P_i = 0.91, 323 K, Figure 4.19).[24] The ligands used, show some similarities with the hybrid ligand prepared in this thesis and thus, its coordination chemistry with group 4 metals, the resultant polymerisation activity and stereoselectivity could be an interesting future option.

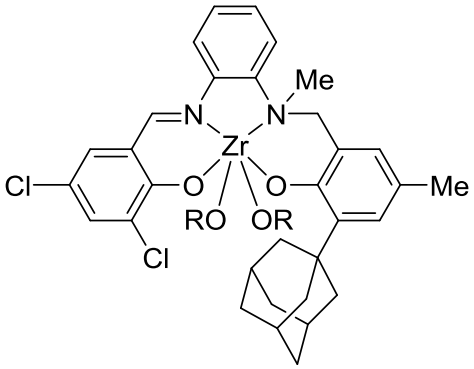

E

Figure 4.19. Isoselective zirconium salalen initiator reported by Kol and co-workers (R = *t*Bu).[24]

In terms of redox switchable catalysts, the short-term aim for complex **4.10** is to synthesise the *tert*-butoxide complex in its reduced and oxidised form. Polymerisation studies using each state should be undertaken to compare both rates and isoselectivites. The aim is to instigate a switch in stereoselectivity between the two states, which has not been previously reported. Long-term aims for the ferrocene-incorporated hybrid initiators would be to utilise the other modifications described in this chapter to optimise the isoselectivity to produce, in one pot, thermoplastic elastomers featuring controllable blocks to crystalline and amorphous PLA.

4.7. References

1 P. Hormnirun, E. L. Marshall, V. C. Gibson, R. I. Pugh and A. J. P. White, *Proc. Natl. Acad. Sci.*, 2006, **103**, 15343–15348.

2 P. McKeown, M. G. Davidson, G. Kociok-Köhn and M. D. Jones, *Chem. Commun.*, 2016, **52**, 10431–10434.

3 A. Pilone, K. Press, I. Goldberg, M. Kol, M. Mazzeo and M. Lamberti, *J. Am. Chem. Soc.*, 2014, **136**, 2940–2943.

4 D. C. Aluthge, B. O. Patrick and P. Mehrkhodavandi, *Chem. Commun.*, 2013, **49**, 4295–4297.

5 D. C. Aluthge, E. X. Yan, J. M. Ahn and P. Mehrkhodavandi, *Inorg. Chem.*, 2014, **53**, 6828–6836.

6 Y. V. Torubaev, A. V. Pavlova, A. A. Pasynskii, A. Raghuvanshi and M. M. Shaikh, *Russ. J. Coord. Chem.*, 2015, **41**, 638–643.

7 Y. Yu, A. D. Bond, P. W. Leonard, U. J. Lorenz, T. V. Timofeeva, K. P. C. Vollhardt, G. D. Whitener and A. A. Yakovenko, *Chem. Commun.*, 2006, 2572–2574.

8 C. Bombis, S. Weigelt, M. M. Knudsen, M. Nørgaard, C. Busse, E. Laegsgaard, F. Besenbacher, K. V Gothelf and T. R. Linderoth, *ACS Nano*, 2010, **4**, 297–311.

9 B. Bildstein, M. Malaun, H. Kopacka, K. Wurst, M. Mitterböck, K.-H. Ongania, G. Opromolla and P. Zanello, *Organometallics*, 1999, **18**, 4325–4336.

10 U. Siemeling, B. Neumann, H.-G. Stammler and O. Kuhnert, *Polyhedron*, 1999, **18**, 1815–1819.

11 K. Shen, X. Liu, Y. Cai, L. Lin and X. Feng, *Chem. Eur. J.*, 2009, **15**, 6008–6014.

12 C. A. Busacca, J. C. Lorenz, N. Grinberg, N. Haddad, M. Hrapchak, B. Latli, H. Lee, P. Sabila, A. Saha, M. Sarvestani, S. Shen, R. Varsolona, X. Wei and C. H. Senanayake, *Org. Lett.*, 2005, **7**, 4277–4280.

13 L. Ding, S. Liang, J. Zhang, C. Ding, Y. Chen and X. Lu, *Inorg. Chem. Commun.*, 2014, **44**, 173–176.

14 L. Chiang, K. Herasymchuk, F. Thomas and T. Storr, *Inorg. Chem.*, 2015, **54**, 5970–5980.

15 J. D. White and S. Shaw, *Org. Lett.*, 2014, **16**, 3880–3883.

16 M. Braun, R. Fleischer, B. Mai, M.-A. Schneider and S. Lachenicht, *Adv. Synth. Catal.*, 2004, **346**, 474–482.

17 M. Nielsen and K. V. Gothelf, *J. Chem. Soc. Perkin Trans. 1*, 2001, 2440–2444.

18 C. A. Tolman, *J. Am. Chem. Soc.*, 1970, **92**, 2953–2956.

19 C. A. Tolman, *Chem. Rev.*, 1977, **77**, 313–348.

20 D. Myers, A. J. P. White, C. M. Forsyth, M. Bown and C. K. Williams, *Angew. Chem. Int. Ed.*, 2017, **56**, 5277–5282.

21 M. Lohan, F. Justaud, T. Roisnel, P. Ecorchard, H. Lang and C. Lapinte, *Organometallics*, 2010, **29**, 4804–4817.

22 A. J. Bard and L. Y. Faulkner, *Electrochemical Methods*, Wiley, 2nd edn., 2004.

23 C. Bakewell, T.-P.-A. Cao, X. F. Le Goff, N. J. Long, A. Auffrant and C. K. Williams, *Organometallics*, 2013, **32**, 1475–1483.

24 A. Stopper, T. Rosen, V. Venditto, I. Goldberg and M. Kol, *Chem. Eur. J.*, 2017, **23**, 11540–11548.

Chapter 5

Half Phosphasalen Ligands: Coordination Chemistry with Zinc and Indium and Activity in ROP of *rac*-lactide

In this chapter, the syntheses of two novel "half-phosphasalen" ligands are described. The aim was to target zinc initiators containing phosphasalen ligands to achieve stereocontrol with an economically viable metal. The scope of the ligand complexations was extended to indium. The coordination chemistry with zinc and indium were explored with NMR spectroscopy, including multinuclear and DOSY experiments, and solid-state X-ray diffraction. Where initiators were synthesised, they were tested in the ROP of rac-lactide.

5.1. Introduction

Homogenous zinc complexes remain some of the fastest initiators for the ROP of LA.[1–7] Zinc is able to bind a wide range of ligands and offer competitive rates whilst maintaining excellent control. Zinc and related Group 2 metals are attractive due to their low cost, combined with high activity, selectivity and low toxicity.[8]

It is typical for zinc initiators to display little/no stereoselectivity and there are only a handful of isoselective examples. Ma and co-workers reported a number of zinc aminophenolate initiators for isotactic ROP of *rac*-LA.[9–11] The most interesting example of which, using a chiral aminophenolate ligand yielded heteroselectivity when coordinated to magnesium (P_s = 0.81, 298 K) and isoselectivity when coordinated to zinc (P_i = 0.84, 298 K) (**A**, Figure 5.1).[12] The stereocontrol mechanism was found to involve both enantiomorphic site control (ESC) and chain-end control (CEC). The chirality induced by the ligand favoured the preferential enchainment of one monomer, which was then further mediated by a CEC mechanism. The magnesium initiators had a higher coordination number and therefore multiple sites for lactide coordination, which was suggested as the reason for heteroselectivity.

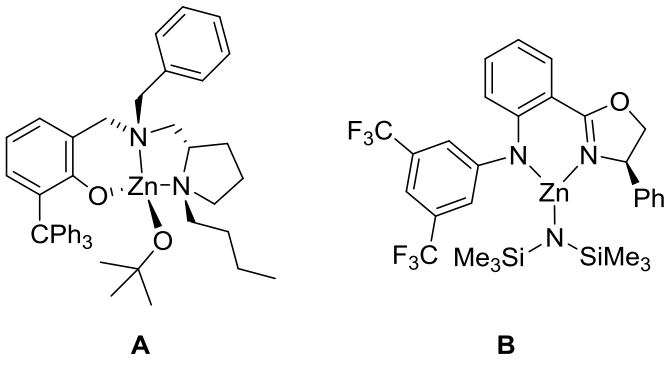

Figure 5.1. Examples of isoselective zinc initiators by Ma (**A**) and Cui (**B**).[12,13]

Another isotactic initiator (**B**), reported by Cui and co-workers, reached P_i = 0.85 (298 K) using an achiral heteroscorpionate zinc complex.[14] The degree of isoselectivity was

solvent dependent, whereby polar solvents reduced P_i. The highest isoselectivity achieved by a zinc initiator was reported by Du and co-workers, using a chiral bidentate amido-oxazolindate zinc initiator (P_i = 0.91, 298 K) which also showed excellent rates and control.[13]

As previously discussed, phosphasalen initiators also show good stereoselectivity, whilst maintaining high polymerisation rates and control with a number of metal centres.[15–17] To date, these phosphasalen ligands have not been coordinated to zinc or Group 2 metals, due to being di-anionic. Hayes and co-workers investigated mono and bis(phosphinimine) zinc complexes to yield cationic initiators for LA polymerisation.[18,19] Despite being cationic, a coordination-insertion mechanism was proposed and exhibited a slight heterotactic bias. Therefore, there is great scope for investigation with ligands containing iminophosphorane bonds to coordinate to zinc.

5.1.1. Aims

The aim was to design and synthesise a series of mono-anionic "half-phosphasalen" ligands, which could be coordinated to zinc and Group 2 metals (Mg, Ca). This requires "halving" the phosphasalen ligand and number of ligand features to be considered (Figure 5.2):

1. One phenolate with *ortho*-*tert*-butyl groups to target mono-anionic ligands suitable to coordinate M(II).
2. Two nitrogen donors: one iminophosphorane group and one amine group.
3. R = alkyl or aromatic: to provide further steric protection of the metal centre and to limit aggregation.

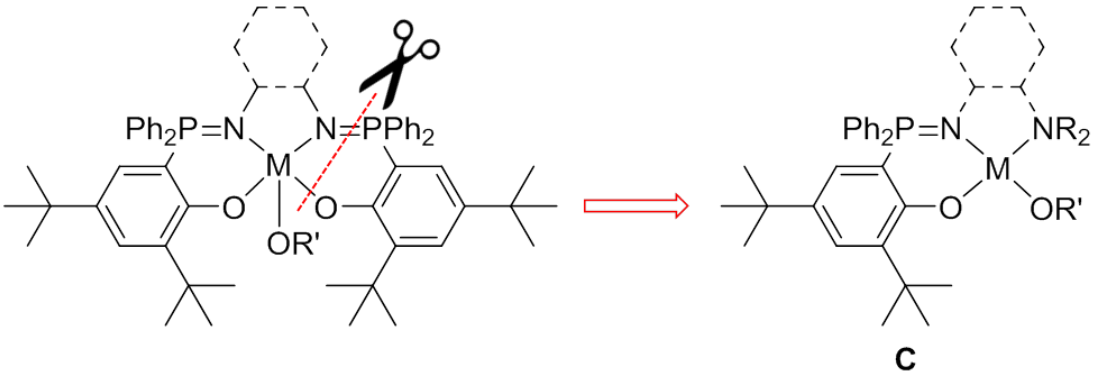

Figure 5.2. Design considerations for half-phosphasalen metal complexes.

The synthesis of half-phosphasalen ligands requires the use of unsymmetrical diamines, containing one NH_2 moiety and one NR_2 moiety. The former amine group is necessary in the Kirsanov reaction, the ligand formation step, whereas the pre-functionalisation of the second amine group will prevent "over-reaction" to a full phosphasalen ligand. Initially, commercially available unsymmetrical diamines will be targeted, but the scope can be broadened by the synthesis of necessary diamines.

Initially, the synthesis of zinc complexes will be the key focus, as (i) they typically have better solubility and stability and (ii) the availability/ease of synthesis of a range of zinc precursors, such as diethyl zinc ($ZnEt_2$), diphenyl zinc ($ZnPh_2$), zinc chloride ($ZnCl_2$) and zinc bis(trimethylsilylamide) ($Zn(N(SiMe_3)_2)_2$). The target co-ligand will be an alkoxide group (complex **C**), such as ethoxide, *iso*-propoxide or *tert*-butoxide, as they are the best initiating groups for LA ROP, but amide co-ligands are also able to initiate. Due to the sensitivity of alkoxide groups to hydrolysis, intermediates such as zinc alkyls, halides or amides will be synthesised to allow for a purification step before introduction of the alkoxide co-ligand.

The coordination of Schiff base ligands has been utilised with other metals, for example Mehrkhodavandi and co-workers reported indium initiators with such ligands (Figure 5.3).[20] Initiator **D** displayed moderate isoselectivity (P_i = 0.62) but good rates were observed. Therefore, in this study, half-phosphasalen ligands will also be coordinated to indium to investigate their catalytic properties.

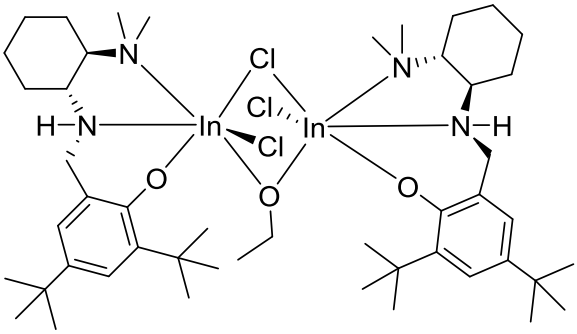

D

Figure 5.3. An isotactic indium Schiff base initiator.[20]

5.2. Ligand Synthesis

The synthesis of half-phosphasalen ligands, **5.1** and **5.2**, used commercially available, unsymmetrical diamines, *N*,*N*-dimethylethylenediamine and 2-amino-*N*-cyclohexyl-*N*-methylbenzylamine, in a Kirsanov reaction with 2,4-di-*tert*-butyl-6-phosphinophenol, the synthesis of which was discussed in Section 3.2 (Figure 5.4). Both reactions used 1,4-diazabicyclo[2.2.2]octane (DABCO) as a base. Ligand **5.1** was isolated as a phosphonium bromide salt, by precipitation from diethyl ether (Et_2O) in good yields, 61%. It was fully characterised by multinuclear NMR spectroscopy and elemental analysis.

Ligand **5.2** was also isolated as a phosphonium bromide salt but elemental analysis revealed impurities from the remaining DABCO salts. It was further purified by column chromatography (alumina, 40:1 DCM:EtOH) which removed the salts and yielded the deprotonated neutral iminophosphorane ligand, **5.2**. This was confirmed by elemental analysis. The ligand was isolated in moderate yields, 55%, and was characterised by multinuclear NMR spectroscopy. Attempts to isolate ligand **5.1** as a deprotonated neutral ligand resulted in the isolation of several species after column chromatography. Thus, because the phosphonium bromide salt was easily isolated, this was the preferred ligand form to take forward.

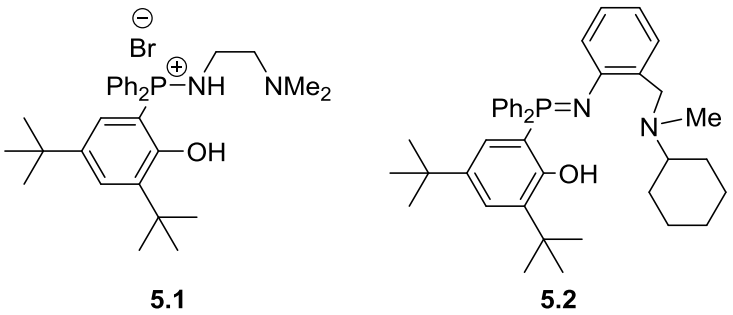

5.1 **5.2**

Figure 5.4. Structure of ligands **5.1** and **5.2**.

5.3. Zinc Complexes

5.3.1. Synthesis of zinc intermediates 5.3-5.5, with ligand 5.1

For both ligands, **5.1** and **5.2**, zinc alkyl, amide and halide intermediates were synthesised. The amide species could be directly tested in the ROP of *rac*-LA and the other complexes as precursors to the alkoxide initiators.

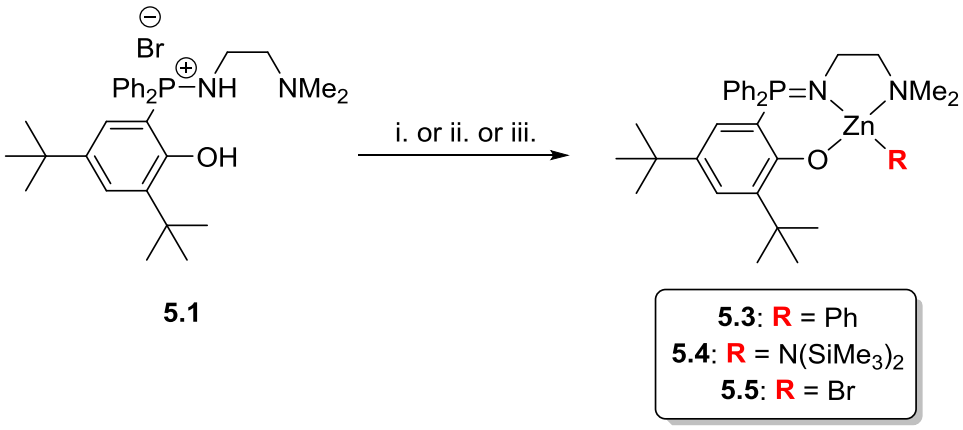

Scheme 5.1. Synthesis of intermediates, **5.3**-**5.5**, utilised in the synthesis of zinc alkoxide with ligand **5.1**. Conditions: i. a) $KN(SiMe_3)_2$ (1 equiv.), THF, 298 K, b) $ZnPh_2$ (1 equiv.), 298 K; ii. a) $KN(SiMe_3)_2$ (1 equiv.), THF, 298 K, b) $Zn(N(SiMe_3)_2)_2$, 298 K; iii. $ZnEt_2$ (1 equiv.) THF, 298 K.

The zinc phenyl complex, **5.3**, was synthesised by reaction of one equivalent of potassium bis(trimethylsilyl)amide ($KN(SiMe_3)_2$) with ligand **5.1**, in THF (Scheme 5.1). The deprotonated intermediate was not isolated and one equivalent of $ZnPh_2$ was subsequently added. Salts were removed by centrifugation and the product was isolated as a white crystalline solid, from a THF/*n*-hexane solution at 243 K, in a moderate yield of 45%. The zinc amide complex, **5.4**, was synthesised in a similar manner, by initial deprotonation using $KN(SiMe_3)_2$ and then addition of one equivalent of a zinc amide precursor ($Zn((SiMe_3)_2)_2$). Complex **5.4** was isolated as a white crystalline solid from *n*-hexane at 298 K. The synthesis of **5.3** and **5.4** was monitored using $^{31}P\{^1H\}$ NMR spectroscopy (C_6D_6). The deprotonation reaction resulted in a shift from 43.3 ppm (ligand

5.1) to 23.8 ppm. Addition of $ZnPh_2$ and $Zn((SiMe_3)_2)_2$, to obtain **5.3** and **5.4**, yielded further shifts to resonances at 32.9 ppm and 36.9 ppm, respectively.

A zinc bromide complex, **5.5**, was synthesised by addition of one equivalent of $ZnEt_2$ to ligand **5.1**, in THF. Both equivalents of ethane were lost due to deprotonation of the remaining amine proton of the phosphonium bromide and phenolic proton. The bromide anion then coordinated to the zinc centre and using mass spectrometry, the presence of a covalent rather than ionic bond was confirmed because the molecular ion corresponded to the mass of the zinc bromide complex. The reaction was also monitored using $^{31}P\{^1H\}$ NMR spectroscopy; a change in the chemical shift to 35.0 ppm was observed and the product was isolated in a good yield of 73%. All complexes were fully characterised using multinuclear NMR spectroscopy and their purity confirmed by elemental analysis.

Inspection of the ^1H NMR spectra before and after complexation to zinc showed distinct changes in the chemical shift environments of the ligand resonances (Figure 5.5). The resonance corresponding to the methyl groups (**E**) present on the amine nitrogen shifted upfield by between 0.41-0.47 ppm for all complexes **5.3** - **5.5**, presumably a consequence of zinc coordination increasing the electron density at the methyl groups. Resonances corresponding to the protons in the backbone of the ligand (**C** and **D**) also shifted upfield, more significantly for the protons closest to the iminophosphorane bond. For complex **5.4**, the resonance corresponding to the protons at **C** were at the same chemical shift as those for methyl groups, **E**. Finally, aromatic resonances, **A** and **B**, were observed to shift downfield along with the *ortho*-protons of the phenyl groups on phosphorus, whereas

the *meta*- and *para*-protons on these phenyl groups shift upfield. All these changes were diagnostic of coordination of ligand **5.1** to a zinc centre.

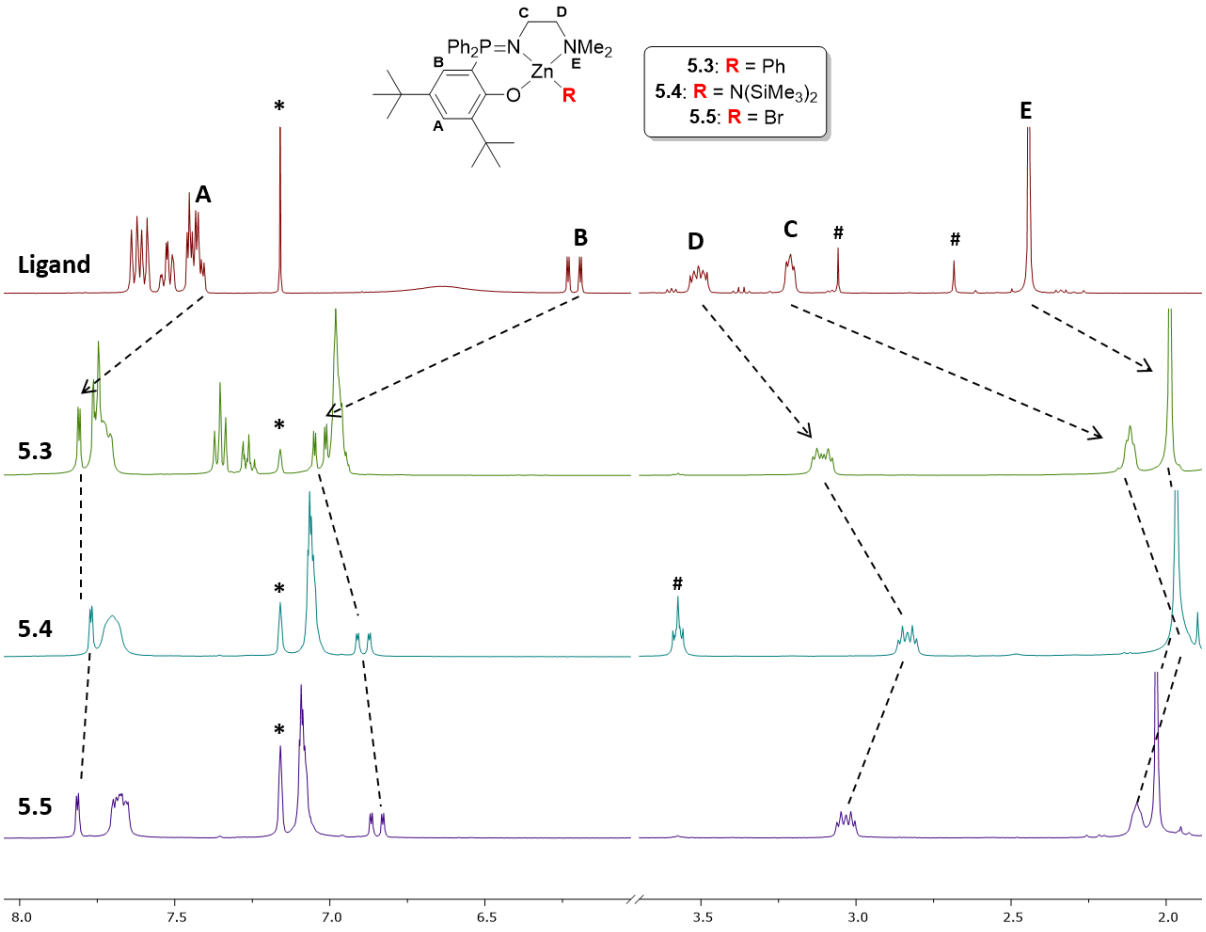

Figure 5.5. ^{1}H NMR spectra of ligand **5.1** and complexes **5.3**-**5.5** demonstrating changes in chemical shifts due to zinc coordination (*tert*-butyl region omitted for clarity) (C_6D_6*, 400 MHz, 298 K, residual solvent#).

5.3.2. X-Ray crystal structures of complexes 5.3 and 5.4

Crystals of complexes **5.3** and **5.4**, suitable for X-ray diffraction experiments were grown by slow evaporation of complex **5.3** in *n*-hexane and a saturated solution of complex **5.4** in THF/*n*-hexane at 298 K, respectively (Figure 5.6 and 5.7). Complex **5.3** crystallised in a monoclinic $P2_1/c$ space group and complex **5.4** in a monoclinic $P2_1/n$ space group. Both complexes show distorted tetrahedral geometries at zinc. For complex **5.3**, τ_4 = 0.78 and for complex **5.4**, τ_4 = 0.77, corresponding to a tetrahedral geometry at metal. In complex **5.3**, the lengths of bonds Zn-O^1 and Zn-C^{40} are very similar, 1.967(2) and 1.975(2) Å, respectively, which reflects the polarity of these bonds. Hence, distortion of the tetrahedral geometry might be attributed to the electrostatic repulsion between the phenyl group and the other coordinated groups around the zinc metal centre. Conversely, the ligand may also be constraining the geometry. For both complexes **5.3** and **5.4**, the N^8-Zn-N^{11} angle is smallest around the zinc centre, 84.00(7) ^{o} and 85.07(7) ^{o}, respectively. The two complexes are otherwise comparable with the P^7-N^8 and Zn-R bonds being within error.

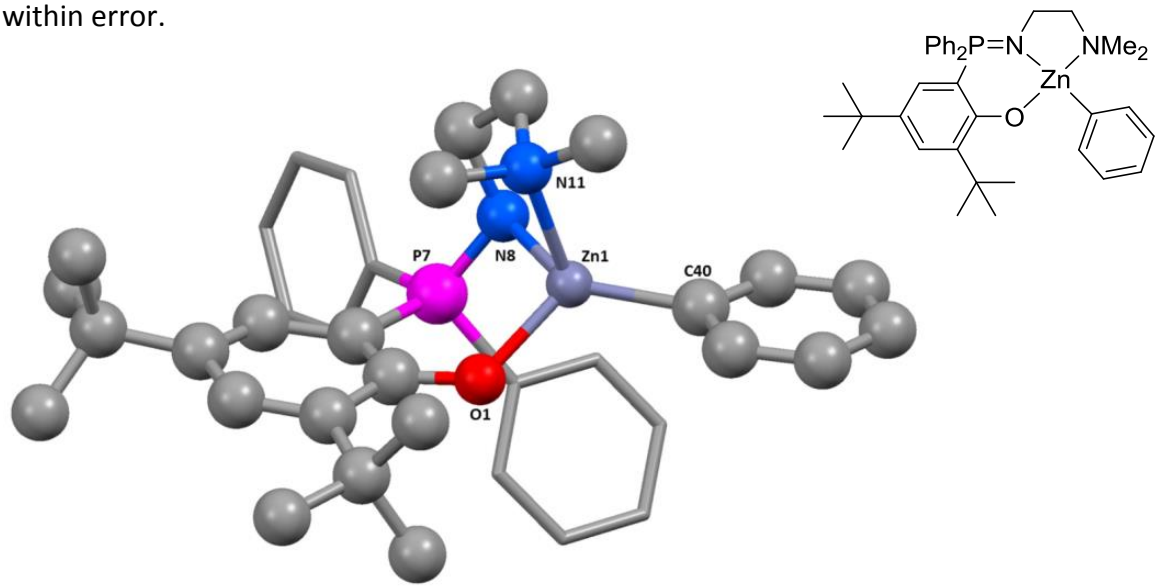

Figure 5.6. Ball and stick representation of complex **5.3** (H-atoms omitted for clarity. See Appendix for complete bond lengths and angles).

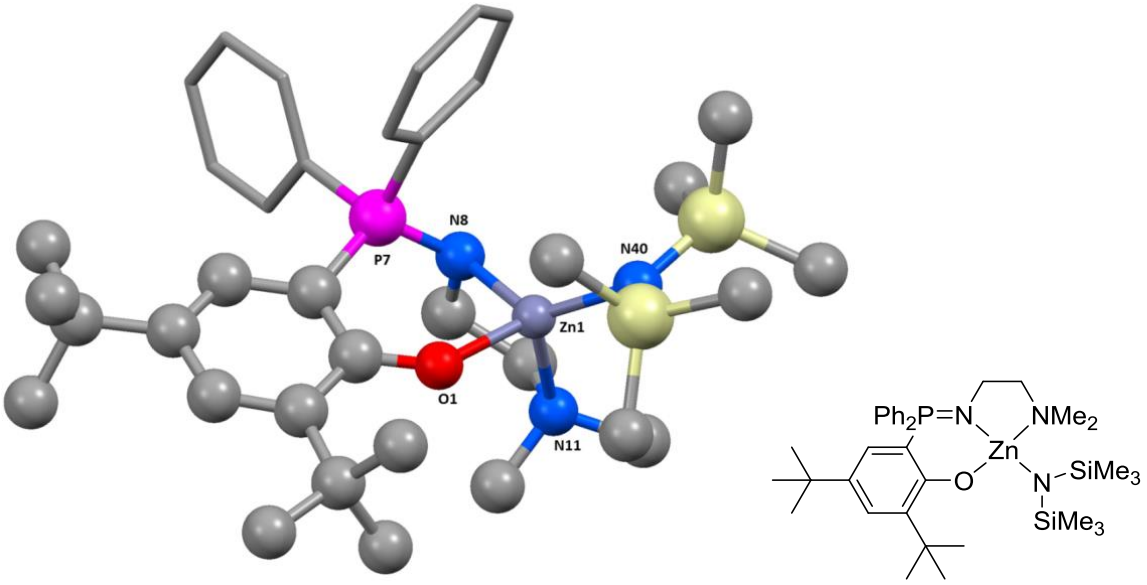

Figure 5.7. Ball and stick representation of complex **5.4** (H-atoms omitted for clarity. See Appendix for complete bond lengths and angles).

5.3.3. Attempted synthesis of zinc alkoxide complexes with ligand 5.1

Complex **5.3** was reacted with one equivalent of *iso*-propyl alcohol (IPA), in THF, and the reaction was monitored over several days using $^{31}P\{^{1}H\}$ NMR spectroscopy. The resonance corresponding to the starting material, **5.5**, disappeared after two days and a resonance appeared at 38.5 ppm. In the ^{1}H NMR spectrum of this new product, no resonances corresponding to the *iso*-propoxide complex were observed.

Complex **5.4** was also reacted with one equivalent of IPA, in THF, but multiple species were observed by $^{31}P\{^{1}H\}$ NMR spectroscopy. One of the major products showed a resonance of 38.5 ppm, as observed in the reaction between complex **5.3** and IPA. Multiple attempts to crystallise the reaction mixture and isolate this species were not successful.

Finally, a salt metathesis reaction between complex **5.5** and potassium ethoxide (KOEt) was carried out. The $^{31}P\{^{1}H\}$ NMR spectrum of the crude mixture showed a species at 38.5 ppm. Crystallisation of this mixture enabled isolation of this product. The ^{1}H NMR spectrum of this product showed resonances corresponding to the ligand, but none that

could be attributed to an ethoxide co-ligand. Variable temperature (VT) NMR spectroscopy did not resolve the spectra further. Crystallisation attempts yielded crystals suitable for analysis by single X-ray crystallography and the product was shown to be homoleptic complex **5.6**, as also confirmed by elemental analysis (Figure 5.8). Furthermore, this structure was consistent with a single resonance in the $^{31}P\{^{1}H\}$ NMR spectra and resonances corresponding to one ligand environment in the ^{1}H NMR spectrum (Figure 5.9).

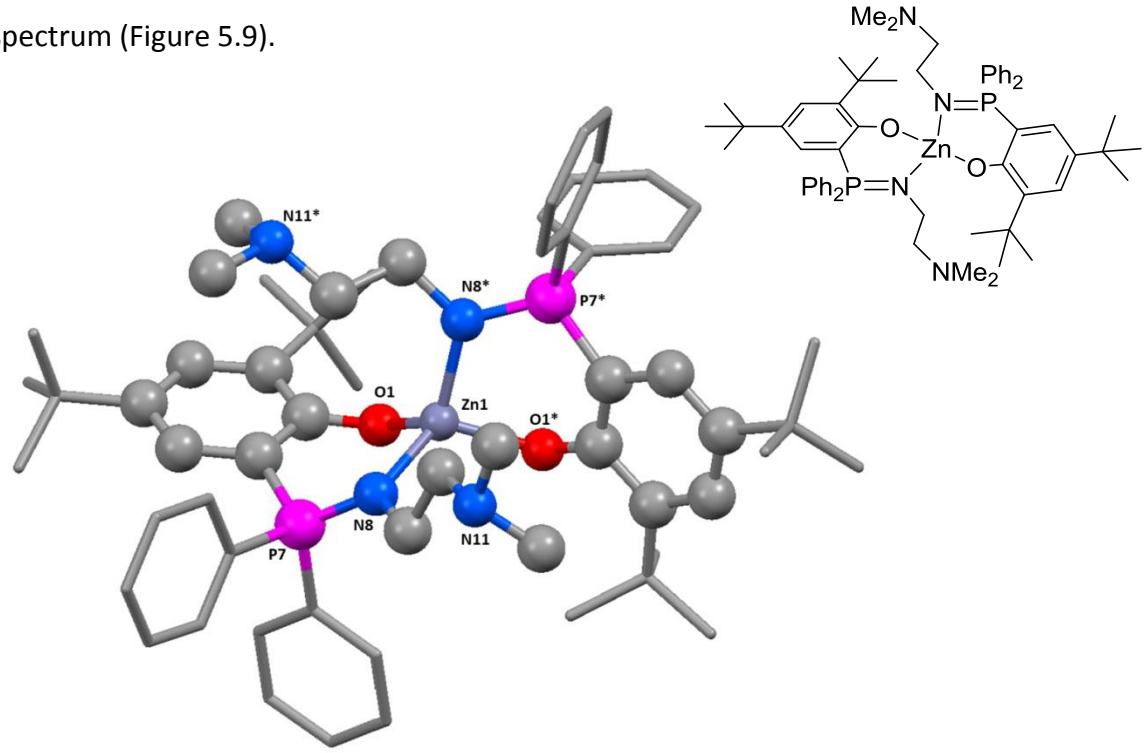

Figure 5.8. Ball and stick representation of complex **5.6**. (H-atoms omitted for clarity. See Appendix for complete bond lengths and angles).

The crystals suitable for X-ray diffraction experiments were grown from a saturated *n*-hexane solution at 298 K. The complex crystallised in an orthorhombic space group (P_{bcn}) and showed a distorted tetrahedral geometry at zinc (τ_4 = 0.87). The complex has C_2 symmetry, which justifies the single phosphorus environment in the $^{31}P\{^{1}H\}$ NMR spectrum. The zinc centre is coordinated by the phenolate oxygen (O1 and O1*) and iminophosphorane nitrogen (N8 and N8*) of each ligand, with the amino nitrogen occupying the free space surrounding the molecule. The electron donating ability of the

iminophosphorane bond is known to be greater than the imine bond e.g. for complex **5.6**, the Zn-N8 bond length is 2.001(2) Å, whereas for the zinc ethyl Schiff-base analogue the zinc imine bond length is 2.147(3) Å.[22] Therefore, it can be hypothesised that the electron donation of two iminophosphorane bonds has a greater stabilising effect at zinc compared to a mono-ligated complex.

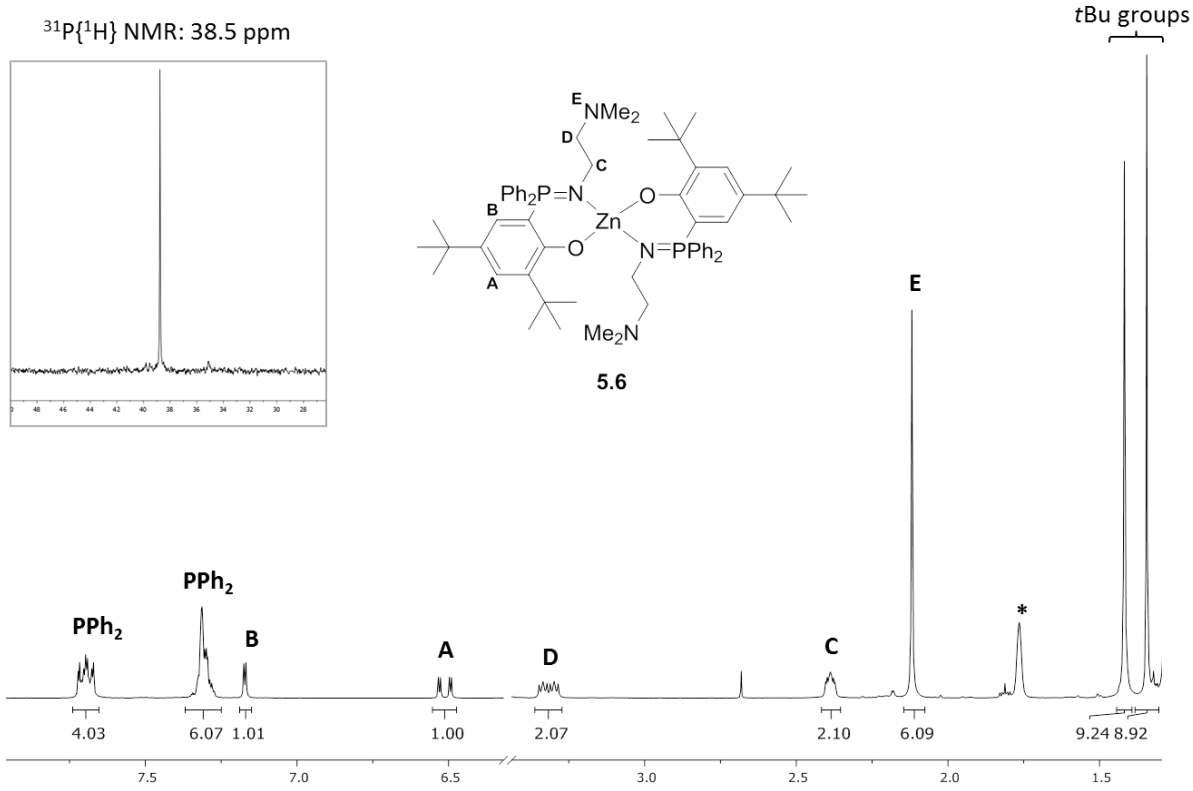

Figure 5.9. ^{1}H and $^{31}P\{^{1}H\}$ NMR spectra of the homoleptic zinc complex **5.6** (d_8-THF*, 400 MHz, 298 K).

The formation and apparent stability of this homoleptic species was not unexpected, as Schlenk equilibria are common with zinc complexes.[23] Nonetheless, the previously reported Schiff base analogue did not display such an equilibrium and the heteroleptic zinc complexes were easily isolated.[22] Attempts to drive the equilibrium towards the desired heteroleptic zinc alkoxide complex utilising lower reaction temperatures, coordinating solvents, such as 1,4-dioxane, and slow addition of the reagents were not successful.

The synthesis of zinc amide complex, **5.4**, was attempted a further three times in order to test its activity in the ROP of *rac*-LA. On two occasions, only the homoleptic product was observed by $^{31}P\{^{1}H\}$ NMR spectroscopy and on the other occasion, a mixture of the desired product and the homoleptic product were observed, but multiple attempts to crystallise complex **5.4** from this mixture, using the same procedure as reported in the experimental section, did not yield the single species. This reactivity demonstrates the propensity of the homoleptic species, **5.6**, to persist.

As discussed earlier, the improved electron-donating ability of a phosphasalen ligand might bias the Schenk equilibrium towards the formation of homoleptic over heteroleptic complexes.[15] Other factors to consider are the groups present on the amine-nitrogen and the flexibility of the ligand backbone. Increasing the rigidity of the backbone might prevent the distal amine group from rotating away from the zinc centre. Furthermore, increasing the steric bulk of the amine-nitrogen groups might provide greater protection at zinc and hinder aggregation. Therefore, ligand **5.2** was investigated to try to bias the equilibrium in favour of a heteroleptic alkoxide complex.

5.3.4. Synthesis of zinc complexes 5.7-5.9, with ligand 5.2

For ligand **5.2**, alkyl, amide and halide intermediate complexes were synthesised, isolated and subsequently reacted after purification (Scheme 5.2). Using ligand **5.2**, a zinc ethyl complex, **5.7**, was synthesised by reaction with one equivalent of $ZnEt_2$, in THF. The reaction was monitored using $^{31}P\{^1H\}$ NMR spectroscopy (C_6D_6) and a single resonance was observed at 27.5 ppm, after addition of $ZnEt_2$. The product was isolated by precipitation from *n*-hexane in good yields (54%). A quantitative yield was not obtained due to the partial solubility of the product in *n*-hexane.

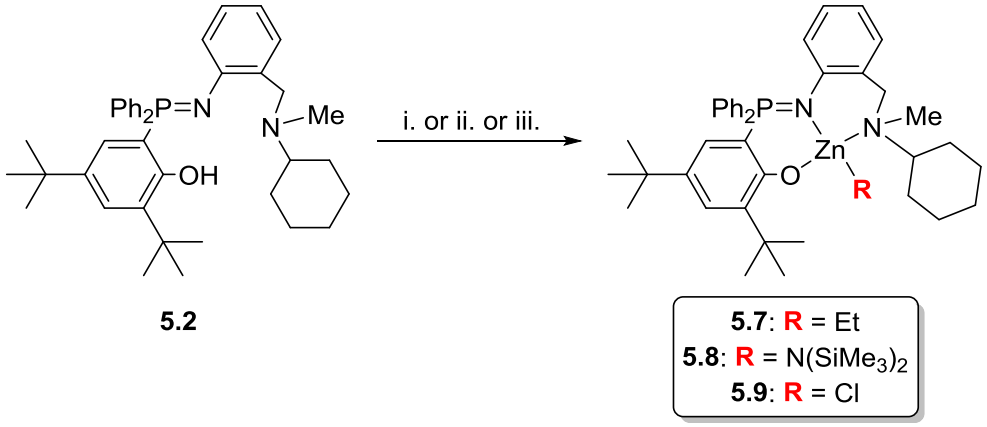

Scheme 5.2. Synthesis of intermediates, **5.7**-**5.9**. Conditions: i. $ZnEt_2$ (1 equiv.), THF, 298 K; ii. $Zn(N(SiMe_3)_2)_2$ (1 equiv.), THF, 298 K; iii. a) $KN(SiMe_3)_2$ (1 equiv.), THF, 298 K; b) $ZnCl_2$ (1 equiv.), THF, 298 K.

The zinc amide complex **5.8** was synthesised by the addition of one equivalent of $Zn(N(SiMe_3)_2)_2$ to ligand **5.2**, in THF. The reaction yielded a product showing a single resonance in the $^{31}P\{^1H\}$ NMR spectrum, at 31.9 ppm. The product was isolated in good yields (57%), by slow evaporation of a cyclohexane solution. Zinc chloride complex, **5.9**, was synthesised, by addition of one equivalent of $KN(SiMe_3)_2$, to a solution of ligand **5.2** in THF, to yield the deprotonated ligand. The deprotonated ligand showed a single resonance of 10.5 ppm in the $^{31}P\{^1H\}$ NMR spectrum. After addition of $ZnCl_2$, another single resonance at 31.9 ppm was observed and the product was isolated by crystallisation from THF/*n*-hexane, at 243 K, in good yields (54%). All complexes were fully

characterised by multinuclear NMR spectroscopy and their purity confirmed by elemental analysis.

For ligand **5.2** and its complexes, **5.7**-**5.9**, increased complexity was observed in the aliphatic region of the ^{1}H NMR spectra, due to the ligand containing a cyclohexane group. This complexity arose from the high degree of coupling between the protons on the ring and the similar chemical environment of which they all occur. Fortunately, upon coordinating to zinc, these resonances were better separated and some, such as **C** or **D**, were diagnostic of coordination to zinc (Figure 5.10). Upfield shifts in the resonances were observed for the benzylic protons, **C**, whereas downfield shifts were observed for the nitrogen methyl group (**D**) and phenolate protons (**A** & **B**). Similar chemical shifts were observed for complexes **5.7** and **5.9**, whereas for complex **5.8**, the peaks were shifted further downfield. This may reflect electron-withdrawing effects of the various co-ligands.

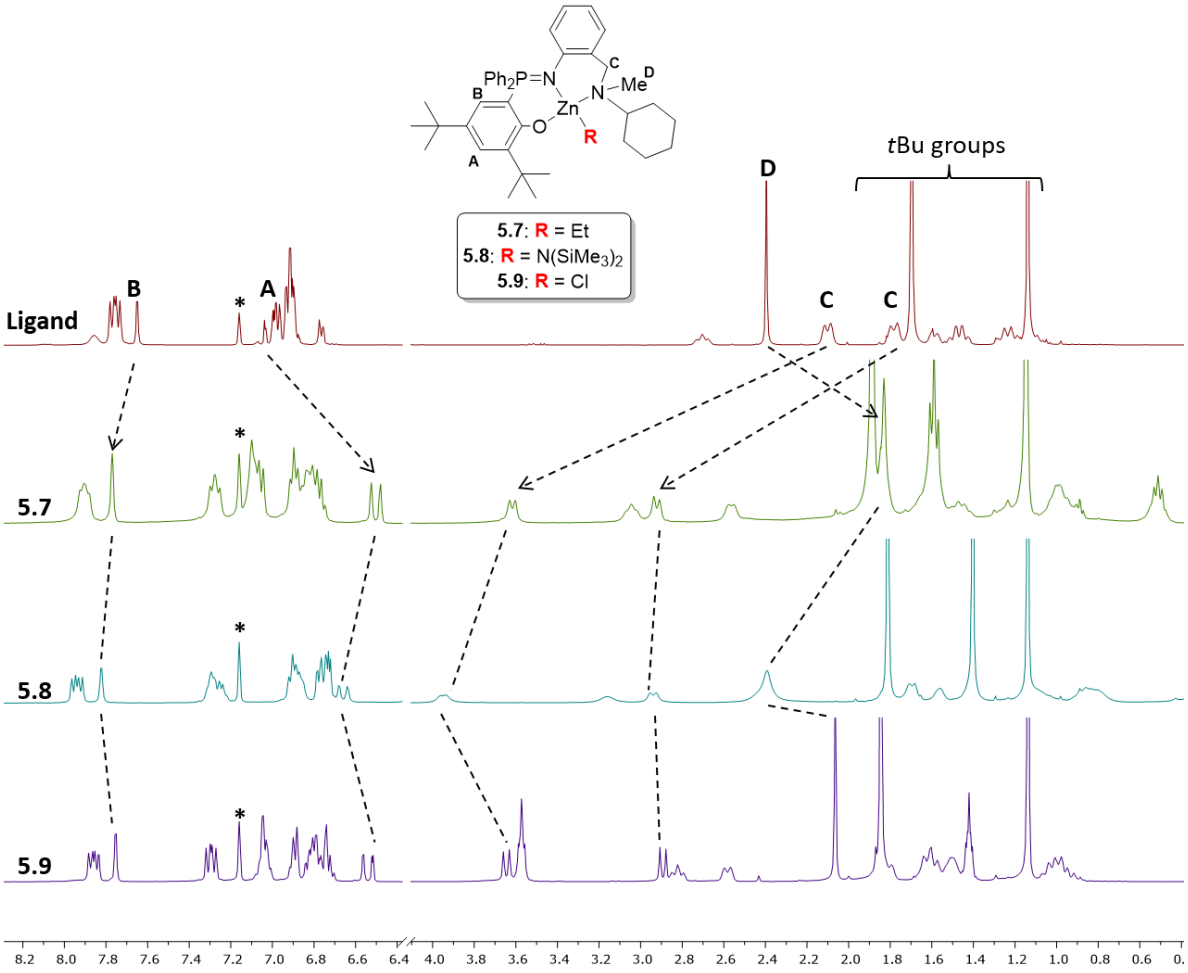

Figure 5.10. ^{1}H NMR spectra of ligand **5.2** and complexes **5.7**-**5.9** demonstrating changes in chemical shift environments due to zinc coordination (C_6D_6*, 400 MHz, 298 K).

5.3.5. X-ray crystal structures of complexes 5.7 and 5.8

Crystals of complexes **5.7** and **5.8** suitable for X-ray diffraction experiments were grown from saturated solutions in THF/*n*-hexane at 298 K (Figure 5.11). Complexes **5.7** and **5.8** crystallised in orthorhombic $Pca2_1$ and $P2_12_12_1$ space groups and with τ_4 values of 0.81 and 0.82, respectively. Complex **5.7** crystallised as two crystallographically independent molecules, where the two differ according to small differences in the orientation of the phenyl groups and the ethyl co-ligand.

The N-Zn-N ligand bite angles are larger (94 ^{o}) with complexes coordinated by ligand **5.2** than with those coordinated by ligand **5.1** (85 ^{o}) which is likely due to a three vs. two atom bridge.

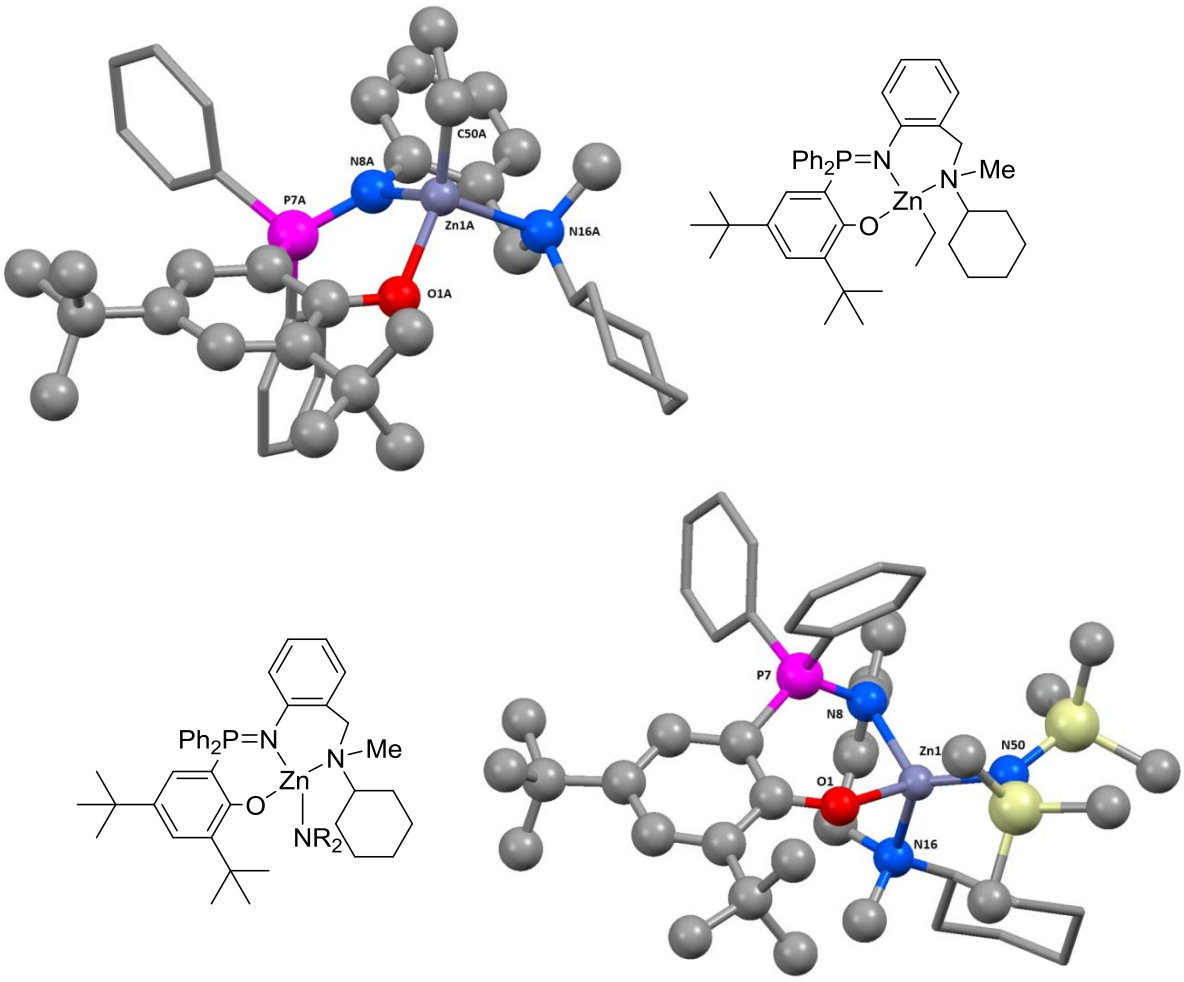

Figure 5.11. Ball and stick representation of complex **5.7** (left – other crystallographically independent molecule omitted for clarity) and **5.8** (right) (H-atoms omitted for clarity. See Appendix for complete bond lengths and angles, R = $SiMe_3$).

5.3.6. Synthesis of zinc alkoxide complex, 5.10, with ligand 5.2

To synthesise a zinc alkoxide complex, the zinc ethyl complex, **5.7**, was reacted with one equivalent of IPA, in THF. Analysis by $^{31}P\{^{1}H\}$ NMR spectroscopy showed no change to the resonance corresponding to complex **5.7** at 27.5 ppm. The reaction was continued for several days, with periods of heating to 353 K and addition of more equivalents of IPA, but the starting material was always present. Zinc alkyl bonds are typically very sensitive to protic sources, due to the entropic driving force to liberate ethane gas, but after loss of the first ethyl group, the reactivity of the second ligand can vary greatly.[24] Therefore, it was concluded that a synthetic route *via* complex **5.7** was not feasible.

Complex **5.9** was reacted with one equivalent of both KOEt and KO*t*Bu to attempt salt metatheses reactions, to form a zinc alkoxide complex. Both reactions were analysed using $^{31}P\{^{1}H\}$ NMR spectroscopy and multiple resonances were observed, with major resonances at 31.4 ppm and 32.6 ppm for the respective reactions with KOEt and KO*t*Bu. The ^{1}H NMR spectra of the products isolated from both reactions did not show any resonances corresponding to the presence of either alkoxide co-ligand. For the solid collected from the KOEt reaction, a small amount was added to a solution of *rac*-LA in d_8-THF and sonicated for two hours, after which no polymer was observed. It could be concluded that the products isolated from these reactions did not contain an alkoxide co-ligand and, therefore, were unsuitable for testing in polymerisation.

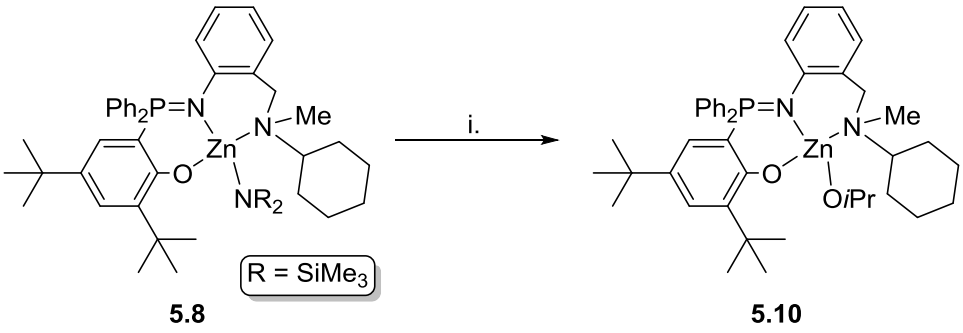

5.8 **5.10**

Scheme 5.3. Synthesis of zinc isopropoxide complex **5.10**. Conditions: i. IPA (0.24 M in THF, 1 equiv.), THF, 298 K.

Finally, zinc amide complex, **5.8**, was reacted with one equivalent of IPA, in THF, and a change in the $^{31}P\{^{1}H\}$ NMR spectrum from 31.9 ppm, corresponding to **5.8**, to 31.3 ppm was observed (Scheme 5.3). The product was isolated by precipitation from *n*-hexane and was analysed by ^{1}H NMR spectroscopy. A multiplet resonance at 4.57 ppm and two doublet resonances at 1.48 and 1.42 ppm were observed, which would be expected for an *iso*-propoxide co-ligand. Further analysis using COSY NMR, demonstrated that these resonances correlated and the presence of an alkoxide co-ligand was confirmed. Complex

5.10 was fully characterised by multinuclear NMR spectroscopy and its purity was confirmed by elemental analysis (Figure 5.12).

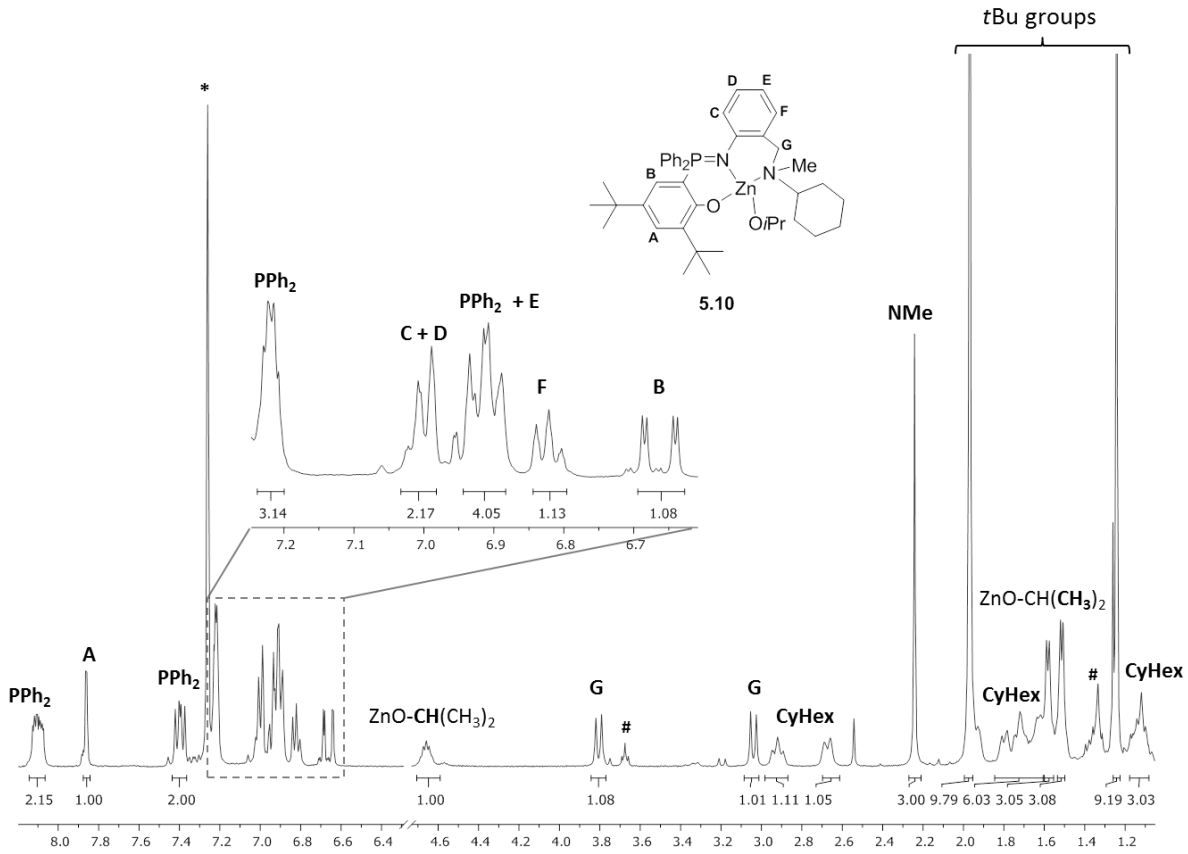

Figure 5.12. ^{1}H NMR spectrum of zinc isopropoxide complex, **5.10** ($CDCl_3$*, 400 MHz, 298 K, residual solvent$^{\#}$).

5.4. Indium Complexes

5.4.1. Synthesis of indium complexes 5.11 and 5.12, with ligand 5.1

Ligand **5.1** was deprotonated, using two equivalents of $KN(SiMe_3)_2$ in THF, and then reacted with one equivalent of indium(III) chloride ($InCl_3$). The reaction was monitored by $^{31}P\{^1H\}$ NMR spectroscopy (C_6D_6) and complete deprotonation was confirmed by a single resonance at 23.8 ppm. After addition of $InCl_3$, another single resonance at 45.7 ppm was observed. The indium dichloride product, **5.11**, was isolated, after centrifugation to remove residual salts, removal of the solvent *in vacuo* and precipitation from *n*-hexane. The successful synthesis of complex **5.11** was confirmed using elemental analysis.

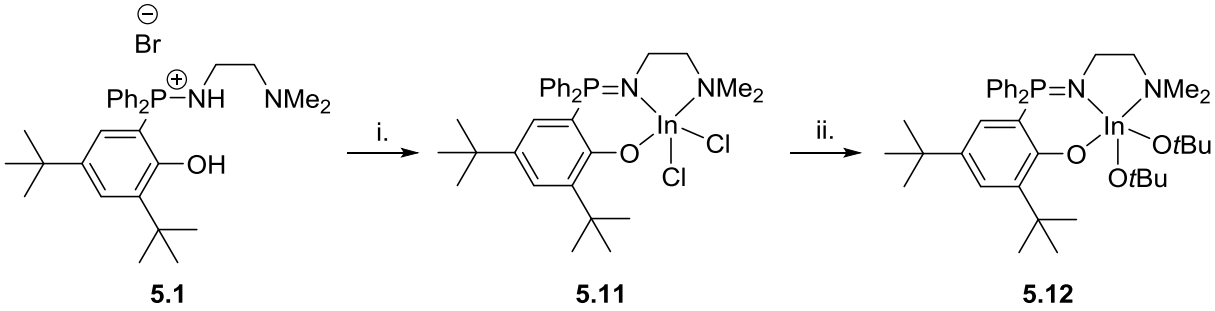

5.1 **5.11** **5.12**

Scheme 5.4. Synthesis of indium dichloride complex, **5.11**, and indium *tert*-butoxide complex, **5.12**, with ligand **5.1**. Conditions: i. a) $KN(SiMe_3)_2$ (2 equiv.), THF, 298 K; b) $InCl_3$ (1 equiv.), THF, 298 K; ii. KO*t*Bu (2 equiv), THF, 298 K.

Two equivalents of KO*t*Bu were added to a THF solution of complex **5.11** and a cloudy solution was obtained. Analysis by $^{31}P\{^1H\}$ NMR spectroscopy showed a single resonance at 43.6 ppm, shifted upfield from the chloride complex, **5.11**. The product was again isolated by centrifugation, removal of solvent and precipitation from *n*-hexane. The ^1H NMR spectrum of this product confirmed the presence of two *tert*-butoxide co-ligands and it was found to be pure by elemental analysis. Complex **5.12** was fully characterised using multinuclear NMR spectroscopy (Figure 5.13).

Complex **5.12** was analysed using DOSY NMR in its polymerisation medium, THF, to investigate the aggregation state. The Schiff-base indium initiators reported by Mehrkhodavandi and co-workers were dimers under polymerisation conditions.[20] Here, a diffusion coefficient of 8.20 x 10^{-10} m^2 s^{-1} was calculated and estimation of the molecular weight was 646 Da. This correlated well with the calculated molecular weight of 737 Da, indicating that complex **5.12** was monomeric, in THF.

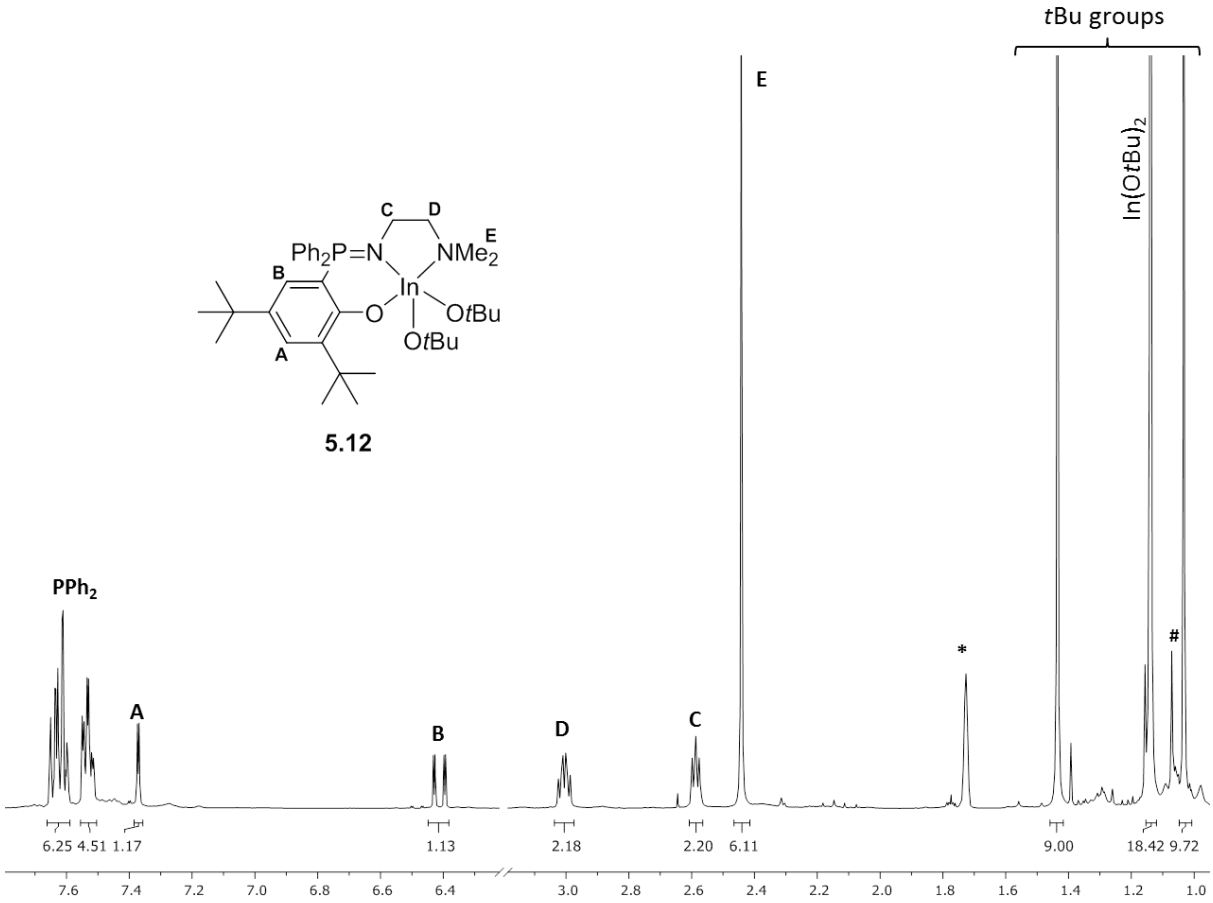

Figure 5.13. ^{1}H NMR spectrum of the indium *tert*-butoxide complex, **5.12** (d_8-THF*, 400 MHz, 298 K, residual solvent$^{\#}$).

5.4.2. X-ray crystal structures of complexes 5.11 and 5.12

Crystals of complexes **5.11** and **5.12**, suitable for X-ray diffraction experiments, were grown from saturated solutions in THF/*n*-hexane, at 243 K (Figure 5.14). Both complexes crystallise in monoclinic C2/*c* space groups, with τ values of 0.59 and 0.37, respectively. Therefore, complex **5.11** lies towards a trigonal bipyramidal geometry at indium whereas

complex **5.12** lies towards a square-based pyramidal geometry at indium with O15 occupying the apex position.

The two *tert*-butoxide co-ligands were equivalent on the NMR timescale whereas, in the solid state, they occupied different spacial environments. O15 is closer to the phenolate ring and the Zn-O15 bond length is 2.035(2) Å, whereas O14 is directed away from the ligand and has a Zn-O14 bond length of 2.021(3) Å. Changing the co-ligands from chloride groups to *tert*-butoxide groups, decreases the bond strength of the Zn-N8 and Zn-N11 bonds, as reflected in their lengths; complex **5.11** (Zn-N8 = 2.133(3) Å, Zn-N11 = 2.355(4) Å) vs. complex **5.12** (Zn-N8 = 2.173(4) Å, Zn-N11 = 2.406(4) Å).

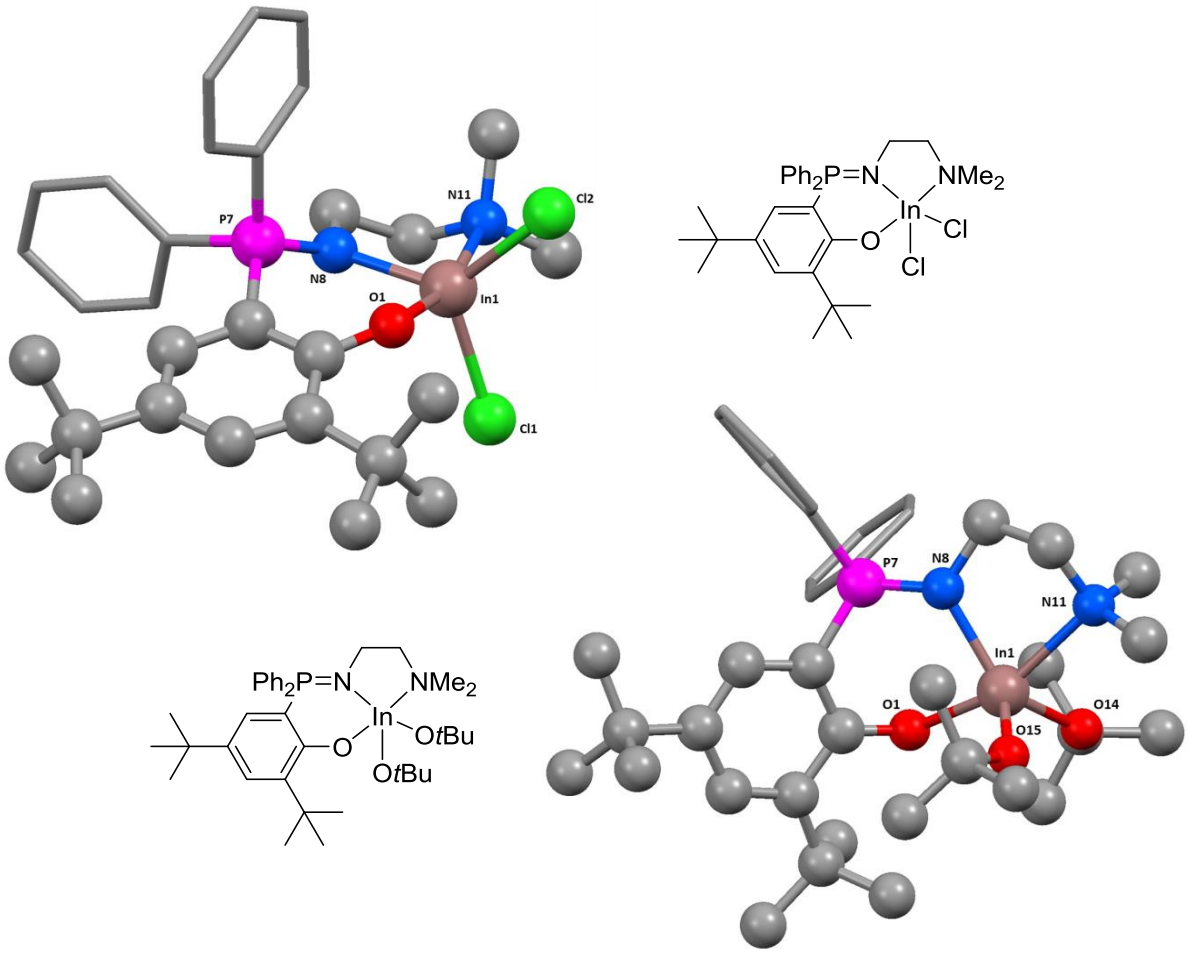

Figure 5.14. Ball and stick representation of complexes **5.11** (left) and **5.12** (right). (H-atoms omitted for clarity. See Appendix for complete bond lengths and angles).

5.4.3. Synthesis of indium complexes 5.13 and 5.14, with ligand 5.2

Ligand **5.2** was reacted with one equivalent of $KN(SiMe_3)_2$, in THF, to yield the deprotonated ligand, as characterised *in situ* with an $^{31}P\{^1H\}$ NMR resonance at 10.5 ppm (C_6D_6). One equivalent of $InCl_3$ was added, and a new singlet resonance at 37.4 ppm was observed. The solution was centrifuged, to remove residual salts, dried *in vacuo* and the product was precipitated from *n*-hexane in good yields (84%). The purity of indium dichloride complex, **5.13**, was then confirmed using elemental analysis.

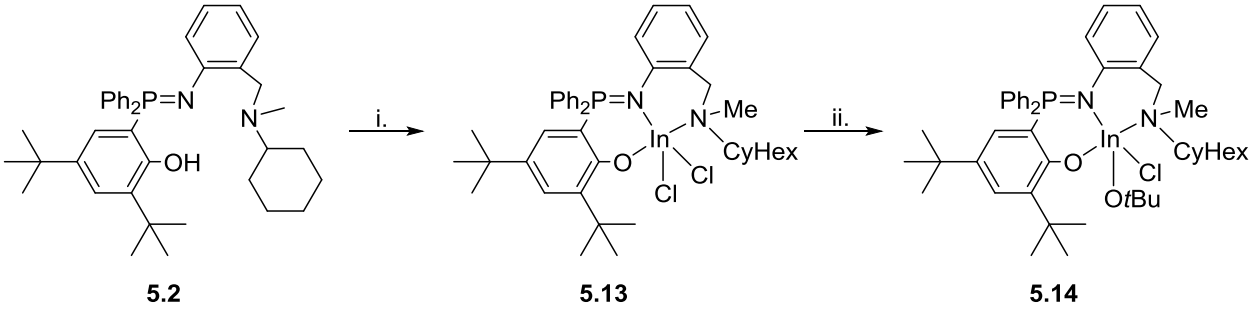

5.2 **5.13** **5.14**

Scheme 5.5. Synthesis of indium dichloride complex, **5.13**, and indium chloride/*tert*-butoxide complex, **5.14**, with ligand **5.2**. Conditions: i. a) $KN(SiMe_3)_2$ (1 equiv.), THF, 298 K; b) $InCl_3$ (1 equiv.), THF, 298 K; ii. KO*t*Bu (1 equiv), THF, 298 K.

Complex **5.13** was reacted with two equivalents of KO*t*Bu, in THF, and multiple new resonances in the $^{31}P\{^1H\}$ NMR spectrum were observed. The major product, complex **5.14**, which was isolated, showed a $^{31}P\{^1H\}$ resonance at 35.6 ppm and the ^1H NMR spectrum showed a 1:1 ratio of *tert*-butoxide to ligand resonances. Complex **5.13** also was reacted with one equivalent of KO*t*Bu, which formed only complex **5.14**, in good yields (62%) and high purity, as confirmed by elemental analysis.

Multiple synthetic attempts to prepare a complex with two *tert*-butoxide co-ligands proved unsuccessful, perhaps due to steric hindrance. Furthermore, the reaction between complex **5.13** and two equivalents of KOEt, a less sterically encumbered co-ligand, also gave multiple products.

Complex **5.14** was fully characterised using multinuclear NMR spectroscopy, suitably concentrated NMR spectra could only be collected in $CDCl_3$, which led to some degradation observed in Figure 5.15, but its overall purity was still confirmed by elemental analysis. It was also analysed using DOSY NMR in its polymerisation medium, THF. The diffusion coefficient was found to be 7.18 x 10^{-10} m^2 s^{-1}, which corresponded to a calculated molecular weight of 818 Da, correlating well with the calculated molecular weight of 829 Da, and showing it to be monomeric in THF.

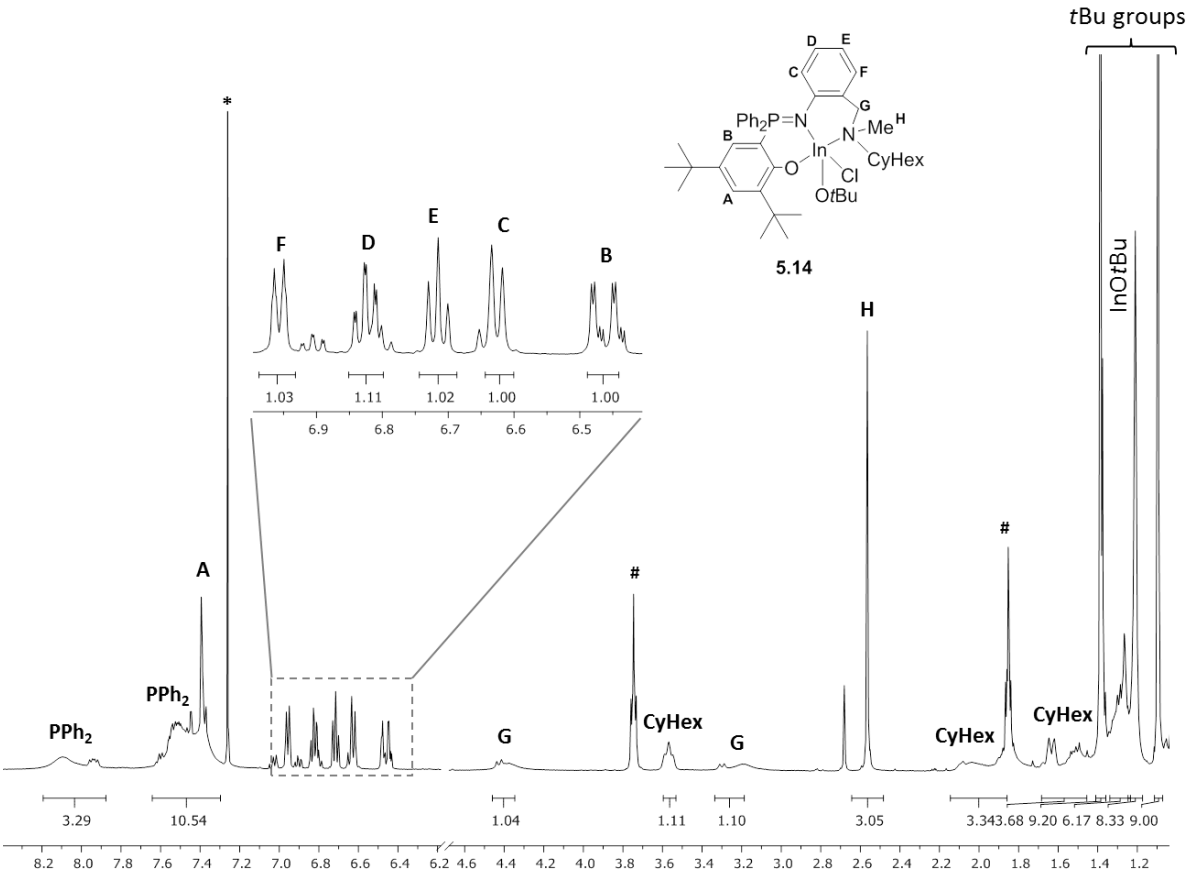

Figure 5.15. ^{1}H NMR spectrum of the indium *tert*-butoxide, chloride complex, **5.14** ($CDCl_3$*, 400 MHz, 298 K, residual solvent$^{\#}$).

5.5. Polymerisation Catalysis

Complexes **5.8**, **5.10**, **5.12** and **5.14** were tested as initiators in the ROP of *rac*-LA (Table 5.1). The polymerisations were carried out under standard conditions: 1 M solution of *rac*-LA in THF and with a catalyst loading of 1 mol%. Complex **5.12** was tested at a range of temperatures from 298 K to 333 K and complex **5.14** was tested at 298 and 333 K. For the polymerisations carried out at room temperature, the polymerisation kinetics were analysed by collecting aliquots, at regular intervals. For high temperature polymerisations, separate runs were quenched at different times. The aliquots were analysed by ^{1}H NMR spectroscopy to determine conversion (%). Complex **5.8** was tested by itself (Entry 1) and with one equivalent of *iso*-propyl alcohol (IPA) (Entry 2), which was proposed to form the alkoxide species *in situ*, and compared with complex **5.10** (Entry 3).

Table 5.1. Polymerisation data using initiators **5.8**, **5.10**, **5.12** and **5.14**.

Entry	Initiator	Conv. (%)[f]	t (mins)	k_{obs} (x 10^{-4} s^{-1})[g]	M_n (g mol^{-1})[h]	M_n^{calc} (g mol^{-1})	Đ[h]	P_i[i]
1[a]	**5.8**	97	210	1.87 ± 0.04	7500	14000	1.44	0.67 ± 0.04
2[b]	**5.8**	94	90	8.41 ± 0.69	10800	13600	1.32	0.67 ± 0.03
3[a]	**5.10**	95	90	9.12 ± 0.42	18500	13700	1.44	0.69 ± 0.04
4[a]	**5.12**	84	2160	0.118 ± 0.002	12900	12100	1.09	0.60 ± 0.06
5[c]	**5.12**	41	240	0.327 ± 0.019	3400	5900	1.06	0.61 ± 0.04
6[d]	**5.12**	62	240	0.580 ± 0.024	4100	8900	1.09	0.61 ± 0.05
7[e]	**5.12**	88	240	2.32 ± 0.16	6700	12700	1.02	0.61 ± 0.04
8[a]	**5.14**	95	900	0.526 ± 0.013	12300	13700	1.01	0.72 ± 0.04
9[e]	**5.14**	96	180	3.22 ± 0.52	12000	14000	1.02	0.65 ± 0.04

[a]Polymerisation conditions: [Initiator]:[LA] = 1:100, [LA] = 1 M, THF, 298 K, [b]Polymerisation conditions: [Initiator]:[IPA]:[LA] = 1:1:100, [LA] = 1 M, THF, 298 K, [c]Polymerisation conditions: [Initiator]:[LA] = 1:100, [LA] = 1 M, THF, 313 K, [d]Polymerisation conditions: [Initiator]:[LA] = 1:100, [LA] = 1 M, THF, 323 K, [e]Polymerisation conditions: [Initiator]:[LA] = 1:100, [LA] = 1 M, THF, 333 K, [f]Determined by integration of the methine region of the ^{1}H NMR spectrum (LA, 5.00 - 5.07 ppm; PLA, 5.10 – 5.24 ppm), [g]Measured by determining the gradients of the plots of $\ln\{[LA]_0/[LA]_t\}$ vs. time, [h]Determined by gel-permeation chromatography in THF, using multiangle laser light scattering (GPC-MALLS), [i]Determined by integrating the average P_i values obtained for each tetrad signal in the methine region of the homonuclear-decoupled ^{1}H NMR spectrum.

5.5.1. Polymerisation Kinetics

5.5.1.1. Zinc Initiators

Complex **5.8** displayed an initiation period of 20 minutes, after which the polymerisation proceeded. Complex **5.8**, complex **5.8** with one equivalent of IPA, and complex **5.10** all showed pseudo first-order rate kinetics as evident by linear fits to plots of $\ln([LA]_0/[LA]_t)$ v.s time (Figure 5.16). The rates of complex **5.10** and complex **5.8** with IPA, were the same within error, as expected as they share a common initiator structure. The value of k_{obs} for complex **5.8** was 5 times lower than the two other systems.

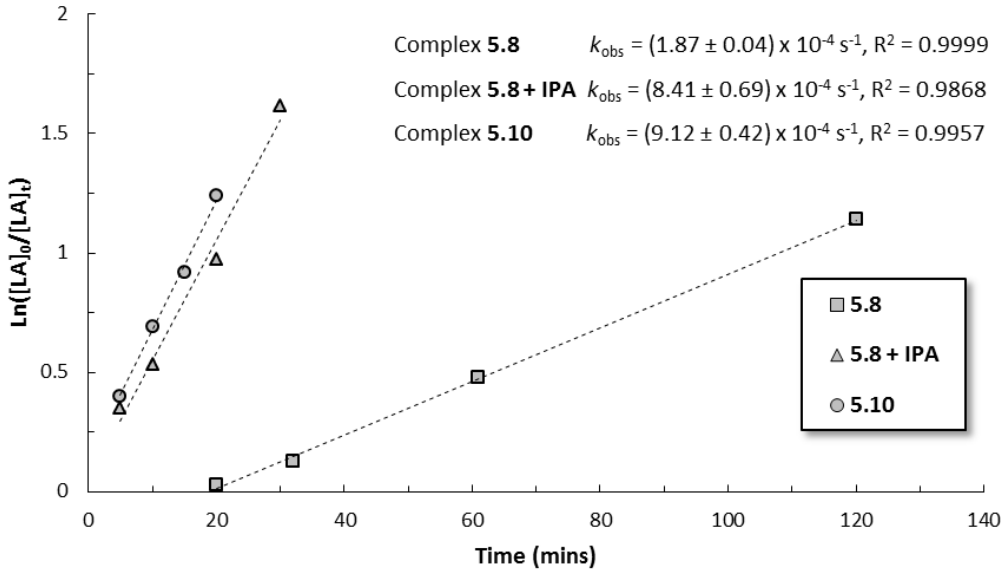

Figure 5.16. Plot of $\ln([LA]_0/[LA]_t)$ vs time of complexes **5.8**, **5.8** + IPA and **5.10**. Conditions: [I]:[LA] = 1:100, [LA] = 1M, THF, 298 K.

5.5.1.2. Indium Initiators

Complex **5.12** displayed pseudo first-order kinetics as observed by its linear fit to the plot of $\ln([LA]_0/[LA]_t)$ vs. time, at all temperatures tested (Figure 5.17). As expected, the observed rate constant increased with temperature, increasing 3-fold from 298 K to 313 K, 2-fold from 313 K to 323 K and 4-fold from 323 – 333 K.

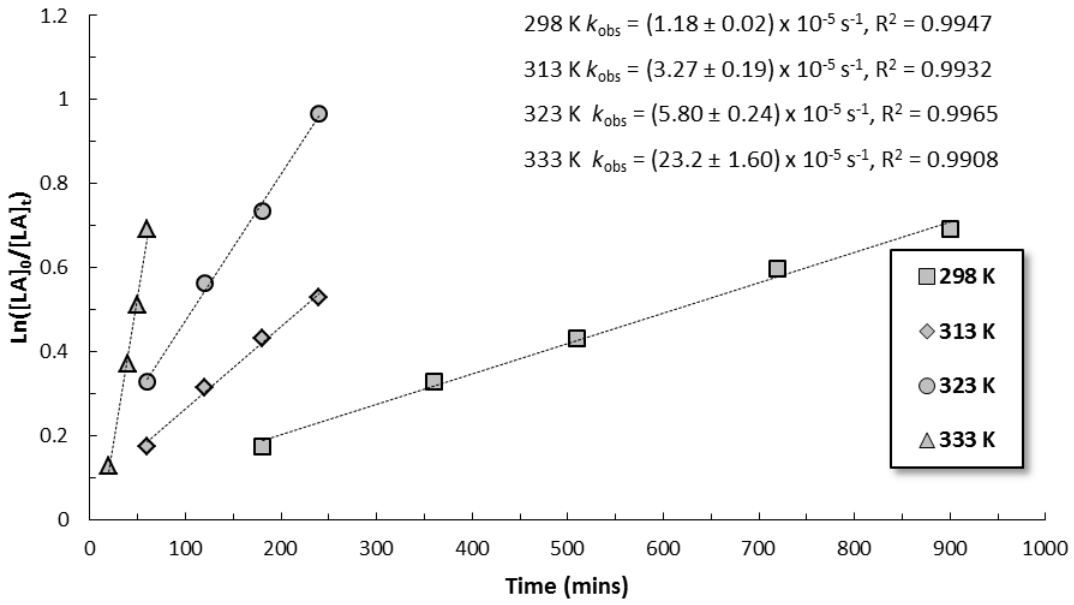

Figure 5.17. Plot of $\ln([LA]_0/[LA]_t)$ vs time of complex **5.12** at 298, 313, 323 and 323 K. Conditions: [I]:[LA] = 1:100, [LA] = 1M, THF.

Complex **5.14** also displayed pseudo first-order kinetics as shown by a linear fit to plots of $\ln([LA]_0/[LA]_t)$ vs. time, at 298 and 333K (Figure 5.18). The observed rates increased with temperature, with a 6-fold increase in rate between the room temperature polymerisation and at 333 K, as seen above.

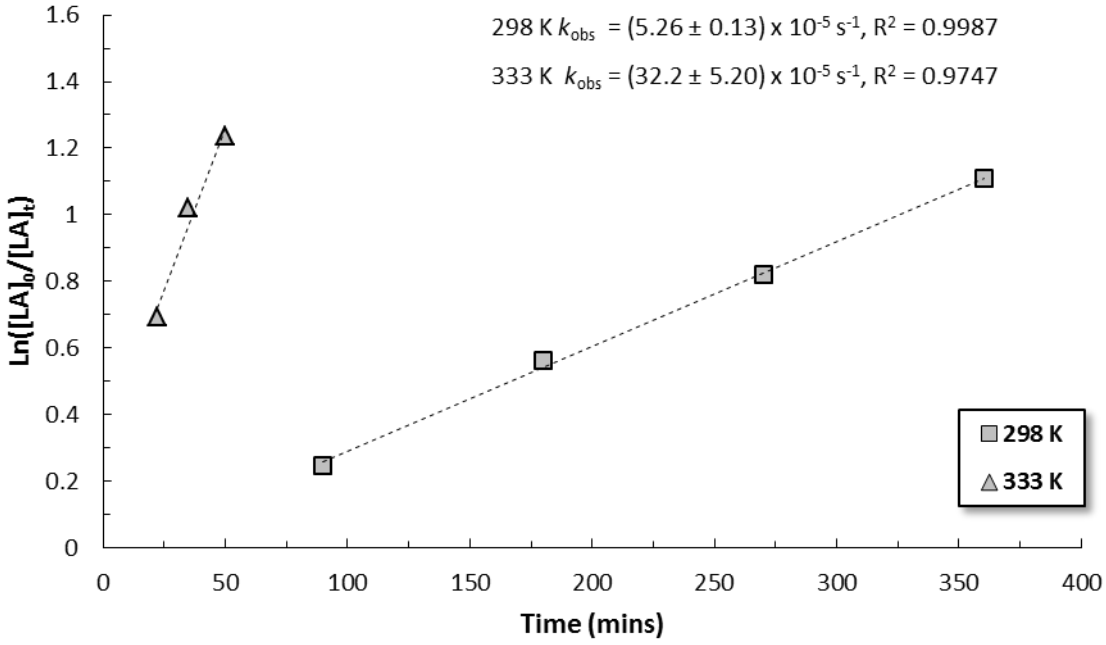

Figure 5.18. Plot of $\ln([LA]_0/[LA]_t)$ vs time of complex **5.14** at 298 and 323 K. Conditions: [I]:[LA] = 1:100, [LA] = 1M, THF.

5.5.2. Polymerisation Control

5.5.2.1. Zinc Initiators

Gel permeation chromatography (GPC) analysis was carried out to determine the molecular weight (M_n) and dispersities (Đ) of each aliquot during the polymerisations. All initiators showed good polymerisation control, as demonstrated by a linear increase in M_n with % conversion (Figure 5.19). For complex **5.8**, the zinc amide complex, higher molecular weights than predicted and broad dispersities (Đ > 1.30) were observed. The M_n values for the polymerisation of complex **5.8** + IPA, were in better agreement with the theoretical values, than complex **5.8** by itself. Similarly, the dispersities throughout the polymerisation were narrower (1.04 < Đ < 1.32).

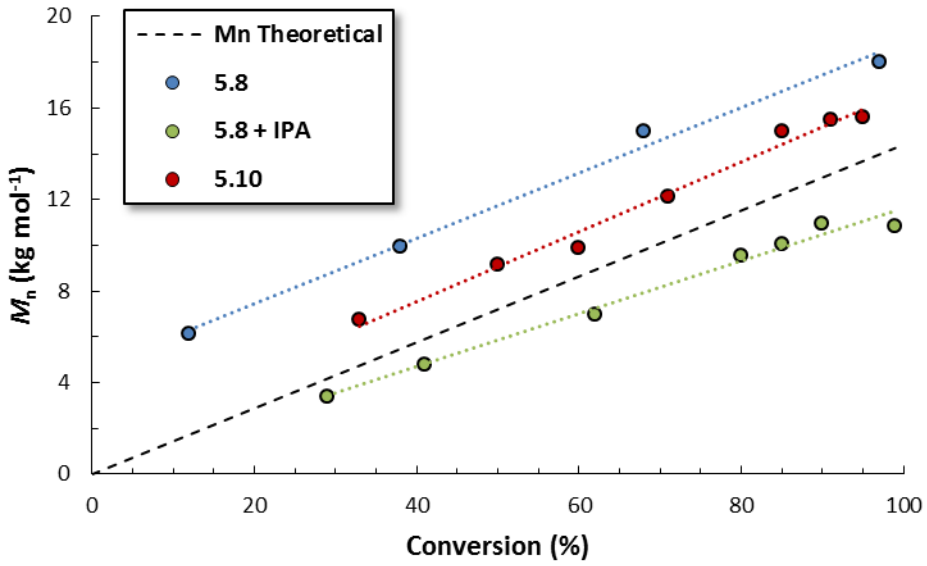

Figure 5.19. Plot of the M_n vs. conversion for the polymerisation of *rac*-LA mediated by complexes **5.8** and **5.10**. Conditions: [**5.8**]:[LA] = 1:100, [LA] = 1M, THF, 298 K - blue; [**5.8**]:[IPA]:[LA] = 1:1:100, [LA] = 1M, THF, 298 K - green; [**5.10**]:[LA] = 1:100, [LA] = 1M, THF, 298 K -red.

A MALDI-ToF spectrum of the low molecular weight polymers produced from initiator **5.8** + IPA was collected and the only polymer series present showed *iso*-propoxide end-groups (Figure 5.20). This first confirmed that the initiating species was the *iso*-propoxide co-ligand, a result of the successful reaction between the amide co-ligand and IPA, and secondly, that no competitive transesterification reactions were present.

For complex **5.10**, the M_n values were greater than predicted and dispersities broader ($1.04 < Đ < 1.44$). It can be assumed that transesterification reactions would not be present in the polymerisation with complex **5.10**, due the presence of the same initiating species in the polymerisation using complex **5.8** and an equivalent of IPA, where no transesterification was observed. Attempts to collect the MALDI-ToF spectrum of low molecular weight polymers were not successful. Therefore, the presence of transesterification reactions was ruled out using $^{13}C\{^1H\}$ spectroscopy. Using the method outlined in Section 2.1, observation of the methine region of all polymer samples found no resonances corresponding to the iss, sss or ssi tetrads, which can only be observed after transesterification. It is also known that transesterification reactions only lead to broad dispersities and not a change in M_n, therefore the poor control observed in complex **5.10** does not arise from transesterification.

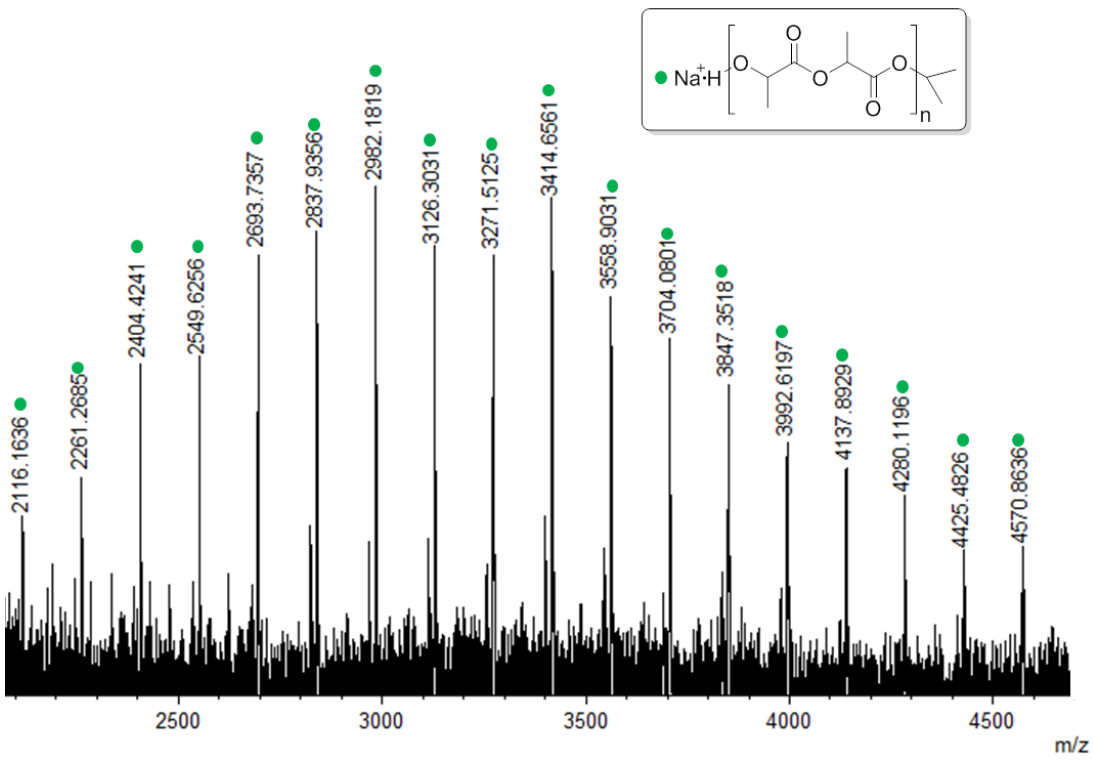

Figure 5.20. MALDI-ToF spectrum obtained from the polymerisation with complex **5.8** and one equivalent of IPA. Conditions: [**5.8**]:[IPA]:[LA] = 1:1:100, [LA] = 1M, THF, 298 K.

5.5.2.2. Indium Initiators

Indium complex, **5.12**, displayed excellent polymerisation control at 298 K with linear increase of M_n against % conversion, good correlation between calculated and experimental M_n values and narrow dispersities throughout (1.01 < Đ < 1.09). For polymerisations carried out at 313, 323 and 333 K, narrow dispersities were observed, but M_n values were half of the calculated values (Figure 5.21). This trend is rationalised by only one *tert*-butoxide group initiating the polymerisation at 298 K whereas at 313 K and above, both *tert*-butoxide groups were proposed to be initiating.

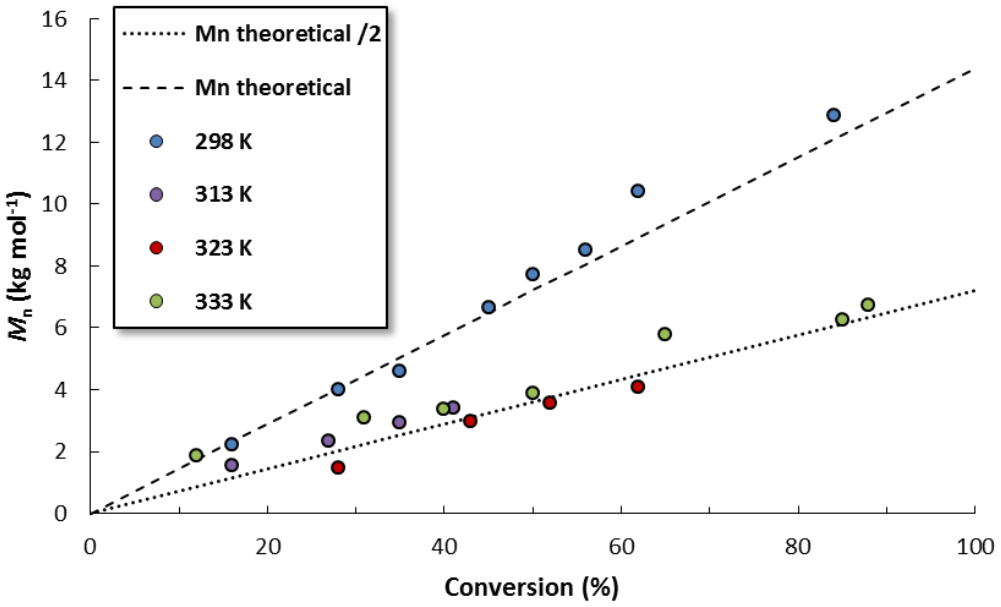

Figure 5.21. Plot of the M_n vs. conversion for the polymerisation of *rac*-LA mediated by complex **5.12**. Conditions: [**5.12**]:[LA] = 1:100, [LA] = 1M, THF, 298, 313, 323 and 333 K.

Complex **5.14** displayed excellent polymerisation control at both 298 K and 333 K with a linear increase of M_n against % conversion and narrow dispersities throughout (Figure 5.22).

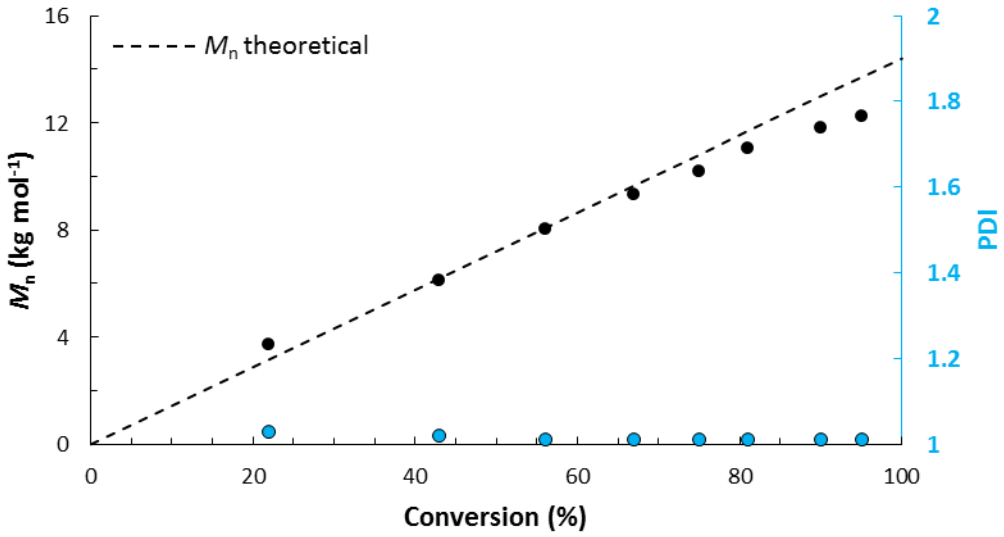

Figure 5.22. Plot of the molecular weight and polydispersity vs. conversion for the polymerisation of *rac*-LA mediated by complex **5.14**. Conditions: [**5.14**]:[LA] = 1:100, [LA] = 1M, THF, 298 K.

5.5.3. Isoselectivity

The isoselectivity of the polymers was determined by analysis of the tetrad resonances, of the methine proton, in the deconvoluted, homonuclear decoupled $^{1}H\{^{1}H\}$ NMR spectrum. Zinc complexes **5.8** and **5.10** yielded P_i values of 0.67 and 0.69 respectively, which correlates to a low degree of isoselectivity. Similarly for indium complex **5.12**, low isoselectivity was displayed at all temperatures (P_i = 0.60-0.61). Interestingly, for indium complex **5.14**, a moderate isoselectivity value was observed at room temperature (P_i = 0.72) (Figure 5.23). At higher temperatures (333 K), this value dropped to 0.65. Inspection of the stereoerrors suggested a CEC mechanism.

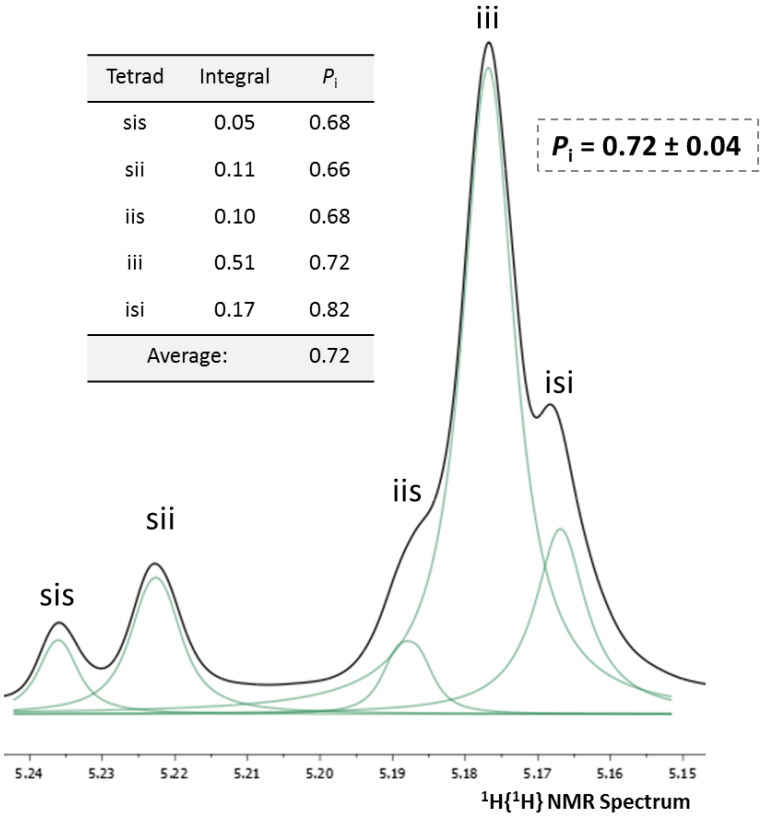

Tetrad	Integral	P_i
sis	0.05	0.68
sii	0.11	0.66
iis	0.10	0.68
iii	0.51	0.72
isi	0.17	0.82
Average:		0.72

Figure 5.23. ^{1}H NMR spectrum ($CDCl_3$, 400 MHz, 298 K) and calculation of P_i value for PLA sample yielded from Complex **5.14**. Conditions: [**5.14**]:[LA] = 1:100, [LA] = 1M, THF, 298 K.

5.5.4. Discussion

5.5.4.1. Zinc Initiators

For the zinc initiators, complex **5.8** with one equivalent of IPA was the most successful system, yielding the fastest rate and good polymerisation control. Complex **5.8** with no additives (exogenous alcohol) showed a 20-minute initiation period, yielded high M_n PLA with broad dispersities (Figure 5.20). These features are characteristic of slow initiation vs. propagation, likely due to the bulky initiating group slowing initiation.[13] After one monomer is inserted, the initiating group has no influence on propagation rate. Due to the slow insertion of the first monomer and the reversibility of lactide coordination, it will inevitably result in a range of initiation times and therefore M_n values for each metal centre in the initiator sample (Figure 5.24). During the initiation period (1/2), only a small proportion of the complex reacts to insert the first monomer and begin polymerisation

(3). As time proceeds, the proportion of active initiator increases (4), resulting in a range of M_n (5). The M_n values are higher than expected because only a proportion of initiator is active.

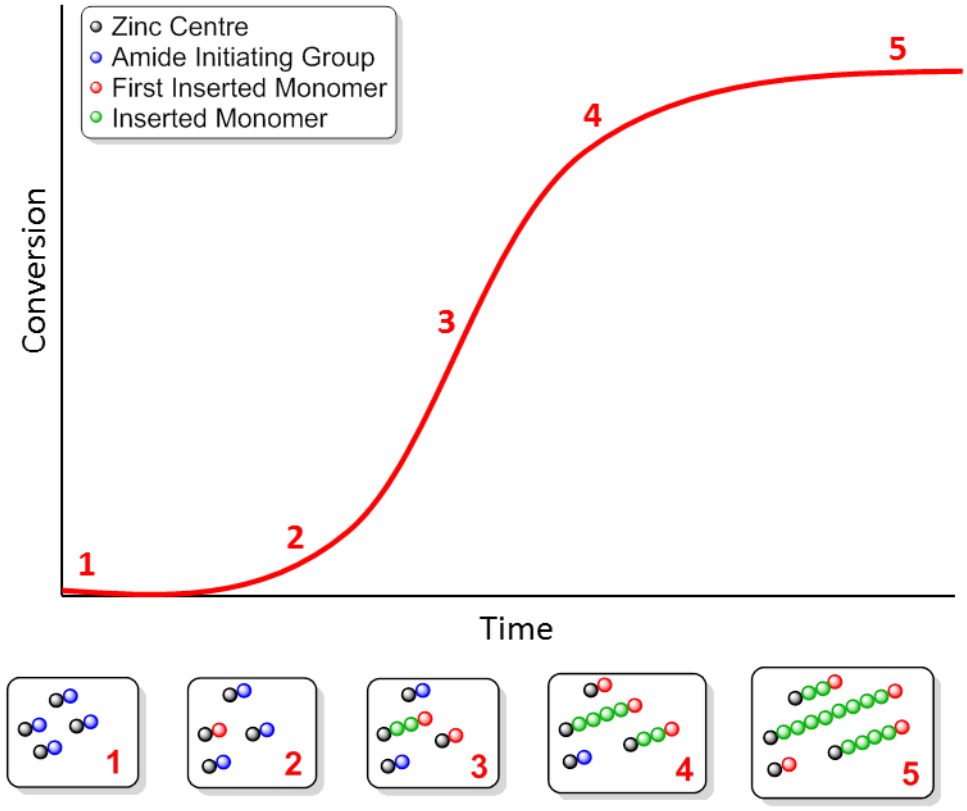

Figure 5.24. Visual schematic of the different initiation times and therefore polymer M_n and dispersities, of complex **5.8**, during the polymerisation. N.B. The first inserted monomer will contain an amide end-group, removed for clarity.

Addition of an equivalent of IPA to complex **5.8**, prior to polymerisation, resulted in the *in situ* formation of an *iso*-propoxide initiating group. This was confirmed by *iso*-propoxide end groups in the MALDI-ToF spectrum (Figure 5.20). Alkoxide co-ligands are better initiators due to a reduced steric hindrance and increased lability of the metal-alkoxide bond.[13] This led to no initiation period, an overall faster rate, more predictable M_n and narrower dispersities.

Complex **5.10**, the isolated *iso*-propoxide complex, yielded a comparable rate to complex **5.8** + IPA, which is expected as they feature the same initiating group. Despite this, the

M_n values were higher and dispersities broader than those obtained from the polymerisation with complex **5.8** + IPA. This is tentatively attributed to the sensitivity of complex **5.10** to hydrolysis/decomposition.

5.5.4.2. Indium Initiators

For indium initiators, complexes **5.12** and **5.14**, the latter yielded the best rates at both 298 K and 333 K, with a 5-fold increase in rate at 298 K and 1.5-fold increase at 333 K between the two. For the polymerisations carried out at 298 K, the rates of propagation (k_p) were determined by carrying out polymerisations at a range of initiator concentrations (Figure 5.25). For both initiators, first-order rate dependence on initiator concentration was observed by linear fits of k_{obs} vs [initiator]. Therefore, the overall rate law was second-order, and the rate-limiting step was proposed to be the nucleophilic attack of the indium-alkoxide bond on the carbonyl bond of the lactide monomer. The k_p values for complexes **5.12** and **5.14** were 0.07 ± 0.0002 and 0.32 ± 0.006 M^{-1} min^{-1}, respectively, and were low compared to other indium initiators both in this thesis (Chapters 3 and 4) and the broader literature.[17,20,25]

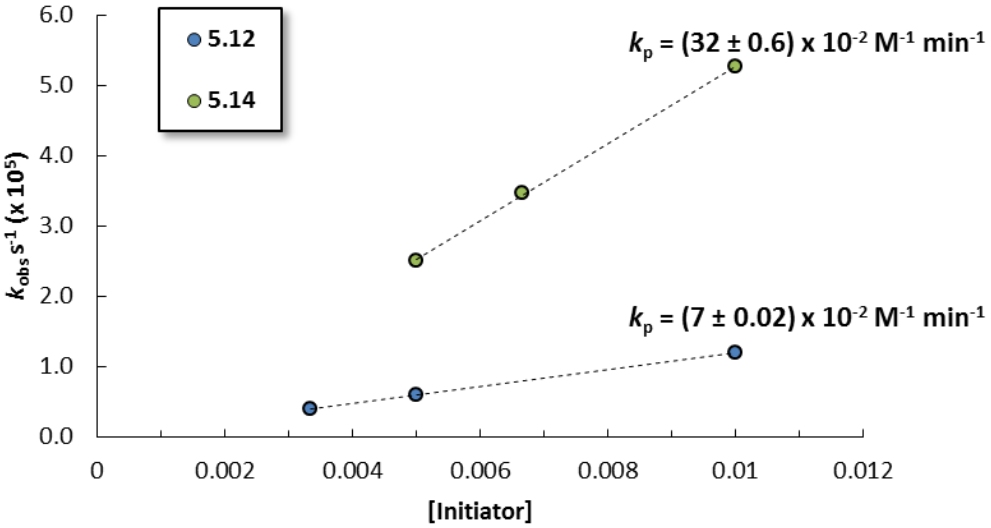

Figure 5.25. Plot of k_{obs} against initiator concentration for calculation of the propagation rate constant, k_p, for complexes **5.12** and **5.14**.

It can be hypothesised that the ligand decreases the lability of the alkoxide bond, resulting in slower rates. This is unexpected, as phosphasalen ligands are typically more electron donating than salen ligands, due to the iminophosphorane bond being a stronger σ- and π- donor than an imine bond.[15] As such, they would be expected to reduce the Lewis acidity of the metal centre and to increase the lability of the metal-alkoxide bond. Therefore, it is proposed that the differences in rates must arise from another feature of the ligands.

Both complex **5.14** and Mehrkhodavandi's Schiff base indium initiator featured one alkoxide initiating group and a chloride co-ligand in the initiating species (**D**, Figure 5.3). Initiator **D** polymerised 200 equivalents of *rac*-LA in 30 minutes (298 K, CH_2Cl_2), so despite the difference in solvent, a large increase in rate compared to complex **5.14** was observed.[20] Therefore, the presence of a chloride co-ligand cannot be attributed to slowing rates in complex **5.14**. For complex **5.12**, featuring two alkoxide co-ligands, a further reduction in rate could be attributed to both ligand effects and the co-ligands present, but without further evidence this cannot be confirmed at this stage.

When increasing the polymerisation temperature, it can be expected that the rate will increase. This phenomenon arises from the greater proportion of molecules that are able to overcome the activation barrier to access the transition state. This increase in rate was observed for both initiators **5.12** and **5.14**.

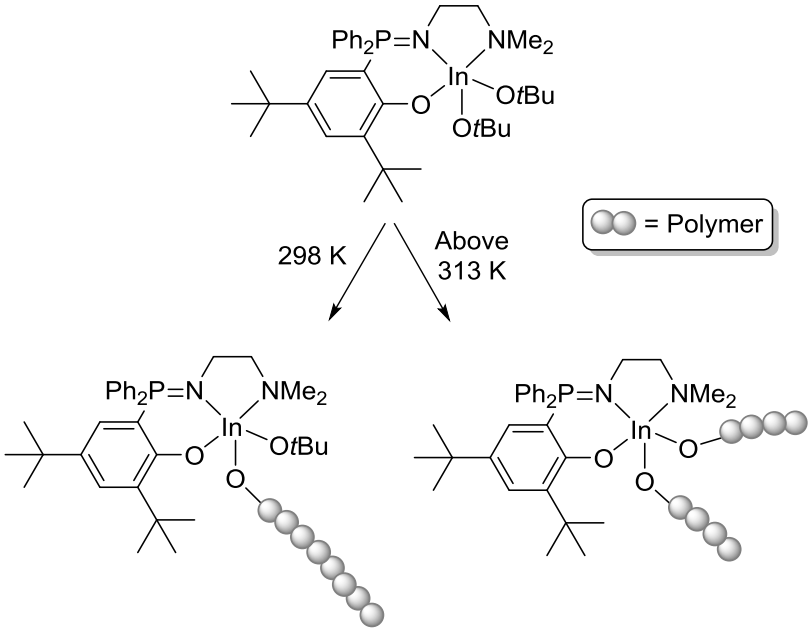

Figure 5.26. Visual representation of the difference in initiating groups for complex **5.12** at different temperatures.

Both initiators yielded excellent polymerisation control, at all temperatures, but for complex **5.12**, a change in the number of initiating groups was observed between 298 K and 313 K. This was confirmed by inspection of the M_n values obtained and comparison to the expected M_n values (Figure 5.21). At 298 K, one alkoxide group initiated the polymerisation whilst at 313 K and above, both alkoxide groups initiated, yielding PLA with M_n values half those as 298 K (Figure 5.26). It was hypothesised that the change in the number of initiating groups might relate to changes in ligand confirmation with temperature. VT NMR studies (^{1}H and ^{31}P{^{1}H} spectra) at 298-333 K (d_8-THF, 500 MHz) showed no change in either spectrum upon heating. Therefore, it was concluded that changes in the ligand conformation were not responsible for the change in number of groups initiating. Rather, an activation barrier for the second alkoxide group was apparently higher and only accessible at higher temperatures.

The activation parameters of the polymerisation in the temperature range 313 – 333 K, when two alkoxide groups were initiating, were obtained from an Eyring plot. Using the

Eyring-Polyani equation and plotting ln(k_{obs}/T) against 1/T, $\Delta H^{\ddagger}$ and $\Delta S^{\ddagger}$ were calculated from the gradient and intercept, respectively (Equation 5.1). The values obtained were $\Delta H^{\ddagger}$ = 64 kJ mol^{-1} and $\Delta S^{\ddagger}$ = -71 J K^{-1} mol^{-1}. For initiator **D** these values were $\Delta H^{\ddagger}$ = 49 kJ mol^{-1} and $\Delta S^{\ddagger}$ = -140 J K^{-1} mol^{-1}.[20] It is worth noting that initiator **D** only features one initiating group, so comparison of these values is somewhat limited, but may provide some information about complex **5.12**. The higher value for $\Delta H^{\ddagger}$ apparently correlates with the higher temperatures and energy required to activate two initiating groups in complex **5.12**.

A negative value for $\Delta S^{\ddagger}$ suggests the transition state is a single activated complex. It is proposed that the rate-limiting step is nucleophilic attack of the alkoxide on the coordinated lactide monomer. This step involves a single species undergoing an intramolecular reaction, which is in line with a negative $\Delta S^{\ddagger}$ and could imply a concerted process. Further investigation would be required to probe this mechanism and understand the steps involved when two initiating groups are present. For greater understanding of the different number of initiating groups, comparison of the activation parameters to the lower temperature range would aid this. Unfortunately, due to the slow rates of polymerisation and experimental difficulties, this could not be completed.

$$ln\left(\frac{k_{obs}}{T}\right) = \frac{\Delta H^{\ddagger}}{R}.\frac{1}{T} + ln\left(\frac{k_B}{h}\right) + \frac{\Delta S^{\ddagger}}{R}$$

Equation 5.1. Eyring-Polyani Equation. *k_{obs} = Observed rate of polymerisation, T = Temperature, $\Delta H^{\ddagger}$ = Enthalpy of activation, R = Gas constant, h = Planks constant, $\Delta H^{\ddagger}$ = Entropy of activation.*

Complex **5.12** resulted in low isoselectivity over a temperature range of 298 to 333 K (P_i = 0.61), whereas complex **5.14** achieved better isoselectivity (P_i = 0.72) at room temperature, which decreased at higher temperatures (P_i = 0.65, 333 K). A reduction in P_i with temperature is expected since stereocontrol is kinetically controlled.[26] The

isoselectivity achieved by **5.14** is also an improvement in comparison to initiator **F**, which yielded P_i = 0.62 (298 K). Both initiators also operated by a chain-end control mechanism. Due to their similarities in terms of co-ligands present (one alkoxide, one chloride), the two offer an interesting comparison. The steric hindrance, in the form of a cyclohexane group, present in the ligand of complex **5.14** could explain this increase in isoselectivity, as initiator **D** features much less bulky methyl groups in the same position. Furthermore, the increased bridge size of complex **5.14** vs. **D** (3- and 2-carbon respectively), could allow for increased steric protection around the indium centre and therefore a more selective approach of a specific monomer after the initial insertion of either enantiomer.

5.6. Summary and Outlook

5.6.1. Summary

The synthesis of two novel half-phosphasalen ligands was described. The first of which, ligand **5.1**, featured a flexible ethylene backbone and methyl substituents at nitrogen. The complexation of **5.1** to zinc resulted in formation of a homoleptic species (complex **5.6**) over the target heteroleptic zinc alkoxide, even *via* a variety of routes (complexes **5.3**-**5.5**). Ligand **5.2**, featured a larger, but less flexible phenylene backbone and bulkier N-substituents - a cyclohexyl group. The syntheses of zinc complexes (**5.7**-**5.9**) and a zinc *iso*-propoxide initiator (complex **5.10**) were successful. Both ligands were also complexed to indium, for ligand **5.1** a complex with two alkoxide co-ligands was synthesised (complex **5.12**), whereas for ligand **5.2**, the main species isolated contained one alkoxide and one chloride co-ligand (complex **5.14**). All complexes were analysed by NMR spectroscopy, elemental analysis and for some complexes, using X-ray diffraction. The indium complexes were also analysed by DOSY NMR to confirm their aggregation state.

Zinc complexes **5.8** (zinc amide) and **5.10** (zinc *iso*-propoxide) were tested in the ROP of *rac*-LA. Complex **5.8** was tested independently and with one equivalent of IPA added prior to addition to the monomer. The differences in rate were **5.8** < **5.10** ~ **5.8** + IPA. The polymerisation control with **5.8** was relatively poor, giving broad dispersities and higher than expected M_n values. These were improved for the polymerisation using **5.8** + IPA, due to the formation of a more efficient initiating group, an alkoxide. All initiators displayed low isoselectivites (P_i = 0.67-0.69, 298 K).

Indium complexes **5.12** and **5.14** were also tested in the ROP of *rac*-LA over range of temperatures (298–333 K). Complex **5.14** was faster than **5.12** but both initiators were

much slower than other initiators reported in the literature.[17,25] They displayed excellent polymerisation control, as expected for indium initiators, with narrow dispersities and predictable M_n values. Complex **5.12** underwent a change in the number of growing polymer chains with temperature, with one at room temperature and two at temperatures above 313 K. The reason for this was attributed to a higher activation barrier for the second chain growth, but further investigation is required. Complex **5.12** displayed low isoselectivites (P_i = 0.60-0.61, 298–313 K) whereas, at room temperature, complex **5.14** yielded a good isoselectivity (P_i = 0.72, 298 K). This was accredited to the increased steric protection provided by ligand **5.2** vs. ligand **5.1**.

5.6.2. Outlook

The origins of the change in number of initiating groups for complex **5.12** and the increased isoselectivity bias of complex **5.14** are currently unknown. Furthermore, the large decrease in rate of these complexes compared to other indium Schiff base initiators (**D**) was unexpected especially as phosphasalen ligands typically increase rates. These phenomena can be further investigated using the following experiments:

1. Determination of $\Delta H^{\ddagger}$ and $\Delta S^{\ddagger}$ for complex **5.12** at low temperatures (273-298 K)
2. Synthesis of an analogue of complex **5.12** with one alkoxide co-ligand and one chloride co-ligand
3. Individual polymerisation reactions using complex **5.14** using *D*-LA and *L*-LA to understand mechanism of stereocontrol
4. Crystallisation of complex **5.14** with one lactide monomer or ethyl lactate
5. Synthesis of the half-salen and half- Schiff base analogues of ligands **5.1** and **5.2** and coordinate to indium

These experiments range in difficulty, but the information elucidated could offer useful insights in the rate and stereocontrol mechanisms. The mechanistic study for complex **5.12** would be of particular interest, due to the presence of two initiating groups. Understanding the origin of stereocontrol would also aid in the development of new, increasingly isoselective initiators.

As well as gaining insight into the complexes reported in this chapter, the scope of these ligands and complexes can be investigated by further modifications to the ligand. Figure 5.27 summarises the range of modifications that could be carried out. The key aim of such modifications would be to increase rate and isoselectivity.

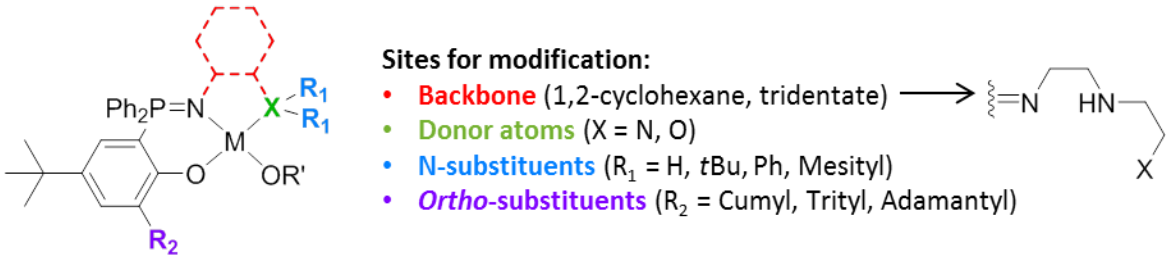

Figure 5.27. Overview of potential modifications to the half-phosphasalen ligand and resultant complexes (M = Zn, Mg, In).

The modifications proposed are inspired by recent reports of other successful initiators in the literature.[27] Kol and co-workers reported a tetradentate monoanionic ligand coordinated to magnesium yielding highly stereoblock PLA, albeit using a sequential addition of enantiomers, but highlighting the potential for additional donor groups.[28] This could be extended to half phosphasalen ligands by using a tridentate backbone (e.g. a derivative of diethylene triamine). The initiators reported by Ma and co-workers feature a chiral tridentate ligand which when coordinated to zinc achieved excellent isoselectivity.[11,12] Whilst a monoanionic ligand is preferable for zinc(II) and magnesium(II) centres, the distal donor group present in the backbone can be varied for use with

indium(III) centres, therefore allowing for only one alkoxide co-ligand. The steric bulk at this position can also be varied, and for complex **5.14**, greater hindrance increased the isotactic bias. Therefore, the influence (if any) of sterically bulky groups at this site can be investigated. Finally, increasing the bulk in the *ortho*-phenolate position has been observed to increase P_i for various zinc(II) and indium(III) initiators, therefore a similar approach should be targeted in the future in these systems.[3,9,17]

5.7. References

1 C. K. Williams, N. R. Brooks, M. A. Hillmyer and W. B. Tolman, *Chem. Commun.*, 2002, 2132–2133.

2 G. Labourdette, D. J. Lee, B. O. Patrick, M. B. Ezhova and P. Mehrkhodavandi, *Organometallics*, 2009, **28**, 1309–1319.

3 D. J. Darensbourg and O. Karroonnirun, *Inorg. Chem.*, 2010, **49**, 2360–2371.

4 F. Drouin, P. O. Oguadinma, T. J. J. Whitehorne, R. E. Prud'homme and F. Schaper, *Organometallics*, 2010, **29**, 2139–2147.

5 V. Poirier, T. Roisnel, J.-F. Carpentier and Y. Sarazin, *Dalton Trans.*, 2011, **40**, 523–534.

6 X.-F. Yu, C. Zhang and Z.-X. Wang, *Organometallics*, 2013, **32**, 3262–3268.

7 M. Honrado, A. Otero, J. Fernández-Baeza, L. F. Sánchez-Barba, A. Lara-Sánchez, J. Tejeda, M. P. Carrión, J. Martínez-Ferrer, A. Garcés and A. M. Rodríguez, *Organometallics*, 2013, **32**, 3437–3440.

8 S. Inkinen, M. Hakkarainen, A.-C. Albertsson and A. Södergård, *Biomacromolecules*, 2011, **12**, 523–532.

9 L. Wang and H. Ma, *Dalton Trans.*, 2010, **39**, 7897–7910.

10 S. Song, X. Zhang, H. Ma and Y. Yang, *Dalton Trans.*, 2012, **41**, 3266–3277.

11 H. Wang and H. Ma, *Chem. Commun.* , 2013, **49**, 8686–8688.

12 H. Wang, Y. Yang and H. Ma, *Macromolecules*, 2014, **47**, 7750–7764.

13 S. Abbina and G. Du, *ACS Macro Lett.*, 2014, **3**, 689–692.

14 Z. Mou, B. Liu, M. Wang, H. Xie, P. Li, L. Li, S. Li and D. Cui, *Chem. Commun.* , 2014, **50**, 11411–11414.

15 C. Bakewell, T.-P.-A. Cao, N. Long, X. F. Le Goff, A. Auffrant and C. K. Williams, *J. Am. Chem. Soc.*, 2012, **134**, 20577–20580.

16 C. Bakewell, A. J. P. White, N. J. Long and C. K. Williams, *Angew. Chem. Int. Ed.*, 2014, **53**, 9226–9230.

17 D. Myers, A. J. P. White, C. M. Forsyth, M. Bown and C. K. Williams, *Angew. Chem. Int. Ed.*, 2017, **56**, 5277–5282.

18 C. A. Wheaton, B. J. Ireland and P. G. Hayes, *Organometallics*, 2009, **28**, 1282–1285.

19 C. A. Wheaton and P. G. Hayes, *Chem. Commun.*, 2010, **46**, 8404–8406.

20 A. F. Douglas, B. O. Patrick and P. Mehrkhodavandi, *Angew. Chem. Int. Ed.*, 2008,

47, 2290–2293.

21 M. Bochmann, G. Bwembya, K. J. Webb, M. A. Malik, J. R. Walsh and P. O'Brien, in *Inorganic Syntheses*, John Wiley & Sons, Inc., Hoboken, NJ, USA, 2007, pp. 19–24.

22 C. K. Williams, L. E. Breyfogle, S. K. Choi, W. Nam, V. G. Young, M. A. Hillmyer and W. B. Tolman, *J. Am. Chem. Soc.*, 2003, **125**, 11350–11359.

23 M. H. Chisholm, N. W. Eilerts, J. C. Huffman, S. S. Iyer, M. Pacold and K. Phomphrai, *J. Am. Chem. Soc.*, 2000, **122**, 11845–11854.

24 S. Inoue, M. Kobayashi and T. Tozuka, *J. Organomet. Chem.*, 1974, **81**, 17–21.

25 D. C. Aluthge, B. O. Patrick and P. Mehrkhodavandi, *Chem. Commun.*, 2013, **49**, 4295–4297.

26 H. R. Kricheldorf, M. Berl and N. Scharnagl, *Macromolecules*, 1988, **21**, 286–293.

27 C. Kan, J. Hu, Y. Huang, H. Wang and H. Ma, *Macromolecules*, 2017, **50**, 7911–7919.

28 T. Rosen, I. Goldberg, V. Venditto and M. Kol, *J. Am. Chem. Soc.*, 2016, **138**, 12041–12044.

Chapter 6

Outlook

In the field of bio-derived polymers, the synthesis of materials, such as PLA, which are biodegradable and have competitive physical and mechanical properties, are desirable. The isotactic ROP of *rac*-LA yields the highest melt temperatures, and consequently the best mechanical properties of PLA. Therefore, this thesis focused on the synthesis of metal initiators, containing ligands that could undertake the isoselective ROP of *rac*-LA with good rates, under mild conditions and exhibit excellent polymerisation control.

The original aims of this thesis were:

1. Synthesis of a hybrid tetradentate ligand containing one imine and iminophosphorane bond and coordinate to Group 13 metals.
2. Investigate structure-activity relationships with the hybrid ligand by steric and electronic modification.
3. Synthesise a ferrocene-containing initiator.
4. Synthesis of half-phosphasalen ligands for coordination to zinc(II).

The hybrid ligand, whilst coordinated to indium(III) yielded higher isoselective control (P_i = 0.71) than its indium salen and phosphasalen analogues (P_i = 0.51 – 0.52). The rates of all aluminium initiators were poor in comparison to indium initiators, due to decreased metal-alkoxide bond lability. Structure-activity investigations of the hybrid ligand found that the size of the *ortho*-phenolate and phosphorus substituents were important in isoselectivity but that when the substituent was too large, e.g. adamantyl, ligand distortion orientated these groups away from the metal centre. Furthermore, electron-withdrawing groups significantly increased polymerisation rates.

The synthesis of a ferrocene-containing indium complex was achieved, but the co-ligand was not suitable for polymerisation studies, therefore, future investigations with this complex are discussed below. Electrochemical studies with this complex found that it underwent a stable and reversible one-electron redox event, which is necessary for future redox-switch catalysis.

Finally, two half-phosphasalen ligands were synthesised for complexation to zinc(II). The less sterically encumbered ligand preferentially formed homoleptic zinc complexes, instead of the desired zinc alkoxide initiators, due to a Schlenk equilibrium. Increasing the size of the nitrogen substituents and decreasing the flexibility of the ligand backbone allowed synthesis of zinc amide and alkoxide initiators. These initiators yielded moderate yields but poor polymerisation control. The ligands were also coordinated to indium(III) and one initiator, with the less sterically encumbered ligand, observed a change in the number of initiating groups with temperature and low isoselectivity (P_i = 0.67). For the bulkier ligand, good isoselectivity control was achieved (P_i = 0.72), due to steric shielding of the metal centre.

6.1. Hybrid Initiators

Following the modifications to the indium hybrid initiators, only a small increase in isoselectivity was observed. Nonetheless the investigations revealed various sites relevant for further substitution studies. The investigation also discovered that electron-withdrawing groups in the *para*-phenolate position on the salen side significantly increased rates.

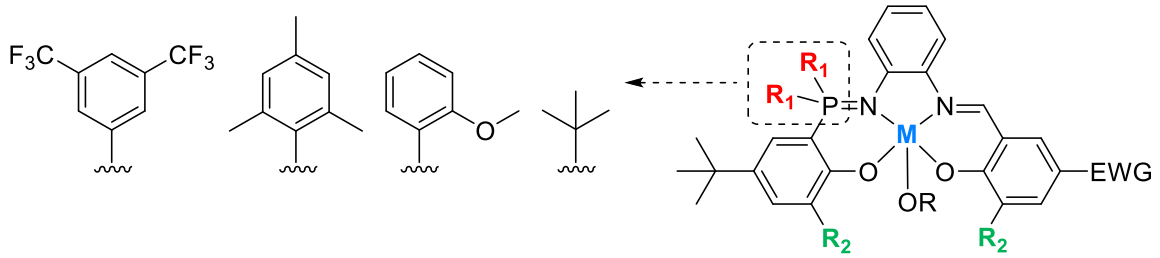

Figure 6.1. Modification of phosphine substituents (R = Et or *t*Bu).

As changing the phosphorus substituents gave the highest isoselectivity, the site is worth further modification (Figure 6.1). Since chloro-di-*tert*-butylphosphine, chloro-di-mesitylphosphine and chloro-bis(3,5-di(trifluoromethyl)phenyl)phosphine are all commercially available, these would be straightforward to apply in the phosphorylation reaction to target novel phosphinophenols. The synthesis of chloro-di-(2-methoxyphenyl)phosphine has been previously reported and, therefore, would also be a suitable candidate.[3] It offers the possibility of additional dative coordination of the methoxy groups to the metal centre, providing further steric constraint.

Chapter 4 showed that adamantyl groups in the *ortho*-phenolate positions were potentially too large to bias isoselectivity but also that chloride groups were too small. There may be scope to reduce the size of the groups in these positions, with respect to adamantyl, but increase with respect to *tert*-butyl groups. Possible groups include phenyl, cumyl or cyclohexyl (Figure 6.2). It was also shown that EWGs are preferred in the *para*-phenolate position on the salen side, therefore, chloride, trifluoromethyl or nitro substitutions should be investigated to optimise rates.

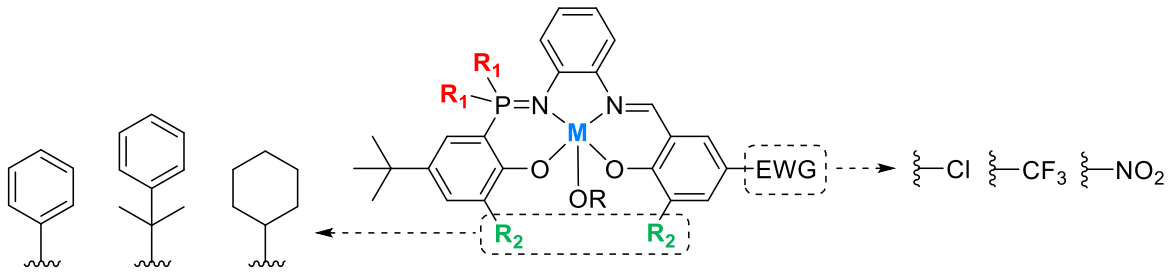

Figure 6.2. Modification of the *ortho*- and *para*-phenolate substituents (R = Et or *t*Bu).

Finally, expanding the scope of the metal centre from indium to other M(III) and M(IV) centres would be of interest. Zirconium(IV) and hafnium(IV) whilst coordinated to unsymmetrical salalen ligands have demonstrated high isoselectivites.[4,5] In our group, initiators based on yttrium(III), lanthanum(III) and lutetium(III) are also highly stereoselective.[6]

6.2. Switchable Initiators

As discussed in Chapter 4, the first goal for the ferrocene-containing indium hybrid complex is to undertake polymerisation studies using the oxidised/reduced initiator. The overall target is to change PLA tacticity by using a redox switch, which has not yet been reported in polymerisation catalysis.[7]

An interesting challenge is to prepare initiators which can greatly discriminate between two lactones. This challenge applies to both isoselective ROP of *rac*-LA and copolymerisation with other monomers. The steric influence of a ligand appears to play the biggest role in isoselectivity, for the initiators reported in this thesis, and others reported in the literature. Mirkin and co-workers reported rate switch on/off by ligand spatial control (using allosteric regulation) and such an approach may be of interest also.[8] Furthermore, photochemical switches have not yet been applied to lactone ROP, and

offer a straightforward switch.[9] It is worth highlighting that counterions in electrochemical polymerisations commonly contaminate the reaction after triggering a switch, by reducing rate or control.

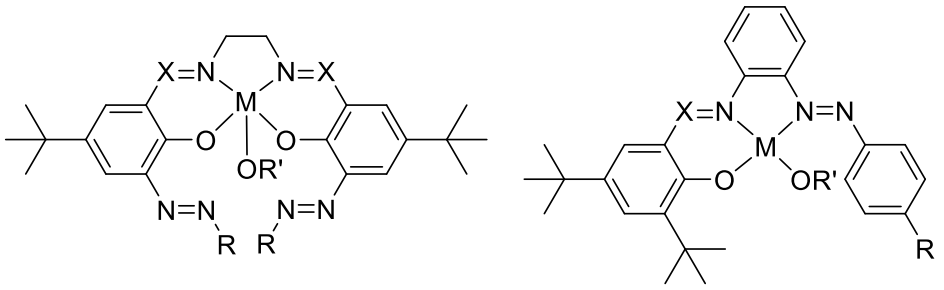

Figure 6.3. Proposed structures of photochemically switchable initiators (X = CH or PPh_2, R = any aliphatic or aromatic group, R' = Et or *t*Bu).

Photochemical switching of azo groups is well documented and introduction of these groups in the *ortho*-phenolate or nitrogen substituents of a metal initiator could allow for a photochemical switch (Figure 6.3).[10] The use of azo groups in LA polymerisation has been previously reported with thiourea catalysts to demonstrate a rate change upon a photochemical switch.[11] It is proposed that in the *cis* configuration, the metal centre would be more sterically encumbered, which might bias high isoselectivity. The *trans* configuration, should allow a reduction in steric hindrance and could produce atactic or heterotactic PLA.

6.3. Half Phosphasalen Initiators

In Chapter 5, the synthesis of two half-phosphasalen ligands were described, therefore there is great scope for modifications of the ligand as well as changing the metal centre beyond zinc(II) and indium(III) (Figure 6.4). The investigation focused on using two commercially available unsymmetrical diamines, *N*,*N*-dimethylethylenediamine and 2-amino-*N*-cyclohexyl-*N*-methylbenzylamine. The synthesis of an unsymmetrical diamine

with a cyclohexane backbone, featuring aliphatic N-substituents can be carried out using known literature procedures.[12,13] By protecting one of the amine groups in 1,2-diaminocyclohexane using *tert*-butoxycarbonyl (Boc), the remaining amine group can be functionalised. Then, the protected amine can be deprotected for use in the Kirsanov reaction to synthesise a half phosphasalen ligand. These methods could be used to investigate the effect of chirality and changing the size of the substituent at nitrogen.

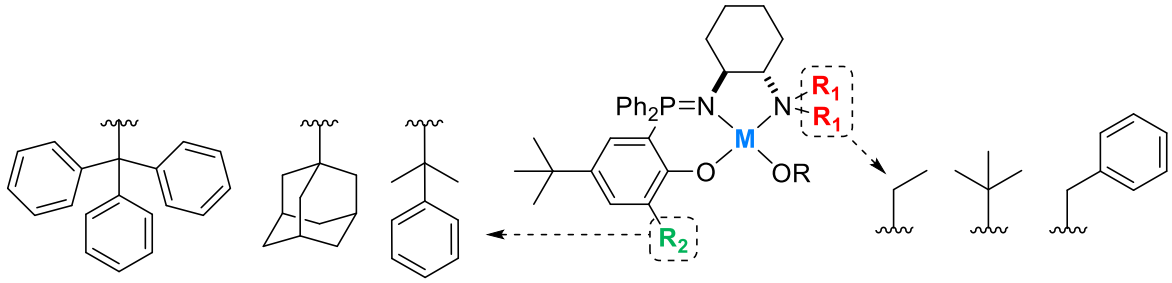

Figure 6.4. N-substituent and *ortho*-phenolate substituent modifications (R = Et or *t*Bu).

The effect of the size of the *ortho*-phenolate substituent is another key location for modification, larger substituents such as cumyl, adamantyl and trityl would be expected to increase isoselectivity but there is scope to reduce the size, to *iso*-propyl or methyl. Furthermore, the metal centre can be varied, as discussed with the hybrid ligands, to: (i) M(II) centres e.g. magnesium or calcium, (ii) M(III) e.g. aluminium, bismuth or yttrium, (iii) M(IV) e.g. titanium, zirconium or hafnium.

There is a range of other lactone and cyclic monomers for which the initiators discussed in this thesis could be tested. Recently, our group have reported yttrium phosphasalen initiators for the ROP of macrolactones.[14] Other monomers with smaller ring sizes include ε-caprolactone, δ-valerolactone, trimethylene carbonate or β-butyrolactone, the latter of which is of interest for stereoselective ROP.[15] It would be interesting if the initiators in this thesis could be used to copolymerise mixtures of these monomers or even

copolymerise with CO_2, as also reported in our group. The potential of these initiators covers a wide range of challenges faced across the bio-sustainable polymer field.

6.4. References

1 P. Hormnirun, E. L. Marshall, V. C. Gibson, R. I. Pugh and A. J. P. White, *Proc. Natl. Acad. Sci.*, 2006, **103**, 15343–15348.

2 A. F. Douglas, B. O. Patrick and P. Mehrkhodavandi, *Angew. Chem. Int. Ed.*, 2008, **47**, 2290–2293.

3 C. Chen, T. M. J. Anselment, R. Fröhlich, B. Rieger, G. Kehr and G. Erker, *Organometallics*, 2011, **30**, 5248–5257.

4 S. M. Kirk, G. Kociok-Köhn and M. D. Jones, *Organometallics*, 2016, **35**, 3837–3843.

5 A. Stopper, T. Rosen, V. Venditto, I. Goldberg and M. Kol, *Chem. Eur. J.*, 2017, **23**, 11540–11548.

6 C. Bakewell, A. J. P. White, N. J. Long and C. K. Williams, *Angew. Chem. Int. Ed.*, 2014, **53**, 9226–9230.

7 S. M. Guillaume, E. Kirillov, Y. Sarazin and J.-F. Carpentier, *Chemistry*, 2015, **21**, 7988–8003.

8 H. J. Yoon, J. Kuwabara, J.-H. Kim and C. A. Mirkin, *Science*, 2010, **330**, 66–69.

9 C. Deo, N. Bogliotti, R. Métivier, P. Retailleau and J. Xie, *Organometallics*, 2015, **34**, 5775–5784.

10 P. Pattanyak, D. Patra, J. L. Pratihar, A. Burrows, M. F. Mahon and S. Chattopadhyay, *Inorganica Chim. Acta*, 2010, **363**, 2865–2873.

11 Z. Dai, Y. Cui, C. Chen and J. Wu, *Chem. Commun.*, 2016, **52**, 8826–8829.

12 X. Zhang, T. J. Emge and K. C. Hultzsch, *Angew. Chem. Int. Ed.*, 2012, **51**, 394–398.

13 L. Li, S. Gou and F. Liu, *Tetrahedron Lett.*, 2013, **54**, 6358–6362.

14 D. Myers, T. Witt, A. Cyriac, M. Bown, S. Mecking and C. K. Williams, *Polym. Chem.*, 2017, **8**, 5780–5785.

15 D. Myers, A. Cyriac and C. K. Williams, *Nat. Chem.*, 2016, 8, 3–4.

Chapter 7

Experimental

7.1. Materials and Methods

All solvents and reagents were obtained from commercial sources (Sigma Aldrich, VWR and Strem) and used as received, unless stated otherwise. *Rac*-lactide was obtained from Purac Plc. and recrystallised twice from anhydrous toluene, sublimed twice under vacuum and stored under nitrogen prior to use. The phosphinophenol, 2-(diphenylphosphino)-4,6-di-*tert*-butylphenol[1], half salen, 2-((2-aminophenylimino)methyl)-4,6-di-*tert*-butylphenol[2], and the salen ligand (**3.1**[3]) used in Chapter 3, were prepared according to literature protocols. The following compounds from Chapter 4 were prepared using literature protocols: 2-adamantyl-4-tert-butylphenol[4], 3-adamantyl-5-*tert*-butyl-2-hydroxybenzaldehyde[5], 5-methoxy-3-*tert*-butyl-2-hydroxybenzaldehyde[6], 5-dimethylamino-3-*tert*-butyl-2-hydroxybenzaldehyde[7], 3-*tert*-butyl-5-iodosalicyaldehyde[8] and monolithioferrocene[9]. Zinc bis(trimethylsilyl)amide[10] used in Chapter 5 was also prepared according to a literature protocol. Potassium *tert*-butoxide was sublimed twice and stored under nitrogen before use. For all moisture-sensitive reactions, all solvents were dry, degassed and stored over activated molecular sieves prior to use. THF, toluene, *n*-hexane and cyclohexane were all distilled from sodium/benzophenone. Isopropanol (IPA) and dichloromethane (DCM) were both distilled from calcium hydride. Diethyl ether (Et_2O) was obtained from Sigma Aldrich as <99% anhydrous and stored over activated molecular sieves before use. THF-d_8, toluene-d_8, chloroform-d_1 and benzene-d_6 were all distilled from calcium hydride and stored over activated molecular sieves before use. All polymerisations were carried out in silanised glassware.

NMR: Nuclear magnetic resonance (NMR) spectra were recorded on a Bruker Av400 spectrometer, operating at 400 MHz for ^{1}H, 100 MHz for $^{13}C\{^{1}H\}$ and 162 MHz for $^{31}P\{^{1}H\}$

spectra. Solvent peaks were used as internal references for ^{1}H and $^{13}C\{^{1}H\}$ NMR chemical shifts (ppm). Additional NMR experiments were performed by Mr Peter Haycock at Imperial College London. Higher resolution NMR experiments (e.g. DOSY) were performed on a Bruker Av500 spectrometer. NMR spectra were processed and analysed using MestReNova and Bruker TopSpin software packages. For homonuclear decoupled $^{1}H\{^{1}H\}$ NMR spectra, the deconvolution tool from MestReNova software package was used to help determine tetrad integrals. DOSY experiments were performed on a Bruker Av500 spectrometer using the ledbpgp2s pulse programme, collecting 32768 data points and employing at least 32 gradient strength increments for each experiment. Processing and analysis was performed on TopSpin 3.5, using exponential fits.

MALDI-TOF MS: Matrix assisted laser desorption ionization time-of-flight (MALDI-ToF) analysis was performed on a Micromass MALDI micro MX spectrometer. Polymers were characterised using dithranol as a matrix and potassium trifluoroacetate as an additive when necessary. The samples were prepared in the following manner: 10 mg/mL THF solutions of the polymer, matrix and additive were separately prepared. Then, the polymer (20 µL) and the matrix solution (20 µL) were mixed, along with the additive solution (10 µL). This mixture (2 µL) was then spotted on the MALDI plate and allowed to dry.

X-ray diffraction: Single crystal X-ray diffraction data was collected and analysed by Dr Andrew White and Dr Christopher Durr at Imperial College London and the University of Oxford respectively.

Elemental analysis: Elemental analyses (C, H, N) for all novel compounds were carried out by Mr Stephen Boyer from London Metropolitan University.

Gel permeation chromatography: Analyses of polylactides were performed on a Shimadzu LC-20AD instrument using two Mixed Bed PSS SDV linear S columns in series at 40 ^{o}C. This was further equipped with a Dawn multi-angle (8+) laser light scattering (GPC-MALLS) detector, with data analysed using Astra Version 6.1. The refractive angle increment used for polylactide (dn/dc) in THF was 0.040 mL g^{-1}.[11] For all runs, THF was used as the eluent at a flow rate of 1 mL min^{-1}.

Cyclic Voltammetry: Cyclic voltammograms were recorded under an atmosphere of argon in using electrolyte solutions as stated on a Gamry reference 600TM (Gamry Instruments, Warminter, PA, USA) with a glassy carbon disc as working electrode (diameter = 2.5 mm) and Pt-wire as reference and counter electrodes. Analyte solutions were [*n*Bu_4N]PF_6 (0.1 M in THF). Potentials are reported relative to $[Cp_2Fe]^+/[Cp_2Fe]$, measured against internal $[Cp^*_2Fe]^+/[Cp^*_2Fe]$ references.

7.2. General Procedures

7.2.1. Typical polymerisation procedure (ambient)

In a nitrogen-filled glovebox, a silanised vial was charged with *rac*-LA (288 mg, 2.0 mmol) and dissolved in THF (1.8 mL). A stock solution of the initiator (0.2 mL, 0.020 M) was injected into the solution of monomer such that the overall concentration of lactide was 1 M and the initiator, 2 mM. Aliquots were taken inside the glovebox at specific time intervals and precipitated in *n*-hexane (~ 1 mL). The aliquots were then removed from the glovebox and left to evaporate. The crude product was analysed by ^{1}H NMR (and $^1H\{^1H\}$ NMR where applicable) spectroscopy and GPC. Polymer conversion yields were determined by relative integration of the methine proton resonances for the polymer and

monomer. The tacticity (P_i) was determined by integration of the tetrad resonances in the $^1H\{^1H\}$ decoupled NMR of the polymer (see Section 2.1 for method of calculation).

7.2.2. Typical polymerisation procedure (high temperature)

In a nitrogen-filled glovebox, a silanised vial was charged with *rac*-LA (288 mg, 2.0 mmol) and suspended in toluene (1.8 mL). A stock solution of the initiator (0.2 mL, 0.020 M) was injected into the solution of monomer such that the overall concentration of lactide was 1 M and the initiator, 2 mM. The vial was then sealed, removed from the glovebox and placed into an oil bath set at the required temperature. Aliquots were taken by taking the vial into the glovebox at specific time intervals and precipitated into *n*-hexane (~ 1 mL). The aliquots were then removed from the glovebox and left to evaporate. The mixture was then analysed using the methods described above.

7.2.3. Silanisation procedure

Hot vials heated in an oven at 383 K were rinsed several times in a solution of dichlorodimethylsilane in DCM (0.8 M, 10 mL) before being left to dry in an oven prior to use.

7.3. Chapter 3 Experimental Section

Compound 3.2

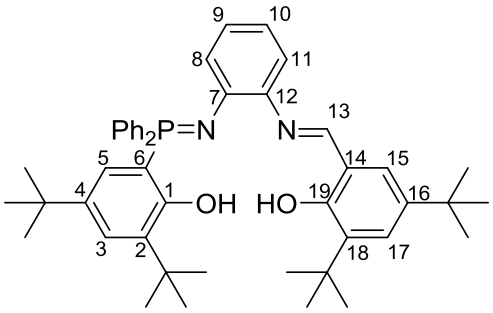

At -78 °C, bromine (70 µL, 1.42 mmol) was added dropwise to a solution of 2-(diphenylphosphino)-4,6-di-*tert*-butylphenol (0.55 g, 1.42 mmol) in DCM (80 mL). The cold bath was removed and stirred was continued for two hours at 25 °C. The solution was again cooled to -78 °C, DABCO (0.16 g, 1.42 mmol) and 2-((2-aminophenylimino)methyl)-4,6-di-*tert*-butylphenol (0.46 g, 1.42 mmol) were added. The cold bath was removed and the solution was left to stir at 25 °C for 20 h. The DCM was evaporated and the residue was suspended in THF (10 mL) and filtered to remove the DABCO salt. THF was removed from the filtrate and *n*-hexane was added to the residue to precipitate a pale yellow solid, which was washed and dried *in vacuo* to yield the product (0.60 g, 0.84 mmol, 54%).

^{1}H NMR (400 MHz, d_8-THF, δ (ppm)): 13.45 (s, 1H, C^{1}-O*H*), 8.36 (s, 1H, C^{13}-*H*), 7.74 (m, 4H, *o*-C*H*(PPh_2)), 7.52 (m, 2H, *p*-C*H*(PPh_2)), 7.44 (d, 1H, C^{17}-*H*, $^{4}J_{HH}$ = 2.50 Hz), 7.42 (m, 4H, *m*-C*H*(PPh_2)), 7.36 (d, 1H, C^{3}-*H*, $^{4}J_{HH}$ = 2.40 Hz), 7.16 (d, 1H, C^{15}-*H*, $^{4}J_{HH}$ = 2.50 Hz), 6.77 (m, 5H, C^{5}-*H*, $C^{8\text{-}11}$-*H*), 1.42 (s, 9H, C^{18}-C(CH_3)$_3$), 1.32 (s, 9H, C^{2}-C(CH_3)$_3$), 1.26 (s, 9H, C^{16}-C(CH_3)$_3$), 1.09 (s, 9H, C^{4}-C(CH_3)$_3$).

^{31}P{^{1}H} NMR (162 MHz, d_8-THF, δ (ppm)): 20.9 (s, P).

^{13}C{^{1}H} NMR (100 MHz, d_8-THF, δ (ppm)): 166.4 (s, C^{13}-H), 163.4 (d, C^{IV}, $^{4}J_{PC}$ = 2.90 Hz), 159.2 (s, C^{IV}), 146.2 (d, C^{IV}, $^{2}J_{PC}$ = 17.1 Hz), 142.3 (d, C^{IV}, $^{3}J_{PC}$ = 5.00 Hz), 140.4 (s, C^{IV}), 139.6 (d, C^{IV}, $^{2}J_{PC}$ = 14.6 Hz), 137.1 (s, C^{IV}), 133.7 (d, *o*-*C*H(PPh_2), $^{2}J_{PC}$ = 9.90 Hz), 132.9 (d, *p*-*C*H(PPh_2), $^{4}J_{PC}$ = 2.80 Hz), 131.8 (s, C^{IV}), 131.2 (s, C^{IV}), 129.5 (d, *m*-*C*H(PPh_2), $^{3}J_{PC}$ = 11.7 Hz), 128.8 (s, C^{3}-H), 127.9 (s, C^{17}-H), 127.6 (s, C^{15}-H), 127.0 (d, C^{5}-H, $^{2}J_{PC}$ = 13.5 Hz), 126.6 (s, C^{9}-

H), 123.6 (d, C^8-H, $^2J_{PC}$ = 10.4 Hz), 121.3 (s, C^{10}-H), 120.3 (s, C^{11}-H), 107.4 (s, C^{IV}), 106.4 (s, C^{IV}), 36.1 (s, C^2-$C(CH_3)_3$), 35.9 (s, C^4-$C(CH_3)_3$), 34.9 (s, C^{18}-$C(CH_3)_3$), 34.8 (s, C^{16}-$C(CH_3)_3$), 31.9 (s, C^2-$C(CH_3)_3$), 31.7 (s, C^4-$C(CH_3)_3$), 30.2 (s, C^{18}-$C(CH_3)_3$), 30.1 (s, C^{16}-$C(CH_3)_3$); MS ES+: *m/z* 713, ($[M+H]^+$ Calc.: 713).

Anal. Calcd for $C_{47}H_{57}N_2O_2P$: C, 79.18; H, 8.06; N, 3.93. Found: C, 79.01; H, 8.57; N, 3.46.

Compound 3.3[12]

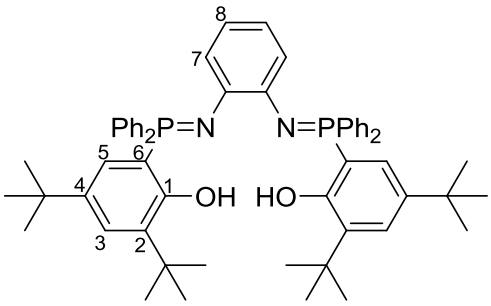

At -78 °C, bromine (26 µL, 5.12 mmol) was added dropwise to a solution of 2-(diphenylphosphino)-4,6-di-*tert*-butylphenol (2.00 g, 5.12 mmol) in DCM (80 mL). The cold bath was removed and stirred was continued for two hours at 25 °C. The solution was again cooled to -78 °C, DABCO (0.29 g, 2.56 mmol) and *o*-phenylenediamine (0.28 g, 2.56 mmol) were added. The cold bath was removed and the solution was left to stir at 25 °C for 20 h. The DCM was evaporated and the residue was suspended in THF (10 mL) and filtered to remove the DABCO salt. THF was removed from the filtrate and Et_2O was added to the residue to precipitate a pale yellow solid which after filtration, washing and drying could be further purified by column chromatography (alumina, DCM: EtOH 40:1) and washing with pentane (30 mL) to give the pure product (0.89 g, 1.00 mmol, 39%).

^{1}H NMR (400 MHz, d_8-THF, δ (ppm)): 7.86 (m, 8H, *o*-*C*H(PPh_2)), 7.45 (m, 12H, *m*/*p*-*CH*(PPh_2)), 7.33 (d, 2H, C^3-*H*, $^4J_{HH}$ = 2.40 Hz), 6.92 (dd, 2H, C^5-*H*, $^4J_{HH}$ = 2.37 Hz, $^3J_{PH}$ = 16.80 Hz), 6.39 (m, 2H, C^7-*H*), 6.23 (m, 2H, C^8-*H*), 1.16 (s, 18H, C^2-C(CH_3)$_3$), 1.13 (s, 18H, C^4-C(CH_3)$_3$).

^{31}P{^{1}H} NMR (162 MHz, d_8-THF, δ (ppm)): 17.7 (s, P).

^{13}C{^{1}H} NMR (100 MHz, d_8-THF, δ (ppm)): 164.2 (s, C^{IV}), 143.3 (s, C^{IV}), 138.8 (s, C^{IV}), 134.2 (d, *o*-*C*H(PPh_2), $^2J_{PC}$ = 10.20 Hz), 133.2 (s, C^{IV}), 132.6 (s, *p*-*C*H(PPh_2)), 132.4 (s, C^{IV}), 129.4 (d, *m*-*C*H(PPh_2), $^3J_{PC}$ = 11.70 Hz), 128.4 (s, C^3-H), 126.9 (d, C^5-H, $^3J_{PC}$ = 13.30 Hz), 122.2 (d, C^7-H, $^3J_{PC}$ = 8.20 Hz), 119.9 (s, C^8-H), 108.2 (s, C^{IV}), 106.9 (s, C^{IV}), 36.0 (s, C^4-*C*(CH_3)$_3$), 34.9 (s, C^2-*C*(CH_3)$_3$), 31.9 (s, C^4-C(*C*H_3)$_3$), 30.2 (s, C^2-C(*C*H_3)$_3$).

Anal. Calcd for $C_{58}H_{66}N_2O_2P_2$: C, 78.70; H, 7.52; N, 3.16. Found: C, 78.81; H, 7.44; N, 3.24.

Compound 3.4

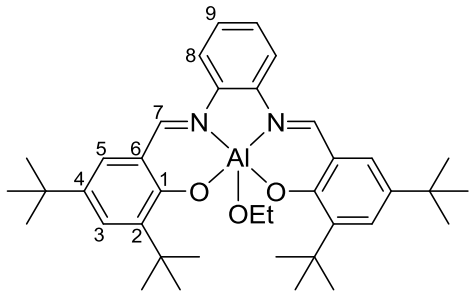

Diethylaluminium chloride (115 µL, 0.92 mmol) was added to a solution of **2.1** (500 mg, 0.92 mmol) in THF (5 mL) and stirred for one hour. Potassium ethoxide (78 mg, 0.92 mmol) was added to achieve a colour change from yellow to red. The solution was stirred for 16 hours and then centrifuged to remove the KCl salt. The solvent was removed *in vacuo* and the residue was washed with cold *n*-hexane to yield a yellow solid (220 mg, 0.36 mmol, 39%).

^{1}H NMR (400 MHz, d_8-THF, δ (ppm)): 9.21 (s, 2H, C^{7}-*H*), 7.95 (m, 2H, C^{8}-*H*), 7.63 (d, 2H, C^{3}-*H*, $^{4}J_{HH}$ = 2.50 Hz), 7.37 (d, 2H, C^{5}-*H*, $^{4}J_{HH}$ = 2.50 Hz), 7.35 (m, 2H, C^{9}-*H*), 3.34 (q, 2H, O-C*H*$_2$-CH$_3$, $^{3}J_{HH}$ = 6.90 Hz), 1.62 (s, 18H, C^{2}-C(C*H*$_3$)$_3$), 1.36 (s, 18H, C^{4}-C(C*H*$_3$)$_3$), 0.64 (t, 3H, O-CH$_2$-C*H*$_3$, $^{3}J_{HH}$ = 6.90 Hz).

^{13}C{^{1}H} NMR (100 MHz, d_8-THF, δ (ppm)): 165.9 (s, *C*^{1}-OH), 163.4 (s, *C*^{7}-H), 141.7 (s, C^{IV}), 140.1 (s, C^{IV}), 138.9 (s, C^{IV}), 132.3 (s, *C*^{3}-H), 129.4 (s, *C*^{5}-H), 128.6 (s, *C*^{9}-H), 120.2 (s, C^{IV}), 116.8 (s, *C*^{8}-H), 58.4 (s, O-*C*H$_2$-CH$_3$), 36.6 (s, C^{4}-*C*(CH$_3$)$_3$), 34.9 (s, C^{2}-*C*(CH$_3$)$_3$), 31.9 (s, C^{4}-(*C*H$_3$)$_3$), 30.7 (s, C^{2}-(*C*H$_3$)$_3$), 21.6 (s, O-CH$_2$-*C*H$_3$).

Anal. Calcd for $C_{38}H_{51}AlN_2O_3$: C, 74.72; H, 8.42; N, 4.59. Found: C, 74.48; H, 8.48; N, 4.64.

Compound 3.5

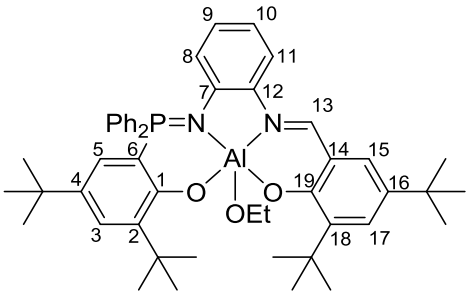

Diethylaluminium chloride (88 µL, 0.70 mmol) was added to a solution of **2.2** (500 mg, 0.70 mmol) in THF (5 mL) and stirred for one hour. Potassium ethoxide (59 mg, 0.70 mmol) was added to achieve a colour change from yellow to red. The solution was stirred for 16 hours and then centrifuged to remove the KCl salt. The solvent was removed *in vacuo* and the residue recrystallised from THF/*n*-hexane to yield an orange solid (50 mg, 0.07 mmol, 10%).

^{1}H NMR (400 MHz, d_8-THF, δ (ppm)): 9.00 (s, 1H, C^{13}-*H*), 8.06 (m, 2H, *o*-C*H*(PPh$_2$)), 7.51-7.70 (m, 9H, *o*/*m*/*p*-C*H*(PPh$_2$), C^{11}-*H* & C^{17}-*H*) 7.40-7.46 (m, 2H, *m*-C*H*(PPh$_2$) & C^{3}-*H*), 7.31 (d, 1H, C^{15}-*H*, $^{4}J_{HH}$ = 2.70 Hz), 6.72-6.79 (m, 2H, C^{5}-*H* & C^{10}-*H*), 6.64 (m, 1H, C^{9}-*H*), 6.39 (m, 1H, C^{8}-*H*), 3.45 (m, 2H, O-C*H*$_2$-CH$_3$), 1.53 (s, 18H, C$^{2\&18}$-C(C*H*$_3$)$_3$), 1.34 (s, 9H, C^{16}-C(C*H*$_3$)$_3$), 1.11 (s, 9H, C^{4}-C(C*H*$_3$)$_3$), 0.69 (t, 3H, O-CH$_2$-C*H*$_3$, $^{3}J_{HH}$ = 7.00 Hz).

^{31}P{^{1}H} NMR (162 MHz, d_8-THF, δ (ppm)): 31.0 (s, P).

^{13}C{^{1}H} NMR (100 MHz, d_8-THF, δ (ppm)): 166.2 (s, *C*^{IV}), 165.9 (s, *C*^{IV}), 163.1 (s, *C*^{13}-H), 143.6 (s, *C*^{IV}), 142.0 (d, *C*^{IV}, $^{3}J_{PC}$ = 9.50 Hz), 141.4 (s, *C*^{IV}), 139.5 (d, *C*^{IV}, $^{2}J_{PC}$ = 14.60 Hz), 138.2 (s, *C*^{IV}), 137.9 (d, *C*^{IV}, $^{2}J_{PC}$ = 15.40 Hz), 135.2 (d, *o*-*C*H(PPh$_2$), $^{2}J_{PC}$ = 9.90 Hz), 133.8 (d, *o*-*C*H(PPh$_2$), $^{2}J_{PC}$ = 9.90 Hz), 133.7 (s, *p*-*C*H(PPh$_2$)), 133.4 (s, *p*-*C*H(PPh$_2$)), 131.5 (s, *C*$^{3/17}$-H), 129.9 (d, *m*-*C*H(PPh$_2$), $^{3}J_{PC}$ = 12.20 Hz), 129.8 (d, *m*-*C*H(PPh$_2$), $^{3}J_{PC}$ = 12.20 Hz), 129.7 (s, *C*$^{3/17}$-H), 128.9 (s, *C*^{15}-H), 127.5 (d, *C*^{5}-H, $^{3}J_{PC}$ = 14.40 Hz), 127.2 (s, *C*$^{9\text{-}11}$-H), 120.9 (s, *C*$^{9\text{-}11}$-H), 120.5 (s, *C*^{IV}), 120.3 (d, *C*^{8}-H, $^{3}J_{PC}$ = 8.80 Hz), 116.1 (s, *C*$^{9\text{-}11}$-H), 109.2 (s, *C*^{IV}), 108.1 (s, *C*^{IV}), 58.5 (s, O-*C*H$_2$-CH$_3$), 36.8 (s, C^{4}-*C*(CH$_3$)$_3$), 36.5 (s, C^{16}-*C*(CH$_3$)$_3$), 34.8 (s, C$^{2/18}$-*C*(CH$_3$)$_3$), 31.9 (s, C^{4}-C(*C*H$_3$)$_3$), 31.8 (s, C^{16}-C(*C*H$_3$)$_3$), 31.1 (s, C$^{2/18}$-C(*C*H$_3$)$_3$), 21.7 (s, O-CH$_2$-*C*H$_3$).

Anal. Calcd for $C_{49}H_{60}AlN_2O_3P$: C, 75.17; H, 7.72; N, 3.58. Found: C, 74.91; H, 7.68; N, 3.73.

Compound 3.6

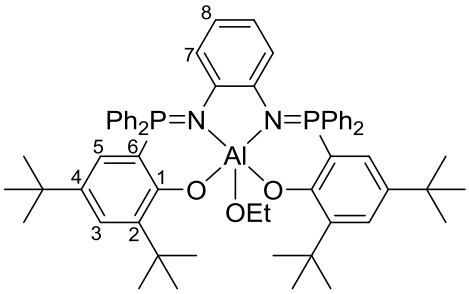

Diethylaluminium chloride (70 µL, 0.56 mmol) was added to a solution of **2.3** (500 mg, 0.56 mmol) in THF (5 mL) and stirred for one hour. Potassium ethoxide (46 mg, 0.56 mmol) was added. The solution was stirred for 16 hours and then centrifuged to remove the KCl salt. The solvent was removed *in vacuo* and the residue was recrystallised from THF/*n*-hexane to achieve a white solid (140 mg, 0.15 mmol, 26%).

^{1}H NMR (400 MHz, d_8-THF, δ (ppm)): 7.92 (m, 4H, *o*-C*H*(PPh_2)), 7.57 (m, 6H, *o/p*-C*H*(PPh_2)), 7.47 (m, 6H, *m/p*-C*H*(PPh_2)), 7.35 (m, 4H, *m*-C*H*(PPh_2)), 7.31 (d, 2H, C^3-*H*, $^4J_{HH}$ = 2.50 Hz), 6.63 (dd, 2H, C^5-*H*, $^4J_{HH}$ = 2.50 Hz, $^3J_{PH}$ = 16.3 Hz), 6.12 (m, 2H, C^7-*H*), 6.05 (m, 2H, C^8-*H*), 3.62 (q, 2H, O-CH_2-CH_3, $^3J_{HH}$ = 6.90 Hz), 1.17 (s, 18H, C^2-C(CH_3)$_3$), 1.08 (s, 18H, C^4-C(CH_3)$_3$), 0.61 (t, 3H, O-CH_2-CH_3, $^3J_{HH}$ = 6.90 Hz).

^{31}P{^{1}H} NMR (162 MHz, d_8-THF, δ (ppm)): 28.9 (s, P).

^{13}C{^{1}H} NMR (100 MHz, d_8-THF, δ (ppm)): 166.1 (d, C^{IV}, $^4J_{PC}$ = 3.0 Hz), 140.4 (s, C^{IV}), 140.1 (d, C^{IV}, $^3J_{PC}$ = 9.20 Hz), 135.6 (d, C^{IV}, $^2J_{PC}$ = 15.1 Hz), 133.6 (d, *o*-*C*H(PPh_2), $^2J_{PC}$ = 10.5 Hz), 133.3 (d, *o*-*C*H(PPh_2), $^2J_{PC}$ = 9.90 Hz), 132.1 (d, *p*-*C*H(PPh_2), $^4J_{PC}$ = 2.80 Hz), 131.8 (d, *p*-*C*H(PPh_2), $^4J_{PC}$ = 2.80 Hz), 129.4 (s, C^{IV}), 128.4 (d, *m*-*C*H(PPh_2), $^3J_{PC}$ = 11.9 Hz), 128.1 (d, *m*-*C*H(PPh_2), $^3J_{PC}$ = 12.6 Hz), 128.0 (s, C^3-H), 127.9 (s, C^{IV}), 125.8 (d, C^5-H, $^2J_{PC}$ = 13.7 Hz), 118.4 (s, C^8-H), 117.4 (d, C^7-H, $^3J_{PC}$ = 7.0 Hz), 108.6 (s, C^{IV}), 107.4 (s, C^{IV}), 57.6 (s, O-*C*H_2-CH_3), 35.1 (s, C^4-*C*(CH_3)$_3$), 33.6(s, C^2-*C*(CH_3)$_3$), 30.8 (s, C^4-C(*C*H_3)$_3$), 29.6 (s, C^2-C(*C*H_3)$_3$), 20.5 (s, O-CH_2-*C*H_3).

Anal. Calcd for $C_{60}H_{69}AlN_2O_3P_2$: C, 75.45; H, 7.28; N, 2.98. Found: C, 75.25; H, 7.38; N, 2.84.

Compound 3.7

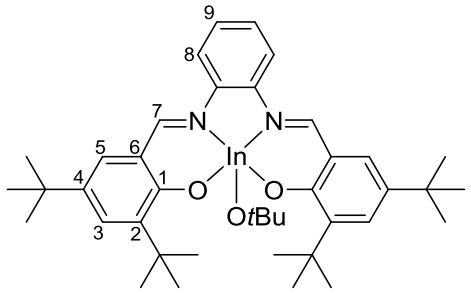

Potassium bis(trimethylsilyl)amide (221 mg, 1.10 mmol) was added to a yellow solution of **3.1** (300 mg, 0.55 mmol) in THF (10 mL) and the resultant orange solution was stirred for two hours. $InCl_3$ (123 mg, 0.55 mmol) was added and stirred for a further two hours. The insoluble salts were removed by centrifugation and the red solution was filtered. Potassium *tert*-butoxide (67 mg, 0.55 mmol) was added giving a dark red solution. Stirring was continued for a further two hours and the insoluble solids were removed by centrifugation. The solvent was evaporated in *vacuo* and the residue was recrystallised from THF/*n*-hexane to give the product as an orange solid (230 mg, 0.32 mmol, 58%).

^{1}H NMR (400 MHz, d_8-THF, δ (ppm)): 8.93 (s, 2H, C^7-*H*), 7.89 (m, 2H, C^8-*H*), 7.54 (d, 2H, C^3-*H*, $^4J_{HH}$ = 2.60 Hz), 7.31 (m, 2H, C^9-*H*), 7.22 (d, 2H, C^5-*H*, $^4J_{HH}$ = 2.60 Hz), 1.55 (s, 18H, C^2-C(C*H*$_3$)$_3$), 1.32 (s, 18H, C^4-C(C*H*$_3$)$_3$), 1.05 (s, 9H, In-O-C(C*H*$_3$)$_3$).

^{13}C{^{1}H} NMR (100 MHz, d_8-THF, δ (ppm)): 170.4 (s, *C*^{1}-OH), 167.3 (s, *C*^{7}-H), 143.0 (s, C^{IV}), 139.3 (s, C^{IV}), 137.9 (s, C^{IV}), 131.9 (s, *C*^{3}-H), 131.4 (s, *C*^{5}-H), 128.9 (s, *C*^{9}-H), 119.6 (s, C^{IV}), 117.9 (s, *C*^{8}-H), 36.4 (s, C^4-*C*(CH$_3$)$_3$), 35.3 (s, In-O-C(*C*H$_3$)$_3$), 34.8 (s, C^2-*C*(CH$_3$)$_3$), 31.9 (s, C^4-(*C*H$_3$)$_3$), 30.6 (s, C^2-(*C*H$_3$)$_3$).

Anal. Calcd for $C_{40}H_{55}InN_2O_3$: C, 66.11; H, 7.63; N, 3.85. Found: C, 65.83; H, 7.71; N, 3.71.

Compound 3.8

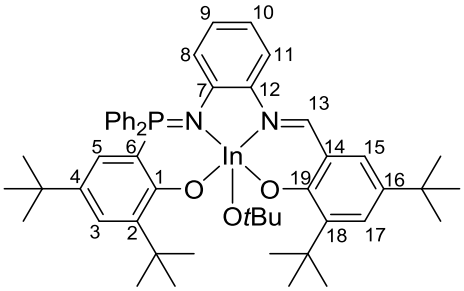

Potassium bis(trimethylsilyl)amide (133 mg, 0.57 mmol) was added to a solution of **3.2** (150 mg, 0.19 mmol) in THF (10 mL). After two hours, a cloudy solution was yielded and the insoluble potassium bromide salt was removed by centrifugation. $InCl_3$ (42 mg, 0.19 mmol) was added and stirred for two hours. Potassium *tert*-butoxide (23 mg, 0.19 mmol) was added to the mixture, giving a cloudy solution. Stirring was continued for two hours and the solid was removed by centrifugation. The solvent was evaporated in *vacuo* and the residue was washed with *n*-hexane to give the product as a yellow solid (60 mg, 0.067 mmol, 35%).

^{1}H NMR (400 MHz, d_8-THF, δ (ppm)): 8.92 (s, 1H, C^{13}-*H*), 8.11 (m, 2H, *o*-C*H*(PPh_2)), 7.66 (m, 7H, C^{11}-*H*, *m*/*p*-C*H*(PPh_2)), 7.55 (d, 1H, C^{17}-*H*, $^{4}J_{HH}$ = 2.60 Hz), 7.47 (d, 1H, C^{3}-*H*, $^{4}J_{HH}$ = 2.50 Hz), 7.45 (m, 2H, *m*-C*H*(PPh_2)), 7.24 (d, 1H, C^{15}-*H*, $^{4}J_{HH}$ = 2.60 Hz), 6.84 (td, 1H, C^{10}-*H*, $^{3}J_{HH}$ = 7.70 Hz, $^{4}J_{HH}$ = 1.50 Hz), 6.74 (td, 1H, C^{9}-*H*, $^{3}J_{HH}$ = 7.70 Hz, $^{4}J_{HH}$ = 1.50 Hz), 6.58 (m, 1H, C^{8}-*H*), 6.57 (dd, 1H, C^{5}-*H*, $^{3}J_{PH}$ = 17.9 Hz, $^{4}J_{HH}$ = 2.50 Hz), 1.57 (s, 9H, C^{18}-C(CH_3)$_3$), 1.55 (s, 9H, C^{2}-C(CH_3)$_3$), 1.36 (s, 9H, C^{16}-C(CH_3)$_3$), 1.10 (s, 9H, C^{4}-C(CH_3)$_3$), 1.03 (s, 9H, InO-C(CH_3)$_3$).

^{31}P{^{1}H} NMR (162 MHz, d_8-THF, δ (ppm)): 33.2 (s, P).

^{13}C{^{1}H} NMR (100 MHz, d_8-THF, δ (ppm)): 171.0 (d, C^{IV}, $^{4}J_{PC}$ = 3.10 Hz), 170.8 (s, C^{IV}), 166.0 (s, C^{13}-H), 142.9 (d, C^{IV}, $^{3}J_{PC}$ = 9.70 Hz), 142.8 (s, C^{IV}), 142.4 (d, C^{IV}, $^{4}J_{PC}$ = 3.40 Hz), 138.1 (d, C^{IV}, $^{2}J_{PC}$ = 14.90 Hz), 137.4 (d, C^{IV}, $^{2}J_{PC}$ = 15.70 Hz), 137.1 (s, C^{IV}), 134.8 (d, *o*-*C*H(PPh_2), $^{2}J_{PC}$ = 9.85 Hz), 133.8 (d, *o*-*C*H(PPh_2), $^{2}J_{PC}$ = 9.85 Hz), 133.7 (d, *p*-*C*H(PPh_2), $^{4}J_{PC}$ = 2.92 Hz), 133.4 (d, *p*-*C*H(PPh_2), $^{4}J_{PC}$ = 2.92 Hz), 131.3 (s, C^{17}-H), 131.2 (s, C^{15}-H), 130.8 (s, C^{IV}), 130.0 (d, *m*-*C*H(PPh_2), $^{3}J_{PC}$ = 12.11 Hz), 129.9 (s, C^{3}-H), 129.8 (d, *m*-*C*H(PPh_2), $^{3}J_{PC}$ = 12.11 Hz), 128.6 (d, C^{5}-H, $^{3}J_{PC}$ = 15.42 Hz), 128.6 (s, C^{IV}), 127.6 (s, C^{9}-H), 121.8 (d, C^{8}-H, $^{3}J_{PC}$ = 9.14 Hz), 121.1 (s, C^{10}-H), 119.4 (s, C^{IV}), 117.2 (s, C^{11}-H), 109.6 (s, C^{IV}), 108.4 (s, C^{IV}), 36.9 (s, C^{4}-*C*(CH_3)$_3$), 36.7

(s, C^{16}-*C*$(CH_3)_3$), 36.6 (s, C^2-*C*$(CH_3)_3$), 34.9 (s, C^{18}-*C*$(CH_3)_3$), 34.8 (s, InO-*C*$(CH_3)_3$), 34.7 (s, InO-C(*C*$H_3)_3$), 31.9 (s, C^4-C(*C*$H_3)_3$), 31.8 (s, C^{16}-C(*C*$H_3)_3$), 30.9 (s, C^2-C(*C*$H_3)_3$), 30.8 (s, C^{18}-C(*C*$H_3)_3$).

Anal. Calcd for $C_{51}H_{64}InN_2O_3P$: C, 68.15; H, 7.18; N, 3.12. Found: C, 68.36; H, 7.51; N, 3.13.

Compound 3.9

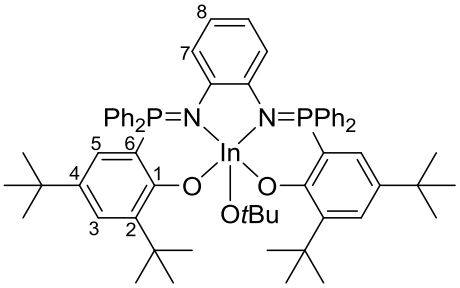

Potassium bis(trimethylsilyl)amide (135 mg, 0.68 mmol) was added to a yellow solution of **3.3** (300 mg, 0.34 mmol) in THF (10 mL) to afford a colour change to orange. After stirring for two hours, $InCl_3$ (75 mg, 0.34 mmol) was added. After a further two hours, a white precipitate was yielded. Potassium *tert*-butoxide (39 mg, 0.34 mmol) was added to achieve a clear solution. After two hours of stirring, the salts were removed by centrifugation and the solvent was removed *in vacuo*. The residue was recrystallised with THF/*n*-hexane to yield a white solid (182 mg, 0.17 mmol, 52%).

^{1}H NMR (400 MHz, d_8-THF, δ (ppm)): 7.91 (m, 4H, *o*-C*H*(PPh_2)), 7.61 (m, 6H, *o*/*m*/*p*-C*H*(PPh_2)), 7.53 (m, 6H, o/*m*/*p*-C*H*(PPh_2)), 7.40 (m, 4H, *m*/*p*-C*H*(PPh_2)), 7.37 (d, 2H, C^3-*H*, $^4J_{HH}$ = 2.50 Hz), 6.51 (dd, 2H, C^5-*H*, $^4J_{HH}$ = 2.50 Hz, $^3J_{PC}$ = 17.6 Hz), 6.31 (m, 2H, C^7-*H*), 6.10 (m, 2H, C^8-*H*), 1.37 (s, 18H, C^2-C(CH_3)$_3$), 1.06 (s, 18H, C^4-C(CH_3)$_3$), 0.97 (s, 9H, In-O-C(CH_3)$_3$).

^{31}P{^{1}H} NMR (162 MHz, d_8-THF, δ (ppm)): 34.4 (s, P).

^{13}C{^{1}H} NMR (100 MHz, d_8-THF, δ (ppm)): 171.2 (s, C^{IV}), 142.5 (s, C^{IV}), 140.2 (s, C^{IV}), 136.1 (s, C^{IV}), 134.9 (d, *o*-*C*H(PPh_2), $^2J_{PC}$ = 9.80 Hz), 134.1 (d, *o*-*C*H(PPh_2), $^2J_{PC}$ = 9.80 Hz), 133.3 (d, *p*-*C*H(PPh_2), $^4J_{PC}$ = 2.20 Hz), 133.2 (d, *p*-*C*H(PPh_2), $^4J_{PC}$ = 2.20 Hz), 130.9 (s, C^{IV}), 129.7 (d, *m*-*C*H(PPh_2), $^3J_{PC}$ = 12.1 Hz), 129.6 (d, *m*-*C*H(PPh_2), $^3J_{PC}$ = 12.1 Hz), 129.5 (s, C^3-H), 128.3 (d, C^5-H, $^2J_{PC}$ = 14.5 Hz), 121.2 (d, C^7-H, $^3J_{PC}$ = 8.20 Hz), 119.8 (s, C^8-H), 110.0 (s, C^{IV}), 108.9 (s, C^{IV}), 36.7 (s, C^4-*C*(CH_3)$_3$), 34.9 (s, In-O-C(*C*H_3)$_3$), 34.7 (s, C^2-*C*(CH_3)$_3$), 31.9 (s, C^4-C(*C*H_3)$_3$), 31.1 (s, C^2-C(*C*H_3)$_3$).

Anal. Calcd for $C_{62}H_{73}InN_2O_3P_2$: C, 69.53; H, 6.87; N, 2.62. Found: C, 69.28; H, 6.32; N, 2.87.

Compound 3.10

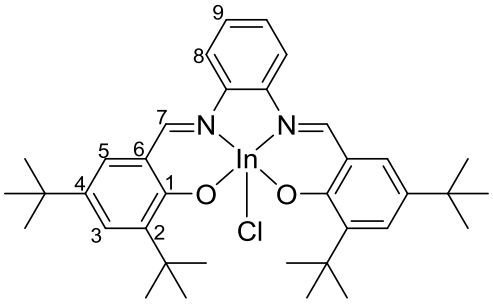

Potassium bis(trimethylsilyl)amide (221 mg, 1.10 mmol) was added to a yellow solution of **2.1** (300 mg, 0.55 mmol) in THF (10 mL) to afford a colour change to orange. After stirring for two hours, $InCl_3$ (122 mg, 0.55 mmol) was added to afford another colour change to orange *via* red. After stirring for a further two hours, the salts were removed by centrifugation and the solvent was removed *in vacuo*. The residue was washed with cold *n*-hexane to yield the product as an orange solid (250 mg, 0.36 mmol, 66%).

^{1}H NMR (400 MHz, C_6D_6, δ (ppm)): 7.99 (s, 2H, C^7-*H*), 7.80 (d, 2H, C^3-*H*, $^4J_{HH}$ = 2.60 Hz), 6.91 (d, 2H, C^5-*H*, $^4J_{HH}$ = 2.60 Hz), 6.84 (m, 2H, C^8-*H*), 6.61 (m, 2H, C^9-*H*), 1.83 (s, 18H, C^2-C(C*H*$_3$)$_3$), 1.39 (s, 18H, C^2-C(C*H*$_3$)$_3$).

^{13}C{^{1}H} NMR (100 MHz, C_6D_6, δ (ppm)): 164.9 (s, *C*^{7}-H), 131.9 (s, *C*^{3}-H), 130.1 (s, *C*^{5}-H), 127.6 (s, *C*^{8}-H), 115.9 (s, *C*^{9}-H), 31.2 (s, C^4-C(*C*H$_3$)$_3$), 29.7 (s, C^2-C(*C*H$_3$)$_3$).

Anal. Calcd for $C_{36}H_{46}ClInN_2O_2$: C, 62.75; H, 6.73; N, 4.07. Found: C, 62.89; H, 6.48; N, 4.34.

Compound 3.11

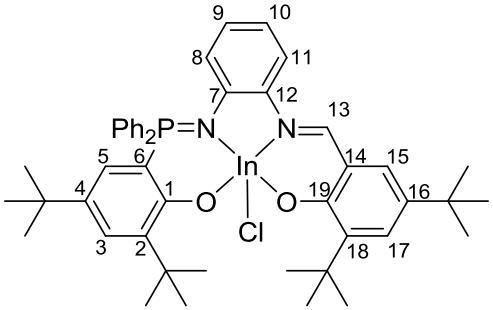

Potassium bis(trimethylsilyl)amide (167 mg, 0.84 mmol) was added to a yellow solution of **2.2** (299 mg, 0.42 mmol) in THF (10 mL) to afford a colour change to orange. After stirring for two hours, $InCl_3$ (93 mg, 0.42 mmol) was added to afford another colour change to yellow *via* red. After stirring for a further two hours, the salts were removed by centrifugation and the solvent was removed *in vacuo*. The residue was washed with cold *n*-hexane to yield the product as a yellow solid (250 mg, 0.26 mmol, 69%).

^{1}H NMR (400 MHz, C_6D_6, δ (ppm)): 8.03 (s, 1H, C^{13}-*H*), 7.87 (m, 2H, *o*-C*H*(PPh_2)), 7.80 (d, 1H, C^{3}-*H*, $^{4}J_{HH}$ = 2.40 Hz), 7.76 (d, 1H, C^{17}-*H*, $^{4}J_{HH}$ = 2.60 Hz), 7.66 (m, 2H, *o*-C*H*(PPh_2)), 6.77 (d, 1H, C^{15}-*H*, $^{4}J_{HH}$ = 2.60 Hz), 6.76-7.05 (m, 6H, *m*/*p*-C*H*(PPh_2)), 6.65 (dd, 1H, C^{5}-*H*, $^{4}J_{HH}$ = 2.40 Hz, $^{3}J_{PH}$ = 17.9 Hz), 6.51-6.73 (m, 4H, $C^{8\text{-}11}$-*H*), 1.91 (s, 9H, C^{18}-C(CH_3)$_3$), 1.83 (s, 9H, C^{2}-C(CH_3)$_3$), 1.39 (s, 9H, C^{16}-C(CH_3)$_3$), 1.10 (s, 9H, C^{4}-C(CH_3)$_3$).

^{31}P{^{1}H} NMR (162 MHz, C_6D_6, δ (ppm)): 34.5 (s, P).

^{13}C{^{1}H} NMR (100 MHz, C_6D_6, δ (ppm)): 165.8 (s, C^{13}-H), 133.2 (d, *o*-*C*H(PPh_2), $^{2}J_{PC}$ = 10.0 Hz), 132.7 (d, *p*-*C*H(PPh_2), $^{4}J_{PC}$ = 2.30 Hz), 132.3 (d, *o*-*C*H(PPh_2), $^{2}J_{PC}$ = 9.50 Hz), 132.3 (s, *p*-*C*H(PPh_2)), 131.1 (s, C^{17}-H), 130.1 (s, C^{3}-H), 129.2 (d, *m*-*C*H(PPh_2), $^{3}J_{PC}$ = 12.2 Hz), 128.8 (d, *m*-*C*H(PPh_2), $^{3}J_{PC}$ = 12.6 Hz), 127.7 (d, C^{5}-H, $^{2}J_{PC}$ = 15.5 Hz), 126.6 (s, C^{15}-H), 120.5 (s, $C^{8\text{-}11}$-H), 120.2 (s, $C^{8\text{-}11}$-H), 120.1 (s, $C^{8\text{-}11}$-H), 116.3 (s, $C^{8\text{-}11}$-H), 31.6 (s, C^{16}-C(CH_3)$_3$), 31.5 (s, C^{4}-C(CH_3)$_3$), 30.6 (s, C^{2}-C(CH_3)$_3$), 30.3 (s, C^{18}-C(CH_3)$_3$).

Anal. Calcd for $C_{47}H_{55}ClInN_2O_2P$: C, 65.55; H, 6.44; N, 3.25. Found: C, 65.78; H, 6.51; N, 3.23.

Compound 3.12

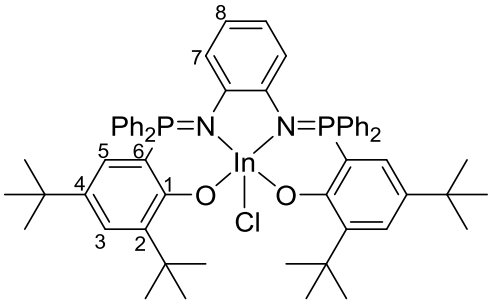

Potassium bis(trimethylsilyl)amide (135 mg, 0.68 mmol) was added to a yellow solution of **2.3** (300 mg, 0.34 mmol) in THF (10 mL) to afford a colour change to orange. After stirring for two hours, $InCl_3$ (75 mg, 0.34 mmol) was added. After a further two hours, a white precipitate was yielded. The solvent was removed *in vacuo* and CH_2Cl_2 was added to precipitate the waste salts which were removed by centrifugation. The solvent was removed *in vacuo* again and the residue was washed with cold *n*-hexane to yield the product as a white solid (240 mg, 0.23 mmol, 68%).

^{1}H NMR (400 MHz, C_6D_6, δ (ppm)): 7.84 (m, 4H, *o*-C*H*(PPh_2)), 7.73 (m, 6H, C^3-*H* & *o*-C*H*(PPh_2)), 6.81-7.00 (m, 12H, *m*/*p*-C*H*(PPh_2)), 6.74 (dd, 2H, C^5-*H*, $^4J_{HH}$ = 2.50 Hz, $^3J_{PH}$ = 17.5 Hz), 6.63 (m, 2H, C^8-*H*), 6.33 (m, 2H, C^7-*H*), 1.78 (s, 18H, C^2-C(CH_3)$_3$), 1.15 (s, 18H, C^4-C(CH_3)$_3$).

^{31}P{^{1}H} NMR (162 MHz, C_6D_6, δ (ppm)): 35.9 (s, P).

^{13}C{^{1}H} NMR (100 MHz, C_6D_6, δ (ppm)): 133.6 (d, *o*-*C*H(PPh_2), $^2J_{PC}$ = 10.2 Hz), 132.7 (d, *o*-*C*H(PPh_2), $^2J_{PC}$ = 9.90 Hz), 132.4 (d, *p*-*C*H(PPh_2), $^4J_{PC}$ = 1.70 Hz), 131.9 (d, *p*-*C*H(PPh_2), $^4J_{PC}$ = 2.00 Hz), 129.6 (s, C^3-H), 128.7 (d, *m*-*C*H(PPh_2), $^3J_{PC}$ = 12.0 Hz), 128.6 (d, *m*-*C*H(PPh_2), $^3J_{PC}$ = 12.0 Hz), 127.5 (d, C^5-H, $^2J_{PC}$ = 14.4 Hz), 120.4 (d, C^7-H, $^3J_{PC}$ = 8.10 Hz), 119.4 (s, C^8-H), 31.2 (s, C^4-C(CH_3)$_3$), 30.5 (s, C^2-C(CH_3)$_3$).

Anal. Calcd for $C_{58}H_{64}ClInN_2O_2P_2$: C, 67.41; H, 6.24; N, 2.71. Found: C, 67.28; H, 6.32; N, 2.87.

7.4. Chapter 4 Experimental Section

Compound S1

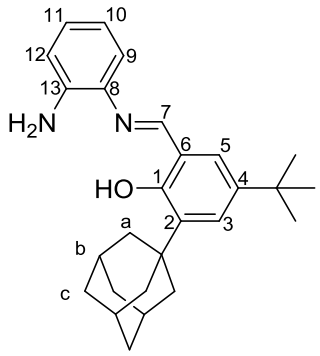

3-Adamantyl-5-*tert*-butyl-2-hydroxybenzaldehyde (1.05 g, 3.36 mmol) was dissolved in a minimum amount of ethanol (5 mL) and added dropwise at 25 ^{o}C to *o*-phenylenediamine (0.73 g, 6.72 mmol) dissolved in a minimum amount of EtOH (10 mL). The yellow solution was left to stir at 25 ^{o}C for 18 hours. A yellow precipitate formed which was filtered, recrystallised from methanol and dried to yield yellow crystals (0.63 g, 1.56 mmol, 47%).

^{1}H NMR (400 MHz, $CDCl_3$, δ (ppm)): 13.43 (s, 1H, C^{1}-O*H*), 8.63 (s, 1H, C^{7}-*H*), 7.40 (d, 1H, C^{3}-*H*, $^{4}J_{HH}$ = 2.40 Hz), 7.23 (d, 1H, C^{5}-*H*, $^{4}J_{HH}$ = 2.40 Hz), 7.09 (td, 1H, C^{12}-*H*, $^{4}J_{HH}$ = 1.40 Hz, $^{3}J_{HH}$ = 7.70 Hz), 7.04 (dd, 1H, C^{11}-*H*, $^{4}J_{HH}$ = 1.40 Hz, $^{3}J_{HH}$ = 8.10 Hz), 6.79 (m, 2H, $C^{9\&10}$-*H*), 4.02 (s, 2H, C^{13}-NH_2), 2.22 (m, 6H, Ad^{a}-CH_2), 2.11 (m, 3H, Ad^{b}-C*H*), 1.81 (m, 6H, Ad^{a}-CH_2), 1.34 (s, 9H, C^{4}-C(CH_3)$_3$).

^{13}C{^{1}H} NMR (100 MHz, $CDCl_3$, δ (ppm)): 163.6 (s, C^{7}-H), 158.2 (s, C^{IV}), 140.9 (s, C^{IV}), 140.7 (s, C^{IV}), 137.2 (s, C^{IV}), 135.7 (s, C^{IV}), 127.9 (s, C^{3}-H), 127.7 (s, C^{12}-H), 126.7 (s, C^{5}-H), 118.8 (s, $C^{9/10}$-H), 118.6 (s, C^{IV}), 118.5 (s, C^{11}-H), 115.7 (s, $C^{9/10}$-H), 40.3 (s, Ad^{a}-CH$_2$), 37.3 (s, Ad(*C*)), 37.2 (s, Ad^{c}-CH$_2$), 34.3 (s, C^{4}-C(CH$_3$)$_3$), 31.5 (s, C^{4}-C(CH$_3$)$_3$), 29.1 (s, Ad^{b}-CH).

Anal. Calcd for $C_{27}H_{34}N_2O$: C, 80.55; H: 8.51; N: 6.96. Found: C, 80.44; H, 8.60; N: 6.76.

Compound S2

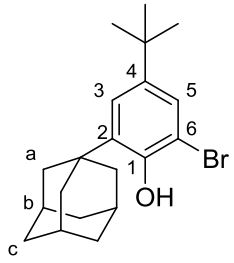

Bromine (540 µl, 10.6 mmol) was added to 2-adamantyl-4-tert-butylphenol (3.00 g, 10.6 mmol) in DCM (50 mL). After stirring for five minutes, the solution was washed with water and dried with $MgSO_4$. The solvent was removed *in vacuo* to yield the product as a white solid (2.95 g, 8.16 mmol, 77%).

^{1}H NMR (400 MHz, $CDCl_3$, δ (ppm)): 7.36 (d, 1H, C^3-*H*, $^4J_{HH}$ = 2.30 Hz), 7.23 (d, 1H, C^5-*H*, $^4J_{HH}$ = 2.30 Hz), 5.69 (s, C^1-O*H*), 2.17 (m, 6H, Ad^a-CH_2), 2.12 (m, 3H, Ad^b-C*H*), 1.82 (m, 6H, Ad^c-CH_2), 1.32 (s, 9H, C^4-C(CH_3)$_3$).

^{13}C{^{1}H} NMR (100 MHz, $CDCl_3$, δ (ppm)): 148.2 (s, *C*^{1}-OH), 143.9 (s, *C*^{2}), 137.2 (s, *C*^{4}), 126.2 (s, *C*^{3}-H), 123.8 (s, *C*^{5}-H), 112.3 (s, *C*^{6}), 40.4 (s, Ad^a-*C*H$_2$), 37.8 (s, Ad(*C*)), 37.2 (s, Ad^c-*C*H$_2$), 34.6 (s, C^4-*C*(CH$_3$)$_3$), 31.6 (s, C^4-C(*C*H$_3$)$_3$), 29.2 (s, Ad^b-*C*H$_2$).

Anal. Calcd for $C_{20}H_{27}BrO$: C, 66.11; H, 7.49. Found: C, 65.95; H, 7.49.

Compound S3

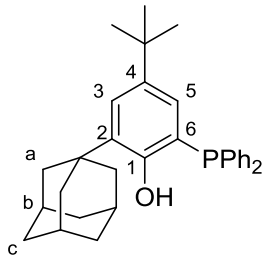

n-Butyllithium (1.6 M in hexanes, 17 mL, 27.7 mmol) was added to a solution of **S2** (4.80 g, 13.2 mmol) in Et_2O (80 mL) at -78 ^oC, giving a white precipitate. The solution was allowed to warm to 25 ^oC and stirred for three hours. Chlorodiphenylphosphine (2.24 mL, 13.2 mmol) was added dropwise at -78^oC forming a white precipitate. The solution was left to stir at 25 ^oC for 15 h. The mixture was extracted with aqueous solutions of NaH_2PO_4 (0.1 M, 3 x 50 mL) and the organic layer was filtered to remove inorganic salts. Acetic acid (10 mL) and the solution was stirred at 25 ^oC for three hours, after which the mixture was extracted with aqueous solutions of NaH_2PO_4 (0.1 M, 3 x 50 mL). The organic layer was dried with $MgSO_4$ and filtered, then methanol (30 mL) was added and the solution was concentrated and then cooled to -20 ^oC to precipitate the product as a white solid (1.32 g, 2.77 mmol, 21%).

^{1}H NMR (400 MHz, $CDCl_3$, δ (ppm)): 7.33-7.38 (m, 10H, PPh_2(C-*H*)), 7.32 (d, 1H, C^3-*H*, $^4J_{HH}$ = 2.40 Hz), 6.89 (dd, 1H, C^5-*H*, $^4J_{HH}$ = 2.40 Hz, $^3J_{PH}$ = 5.80 Hz), 6.68 (d, 1H, C^1-O*H*), 2.17 (s, 6H, Ad^a-CH_2), 2.09 (s, 3H, Ad^b-C*H*), 1.79 (s, 6H, Ad^c-CH_2), 1.18 (s, 9H, C^4-C(CH_3)$_3$).

^{31}P{^{1}H} NMR (162 MHz, $CDCl_3$, δ (ppm)): -29.8 (s, P).

^{13}C{^{1}H} NMR (100 MHz, $CDCl_3$, δ (ppm)): 156.1 (d, C^{IV}, $^2J_{PC}$ = 19.1 Hz), 142.4 (d, C^{IV}, $^4J_{PC}$ = 2.90 Hz), 135.6 (d, C^{IV}, $^4J_{PC}$ = 1.50 Hz), 135.5 (d, C^{IV}, $^4J_{PC}$ = 3.70 Hz), 133.4 (d, *o*-*C*H(PPh_2), $^2J_{PC}$ = 18.2 Hz), 128.9 (d, C^5-H, $^2J_{PC}$ = 4.10 Hz), 128.8 (s, *p*-*C*H(PPh_2)), 128.6 (d, *m*-*C*H(PPh_2), $^3J_{PC}$ = 7.20 Hz), 126.2 (s, C^3-H), 120.1 (s, C^{IV}), 40.5 (s, Ad^a-*C*H_2), 37.3 (s, Ad(*C*)), 37.2 (s, Ad^c-*C*H_2), 34.5 (s, C^4-*C*(CH_3)$_3$), 31.5 (s, C^4-C(*C*H_3)$_3$), 29.2 (s, Ad^b-*C*H).

Anal. Calcd for $C_{32}H_{37}OP$: C, 82.02; H, 7.96. Found: C, 82.31; H, 7.71.

Compound S4

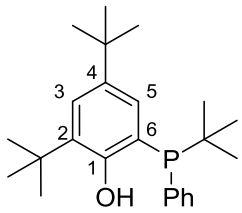

n-Butyllithium (1.6 M in hexanes, 12 mL, 19.5 mmol) was added to a solution of 2-bromo-4,6-di-*tert*-butylphenol (2.64 g, 9.30 mmol) in Et_2O (80 mL) at -78 °C, giving a white precipitate. The solution was allowed to warm to 25 °C and stirred for 30 minutes, giving a yellow solution. Chloro(*tert*-butyl)phenylphosphine (1.75 mL, 9.30 mmol) was added dropwise at -78°C forming a white precipitate. The solution was left to stir at 25 °C for 15 h. The mixture was extracted with aqueous solutions of NaH_2PO_4 (0.1 M, 3 x 50 mL) and the organic layer was filtered to remove inorganic salts. The solvent was removed *in vacuo* and to the oily precipitate, methanol was added to yield the product as a white crystalline sold (1.42 g, 3.81 mmol, 41 %).

^{1}H NMR (400 MHz, $CDCl_3$, δ (ppm)): 7.57 (m, 2H, Ar(C-*H*)), 7.33 (m, 5H, Ar(C-*H*)), 1.42 (s, 9H, C^2-C(C*H*$_3$)$_3$), 1.28 (s, 9H, C^4-C(C*H*$_3$)$_3$), 1.20 (d, 9H, P^{III}-C(C*H*$_3$), $^2J_{PH}$ = 13.7 Hz);

^{31}P{^{1}H} NMR (162 MHz, $CDCl_3$, δ (ppm)): 19.2 ppm;

^{13}C{^{1}H} NMR (100 MHz, $CDCl_3$, δ (ppm)): 157.3 (d, *C*^{IV}, $^2J_{PC}$ = 20.7 Hz), 140.8 (s, *C*^{IV}), 135.1 (d, *C*^{IV}, $^3J_{PC}$ = 9.10 Hz), 134.8 (s, *C*^{IV}), 133.6 (d, *o*-*C*H(PPh), $^2J_{PC}$ = 16.9 Hz), 129.2 (s, *p*-*C*H(PPh)), 128.2 (s, *C*^{IV}), 128.1 (d, *m*-*C*H(PPh), $^3J_{PC}$ = 8.00 Hz), 125.9 (s, *C*^{3}-H), 118.3 (s, *C*^{5}-H), 35.1 (s, C^4-*C*(CH$_3$)$_3$), 34.3 (C^2-*C*(CH$_3$)$_3$), 31.6 (s, C^4-C(*C*H$_3$)$_3$), 31.4 (d, P^{III}-*C*(CH$_3$)$_3$, $^1J_{PC}$ = 7.8 Hz, C(CH$_3$)$_3$), 29.5 (s, C^2-C(*C*H$_3$)$_3$), 28.6 (d, P^{III}-C(*C*H$_3$)$_3$, $^2J_{PC}$ = 14.4 Hz).

Anal. Calcd for $C_{24}H_{35}OP$: C, 77.80; H, 9.52. Found: C, 77.32; H, 9.89.

Compound S5

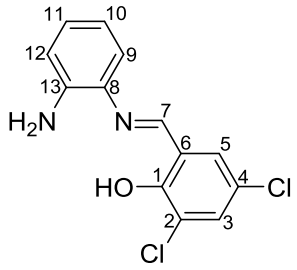

3, 5-Dichloro-2-hydroxybenzaldehyde (2.50 g, 13.1 mmol) was dissolved in a minimum amount of ethanol (20 mL) and added dropwise, at 25 ^{o}C, to *o*-phenylenediamine (2.83 g, 26.2 mmol) dissolved in a minimum amount of EtOH (30 mL). The solution formed a red precipitate immediately, which was filtered, washed with cold ethanol and dried to yield a red solid (3.23 g, 11.5 mmol, 88%).

^{1}H NMR (400 MHz, $CDCl_3$, δ (ppm)): 14.00 (s, 1H, C^{1}-O*H*), 8.55 (s, 1H, C^{7}-*H*), 7.46 (d, 1H, C^{3}-*H*, $^{4}J_{HH}$ = 2.50 Hz), 7.32 (d, 1H, C^{5}-*H*, $^{4}J_{HH}$ = 2.50 Hz), 7.15 (s, 1H, C^{12}-*H*), 7.07 (s, 1H, C^{9}-*H*), 6.80 (m, 2H, $C^{10/11}$-*H*), 4.03 (s, 2H, NH_2).

^{13}C{^{1}H} NMR (100 MHz, $CDCl_3$, δ (ppm)): 159.4 (s, C^{7}-H), 155.5 (s, C^{IV}), 141.3 (s, C^{IV}), 133.6 (s, C^{IV}), 132.6 (s, C^{3}-H), 129.7 (s, C^{5}-H), 129.3 (s, C^{12}-H), 123.7 (s, C^{IV}), 122.7 (s, C^{IV}), 120.7 (s, C^{IV}), 119.0 (s, $C^{10/11}$-H), 118.3 (s, C^{9}-H), 116.3 (s, $C^{10/11}$-H).

Anal. Calcd for $C_{13}H_{10}Cl_2N_2O$: C, 55.54; H, 3.59; N, 9.96. Found: C, 55.69; H, 3.73; N, 10.12.

Compound S6

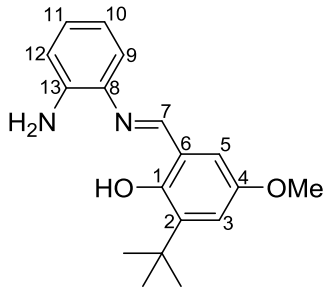

5-methoxy-3-*tert*-butyl-2-hydroxybenzaldehyde (1.27 g, 6.09 mmol) was dissolved in a minimum amount of ethanol (5 mL) and added dropwise at 25 °C to *o*-phenylenediamine (1.32 g, 12.2 mmol) dissolved in a minimum amount of EtOH (10 mL). The orange solution was left to stir at 25 °C for 18 hours. A yellow precipitate formed which was filtered, recrystallised from methanol and dried to yield yellow crystals (0.89 g, 2.98 mmol, 49%).

^{1}H NMR (400 MHz, $CDCl_3$, δ (ppm)): 13.23 (s, 1H, C^{1}-O*H*), 8.60 (s, 1H, C^{7}-*H*), 7.11 (m, 1H, C^{12}-*H*), 7.06 (d, 1H, C^{3}-*H*, $^{4}J_{HH}$ = 3.10 Hz), 7.00 (m, 1H, C^{9}-*H*), 6.80 (m, 2H, $C^{10/11}$-*H*), 6.75 (d, 1H, C^{5}-*H*, $^{4}J_{HH}$ = 3.10 Hz), 4.04 (s, 2H, NH_2), 3.82 (s, 3H, OCH_3), 1.47 (s, 9H, C^{2}-C(CH_3)$_3$).

^{13}C{^{1}H} NMR (100 MHz, $CDCl_3$, δ (ppm)): 162.7 (s, C^{7}-H), 154.9 (s, C^{IV}), 151.9 (s, C^{IV}), 140.9 (s, C^{IV}), 139.4 (s, C^{IV}), 135.5 (s, C^{IV}), 128.1 (s, C^{12}-H), 119.5 (s, C^{9}-H), 118.9 (s, $C^{10/11}$-H), 118.8 (s, C^{IV}), 118.5 (s, C^{3}-H), 115.9 (s, $C^{10/11}$-H), 112.0 (s, C^{5}-H), 55.9 (s, OCH_3), 35.2 (s, C^{2}-$C(CH_3)_3$), 29.4 (s, C^{2}-C(CH_3)$_3$).

Anal. Calcd for $C_{18}H_{22}N_2O_2$: C, 72.46; H, 7.42; N, 9.39. Found: C, 72.67; H, 7.23; N 9.33.

Compound S7

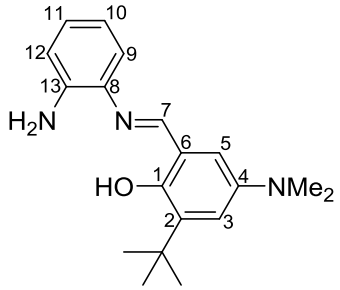

5-Dimethylamino-3-*tert*-butyl-2-hydroxybenzaldehyde (0.47 g, 2.12 mmol) was dissolved in a minimum amount of ethanol (5 mL) and added dropwise at 25 ^{o}C to *o*-phenylenediamine (0.46 g, 4.25 mmol) dissolved in a minimum amount of EtOH (10 mL). The orange solution was left to stir at 25 ^{o}C for 18 hours. A yellow precipitate formed which was filtered, washed with methanol and dried to yield yellow crystals (0.17 g, 0.55 mmol, 26%).

^{1}H NMR (400 MHz, $CDCl_3$, δ (ppm)): 13.03 (s, 1H, C^{1}-O*H*), 8.61 (s, 1H, C^{7}-*H*), 7.09 (m, 1H, C^{12}-*H*), 7.04 (m, 2H, $C^{3\&9}$-*H*), 6.79 (m, 2H, $C^{10\&11}$-*H*), 6.67 (d, 1H, C^{5}-*H*, $^{4}J_{HH}$ = 3.00 Hz), 4.04 (s, 2H, NH_2), 2.89 (s, 6H, N(CH_3)$_2$), 1.47 (s, 9H, C^{2}-C(CH_3)$_3$).

^{13}C{^{1}H} NMR (100 MHz, $CDCl_3$, δ (ppm)): 163.4 (s, *C*^{7}-H), 153.4 (s, *C*^{IV}), 143.9 (s, *C*^{IV}), 140.9 (s, *C*^{IV}), 138.3 (s, *C*^{IV}), 135.8 (s, *C*^{IV}), 127.9 (s, *C*^{12}-H), 119.5 (s, *C*^{3}-H), 119.2 (s, *C*^{IV}), 118.9 (s, *C*$^{10/11}$-H), 118.5 (s, *C*^{9}-H), 115.8 (s, *C*$^{10/11}$-H), 114.9 (s, *C*^{5}-H), 42.5 (s, N(*C*H$_3$)$_2$), 35.3 (s, C^{2}-*C*(CH$_3$)$_3$), 29.5 (s, C^{2}-C(*C*H$_3$)$_3$).

Anal. Calcd for $C_{19}H_{25}N_3O_1$: C, 73.28; H, 8.09; N, 13.49. Found: C, 73.56; H, 7.99; N 13.34.

Compound S8

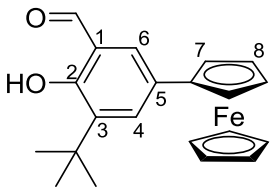

Monolithioferrocene (0.79 g, 4.14 mmol) and zinc(II) chloride (0.56 g, 4.14 mmol) were dissolved in THF (20 mL) and stirred at 25 ^{o}C for one hour. In a separate Schlenk flask, a few mgs of $Pd(PPh_3)_4$ and 3-*tert*-butyl-5-iodosalicyaldehyde (0.63 g, 2.07 mmol) were dissolved in THF (50 mL). The first solution was added dropwise to the second and the dark brown solution was left stirring at 60 ^{o}C for 24 hours. The solution was cooled and 0.1 M HCl (50 mL) was added dropwise, the resultant solution was subsequently extracted with chloroform (2 x 50 mL), dried, filtered and the solvent was removed *in vacuo*. The dark orange residue was purified by column chromatography (silica, 7:3 *n*-hexane:DCM, R_f = 0.26) to yield the product as an orange solid (0.36 g, 9.94 mmol, 48%).

^{1}H NMR (400 MHz, $CDCl_3$, δ (ppm)): 11.71 (s, 1H, C^2-O*H*), 9.90 (s, 1H, C^1-C*H*=N), 7.69 (d, 1H, C^6-*H*), $^{4}J_{HH}$ = 2.08 Hz), 7.44 (d, 1H, C^4-*H*, $^{4}J_{HH}$ = 2.08 Hz), 4.57 (pseudo-t, 2H, Cp^7-*H*), 4.31 (pseudo-t, 2H, Cp^8-*H*), 4.06 (s, 5H, Cp-*H*), 1.47 (s, 9H, C^3-C(CH_3)$_3$).

^{13}C{^{1}H} NMR (100 MHz, $CDCl_3$, δ (ppm)): 197.3 (s, C^1-*C*H=O), 159.8 (s, *C*^{2}-OH), 138.3 (s, *C*^{1}-CH=N), 132.9 (s, *C*^{6}-H), 130.3 (s, *C*^{5}-C(Fc)), 128.7 (s, *C*^{4}-H), 120.7 (s, *C*^{3}-C(CH_3)$_3$), 85.6 (s, C^5-*C*(Fc)), 69.7 (s, Cp-*C*H), 68.9 (s, Cp^8-*C*H), 66.5 (s, Cp^7-*C*H), 35.0 (s, C^3-*C*(CH_3)$_3$), 29.5 (s, C^3-C(*C*H_3)$_3$); MS ES+: *m/z* 362, ($[M+H]^+$ Calc.: 362).

Anal. Calcd for $C_{21}H_{22}FeO_2$: C, 69.63; H, 6.12. Found: C, 69.93; H, 6.24.

Compound S9

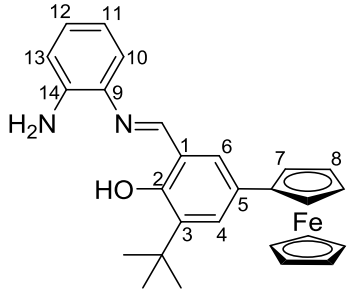

S8 (0.30 g, 0.83 mmol) was dissolved in a minimum amount of ethanol (5 mL) and added dropwise at 25 °C to *o*-phenylenediamine (0.17 g, 1.66 mmol) dissolved in a minimum amount of EtOH (10 mL). The orange solution was left to stir at 25 °C for 18 hours. An orange precipitate formed which was filtered, washed with cold ethanol and dried to yield orange crystals (0.084 g, 0.186 mmol, 22%).

^{1}H NMR (400 MHz, $CDCl_3$, δ (ppm)): 13.55 (s, 1H, C^2-O*H*), 8.63 (s, 1H, C^1-C*H*=O), 7.54 (d, 1H, C^6-*H*, $^4J_{HH}$ = 2.20 Hz), 7.32 (d, 1H, C^4-*H*, $^4J_{HH}$ = 2.20 Hz), 7.05-7.11 (m, 2H, $C^{10\&13}$-*H*), 6.77-6.81 (m, 2H, $C^{11\&12}$-*H*), 4.56 (pseudo-t, 2H, Cp^7-*H*), 4.27 (pseudo-t, 2H, Cp^8-*H*), 4.07 (brs, 2H, C^{14}-NH_2), 4.04 (s, 5H, Cp-*H*), 1.49 (s, 9H, C^3-C(CH_3)$_3$).

^{13}C{^{1}H} NMR (100 MHz, $CDCl_3$, δ (ppm)): 162.9 (s, C^1-*C*H=N), 158.8 (s, *C*^{2}-OH), 140.9 (s, *C*^{14}-NH_2), 137.6 (s, *C*^{1}-CH=N), 135.5 (s, *C*^{9}-N=CH), 129.1 (s, *C*^{6}-H), 129.0 (s, *C*^{5}-C(Fc)), 128.0 (s, *C*^{13}-H), 127.8 (s, *C*^{4}-H), 119.3 (s, *C*^{3}-C(CH_3)$_3$), 118.9 (s, *C*^{12}-H), 118.5 (s, *C*^{10}-H), 115.9 (s, *C*^{11}-H), 86.5 (s, C^5-*C*(Fc)), 69.6 (s, Cp-*C*H), 68.6 (s, Cp^8-*C*H), 66.4 (s, Cp^7-*C*H), 35.0 (s, C^3-*C*(CH_3)$_3$), 29.5 (s, C^3-C(*C*H_3)$_3$); MS ES+: *m/z* 453, ([M+H]$^+$ Calc.: 453).

Anal. Calcd for $C_{27}H_{28}FeN_2O$: C, 71.69; H, 6.24; N, 6.19. Found: C, 71.58; H, 6.16; N, 6.25.

Compound 4.1

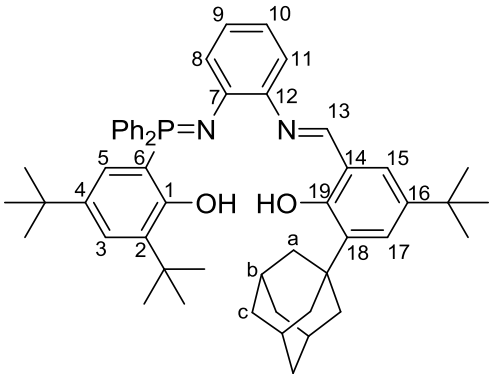

At -78 °C, bromine (80 µL, 1.56 mmol) was added dropwise to a solution of 2-(diphenylphosphino)-4,6-di-*tert*-butylphenol (0.61 g, 1.56 mmol) in DCM (80 mL). The cold bath was removed and stirring was continued for two hours at 25 °C. The solution was again cooled to -78 °C, DABCO (0.19 g, 1.56 mmol) and **S1** (0.63 g, 1.56 mmol) were added. The cold bath was removed and the solution was left to stir at 25 °C for 20 h. The DCM was evaporated and the residue was suspended in THF (10 mL) and filtered to remove the DABCO salt. THF was removed from the filtrate and *n*-hexane was added to the residue to precipitate a pale yellow solid, which was washed and dried *in vacuo* to yield the product (0.27 g, 0.34 mmol, 22%).

^{1}H NMR (400 MHz, d_8-THF, δ (ppm)): 14.57 (s, 1H, C-O*H*), 13.77 (s, 1H, C-O*H*), 8.44 (s, 1H, C^{13}-*H*), 7.78 (m, 4H, *o*-C*H*(PPh_2)), 7.55 (m, 2H, *p*-C*H*(PPh_2)), 7.46 (m, 4H, *m*-C*H*(PPh_2)), 7.36 (d, 1H, C^{3}-*H*, $^{4}J_{HH}$ = 2.40 Hz), 7.34 (d, 1H, C^{17}-*H*, $^{4}J_{HH}$ = 2.50 Hz), 7.19 (d, 1H, C^{15}-*H*, $^{4}J_{HH}$ = 2.50 Hz), 6.81 (m, 2H, C^{5}-*H* & C^{11}-*H*), 6.73 (m, 1H, C^{10}-*H*), 6.67 (m, 1H, C^{9}-*H*), 6.63 (m, 1H, C^{8}-*H*), 2.24 (s, 6H, Ad^{a}-CH_2), 2.06 (s, 3H, Ad^{b}-C*H*), 1.81 (m, 6H, Ad^{c}-CH_2), 1.32 (s, 9H, C^{2}-C(CH_3)$_3$), 1.25 (s, 9H, C^{16}-C(CH_3)$_3$), 1.09 (s, 9H, C^{4}-C(CH_3)$_3$).

^{31}P{^{1}H} NMR (162 MHz, d_8-THF, δ (ppm)): 18.6 (s, P).

^{13}C{^{1}H} NMR (100 MHz, d_8-THF, δ (ppm)): 164.0 (s, C^{13}-H), 160.4 (s, C^{IV}), 156.5 (s, C^{IV}), 143.3 (d, C^{IV}, $^{2}J_{PC}$ = 18.1 Hz), 139.5 (s, C^{IV}), 137.6 (s, C^{IV}), 136.8 (d, C^{IV}, $^{2}J_{PC}$ = 14.7 Hz), 136.0 (d, C^{IV}, $^{3}J_{PC}$ = 9.50 Hz), 134.5 (s, C^{IV}), 130.9 (d, *o*-*C*H(PPh_2), $^{2}J_{PC}$ = 9.90 Hz), 130.1 (d, *p*-*C*H(PPh_2), $^{4}J_{PC}$ = 2.80 Hz), 128.4 (d, C^{IV}, $^{1}J_{PC}$ = 83.8 Hz), 126.7 (d, *m*-*C*H(PPh_2), $^{3}J_{PC}$ = 11.5 Hz), 125.8 (s, C^{3}-H), 124.9 (s, C^{17}-H), 124.7 (s, C^{15}-H), 124.2 (d, C^{5}-H, $2J_{PC}$ = 13.7 Hz), 123.6 (s, C^{11}-H), 119.9 (d, C^{8}-H, $^{2}J_{PC}$ = 11.1 Hz), 118.8 (s, C^{10}-H), 117.3 (s, C^{IV}), 117.1 (s, C^{9}-H),

104.5 (d, C^{IV}, $^{1}J_{PC}$ = 124.8 Hz), 38.5 (s, Ad^{a}-CH_2), 35.3 (s, Ad^{c}-CH_2), 35.2 (s, Ad(*C*)), 33.2 (s, C^{2}-$C(CH_3)_3$), 31.9 (s, C^{4}-$C(CH_3)_3$), 31.8 (s, C^{16}-$C(CH_3)_3$), 29.1 (s, C^{2}-$C(CH_3)_3$), 28.8 (s, C^{4}-$C(CH_3)_3$), 27.5 (s, Ad^{b}-CH), 27.2 (s, C^{16}-$C(CH_3)_3$).

Anal. Calcd for $C_{53}H_{63}N_2O_2P$: C, 80.47; H, 8.03; N, 3.54. Found: C, 80.28; H, 8.16; N 3.67.

Compound 4.2

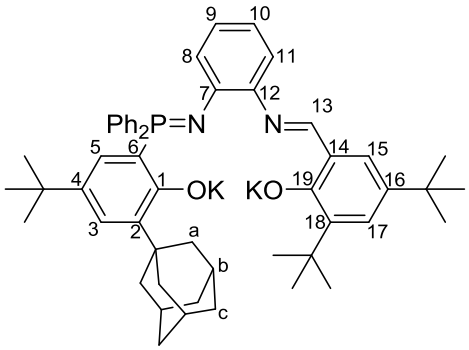

At -78 °C, bromine (130 µL, 2.56 mmol) was added dropwise to a solution of **S3** (1.20 g, 2.56 mmol) in DCM (80 mL). The cold bath was removed and stirring was continued for two hours at 25 °C. The solution was again cooled to -78 °C, DABCO (0.37 g, 3.07 mmol) and 2-((2-aminophenylimino)methyl)-4,6-di-*tert*-butylphenol (0.83 g, 2.56 mmol) were added. The cold bath was removed and the solution was left to stir at 25 °C for 20 h. The DCM was evaporated and the residue was suspended in THF (10 mL) and filtered to remove the DABCO salt. THF was removed from the filtrate and pentane was added to the residue to precipitate a pale yellow solid, which was washed and dried *in vacuo* to yield a mixture of both the phosphonium bromide salt product and the deprotonated iminophosphorane product in a ratio of 0.25:1 respectively. The solid mixture (1.20 g) was dissolved in THF (10 mL) and potassium bis(trimethylsilyl)amide (0.62 g, 3.12 mmol) was added. The solution was stirred at room temperature for two hours before being centrifuged to remove any insoluble salts and the solvent was subsequently removed *in vacuo*. The residue was recrystallised from THF/*n*-hexane to yield the product as a yellow solid (300 mg, 0.346 mmol, 25%).

^{1}H NMR (400 MHz, d_8-THF, δ (ppm)): 8.37 (s, 1H, C^{13}-*H*), 7.62 (m, 4H, *o*-C*H*(PPh_2)), 7.46 (m, 2H, *p*-C*H*(PPh_2)), 7.38 (m, 4H, *m*-C*H*(PPh_2)), 7.13 (d, 1H, C^{3}-*H*, $^{4}J_{HH}$ = 2.70 Hz), 7.09 (d, 1H, C^{17}-*H*, $^{4}J_{HH}$ = 2.80 Hz), 6.94 (m, 1H, C^{11}-*H*), 6.92 (d, 1H, C^{15}-*H*, $^{4}J_{HH}$ = 2.80), 6.60 (m, 1H, C^{8}-*H*), 6.48 (m, 2H, $C^{9/10}$-*H*), 6.17 (dd, 1H, C^{5}-*H*, $^{4}J_{HH}$ = 2.70 Hz, $^{3}J_{PH}$ = 17.0 Hz), 2.24 (m, 6H, Ad^{a}-CH_2), 2.01 (m, 3H, Ad^{b}-C*H*), 1.81 (m, 3H, Ad^{a}-CH_2), 1.72 (m, 3H, Ad^{a}-CH_2), 1.41 (s, 9H, C^{18}-C(CH_3)$_3$), 1.25 (s, 9H, C^{16}-C(CH_3)$_3$), 0.97 (s, 9H, C^{4}-C(CH_3)$_3$).

^{31}P{^{1}H} NMR (162 MHz, d_8-THF, δ (ppm)): 12.2 (s, P).

$^{13}C\{^1H\}$ NMR (100 MHz, d_8-THF, δ (ppm)): 171.3 (d, C^{IV}, $^4J_{PC}$ = 3.80 Hz), 169.9 (s, C^{IV}), 159.6 (s, C^{13}-H), 146.1 (d, C^{IV}, $^4J_{PC}$ = 4.50 Hz), 145.5 (d, C^{IV}, $^1J_{PC}$ = 22.6 Hz), 138.4 (s, C^{IV}), 137.8 (d, C^{IV}, $^3J_{PC}$ = 9.10 Hz), 133.0 (s, C^{IV}), 132.4 (s, C^{IV}), 130.5 (d, *o*-*C*H(PPh_2), $^2J_{PC}$ = 8.80 Hz), 128.4 (d, *p*-*C*H(PPh_2), $^4J_{PC}$ = 82.40 Hz), 127.6 (s, C^{15}-H), 126.4 (d, C^5-H, $^2J_{PC}$ = 15.7 Hz), 126.1 (d, *m*-*C*H(PPh_2), $^3J_{PC}$ = 11.2 Hz), 125.6 (s, C^3-H), 123.8 (s, C^{17}-H), 121.7 (s, $C^{9/10}$-H), 119.5 (d, C^8-H, $^3J_{PC}$ = 11.0 Hz), 119.4 (s, C^{IV}), 115.2 (s, C^{11}-H), 114.3 (s, $C^{9/10}$-H), 109.5 (s, C^{IV}), 108.4 (s, C^{IV}), 38.1 (s, Ad^a-CH_2), 35.6 (s, Ad^c-CH_2), 35.5 (s, Ad(*C*)), 33.3 (s, C^{18}-$C(CH_3)_3$), 31.5 (s, C^4-$C(CH_3)_3$), 31.4 (s, C^{16}-$C(CH_3)_3$), 29.4 (s, C^{16}-C(CH_3)$_3$), 29.2 (s, C^4-C(CH_3)$_3$), 27.6 (s, Ad^b-CH), 27.5 (s, C^{18}-C(CH_3)$_3$).

Anal. Calcd for $C_{53}H_{61}K_2N_2O_2P$: C, 73.40; H, 7.09; N, 3.23. Found: C, 72.97; H, 7.08; N, 3.16.

Compound 4.3

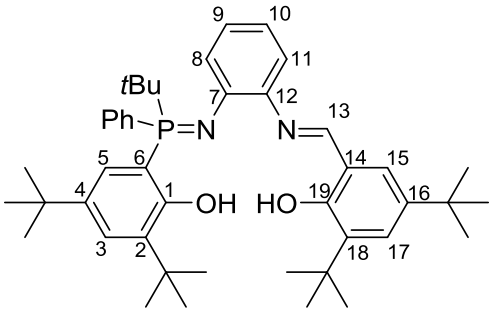

At -78 °C, bromine (190 µL, 3.78 mmol) was added dropwise to a solution of **S4** (1.40 g, 3.78 mmol) in DCM (80 mL). The cold bath was removed and stirring was continued for two hours at 25 °C. The solution was again cooled to -78 °C, DABCO (0.46 g, 3.78 mmol) and 2-((2-aminophenylimino)methyl)-4,6-di-*tert*-butylphenol (1.23 g, 3.78 mmol) were added. The cold bath was removed and the solution was left to stir at 25 °C for 20 h. The DCM was evaporated and the residue was suspended in THF (10 mL) and filtered to remove the DABCO salt. THF was removed from the filtrate and pentane was added to the residue to precipitate a pale yellow solid, which was washed and dried *in vacuo* to yield the product (0.92 g, 1.32 mmol, 35%).

^{1}H NMR (400 MHz, d_8-THF, δ (ppm)): 14.44 (s, 1H, C-O*H*), 13.74 (s, 1H, C-O*H*), 8.56 (s, 1H, C^{13}-*H*), 7.99 (m, 2H, *o*-C*H*(PPh_2)), 7.59 (m, 1H, *p*-C*H*(PPh_2)), 7.51 (m, 2H, *m*-C*H*(PPh_2)), 7.42 (d, 1H, C^{17}-*H*, $^{4}J_{HH}$ = 2.50 Hz), 7.35 (d, 1H, C^{3}-*H*, $^{4}J_{HH}$ = 2.40 Hz), 7.27 (d, 1H, C^{15}-*H*, $^{4}J_{HH}$ = 2.50 Hz), 6.87 (m, 1H, C^{11}-*H*), 6,67 (dd, 1H, C^{5}-*H*, $^{4}J_{HH}$ = 2.40 Hz, $^{3}J_{PH}$ = 14.8 Hz), 6.63 (m, 2H, $C^{9/10}$-*H*), 6.28 (m, 1H, C^{8}-*H*), 1.45 (s, C^{18}-C(CH_3)$_3$), 1.42 (d, 9H, P-C(CH_3)$_3$, $^{3}J_{PH}$ = 15.1 Hz), 1.34 (s, C^{2}-C(CH_3)$_3$), 1.23 (s, C^{16}-C(CH_3)$_3$), 1.10 (s, C^{4}-C(CH_3)$_3$).

^{31}P{^{1}H} NMR (162 MHz, d_8-THF, δ (ppm)): 34.3 (s, P).

^{13}C{^{1}H} NMR (100 MHz, d_8-THF, δ (ppm)): 165.9 (s, C^{13}-H), 164.1 (s, C^{IV}), 159.6 (s, C^{IV}), 145.7 (d, C^{IV}, $^{2}J_{PC}$ = 16.9 Hz), 143.9 (d, C^{IV}, $^{4}J_{PC}$ = 3.90 Hz), 140.5 (s, C^{IV}), 138.7 (d, C^{IV}, $^{3}J_{PC}$ = 8.30 Hz), 138.5 (s, C^{IV}), 137.2 (s, C^{IV}), 134.2 (d, *o*-C*H*(PPh_2), $^{2}J_{PC}$ = 8.60 Hz), 132.9 (d, *p*-C*H*(PPh_2), $^{4}J_{PC}$ = 2.70 Hz), 131.3 (d, C^{IV}, $^{1}J_{PC}$ = 65.4 Hz), 129.9 (d, *m*-C*H*(PPh_2), $^{3}J_{PC}$ = 10.3 Hz), 128.4 (d, C^{3}-H, $^{4}J_{PC}$ = 2.40 Hz), 128.0 (d, C^{5}-H, $^{2}J_{PC}$ = 12.9 Hz), 127.8 (s, C^{17}-H), 127.7 (s, C^{15}-H), 126.7 (s, C^{9}-H), 122.2 (d, C^{8}-H, $^{3}J_{PC}$ = 8.10 Hz), 120.9 (s, C^{11}-H), 120.4 (s, C^{IV}), 119.5 (s, C^{10}-H), 106.4 (d, C^{IV}, $^{1}J_{PC}$ = 111.9 Hz), 39.4 (d, P-*C*(CH_3)$_3$, $^{1}J_{PC}$ = 59.4 Hz), 36.0 (s, C^{2}-

C(CH_3)$_3$), 35.9 (s, C^4-*C*(CH_3)$_3$), 34.9 (s, C^{18}-*C*(CH_3)$_3$), 34.8 (s, C^{16}-*C*(CH_3)$_3$), 32.1 (s, C^2-C(*C*H_3)$_3$), 31.8 (s, C^4-C(*C*H_3)$_3$), 30.3 (s, C^{18}-C(*C*H_3)$_3$), 30.2 (s, C^{16}-C(*C*H_3)$_3$), 27.1 (s, P-C(*C*H_3)$_3$).

Anal. Calcd for $C_{45}H_{61}N_2O_2P$: C, 78.00; H, 8.87; N, 4.04. Found: C, 77.25; H, 9.14; N, 4.58.

Compound 4.4

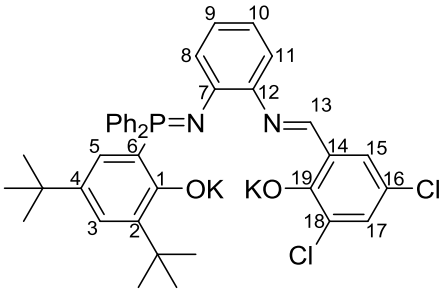

At -78 °C, bromine (0.13 mL, 2.56 mmol) was added dropwise to a solution of 2-(diphenylphosphino)-4,6-di-*tert*-butylphenol (1.00 g, 2.56 mmol) in DCM (80 mL). The cold bath was removed and stirring was continued for two hours at 25 °C. The solution was again cooled to -78 °C, DABCO (0.31 g, 2.56 mmol) and **S5** (0.72 g, 2.56 mmol) were added. The solution was left to stir at 25 °C for 20 h. The DCM was evaporated and the residue was suspended in THF (10 mL) and filtered to remove the DABCO salt. THF was removed from the filtrate and *n*-hexane was added to the residue to precipitate a pale yellow solid, which was washed and dried *in vacuo* to yield a mixture of both the phosphonium bromide salt product and the deprotonated iminophosphorane product in a ratio of 0.37:1 respectively. The solid mixture (640 mg) was dissolved in THF (10 mL) and potassium bis(trimethylsilyl)amide (417 mg, 2.09 mmol) was added. The solution was stirred at room temperature for two hours before being centrifuged to remove any insoluble salts and the solvent was subsequently removed *in vacuo*. The residue was recrystallised from THF/*n*-hexane to yield the product as a yellow solid (178 mg, 0.24 mmol, 26%).

^{1}H NMR (400 MHz, d_8-THF, δ (ppm)): 8.38 (s, 1H, C^{13}-*H*), 7.67 (m, 4H, *o*-C*H*(PPh_2)), 7.47 (m, 2H, *p*-C*H*(PPh_2)), 7.38 (m, 4H, *m*-C*H*(PPh_2)), 7.25 (d, 1H, C^{3}-*H*, $^{4}J_{HH}$ = 2.70 Hz), 7.08 (d, 1H, C^{17}-*H*, $^{4}J_{HH}$ = 3.00 Hz), 7.03 (d, 1H, C^{15}-*H*, $^{4}J_{HH}$ = 3.00 Hz), 7.01 (m, 1H, C^{11}-*H*), 6.58 (m, 2H, $C^{8/9}$-*H*), 6.50 (m, 1H, C^{10}-*H*), 6.23 (dd, 1H, C^{5}-*H*, $^{4}J_{HH}$ = 2.70 Hz, $^{3}J_{PH}$ = 16.5 Hz), 1.43 (s, 9H, C^{2}-C(CH_3)$_3$), 0.99 (s, 9H, C^{4}-C(CH_3)$_3$).

^{31}P{^{1}H} NMR (162 MHz, d_8-THF, δ (ppm)): 12.6 (s, P).

^{13}C{^{1}H} NMR (100 MHz, d_8-THF, δ (ppm)): 166.9 (s, C^{IV}), 159.7 (s, C^{13}-H), 149.4 (d, C^{IV}, $^{4}J_{PC}$ = 4.00 Hz), 146.6 (d, C^{IV}, $^{1}J_{PC}$ = 23.0 Hz), 140.8 (d, C^{IV}, $^{3}J_{PC}$ = 9.00 Hz), 135.2 (s, C^{IV}), 134.6 (s, C^{IV}), 133.6 (s, C^{17}-H), 133.5 (d, *o*-*C*H(PPh_2), $^{2}J_{PC}$ = 9.00 Hz), 131.5 (d, *p*-*C*H(PPh_2), $^{4}J_{PC}$ = 2.70

Hz), 131.1 (s, C^{15}-H), 129.4 (s, C^{IV}), 129.1 (d, *m*-*C*H(PPh_2), $^3J_{PC}$ = 11.0 Hz), 129.0 (d, C^5-H, $^2J_{PC}$ = 15.2 Hz), 128.7 (d, C^3-H, $^3J_{PC}$ = 1.90 Hz), 126.2 (s, C^9-H), 124.8 (s, C^{IV}), 123.2 (d, C^8-H, $^3J_{PC}$ = 11.4 Hz), 118.2 (s, C^{11}-H), 117.2 (s, C^{10}-H), 112.0 (s, C^{IV}), 111.0 (s, C^{IV}), 110.9 (s, C^{IV}), 36.1 (s, C^4-*C*(CH_3)$_3$), 34.5 (s, C^2-*C*(CH_3)$_3$), 32.3 (s, C^4-C(*C*H_3)$_3$), 30.1 (s, C^2-C(*C*H_3)$_3$).

Anal. Calcd for $C_{39}H_{37}Cl_2K_2N_2O_2P$: C, 62.81; H, 5.00; N, 3.76. Found: C, 62.31; H, 5.11; N 3.64.

Compound 4.5

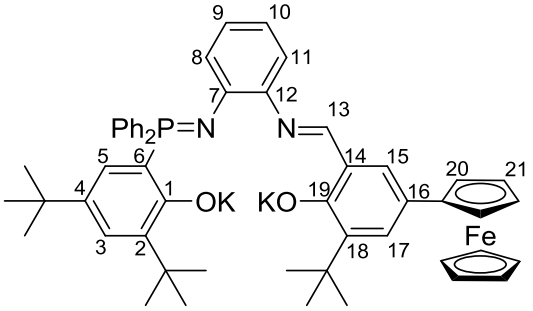

At -78 °C, bromine (60 µL, 1.11 mmol) was added dropwise to a solution of 2-(diphenylphosphino)-4,6-di-*tert*-butylphenol (430 mg, 1.11 mmol) in DCM (80 mL). The cold bath was removed and stirring was continued for two hours at 25 °C. The solution was again cooled to -78 °C, DABCO (140 mg, 1.11 mmol) and **S9** (500 mg, 1.11 mmol) were added. The cold bath was removed and the solution was left to stir at 25 °C for 20 h. The DCM was evaporated and the residue was suspended in THF (10 mL) and filtered to remove the DABCO salt. THF was removed from the filtrate and *n*-hexane was added to the residue to precipitate a pale yellow solid, which was washed and dried *in vacuo* to yield a mixture of both the phosphonium bromide salt product and the deprotonated iminophosphorane product in a ratio of 0.41:1 respectively. The solid mixture (250 mg) was dissolved in THF (10 mL) and potassium bis(trimethylsilyl)amide (131 mg, 0.66 mmol) was added to yield a colour change from yellow to red. The solution was stirred at room temperature for two hours before being centrifuged to remove any insoluble salts and the solvent was subsequently removed *in vacuo*. The residue was recrystallised from THF/*n*-hexane to yield the product as an orange solid (50 mg, 0.05 mmol, 5%).

^{1}H NMR (400 MHz, d_8-THF, δ (ppm)): 8.40 (s, 1H, C^{13}-*H*), 7.66 (m, 4H, *o*-C*H*(PPh_2)), 7.48 (m, 2H, *p*-C*H*(PPh_2)), 7.39 (m, 4H, *m*-C*H*(PPh_2)), 7.27 (d, 1H, C^{17}-*H*, $^{4}J_{HH}$ = 2.50 Hz), 7.23 (d, 1H, C^{3}-*H*, $^{4}J_{HH}$ = 2.70 Hz), 7.13 (d, 1H, C^{15}-*H*, $^{4}J_{HH}$ = 2.50 Hz), 6.98 (m, 1H, C^{11}-*H*), 6.61 (m, 1H, C^{8}-*H*), 6.52 (m, 2H, $C^{9/10}$-*H*), 6.20 (dd, 1H, C^{5}-*H*, $^{4}J_{HH}$ = 2.70 Hz, $^{3}J_{PH}$ = 16.8 Hz), 4.43 (pseudo-t, 2H, Cp^{20}-*H*), 4.08 (pseudo-t, 2H, Cp^{21}-*H*), 3.95 (s, 5H, Cp-*H*), 1.44 (s, 9H, C^{18}-C(CH_3)$_3$), 1.43 (s, 9H, C^{2}-C(CH_3)$_3$), 0.98 (s, 9H, C^{4}-C(CH_3)$_3$).

^{31}P{^{1}H} NMR (162 MHz, d_8-THF, δ (ppm)): 11.9 (s, P).

^{13}C{^{1}H} NMR (100 MHz, d_8-THF, δ (ppm)): 173.9 (s, C^{IV}), 162.3 (s, C^{13}-H), 149.1 (d, C^{IV}, $^{4}J_{PC}$ = 4.30 Hz), 148.2 (d, C^{IV}, $^{1}J_{PC}$ = 22.7 Hz), 142.0 (s, C^{IV}), 140.7 (d, C^{IV}, $^{3}J_{PC}$ = 9.40 Hz), 135.7 (s,

C^{IV}), 135.1 (s, C^{IV}), 133.5 (d, *o*-*C*H(PPh_2), $^2J_{PC}$ = 8.90 Hz), 132.9 (d, C^{IV}, $^3J_{PC}$ = 8.80 Hz), 132.5 (s, C^{15}-H), 131.4 (d, *p*-*C*H(PPh_2), $^4J_{PC}$ = 2.70 Hz), 130.5 (s, C^{IV}), 129.4 (d, C^5-H, $^2J_{PC}$ = 15.4 Hz), 129.1 (d, *m*-*C*H(PPh_2), $^3J_{PC}$ = 10.8 Hz), 128.6 (d, C^3-H, $^4J_{PC}$ = 2.20 Hz), 128.5 (s, C^{17}-H), 125.0 (s, C^9-H), 123.3 (s, C^{IV}), 122.6 (d, C^8-H, $^3J_{PC}$ =11.0 Hz), 118.2 (s, C^{11}-H), 117.4 (s, C^{10}-H), 117.0 (s, C^{IV}), 91.8 (s, *C*(Fc)), 69.8 (s, Cp^{20}-*C*H), 68.1 (s, Cp^{21}-*C*H), 65.7 (s, Cp-*C*H), 36.2 (s, C^4-*C*(CH_3)$_3$), 36.1 (s, C^2-*C*(CH_3)$_3$), 34.5 (s, C^{18}-*C*(CH_3)$_3$), 32.2 (s, C^4-C(*C*H_3)$_3$), 30.5 (s, C^2-C(*C*H_3)$_3$), 30.3 (s, C^{18}-C(*C*H_3)$_3$).

Anal. Calcd for $C_{53}H_{55}FeK_2N_2O_2P$: C, 69.42; H, 6.05; N, 3.05. Found: C, 69.25; H, 6.14; N, 3.28.

Compound 4.6

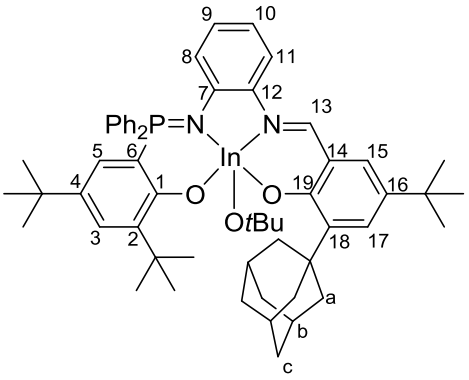

Potassium bis(trimethylsilyl)amide (135 mg, 0.68 mmol) was added to a solution of **4.1** (270 mg, 0.34 mmol) in THF (10 mL) to yield a colour change from yellow to red. After two hours, $InCl_3$ (75 mg, 0.34 mmol) was added to give an orange solution and stirred for two hours. Potassium *tert*-butoxide (38 mg, 0.34 mmol) was added to the mixture, giving a cloudy orange solution. Stirring was continued for two hours and the solid was removed by centrifugation. The solvent was evaporated in *vacuo* and the residue was washed with *n*-hexane to give the product as a yellow solid (170 mg, 0.17 mmol, 51%).

^{1}H NMR (400 MHz, d_8-THF, δ (ppm)): 8.71 (s, 1H, C^{13}-*H*), 8.10 (m, 2H, *o*-C*H*(PPh_2)), 7.67 (m, 1H, *p*-C*H*(PPh_2)), 7.57 (m, 5H, *o*/*m*/*p*-C*H*(PPh_2)), 7.43 (d, 1H, C^{17}-*H*, $^{4}J_{HH}$ = 2.60 Hz), 7.42 (m, 3H, C^{11}-*H*, *m*-C*H*(PPh_2)), 7.41 (d, 1H, C^{3}-*H*, $^{4}J_{HH}$ = 2.60 Hz), 7.14 (d, 1H, C^{15}-*H*, $^{4}J_{HH}$ = 2.60 Hz), 6.79 (m, 1H, C^{10}-*H*), 6.71 (m, 1H, C^{9}-*H*), 6.54 (dd, 1H, C^{5}-*H*, $^{4}J_{HH}$ = 2.60 Hz, $^{3}J_{PH}$ = 18.2 Hz), 6.48 (m, 1H, C^{8}-*H*), 2.34 (m, 6H, Ad^{a}-CH_2), 2.09 (m, 3H, Ad^{b}-C*H*), 1.90 (m, 3H, Ad^{c}-CH_2), 1.75 (m, 3H, Ad^{c}-CH_2), 1.46 (s, 9H, C^{2}-C(CH_3)$_3$), 1.31 (s, 9H, C^{16}-C(CH_3)$_3$), 1.04 (s, 9H, C^{4}-C(CH_3)$_3$), 1.03 (s, 9H, In-OC(CH_3)$_3$).

^{31}P{^{1}H} NMR (162 MHz, d_8-THF, δ (ppm)): 33.2 (s, P).

^{13}C{^{1}H} NMR (100 MHz, d_8-THF, δ (ppm)): 168.8 (s, C^{IV}), 167.4 (d, C^{IV}, $^{4}J_{PC}$ = 3.00 Hz), 164.2 (s, C^{13}-*H*), 139.8 (d, C^{IV}, $^{2}J_{PC}$ = 10.2 Hz), 139.1 (d, C^{IV}, $^{4}J_{PC}$ = 3.70 Hz), 136.5 (d, C^{IV}, $^{2}J_{PC}$ = 14.8 Hz), 134.1 (s, C^{IV}), 134.0 (d, C^{IV}, $^{2}J_{PC}$ = 15.7 Hz), 131.9 (d, *o*-*C*H(PPh_2), $^{2}J_{PC}$ = 10.2 Hz), 130.1 (d, *o*-*C*H(PPh_2), $^{2}J_{PC}$ = 9.70 Hz), 130.6 (d, *p*-*C*H(PPh_2), $^{4}J_{PC}$ = 2.90 Hz), 130.3 (d, *p*-*C*H(PPh_2), $^{4}J_{PC}$ = 2.80 Hz), 128.5 (s, C^{17}-H), 128.2 (s, C^{15}-H), 127.5 (s, C^{IV}), 126.9 (d, *m*-*C*H(PPh_2), $^{3}J_{PC}$ = 12.5 Hz), 126.7 (d, *m*-*C*H(PPh_2), $^{3}J_{PC}$ = 12.1 Hz), 126.7 (s, C^{3}-H), 126.2 (s, C^{IV}), 125.7 (d, C^{5}-H, $^{2}J_{PC}$ = 15.2 Hz), 124.4 (s, C^{9}-H), 118.8 (d, C^{8}-H, $^{3}J_{PC}$ = 8.80 Hz), 118.2 (s, C^{10}-H), 116.7 (s,

C^{IV}), 115.0 (s, C^{11}-H), 106.3 (s, C^{IV}), 105.3 (s, C^{IV}), 38.7 (s, Ad^{a}-CH_2), 35.8 (s, Ad(*C*)), 35.3 (s, Ad^{c}-CH_2), 33.6 (s, C^{2}-$C(CH_3)_3$), 32.6 ((s, In-O$C(CH_3)_3$), 32.2 (s, In-OC$(CH_3)_3$), 31.7 (s, C^{16}-$C(CH_3)_3$), 29.7 (s, C^{4}-$C(CH_3)_3$), 28.9 (s, C^{16}-C$(CH_3)_3$), 28.8 (s, C^{4}-C$(CH_3)_3$), 27.7 (s, C^{2}-C$(CH_3)_3$), 27.6 (s, Ad^{b}-CH).

Anal. Calcd for $C_{57}H_{70}InN_2O_3P$: C, 70.08; H, 7.22; N, 2.87. Found: C, 70.22; H, 7.28; N 2.75.

Compound 4.7

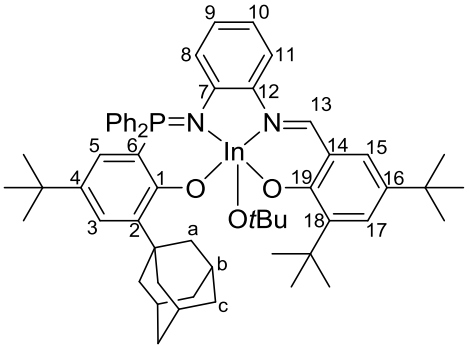

$InCl_3$ (27 mg, 0.12 mmol) was added to a solution of **4.2** (107 mg, 0.12 mmol) in THF (10 mL) and stirred for two hours. Potassium *tert*-butoxide (14 mg, 0.12 mmol) was added to the mixture, giving a cloudy solution. Stirring was continued for two hours and the solid was removed by centrifugation. The solvent was evaporated in *vacuo* and the residue was washed with *n*-hexane to give the product as a yellow solid (60 mg, 0.067 mmol, 35%).

^{1}H NMR (400 MHz, d_8-THF, δ (ppm)): 8.82 (s, 1H, C^{13}-*H*), 7.95 (m, 2H, *o*-C*H*(PPh_2)), 7.57 (m, 7H, C^{11}-*H* & *o*/*m*/*p*-C*H*(PPh_2)), 7.47 (d, 1H, C^{17}-*H*, $^{4}J_{HH}$ = 2.80 Hz), 7.46 (m, 2H, *m*/*p*-C*H*(PPh_2)), 7.34 (d, 1H, C^{3}-*H*, $^{4}J_{HH}$ = 7.46 Hz), 7.19 (d, 1H, C^{15}-*H*, $^{4}J_{HH}$ = 2.80 Hz), 6.75 (td, 1H, C^{10}-*H*, $^{4}J_{HH}$ = 1.40 Hz, $^{3}J_{HH}$ = 7.60 Hz), 6.67 (td, 1H, C^{9}-*H*, $^{4}J_{HH}$ = 1.50 Hz, $^{3}J_{HH}$ = 7.30 Hz), 6.44 (m, 1H, C^{8}-*H*), 6.42 (dd, 1H, C^{5}-*H*, $^{4}J_{HH}$ = 2.46 Hz, $^{3}J_{PH}$ = 17.8 Hz), 2.24 (m, 6H, Ad^{a}-CH_2), 2.04 (m, 3H, Ad^{b}-C*H*), 1.82 (m, 3H, Ad^{c}-CH_2), 1.71 (m, 3H, Ad^{c}-CH_2), 1.48 (s, 9H, C^{18}-C(CH_3)$_3$), 1.32 (s, 9H, C^{16}-C(CH_3)$_3$), 1.05 (s, 9H, C^{4}-C(CH_3)$_3$), 0.92 (s, 9H, In-OC(CH_3)$_3$).

^{31}P{^{1}H} NMR (162 MHz, d_8-THF, δ (ppm)): 33.7 (s, P).

^{13}C{^{1}H} NMR (100 MHz, d_8-THF, δ (ppm)): 168.6 (d, C^{IV}, $^{4}J_{PC}$ = 3.10 Hz), 167.3 (s, C^{IV}), 161.9 (s, C^{13}-H), 139.6 (s, C^{IV}), 139.4 (d, C^{IV}, $^{4}J_{PC}$ = 3.70 Hz), 139.2 (d, C^{IV} $^{3}J_{PC}$ = 9.50 Hz), 135.1 (d, C^{IV}, $^{2}J_{PC}$ = 15.1 Hz), 133.9 (d, C^{IV}, $^{4}J_{PC}$ = 3.40 Hz), 131.9 (d, *o*-*C*H(PPh_2), $^{2}J_{PC}$ = 10.2 Hz), 131.1 (d, *o*-*C*H(PPh_2), $^{2}J_{PC}$ = 9.80 Hz), 130.6 (d, *p*-*C*H(PPh_2), $^{4}J_{PC}$ = 2.90 Hz), 130.5 (d, *p*-*C*H(PPh_2), $^{4}J_{PC}$ = 2.90 Hz), 128.4 (s, C^{15}-H), 127.7 (s, C^{17}-H), 126.8 (d, *m*-*C*H(PPh_2), $^{3}J_{PC}$ = 14.6 Hz), 126.7 (d, *m*-*C*H(PPh_2), $^{3}J_{PC}$ = 14.8 Hz), 126.6 (s, C^{3}-H), 126.1 (s, C^{IV}), 125.8 (s, C^{IV}), 125.3 (s, C^{IV}), 124.8 (d, C^{5}-H, $^{3}J_{PC}$ = 14.7 Hz), 124.8 (s, C^{9}-H), 124.3 (s, C^{IV}), 118.8 (d, C^{8}-H, $^{3}J_{PC}$ = 8.90 Hz), 117.5 (s, C^{10}-H), 116.9 (s, C^{IV}), 113.8 (s, C^{11}-H), 107.5 (d, C^{IV}, $^{1}J_{PC}$ = 119.1 Hz), 38.7 (s, Ad^{a}-CH$_2$), 35.8 (s, Ad(*C*)), 35.3 (s, Ad^{c}-CH$_2$), 33.4 (s, C^{4}-*C*(CH$_3$)$_3$), 31.8 (s, C^{16}-*C*(CH$_3$)$_3$), 31.7

(s, C^{18}-*C*(CH_3)$_3$), 29.7 (s, Ad^b-*C*H), 28.9 (s, C^{18}-C(*C*H_3)$_3$), 28.9 (s, C^{16}-C(*C*H_3)$_3$), 27.7 (s, C^4-C(*C*H_3)$_3$), 27.5 (s, In-OC(*C*H_3)$_3$), 20.7 (s, In-O*C*(CH_3)$_3$).

Anal. Calcd for $C_{57}H_{70}InN_2O_3P$: C, 70.08; H, 7.22; N, 2.87. Found: C, 70.31; H, 7.19; N 2.74.

Compound 4.8

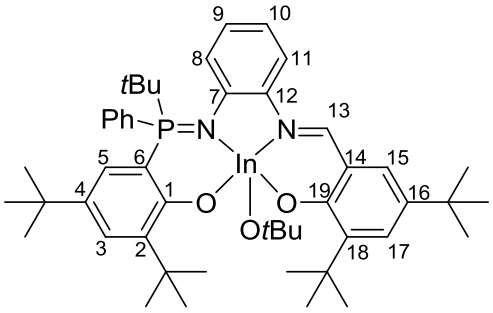

Potassium bis(trimethylsilyl)amide (259 mg, 1.30 mmol) was added to a solution of **4.3** (450 mg, 0.65 mmol) in THF (10 mL) to yield a colour change from yellow to red and back to yellow. After two hours, $InCl_3$ (143 mg, 0.65 mmol) was added to give a bright orange solution and stirred for two hours after which it became a dark yellow solution. Potassium *tert*-butoxide (73 mg, 0.65 mmol) was added to the mixture, giving a cloudy orange solution. Stirring was continued for two hours and the solid was removed by centrifugation. The solvent was evaporated in *vacuo* and the residue was washed with *n*-hexane to give the product as a yellow solid (150 mg, 0.17 mmol, 26%).

^{1}H NMR (400 MHz, d_8-THF, δ (ppm)): 8.86 (s, 1H, C^{13}-*H*), 8.43 (m, 1H, *o*-C*H*(PPh)), 8.31 (m, 1H, *o*-C*H*(PPh)), 7.70 (m, 2H, *m/p*-C*H*(PPh)), 7.59 (m, 1H, *m*-C*H*(PPh)), 7.55 (d, 1H, C^{11}-*H*, $^{3}J_{HH}$ = 8.30 Hz), 7.52 (d, 1H, C^{17}-*H*, $^{4}J_{HH}$ = 2.70 Hz), 7.39 (d, 1H, C^{3}-*H*, $^{4}J_{HH}$ = 2.50 Hz), 7.20 (d, 1H, C^{15}-*H*, $^{4}J_{HH}$ = 2.70 Hz), 6.76 (td, 1H, C^{10}-*H*, $^{4}J_{HH}$ = 1.30 Hz, $^{3}J_{HH}$ = 7.30 Hz), 6.67 (ddd, 1H, C^{9}-*H*, $^{4}J_{HH}$ = 1.30 Hz, $^{3}J_{HH}$ = 8.30 Hz, $^{3}J_{HH}$ = 7.30 Hz), 6.44 (d, 1H, C^{8}-*H*, $^{3}J_{HH}$ = 8.30 Hz), 6.31 (dd, 1H, C^{5}-*H*, $^{4}J_{HH}$ = 2.50 Hz, $^{3}J_{PH}$ = 17.3 Hz), 1.55 (s, 9H, C^{18}-C(CH_3)$_3$), 1.54 (s, 9H, C^{2}-C(CH_3)$_3$), 1.37 (d, 9H, P-C(CH_3)$_3$, $^{3}J_{PH}$ = 15.4 Hz), 1.33 (s, 9H, C^{16}-C(CH_3)$_3$), 1.01 (s, 9H, C^{4}-C(CH_3)$_3$), 0.96 (s, 9H, In-OC(CH_3)$_3$).

^{31}P{^{1}H} NMR (162 MHz, d_8-THF, δ (ppm)): 50.7 (s, P).

^{13}C{^{1}H} NMR (100 MHz, d_8-THF, δ (ppm)): 168.1 (s, C^{IV}), 167.9 (d, C^{IV}, $^{4}J_{PC}$ = 2.80 Hz), 163.1 (s, C^{13}-H), 140.2 (d, C^{IV}, $^{4}J_{PC}$ = 2.90 Hz), 139.8 (s, C^{IV}), 139.7 (d, C^{IV}, $^{3}J_{PC}$ = 9.60 Hz), 135.4 (d, C^{IV}, $^{2}J_{PC}$ = 13.9 Hz), 134.0 (s, C^{IV}), 133.7 (s, *o*-*C*H(PPh)), 132.5 (d, C^{IV}, $^{2}J_{PC}$ = 14.9 Hz), 130.4 (d, *p*-*C*H(PPh), $^{4}J_{PC}$ = 2.80 Hz), 129.3 (s, *o*-*C*H(PPh)), 128.7 (s, C^{IV}), 128.5 (s, *m*-*C*H(PPh)), 128.4 (s, C^{17}-H), 128.2 (s, C^{15}-H), 128.1 (s, C^{IV}), 127.3 (d, C^{5}-H, $^{2}J_{PC}$ = 15.0 Hz), 126.3 (d, C^{3}-H, $^{4}J_{PC}$ = 2.70 Hz), 126.2 (s, *m*-*C*H(PPh)), 124.2 (s, C^{9}-H), 119.2 (d, C^{8}-H, $^{3}J_{PC}$ = 7.20 Hz),

117.8 (s, C^{10}-H), 116.1 (s, C^{IV}), 114.6 (s, C^{11}-H), 37.7 (d, P-$C(CH_3)_3$, $^1J_{PC}$ = 56.8 Hz), 33.7 (s, C^{16}-$C(CH_3)_3$), 33.6 (s, C^4-$C(CH_3)_3$), 32.3 (s, In-OC(CH_3)$_3$), 31.8 (s, C^2-$C(CH_3)_3$), 31.7 (s, C^{18}-$C(CH_3)_3$), 29.7 (s, In-O$C(CH_3)_3$), 28.9 (s, C^{16}-C(CH_3)$_3$), 28.7 (s, C^4-C(CH_3)$_3$), 27.8 (s, C^2-C(CH_3)$_3$), 27.7 (s, C^{18}-C(CH_3)$_3$), 25.5 (s, P-C(CH_3)$_3$).

Anal. Calcd for $C_{49}H_{68}InN_2O_3P$: C, 66.96; H, 7.80; N, 3.19. Found: C, 66.25; H, 7.14; N, 3.58.

Compound 4.9

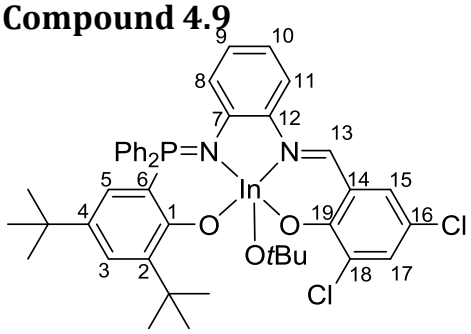

$InCl_3$ (53 mg, 0.24 mmol) was added to a solution of **4.4** (178 mg, 0.24 mmol) in THF (10 mL) and stirred for two hours. Potassium *tert*-butoxide (27 mg, 0.24 mmol) was added to the mixture, giving a cloudy solution. Stirring was continued for two hours and the solid was removed by centrifugation. The solvent was evaporated in *vacuo* and the residue was washed with *n*-hexane to give the product as a yellow solid (75 mg, 0.088 mmol, 37%).

^{1}H NMR (400 MHz, $CDCl_3$, δ (ppm)): 8.57 (s, 1H, C^{13}-*H*), 7.74 (m, 2H, *o*-C*H*(PPh_2)), 7.66 (m, 1H, *p*-C*H*(PPh_2)), 7.61 (m, 1H, *p*-C*H*(PPh_2)), 7.56 (m, 2H, *o*-C*H*(PPh_2)), 7.49 (d, 1H, C^3-*H*, $^4J_{HH}$ = 2.60 Hz), 7.44 (m, 4H, C^{11}-*H* & *m*-C*H*(PPh_2)), 7.39 (d, 1H, C^{17}-*H*, $^4J_{HH}$ = 2.80 Hz), 7.17 (m, 2H, C^{15}-*H* & *m*-C*H*(PPh_2)), 6.74 (m, 1H, C^{10}-*H*), 6.69 (m, 1H, C^9-*H*), 6.29 (m, 1H, C^8-*H*), 6.28 (dd, 1H, C^5-*H*, $^4J_{HH}$ = 2.60 Hz, $^3J_{PH}$ = 17.20 Hz), 1.51 (s, 9H, C^2-C(CH_3)$_3$), 1.10 (s, 9H, In-OC(CH_3)$_3$), 1.04 (s, 9H, C^4-C(CH_3)$_3$).

^{31}P{^{1}H} NMR (162 MHz, $CDCl_3$, δ (ppm)): 36.6 (s, P).

^{13}C{^{1}H} NMR (100 MHz, $CDCl_3$, δ (ppm)): 168.9 (d, C^{IV}, $^4J_{PC}$ = 3.10 Hz), 164.3 (s, C^{IV}), 161.8 (s, C^{13}-H), 142.3 (d, C^{IV}, $^3J_{PC}$ = 9.10 Hz), 141.2 (d, C^{IV}, $^4J_{PC}$ = 3.20 Hz), 138.0 (s, C^{IV}), 137.1 (d, C^{IV}, $^2J_{PC}$ = 15.2 Hz), 136.6 (d, C^{IV}, $^2J_{PC}$ = 14.3 Hz), 134.1 (s, C^{15}-H), 133.5 (d, *o*-*C*H(PPh_2), $^2J_{PC}$ = 9.70 Hz), 133.3 (d, *o*-*C*H(PPh_2), $^2J_{PC}$ = 11.1 Hz), 133.2 (d, *m*-*C*H(PPh_2), $^4J_{PC}$ = 2.90 Hz), 132.3 (s, C^3-H), 130.3 (s, C^{17}-H), 129.3 (d, *m*-*C*H(PPh_2), $^3J_{PC}$ = 3.90 Hz), 129.2 (d, *m*-*C*H(PPh_2), $^3J_{PC}$ = 4.70 Hz), 128.8 (s, C^{IV}), 128.1 (s, C^9-H), 127.0 (d, C^5-H, $^2J_{PC}$ = 14.5 Hz), 125.9 (s, C^{IV}), 125.2 (s, C^{IV}), 121.6 (d, C^8-H, $^3J_{PC}$ = 7.60 Hz), 120.5 (s, C^{10}-H), 120.3 (s, C^{IV}), 118.8 (s, C^{IV}), 116.8 (s, C^{11}-H), 35.7 (s, C^4-*C*(CH_3)$_3$), 35.7 (s, C^2-*C*(CH_3)$_3$), 34.1 (s, In-OC(*C*H_3)$_3$), 31.4 (s, C^4-C(*C*H_3)$_3$), 30.1 (s, C^2-C(*C*H_3)$_3$).

Anal. Calcd for $C_{43}H_{46}Cl_2InN_2O_3P$: C, 60.37; H, 5.42; N, 3.27. Found: C, 60.31; H, 5.21; N 3.44.

Compound 4.10

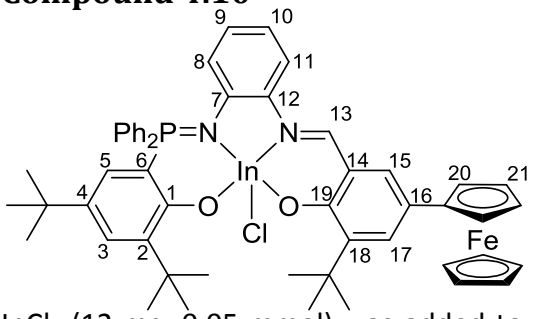

$InCl_3$ (12 mg, 0.05 mmol) was added to a solution of **4.5** (50 mg, 0.05 mmol) in THF (10 mL) and stirred for two hours. The solids were removed by centrifugation, the solvent was evaporated in vacuo, and the residue was washed with *n*-hexane to give the product as a red solid (25 mg, 0.03 mmol, 50%).

^{1}H NMR (400 MHz, d_8-THF, δ (ppm)): 9.00 (s, 1H, C^{13}-*H*), 7.92 (m, 2H, *o*-C*H*(PPh_2)), 7.72 (m, 4H, C^{11}-*H* & *o*/*m*-C*H*(PPh_2)), 7.67 (d, 1H, C^{17}-*H*, $^{4}J_{HH}$ = 2.40 Hz), 7.64 (m, 3H, *m*/*p*-C*H*(PPh_2)), 7.53 (m, 2H, *m*/*p*-C*H*(PPh_2)), 7.50 (d, 1H, C^{3}-*H*, $^{4}J_{HH}$ = 2.50 Hz), 7.40 (d, 1H, C^{15}-*H*, $^{4}J_{HH}$ = 2.40 Hz), 6.83 (m, 1H, C^{10}-*H*), 8.75 (m, 1H, C^{9}-*H*), 6.61 (dd, 1H, C^{8}-*H*, $^{4}J_{PH}$ = 1.30 Hz, $^{3}J_{HH}$ = 8.20 Hz), 6.50 (dd, 1H, C^{5}-*H*, $^{4}J_{HH}$ = 2.50 Hz, $^{3}J_{PH}$ = 18.0 Hz), 4.58 (ddd, 2H, C^{20}-*H*, $^{4}J_{HH}$ = 1.40 Hz, $^{4}J_{HH}$ = 3.20 Hz, $^{3}J_{HH}$ = 7.70 Hz), 4.25 (pseudo-t, 2H, C^{21}-*H*), 4.08 (s, 5H, Cp-C*H*), 1.58 (s, 9H, C^{2}-C(CH_3)$_3$), 1.55 (s, 9H, C^{18}-C(CH_3)$_3$), 1.11 (s, 9H, C^{4}-C(CH_3)$_3$).

^{31}P{^{1}H} NMR (162 MHz, d_8-THF, δ (ppm)): 32.9 (s, P).

^{13}C{^{1}H} NMR (100 MHz, d_8-THF, δ (ppm)): 171.6 (s, C^{IV}), 170.2 (d, C^{IV}, $^{4}J_{PC}$ = 2.90 Hz), 164.4 (s, C^{13}-H), 143.2 (s, C^{IV}), 142.8 (d, C^{IV}, $^{3}J_{PC}$ = 9.60 Hz), 142.2 (d, C^{IV}, $^{4}J_{PC}$ = 2.90 Hz), 137.8 (d, C^{IV}, $^{2}J_{PC}$ = 15.9 Hz), 136.5 (d, C^{IV}, $^{2}J_{PC}$ = 15.4 Hz), 134.4 (d, *o*-*C*H(PPh_2), $^{2}J_{PC}$ = 9.90 Hz), 133.9 (s, *p*-*C*H(PPh_2), 133.9 (d, *o*-*C*H(PPh_2), $^{2}J_{PC}$ = 9.90 Hz), 133.5 (d, *p*-*C*H(PPh_2), $^{4}J_{PC}$ = 2.90 Hz), 132.7 (s, C^{15}-H), 132.5 (s, C^{17}-H), 130.3 (d, *m*-*C*H(PPh_2), $^{3}J_{PC}$ = 12.1 Hz), 130.1 (d, C^{3}-H, $^{4}J_{PC}$ = 2.50 Hz), 129.8 (d, *m*-*C*H(PPh_2), $^{3}J_{PC}$ = 12.1 Hz), 129.6 (s, C^{IV}), 129.1 (s, C^{IV}), 128.8 (s, C^{IV}), 128.7 (d, C^{5}-H, $^{2}J_{PC}$ = 15.4 Hz), 127.6 (s, C^{9}-H), 125.5 (s, C^{IV}), 121.6 (d, C^{8}-H, $^{3}J_{PC}$ = 9.20 Hz), 120.5 (s, C^{10}-H), 120.3 (s, C^{IV}), 116.8 (s, C^{11}-H), 70.1 (s, Cp-*C*H), 68.9 (s, Cp-C^{21}-H), 66.9 (Cp-C^{20}-H), 66.7 (Cp-C^{20}-H), 36.5 (d, C^{4}-*C*(CH_3)$_3$, $^{3}J_{PC}$ = 1.80 Hz), 36.4 (s, C^{18}-*C*(CH_3)$_3$), 34.9 (s, C^{2}-*C*(CH_3)$_3$), 31.9 (s, C^{4}-C(CH_3)$_3$), 31.0 (s, C^{18}-C(CH_3)$_3$), 30.6 (s, C^{2}-C(CH_3)$_3$).

Anal. Calcd for $C_{53}H_{55}ClFeInN_2O_2P$: C, 64.36; H, 5.60; N, 2.83. Found: C, 64.29; H, 5.44; N, 2.90.

7.5. Chapter 5 Experimental Section

Compound 5.1

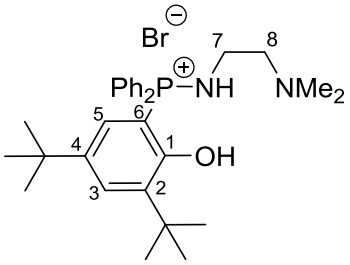

At -78 °C, bromine (0.26 mL, 5.12 mmol) was added dropwise to a solution of 2-(diphenylphosphino)-4,6-di-*tert*-butylphenol (2.00 g, 5.12 mmol) in DCM (40 mL). The cold bath was removed and stirring was continued for two hours at 25 °C. The solution was again cooled to -78 °C, DABCO (0.31 g, 5.12 mmol) and *N*, *N*-dimethylethylenediamine (0.56 mL, 5.12 mmol) were added. The cold bath was removed and the solution was left to stir at 25 °C for 20 h. The DCM was evaporated and the residue was dissolved in THF and filtered to remove the DABCO salt. The solvent was removed and Et_2O was added to precipitate a white solid, which after filtration, washing and drying yielded the pure product (1.79 g, 3.21 mmol, 61%).

^{1}H NMR (400 MHz, $CDCl_3$, δ (ppm)): 7.64 (m, 11H, $P(C_6H_5)_2$ + C^3-*H*), 6.32 (dd, 1H, C^5-*H*, $^4J_{HH}$ = 2.40 Hz, $^3J_{PH}$ = 15.8), 3.62 (m, 2H, C^7-H_2), 3.32 (m, 2H, C^8-H_2), 2.55 (s, 6H, $N(CH_3)_2$), 1.44 (s, 9H, C^2-$(CH_3)_3$), 1.06 (s, 9H, C^4-$(CH_3)_3$).

^{31}P{^{1}H} NMR (162 MHz, $CDCl_3$, δ (ppm)): 43.3 (s, P).

^{13}C{^{1}H} NMR (100 MHz, $CDCl_3$, δ (ppm)): 141.4 (d, C^1-OH, $^2J_{PC}$ = 7.80 Hz), 133.5 (d, *p*-*C*H(PPh_2), $^4J_{PC}$ = 2.50 Hz), 132.1 (d, *o*-*C*H(PPh_2), $^2J_{PC}$ = 11.3 Hz), 131.9 (s, C^3-H), 129.3 (d, *m*-*C*H(PPh_2), $^3J_{PC}$ = 13.3 Hz), 128.9 (d, C^5-H, $^2J_{PC}$ = 14.3 Hz), 124.9 (d, C^6-PPh_2, $^1J_{PC}$ = 105.7 Hz), 106.4 (d, C^{IV}, J_{PC} = 108.7 Hz), 59.6 (s, C^8-H_2); 46.1 (s, $N(CH_3)_2$), 41.1 (s, C^7-H_2), 35.4 (s, C^2-$C(CH_3)_3$), 34.3 (s, C^4-$C(CH_3)_3$), 31.2 (s, C^4-$C(CH_3)_3$), 29.9 (s, C^2-$C(CH_3)_3$). MS ES+: *m/z* 477, ($[M-Br]^+$ Calc.: 477).

Anal. Calcd for $C_{30}H_{42}BrN_2OP$: C, 64.63; H, 7.59; N, 5.02. Found: C, 65.02; H, 7.89; N, 4.96.

Compound 5.2

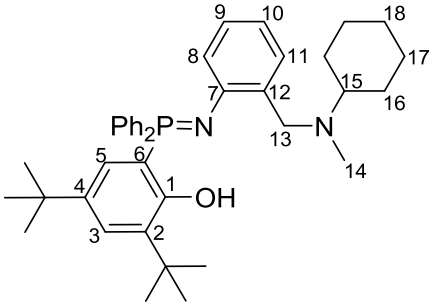

At -78 °C, bromine (0.13 mL, 2.56 mmol) was added dropwise to a solution of 2-(diphenylphosphino)-4,6-di-*tert*-butylphenol (1.00 g, 2.56 mmol) in DCM (40 mL). The cold bath was removed and stirring was continued for two hours at 25 °C. The solution was again cooled to -78 °C, DABCO (0.16 g, 1.28 mmol) and 2-amino-*N*-cyclohexyl-*N*-methylbeznylamine (0.55 g, 2.56 mmol) were added. The cold bath was removed and the solution was left to stir at 25 °C for 20 h. The DCM was evaporated and the residue was dissolved in THF (10 mL) and filtered to remove the DABCO salt. The solvent was removed and Et_2O (10 mL) was added to precipitate a white solid, which after filtration, washing (20 mL) and drying yielded a white solid which could be further purified by column chromatography (alumina, DCM: EtOH 40:1) to give the deprotonated product (0.72 g, 1.19 mmol, 55%).

^{1}H NMR (400 MHz, C_6D_6, δ (ppm)): 7.76 (m, 4H, *o*-C*H*(PPh_2)), 7.65 (d, 1H, C^3-*H*, $^4J_{HH}$ = 2.20 Hz), 6.88-7.04 (m, 10H, C^5-*H*, $C^{9\text{-}11}$-*H* & C*H*(PPh_2)), 6.77 (m, 1H, C^8-*H*), 4.22 (brs, 2H, C^{13}-H_2), 2.70 (t, 1H, C^{15}-*H*, $^3J_{HH}$ = 11.30 Hz), 2.40 (s, 3H, C^{14}-H_3), 2.10 (d, 2H, C^{16}-H_2, $^3J_{HH}$ = 11.4 Hz), 1.78 (d, 2H, C^{16}-H_2, $^3J_{HH}$ = 12.6 Hz), 1.70 (s, 9H, C^2-C(CH_3)$_3$), 1.58 (m, 2H, C^{17}-H_2), 1.47 (m, 2H, C^{17}-H_2), 1.24 (m, 2H, C^{18}-H_2), 1.14 (s, 9H, C^4-C(CH_3)$_3$).

^{31}P{^{1}H} NMR (162 MHz, C_6D_6, δ (ppm)): 20.6 (s, P).

^{13}C{^{1}H} NMR (100 MHz, C_6D_6, δ (ppm)): 132.7 (d, *o*-*C*H(PPh_2), $^2J_{PC}$ = 9.70 Hz), 131.8 (s, $C^{9\text{-}11}$-H), 128.5 (d, *m*-*C*H(PPh_2), $^3J_{PC}$ = 11.7 Hz), 128.2 (s, C^3-H), 127.9 (s, *p*-*C*H(PPh_2)), 126.3 (d, C^5-H & $C^{9\text{-}11}$-H, $^2J_{PC}$ = 13.6 Hz), 120.3 (d, C^8-H, $^3J_{PC}$ = 10.8 Hz), 119.3 (s, $C^{9\text{-}11}$), 63.7 (s, C^{15}-H), 55.5 (s, C^{13}-H_2), 37.7 (s, C^{14}-H_3), 35.9 (s, C^4-$C(CH_3)_3$), 34.3 (s, C^2-$C(CH_3)_3$), 31.6 (s, C^4-C(CH_3)$_3$), 29.9 (s, C^2-C(CH_3)$_3$), 28.9 (s, C^{16}-H_2), 26.9 (s, C^{17}-H_2), 26.6 (s, C^8-H_2).

Anal. Calcd for $C_{40}H_{51}N_2OP$: C, 79.17; H, 8.47; N, 4.62. Found: C, 79.08; H, 8.40; N, 4.71.

Compound 5.3

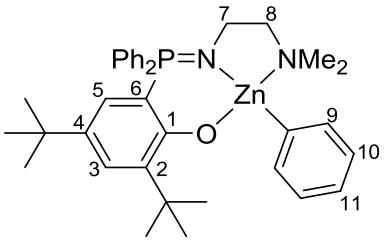

Potassium bis(trimethylsilyl)amide (107 mg, 0.54 mmol) was added to a suspension of **5.1** (300 mg, 0.54 mmol) in THF (10 mL). After one hour, a cloudy green solution was yielded and the insoluble solids were removed by centrifugation. Diphenyl zinc (130 mg, 0.59 mmol) was added to achieve a clear solution. The solvent was removed in *vacuo* and the residue recrystallised from THF/*n*-hexane to yield colourless crystals (150 mg, 0.24 mmol, 45%).

^{1}H NMR (400 MHz, C_6D_6, δ (ppm)): 7.81 (d, 1H, C^3-*H*, $^4J_{HH}$ = 2.60 Hz), 7.71-7.77 (m, 6H, *o*-C*H*(PPh_2) & C^9-*H*), 7.35 (m, 2H, C^{10}-*H*), 7.26 (m, 1H, C^{11}-*H*), 7.03 (dd, 1H, C^5-*H*, $^4J_{HH}$ = 2.60 Hz, $^3J_{PH}$ = 14.2 Hz), 6.93-6.99 (m, 6H, *m*-, *p*-C*H*(PPh_2)), 3.11 (m, 2H, C^8-H_2), 2.12 (m, 2H, C^7-H_2), 1.99 (s, 6H, N(CH_3)$_2$), 1.80 (s, 9H, C^2-C(CH_3)$_3$), 1.28 (s, 9H, C^4-C(CH_3)$_3$).

^{31}P{^{1}H} NMR (162 MHz, C_6D_6, δ (ppm)): 32.9 (s, P).

^{13}C{^{1}H} NMR (100 MHz, C_6D_6, δ (ppm)): 173.4 (s, C^{IV}), 155.7 (s, C^1-OH), 141.5 (s, C^{IV}), 139.6 (s, C^9-H), 133.2 (d, *o*-*C*H(PPh_2), $^2J_{PC}$ = 9.10 Hz), 131.9 (s, *m*-*C*H(PPh_2)), 130.0 (s, C^{IV}), 129.5 (s, C^3-H), 128.9 (s, C^{IV}), 128.6 (s, *o*-*C*H(PPh_2)), 128.5 (s, C^5-H), 126.9 (s, C^{10}-H), 125.6 (s, C^{11}-H), 106.9 (d, C^{IV}, J_{PC} = 94.7 Hz), 63.1 (s, C^7-H_2), 46.2 (s, N(*C*H_3)$_2$), 43.3 (s, C^8-H_2), 36.1 (s, C^4-*C*(CH_3)$_3$), 34.2 (s, C^2-*C*(CH_3)$_3$), 31.9 (s, C^4-C(*C*H_3)$_3$), 30.3 (s, C^2-C(*C*H_3)$_3$.

Anal. Calcd for $C_{36}H_{45}N_2OPZn$: C, 69.95; H, 7.34; N, 4.53. Found: C, 69.84; H, 7.45; N, 4.43.

Compound 5.4

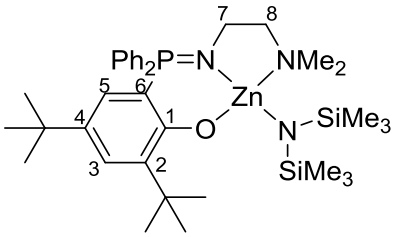

Potassium bis(trimethylsilyl)amide (72 mg, 0.36 mmol) was added to a suspension of **5.1** (200 mg, 0.36 mmol) in THF (10 mL) and stirred for two hours. A solution of $Zn(N(SiMe_3)_2)_2$ (138 mg, 0.36 mmol) in THF (2 mL) was added and the cloudy solution was stirred for a further two hours. The insoluble solids were removed by centrifugation and the solvent was removed to yield a white residue. *n*-Hexane was added and the solution cooled to -30 ^{o}C to yield the homoleptic impurity as a white solid. The supernatant was decanted and left standing at 25 ^{o}C to yield the product as clear colourless crystals (93 mg, 0.13 mmol, 38%).

^{1}H NMR (400 MHz, C_6D_6, δ (ppm)): 7.81 (d, 1H, C^3-*H*, $^{4}J_{HH}$ = 2.70 Hz), 7.68 (m, 4H, *o*-C*H*(PPh_2)), 7.09 (m, 6H, *m*/*p*-C*H*(PPh_2)), 6.85 (dd, 1H, C^5-*H*, $^{4}J_{HH}$ = 2.70 Hz, $^{3}J_{PH}$ = 14.9 Hz), 3.04 (m, 2H, C^8-H_2), 2.10 (m, 2H, C^7-H_2), 2.03 (s, 6H, N(CH_3)$_2$), 1.77 (s, 9H, C^2-C(CH_3)$_3$), 1.21 (s, 9H, C^4-C(CH_3)$_3$), 0.38 (s, 18H, N(Si(CH_3)$_3$)$_2$).

^{31}P{^{1}H} NMR (162 MHz, C_6D_6, δ (ppm)): 36.9 (s, P).

^{13}C{^{1}H} NMR (100 MHz, C_6D_6, δ (ppm)): 133.5 (d, *o*-*C*H(PPh_2), $^{2}J_{PC}$ = 9.10 Hz), 132.1 (d, *p*-*C*H(PPh_2), $^{4}J_{PC}$ = 2.30 Hz), 130.1 (s, C^3-H), 128.9 (d, C^5-H, $^{3}J_{PC}$ = 11.1 Hz), 128.8 (d, *m*-*C*H(PPh_2), $^{3}J_{PC}$ = 11.9 Hz), 62.1 (s, C^7-H_2), 46.6 (s, N(*C*H_3)$_2$), 43.2 (s, C^8-H_2), 36.8 (s, C^4-C(*C*H_3)$_3$), 30.6 (s, C^2-C(*C*H_3)$_3$), 6.6 (s, N(Si(*C*H_3)$_3$)$_2$).

Anal. Calcd for $C_{36}H_{58}N_3OPSi_2Zn$: C, 61.65; H, 8.34; N, 5.99. Found: C, 61.55; H, 8.48; N, 5.76.

Compound 5.5

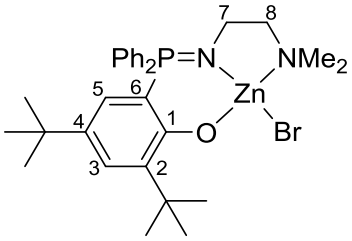

Diethylzinc (92 µL, 0.89 mmol) was added to a suspension of **5.1** (500 mg, 0.89 mmol) in THF (10 mL) and a colourless solution was afforded. The solution was left to stir at 25 ^{o}C after which the solvent was removed to yield a white solid (405 mg, 0.65 mmol, 73%).

^{1}H NMR (400 MHz, C_6D_6, δ (ppm)): 7.77 (d, 1H, C^3-*H*, $^{4}J_{HH}$ = 2.60 Hz), 7.70 (m, 4H, *o*-C*H*(PPh_2)), 7.07 (m, 6H, *m*-, *p*-C*H*(PPh_2)), 6.89 (dd, 1H, C^5-*H*, $^{4}J_{HH}$ = 2.60 Hz, $^{3}J_{PH}$ = 15.3 Hz), 2.84 (m, 2H, C^8-H_2), 1.97 (m, 8H, N(CH_3)$_2$ & C^7-H_2), 1.77 (s, 9H, C^2-C(CH_3)$_3$), 1.20 (s, 9H, C^4-C(CH_3)$_3$).

^{31}P{^{1}H} NMR (162 MHz, C_6D_6, δ (ppm)): 35.0 (s, P).

^{13}C{^{1}H} NMR (100 MHz, C_6D_6, δ (ppm)): 172.3 (s, C^1-OH), 142.3 (s, C^2-C(CH_3)$_3$), 134.9 (s, C^4-C(CH_3)$_3$), 133.5 (d, *o*-*C*H(PPh_2), $^{2}J_{PC}$ = 9.20 Hz), 132.4 (s, *p*-*C*H(PPh_2)), 129.9 (s, C^3-H), 128.8 (d, *m*-*C*H(PPh_2), $^{3}J_{PC}$ = 11.9 Hz), 127.9 (d, C^5-H, $^{2}J_{PC}$ = 11.9), 107.3 (d, C^{IV}, $^{1}J_{PC}$ = 99.9 Hz), 62.4 (s, C^7-H_2), 46.1 (s, N(CH_3)$_2$), 42.4 (s, C^8-H_2), 36.2 (s, C^4-*C*(CH_3)$_3$), 34.2 (s, C^2-*C*(CH_3)$_3$), 31.7 (s, C^4-C(*C*H_3)$_3$), 30.3 (s, C^2-C(*C*H_3)$_3$).

Anal. Calcd for $C_{30}H_{40}BrN_2OPZn$: C, 58.03; H, 6.49; N, 4.51. Found: C, 57.50; H, 6.54; N, 4.84.

Compound 5.7

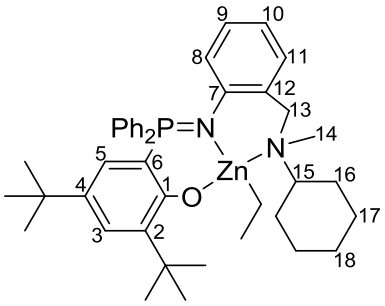

Diethylzinc (30 µL, 0.29 mmol) was added to a suspension of **5.2** (150 mg, 0.29 mmol) in THF (10 mL) and a colourless solution was afforded. The solution was left to stir at 25 ^{o}C after which the solvent was removed to yield a white solid, which was recrystallised from *n*-hexane to afford clear crystals (110 mg, 0.16 mmol, 54%).

^{1}H NMR (400 MHz, C_6D_6, δ (ppm)): 7.91 (m, 2H, *o*-C*H*(PPh_2)), 7.77 (s, 1H, C^{3}-*H*), 7.28 (m, 2H, *o*-C*H*(PPh_2)), 7.04-7.10 (m, 4H, *p*-&*m*-C*H*(PPh_2) & $C^{8\text{-}11}$-*H*), 6.75-6.91 (m, 6H, *p*-&*m*-C*H*(PPh_2) & $C^{8\text{-}11}$-*H*), 6.50 (d, 1H, C^{5}-*H*, $^{3}J_{PH}$ = 17.5 Hz), 3.62 (d, 1H, C^{13}-H_2, $^{2}J_{HH}$ = 10.64 Hz), 3.04 (m, 1H, C^{15}-*H*), 2.93 (d, 1H, C^{13}-H_2, $^{2}J_{HH}$ = 10.6 Hz), 2.56 (m, 1H, $C^{16\text{-}18}$-H_2), 1.89 (s, 9H, C^{2}-C(CH_3)$_3$), 1.83 (s, 3H, C^{14}-H_3), 1.59 (t, 3H, Zn-CH_2-CH_3, $^{3}J_{HH}$ = 7.50 Hz), 1.22-1.72 (m, 5H, $C^{16\text{-}18}$-H_2), 1.15 (s, 9H, C^{4}-C(CH_3)$_3$), 0.84-1.06 (m, 4H, $C^{16\text{-}18}$-H_2), 0.51 (m, 2H, Zn-CH_2-CH_3).

^{31}P{^{1}H} NMR (162 MHz, C_6D_6, δ (ppm)): 27.5 (s, P).

^{13}C{^{1}H} NMR (100 MHz, C_6D_6, δ (ppm)): 133.9 (d, *o*-*C*H(PPh_2), $^{2}J_{PC}$ = 8.70 Hz), 132.3 (s, *o*-*C*H(PPh_2)), 132.2 (s, $C^{8\text{-}11}$-H), 131.7 (s, $C^{8\text{-}11}$-H), 131.1 (s, *m*/*p*-*C*H(PPh_2)), 129.1 (s, *m*/*p*-*C*H(PPh_2)), 128.9 (s, C^{3}-H), 128.3 (d, *m*-*C*H(PPh_2), $^{3}J_{PC}$ = 11.16 Hz), 128.2 (s, *m*/*p*-*C*H(PPh_2)), 128.1 (d, C^{5}-H, $^{2}J_{PC}$ = 11.7 Hz), 125.7 (s, $C^{8\text{-}11}$-H), 121.2 (s, $C^{8\text{-}11}$-H), 64.1 (s, C^{15}-H), 58.9 (s, C^{13}-H_2), 36.1 (s, C^{14}-H_3), 35.8 (s, C^{4}-*C*(CH_3)$_3$), 34.1 (s, C^{2}-*C*(CH_3)$_3$), 31.7 (s, C^{4}-C(*C*H_3)$_3$), 30.2 (s, C^{2}-C(*C*H_3)$_3$), 26.5 (s, $C^{16\text{-}18}$-H_2), 26.0 (s, $C^{16\text{-}18}$-H_2), 23.7 (s, $C^{16\text{-}18}$-H_2), 14.5 (s, Zn-CH_2-*C*H_3), 0.51 (s, Zn-*C*H_2-CH_3).

Anal. Calcd for $C_{42}H_{55}N_2OPZn$: C, 72.04; H, 7.92; N, 4.00. Found: C, 71.97; H, 7.85; N, 4.03.

Compound 5.8

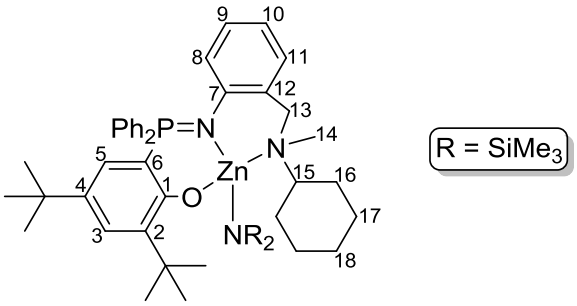

A solution of **5.2** (141 mg, 0.36 mmol) in THF (2 mL) was added to a solution of $Zn(N(SiMe_3)_2)_2$ (200 mg, 0.39 mmol) in THF (10 mL) and the yellow solution was stirred for two hours. The solvent was removed *in vacuo* and the residue was recrystallised by slow evaporation of cyclohexane (5 mL) to yield the product as colourless crystals (170 mg, 0.20 mmol, 57%).

^{1}H NMR (400 MHz, C_6D_6, δ (ppm)): 7.95 (m, 2H, *o*-C*H*(PPh_2)), 7.83 (d, 1H, C^3-*H*, $^4J_{HH}$ = 1.80 Hz), 7.27 (m, 3H, *o*/*m*/*p*-C*H*(PPh_2)), 6.90 (m, 4H, $C^{8\text{-}11}$-*H*, *m*/*p*-C*H*(PPh_2)), 6.75 (m, 4H, $C^{8\text{-}11}$-*H*, *m*/*p*-C*H*(PPh_2)), 6.66 (dd, 1H, C^5-*H*, $^4J_{HH}$ = 1.80 Hz, $^3J_{PC}$ = 16.3 Hz), 6.30 (s, 1H, $C^{8\text{-}11}$-*H*), 3.94 (d, 1H, C^{13}-H_2, $^2J_{HH}$ = 12.3 Hz), 3.16 (s, 1H, C^{15}-*H*), 2.94 (d, 1H, C^{13}-H_2, $^2J_{HH}$ = 12.3 Hz), 2.39 (s, 3H, C^{14}-H_3), 1.81 (s, 9H, C^2-C(CH_3)$_3$), 1.63 (m, 5H, $C^{16\text{-}18}$-H_2), 1.14 (s, 9H, C^4-C(CH_3)$_3$), 0.88 (m, 5H, $C^{16\text{-}18}$-H_2), 0.29 (s, 18H, N(Si(CH_3)$_3$)$_2$).

^{31}P{^{1}H} NMR (162 MHz, C_6D_6, δ (ppm)): 31.9 (s, P).

^{13}C{^{1}H} NMR (100 MHz, C_6D_6, δ (ppm)): 133.8 (d, *o*-*C*H(PPh_2), $^2J_{PC}$ = 11.2 Hz), 132.5 (s, *p*-*C*H(PPh_2)), 131.4 (s, $C^{8\text{-}11}$-H), 129.8 (s, C^3-H), 128.9 (d, *m*-*C*H(PPh_2), $^3J_{PC}$ = 12.8 Hz), 128.3 (s, $C^{8\text{-}11}$-H), 127.9 (s, $C^{8\text{-}11}$-H), 127.6 (d, C^5-H, $^2J_{PC}$ = 11.1 Hz), 121.5 (s, $C^{8\text{-}11}$-H), 58.3 (s, C^{13}-H_2), 39.1 (s, C^{14}-H_3), 31.3 (s, C^4-C(CH_3)$_3$), 30.8 (s, C^2-C(CH_3)$_3$), 29.9 (s, C^{15}-H), 26.8 (s, $C^{16\text{-}18}$-H_2), 26.2 (s, $C^{16\text{-}18}$-H_2), 6.22 (s, N(Si(CH_3)$_3$)$_2$).

Anal. Calcd for $C_{46}H_{68}N_3OPSi_2Zn$: C, 66.44; H, 8.24; N, 5.05. Found: C, 66.87; H, 8.22; N, 5.78.

Compound 5.9

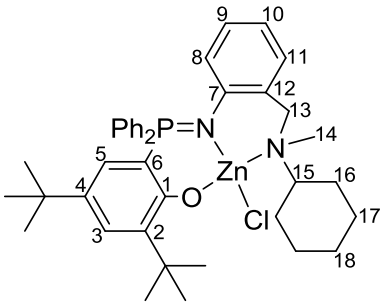

Potassium bis(trimethylsilyl)amide (78 mg, 0.39 mmol) was added to a solution of **5.2** (200 mg, 0.39 mmol) in THF (10 mL) and stirred for two hours. $ZnCl_2$ (53 mg, 0.39 mmol) was added and the solution was stirred for 18 hours. The insoluble salts were removed by centrifugation and the solution was dried *in vacuo*. The residue was recrystallised from THF/*n*-hexane to give a white solid (129 mg, 0.21 mmol, 54%).

^{1}H NMR (400 MHz, C_6D_6, δ (ppm)): 7.86 (m, 2H, *o*-C*H*(PPh_2)), 7.75 (d, 1H, C^3-*H*, $^4J_{HH}$ = 2.30), 7.29 (m, 2H, *o*-C*H*(PPh_2)), 7.04 (m, 3H, *m*/*p*-C*H*(PPh_2)), 6.89 (m, 2H, $C^{8\text{-}11}$-*H*), 6.77 (m, 5H, *m*/*p*-C*H*(PPh_2) & $C^{8\text{-}11}$-*H*), 6.54 (dd, 1H, C^5-*H*, $^4J_{HH}$ = 2.30 Hz, $^3J_{PH}$ = 17.9 Hz), 3.65 (d, 1H, C^{13}-H_2, $^2J_{HH}$ = 11.4 Hz), 2.89 (d, 1H, C^{13}-H_2, $^2J_{HH}$ = 11.4 Hz), 2.82 (m, 1H, C^{15}-*H*), 2.58 (m, 1H, C^{16}-H_2), 2.06 (s, 3H, C^{14}-H_3), 1.85 (s, 9H, C^2-C(CH_3)$_3$), 1.57 (m, 5H, $C^{16\text{-}18}$-H_2), 1.04 (s, 9H, C^4-C(CH_3)$_3$), 1.00 (m, 4H, $C^{16\text{-}18}$-H_2).

^{31}P{^{1}H} NMR (162 MHz, C_6D_6, δ (ppm)): 31.9 (s, P).

^{13}C{^{1}H} NMR (100 MHz, C_6D_6, δ (ppm)): 133.9 (d, *o*-*C*H(PPh_2), $^2J_{PC}$ = 9.60 Hz), 132.4 (s, $C^{8\text{-}11}$-H), 132.3 (d, *o*-*C*H(PPh_2), $^2J_{PC}$ = 9.60 Hz), 132.1 (s, *p*-*C*H(PPh_2)) 131.6 (s, *p*-*C*H(PPh_2)), 129.4 (s, C^3-H), 129.3 ($C^{8\text{-}11}$-H), 128.5 (d, *m*-*C*H(PPh_2), $^3J_{PC}$ = 12.0 Hz), 128.2 (d, *m*-*C*H(PPh_2), $^3J_{PC}$ = 11.57 Hz), 128.0 (d, C^5-H, $^2J_{PC}$ = 15.1 Hz), 125.4 (s, $C^{8\text{-}11}$-H), 121.7 (s, $C^{8\text{-}11}$-H), 65.7 (s, C^{15}-H), 59.6 (s, C^{13}-H_2), 37.3 (s, C^{14}-H_3), 31.7 (s, C^{16}-H_2), 31.6 (s, C^4-C(CH_3)$_3$), 30.4 (s, C^2-C(CH_3)$_3$), 26.4 (s, $C^{16\text{-}18}$-H_2), 26.1 (s, $C^{16\text{-}18}$-H_2), 25.9 (s, $C^{16\text{-}18}$-H_2), 25.6 (s, $C^{16\text{-}18}$-H_2).

Anal. Calcd for $C_{40}H_{50}ClN_2OPZn$: C, 67.99; H, 7.13; N, 3.96. Found: C, 67.87; H, 7.22; N, 3.78.

Compound 5.10

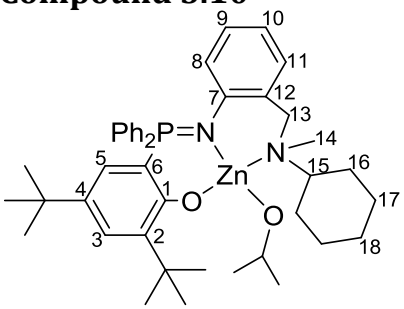

IPA (2.50 mL, 0.24 M solution in THF, 0.59 mmol) was added to a solution of **5.8** (488 mg, 0.59 mmol) in THF and stirred for two hours. THF was removed *in vacuo* and the residue was recrystallised from THF/*n*-hexane at -30 ^{o}C to yield the product as a white solid (148 mg, 0.21 mmol, 35%).

^{1}H NMR (400 MHz, C_6D_6, δ (ppm)): 8.00 (m, 2H, *o*-C*H*(PPh_2)), 7.76 (d, 1H, C^3-*H*, $^4J_{HH}$ = 2.60 Hz), 7.29 (m, 2H, *o*-C*H*(PPh_2)), 7.12 (m, 3H, *m*/*p*-C*H*(PPh_2)), 6.90 (m, 2H, $C^{8\&9}$-*H*), 6.81 (m, 4H, C^{10}-*H* & *m*/*p*-C*H*(PPh_2)), 6.72 (m, 1H, C^{11}-*H*), 6.56 (dd, 1H, C^5-*H*, $^4J_{HH}$ = 2.60 Hz, $^3J_{PH}$ = 17.6 Hz), 4.57 (m, 1H, O-C*H*(CH_3)$_2$), 3.71 (d, 1H, C^{13}-H_2, $^2J_{HH}$ = 11.3 Hz), 2.94 (d, 1H, C^{13}-H_2, $^2J_{HH}$ = 11.3 Hz), 2.82 (t, 1H, C^{15}-*H*, $^3J_{HH}$ = 11.1 Hz), 2.57 (d, 1H, C^{16}-H_2, $^3J_{HH}$ = 12.1 Hz), 2.14 (s, 3H, C^{14}-H_3), 1.87 (s, 9H, C^2-C(CH_3)$_3$), 1.56 (m, 6H, $C^{16\text{-}18}$-H_2), 1.48 (d, 3H, O-CH(CH_3)$_2$, $^3J_{HH}$ = 5.80 Hz), 1.42 (d, 3H, O-CH(CH_3)$_2$, $^3J_{HH}$ = 5.80 Hz), 1.14 (s, 9H, C^4-C(CH_3)$_3$), 1.03 (m, 3H, $C^{16\text{-}18}$-H_2).

^{31}P{^{1}H} NMR (162 MHz, C_6D_6, δ (ppm)): 31.3 (s, P).

^{13}C{^{1}H} NMR (100 MHz, C_6D_6, δ (ppm)): 172.8 (d, C^{IV}, $^4J_{PC}$ = 3.20 Hz), 148.5 (d, C^{IV}, $^3J_{PC}$ = 7.30 Hz), 141.8 (d, C^{IV}, $^3J_{PC}$ = 9.50 Hz), 134.4 (d, *o*-*C*H(PPh_2), $^2J_{PC}$ = 10.3 Hz), 133.2 (s, C^{IV}), 133.1 (s, C^{IV}), 132.9 (d, *o*-*C*H(PPh_2), $^2J_{PC}$ = 9.00 Hz), 132.7 (s, $C^{9/10}$-H), 132.3 (d, *p*-*C*H(PPh_2), $^4J_{PC}$ = 2.90 Hz), 131.9 (s, C^{IV}), 131.9 (s, $C^{9/10}$-H), 131.8 (d, *p*-*C*H(PPh_2), $^4J_{PC}$ = 2.30 Hz), 131.1 (s, C^{IV}), 129.5 (s, C^3-H), 129.2 (s, C^{IV}), 128.9 (d, *m*-*C*H(PPh_2), $^3J_{PC}$ = 11.5 Hz), 128.5 (d, *m*-*C*H(PPh_2), $^3J_{PC}$ = 12.0 Hz), 128.1 (s, C^5-H), 125.7 (d, C^8-H, $^3J_{PC}$ = 6.50 Hz), 121.6 (s, C^{11}-H), 66.4 (s, O-*C*H(CH_3)$_2$), 65.1 (s, C^{15}-H), 59.4 (s, C^{13}-H_2), 36.7 (s, C^{14}-H_3), 36.2 (s, C^4-*C*(CH_3)$_3$), 34.1 (s, C^2-*C*(CH_3)$_3$), 31.9 (s, C^{16}-H_2), 31.6 (s, C^4-C(*C*H_3)$_3$), 30.8 (s, O-CH(CH_3)$_2$), 30.4 (s, C^2-C(*C*H_3)$_3$), 26.5 (s, $C^{16\text{-}18}$-H_2), 26.2 (s, $C^{16\text{-}18}$-H_2), 25.9 (s, $C^{16\text{-}18}$-H_2), 24.5 (s, $C^{16\text{-}18}$-H_2).

Anal. Calcd for $C_{43}H_{57}N_2O_2PZn$: C, 70.72; H, 7.87; N, 3.84. Found: C, 70.34; H, 7.55; N, 3.92.

Compound 5.11

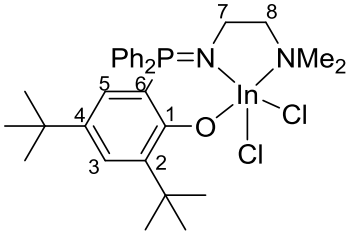

Potassium bis(trimethylsilyl)amide (215 mg, 1.08 mmol) was added to a suspension of **5.1** (300 mg, 0.54 mmol) in THF (10 mL). After one hour, a cloudy green solution was yielded and $InCl_3$ (119 mg, 0.54 mmol) was added to achieve a colourless solution. The insoluble salts were removed by centrifugation and the solvent was removed in *vacuo*. The residue recrystallised from THF/*n*-hexane to yield clear crystals (220 mg, 0.33 mmol, 61%).

^{1}H NMR (400 MHz, d_8-THF, δ (ppm)): 7.61 (m, 10H, *o*/*m*/*p*-C*H*(PPh_2)), 7.41 (d, 1H, C^3-*H*, $^4J_{HH}$ = 2.50 Hz), 6.42 (dd, 1H, C^5-*H*, $^3J_{PH}$ = 16.6 Hz, $^4J_{HH}$ = 2.50 Hz), 3.08 (m, 2H, C^8-H_2), 2.74 (m, 2H, C^7-H_2), 2.48 (s, 6H, N(CH_3)$_2$), 1.39 (s, 9H, C^2-C(CH_3)$_3$), 1.05 (s, 9H, C^4-C(CH_3)$_3$).

^{31}P{^{1}H} NMR (162 MHz, d_8-THF, δ (ppm)): 45.7 (s, P).

^{13}C{^{1}H} NMR (100 MHz, d_8-THF, δ (ppm)): 170.2 (d, C^{IV}, $^4J_{PC}$ = 3.70 Hz), 142.9 (d, C^{IV}, $^2J_{PC}$ = 14.9 Hz), 137.1 (d, C^{IV}, $^2J_{PC}$ = 14.9 Hz), 134.1 (d, *o*-*C*H(PPh_2), $^2J_{PC}$ = 9.70 Hz), 133.8 (d, *p*-*C*H(PPh_2), $^4J_{PC}$ = 2.80 Hz), 130.1 (d, *m*-*C*H(PPh_2), $^3J_{PC}$ = 12.1 Hz), 130.0 (s, C^3-H), 128.9 (s, C^{IV}), 128.2 (s, C^{IV}), 127.3 (d, C^5-H, $^3J_{PC}$ = 13.5 Hz), 109.1 (d, C^{IV}, $^1J_{PC}$ = 113.9 Hz), 59.6 (d, C^7-H_2, $^2J_{PC}$ = 15.2 Hz), 45.1 (s, N(CH_3)$_2$), 42.6 (s, C^8-H_2), 36.3 (s, C^4-C(CH_3)$_3$), 34.8 (s, C^2-C(CH_3)$_3$), 31.9 (s, C^4-C(CH_3)$_3$), 30.7 (s, C^2-C(CH_3)$_3$).

Anal. Calcd for $C_{30}H_{40}Cl_2InN_2OP$: C, 54.48; H, 6.10; N, 4.24. Found: C, 54.23; H, 5.97; N, 4.22.

Compound 5.12

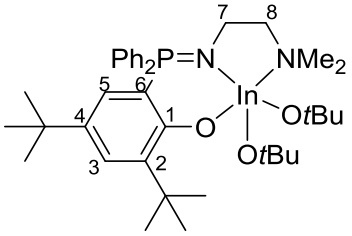

Potassium *tert*-butoxide (127 mg, 1.13 mmol) was added to a solution of **5.11** (375 mg, 0.57 mmol) in THF (10 mL). A cloudy solution was immediately yielded and the reaction mixture was stirred for two hours. The insoluble salts were removed by centrifugation and the solvent removed *in vacuo*. The product was precipitated from *n*-hexane to give a white solid (245 mg, 0.33 mmol, 58%).

^{1}H NMR (400 MHz, d_8-THF, δ (ppm)): 7.63 (m, 6H, *o*/*p*-C*H*(PPh_2)), 7.54 (m, 4H, *m*-C*H*(PPh_2)), 7.37 (d, 1H, C^3-*H*, $^4J_{HH}$ = 2.60 Hz), 6.41 (dd, 1H, C^5-*H*, $^4J_{HH}$ = 2.60 Hz, $^3J_{PH}$ = 16.9 Hz), 3.00 (m, 2H, C^8-H_2), 2.59 (m, 2H, C^7-H_2), 2.44 (s, 6H, N(CH_3)$_2$), 1.44 (s, 9H, C^2-C(CH_3)$_3$), 1.14 (s, 18H, In-(OC(CH_3)$_3$)$_2$), 1.03 (s, 9H, C^4-C(CH_3)$_3$).

^{31}P{^{1}H} NMR (162 MHz, d_8-THF, δ (ppm)): 43.6 (s, P).

^{13}C{^{1}H} NMR (100 MHz, d_8-THF, δ (ppm)): 171.4 (d, $^4J_{PC}$ = 3.80 Hz, C^{IV}), 141.4 (d, $^3J_{PC}$ = 9.80 Hz, C^{IV}), 135.8 (d, $^2J_{PC}$ = 15.2 Hz, C^{IV}), 134.2 (d, *o*-*C*H(PPh_2), $^2J_{PC}$ = 9.30 Hz), 133.2 (d, *p*-*C*H(PPh_2), $^4J_{PC}$ = 2.80 Hz), 129.9 (s, C^{IV}), 129.8 (d, *m*-*C*H(PPh_2), $^3J_{PC}$ = 11.7 Hz), 129.6 (d, C^3-H, $^4J_{PC}$ = 2.30 Hz), 129.2 (s, C^{IV}), 127.4 (d, C^5-H, $^2J_{PC}$ = 13.4 Hz), 69.9 (s, In-(O*C*(CH_3)$_3$)$_2$), 60.1 (d, C^7-H_2, $^2J_{PC}$ = 15.8 Hz), 46.0 (s, N(*C*H_3)$_2$), 43.5 (d, C^8-H_2, $^3J_{PC}$ = 3.90 Hz), 36.4 (s, C^4-*C*(CH_3)$_3$), 35.5 (s, In-(OC(*C*H_3)$_3$)$_2$), 34.7 (s, C^2-*C*(CH_3)$_3$), 31.9 (s, C^4-C(*C*H_3)$_3$), 30.9 (s, C^2-C(*C*H_3)$_3$).

Anal. Calcd for $C_{38}H_{58}InN_2O_3P$: C, 61.96; H, 7.94; N, 3.80. Found: C, 61.68; H, 7.78; N, 3.99.

Compound 5.13

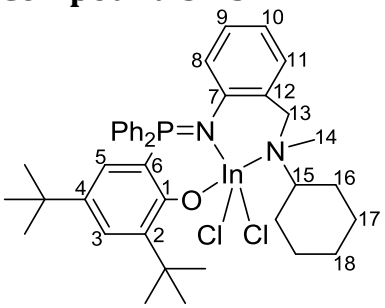

Potassium bis(trimethylsilyl)amide (180 mg, 0.91 mmol) was added to a solution of **5.2** (550 mg, 0.91 mmol) in THF (10 mL). After one hour, $InCl_3$ (200 mg, 0.91 mmol) was added. The insoluble salts were removed by centrifugation and the solvent was removed in *vacuo*. The residue recrystallised from THF/*n*-hexane to yield a white solid (600 mg, 0.76 mmol, 84%).

^{1}H NMR (400 MHz, $CDCl_3$, δ (ppm)): 7.94 (m, 2H, *o*-C*H*(PPh_2)), 7.60 (m, 1H, *p*-C*H*(PPh_2)), 7.53 (m, 3H, *m*/*p*-C*H*(PPh_2)), 7.45 (d, 1H, C^3-*H*, $^4J_{HH}$ = 2.50 Hz), 7.38 (m, 4H, *o*/*m*-C*H*(PPh_2)), 7.02 (dd, 1H, C^{11}-*H*, $^4J_{HH}$ = 1.70 Hz, $^3J_{HH}$ = 7.40 Hz), 6.90 (td, 1H, C^9-*H*, $^4J_{HH}$ = 1.70 Hz, $^3J_{HH}$ = 7.80 Hz), 6.80 (tt, 1H, C^{10}-*H*, $^4J_{HH}$ = 1.10 Hz, $^3J_{HH}$ = 7.40 Hz), 6.64 (dt, 1H, C^8-*H*, $^4J_{HH}$ = 1.30 Hz, $^3J_{HH}$ = 8.00 Hz), 6.45 (dd, 1H, C^5-*H*, $^4J_{HH}$ = 2.50 Hz, $^3J_{PH}$ = 16.1 Hz), 4.42 (d, 1H, C^{13}-H_2, $^2J_{HH}$ = 11.7 Hz), 3.56 (t, 1H, C^{15}-*H*, $^3J_{HH}$ = 11.0 Hz), 3.30 (d, 1H, C^{13}-H_2, $^2J_{HH}$ = 11.7 Hz), 2.68 (s, 3H, C^{14}-H_3), 2.10 (m, 1H, $C^{16\text{-}18}$-H_2), 1.67 (m, 1H, $C^{16\text{-}18}$-H_2), 1.52 (m, 2H, $C^{16\text{-}18}$-H_2), 1.32 (s, 9H, C^2-C(CH_3)$_3$), 1.29 (m, 5H, $C^{16\text{-}18}$-H_2), 1.10 (s, 9H, C^4-C(CH_3)$_3$), 1.04 (m, 1H, $C^{16\text{-}18}$-H_2).

^{31}P{^{1}H} NMR (162 MHz, $CDCl_3$, δ (ppm)): 37.4 (s, P).

^{13}C{^{1}H} NMR (100 MHz, $CDCl_3$, δ (ppm)): 167.4 (d, C^{IV}, $^4J_{PC}$ = 3.40 Hz), 147.3 (d, C^{IV}, $^4J_{PC}$ = 5.50 Hz), 142.5 (d, C^{IV}, $^3J_{PC}$ = 9.00 Hz), 137.5 (d, C^{IV}, $^2J_{PC}$ = 14.7 Hz), 133.7 (d, *o*-*C*H(PPh_2), $^2J_{PC}$ = 14.7 Hz), 133.6 (d, *o*-*C*H(PPh_2), $^2J_{PC}$ = 9.50 Hz), 133.1 (d, *p*-*C*H(PPh_2), $^4J_{PC}$ = 2.70 Hz), 132.6 (d, *p*-*C*H(PPh_2), $^4J_{PC}$ = 3.00 Hz), 131.8 (s, C^{11}-H), 129.7 (d, C^3-H, $^4J_{PC}$ = 2.20 Hz), 129.5 (s, C^9-H), 128.9 (d, *m*-*C*H(PPh_2), $^3J_{PC}$ = 12.0 Hz), 128.8 (d, *m*-*C*H(PPh_2), $^3J_{PC}$ = 12.8 Hz), 128.6 (s, C^{IV}), 126.7 (d, C^{IV}, $^2J_{PC}$ = 13.5 Hz), 125.7 (d, C^8-H, $^3J_{PC}$ = 6.90 Hz), 124.9 (d, C^5-H, $^2J_{PC}$ = 13.0 Hz), 124.6 (s, C^{IV}), 123.9 (s, C^{IV}), 122.0 (s, C^{10}-H), 63.9 (s, C^{15}-H), 55.3 (s, C^{13}-H_2), 41.4 (s, C^{14}-H_3), 35.5 (s, C^4-*C*(CH_3)$_3$), 34.2 (s, C^2-*C*(CH_3)$_3$), 32.0 (s, $C^{16\text{-}18}$-H_2), 31.5 (s, C^4-C(*C*H_3)$_3$), 30.1 (s, C^2-C(*C*H_3)$_3$), 26.7 (s, $C^{16\text{-}18}$-H_2), 26.1 (s, $C^{16\text{-}18}$-H_2), 25.7 (s, $C^{16\text{-}18}$-H_2), 23.7 (s, $C^{16\text{-}18}$-H_2).

Anal. Calcd for $C_{40}H_{50}Cl_2N_2OPIn$: C, 60.70; H, 6.37; N, 3.54. Found: C, 60.85; H, 6.25; N, 3.52.

Compound 5.14

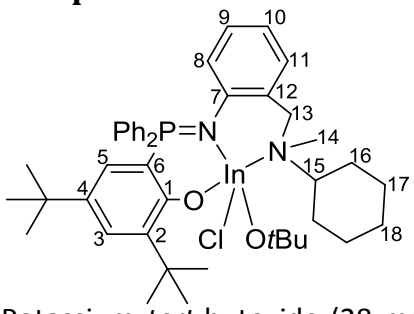

Potassium *tert*-butoxide (28 mg, 0.25 mmol) was added to a solution of **5.13** (200 mg, 0.25 mmol) in THF (10 mL). A cloudy solution was immediately yielded and the reaction mixture was stirred for two hours. The insoluble salts were removed by centrifugation and the solvent removed *in vacuo*. The product was precipitated from *n*-hexane to give a white solid (129 mg, 0.16 mmol, 62%).

^{1}H NMR (400 MHz, $CDCl_3$, δ (ppm)): 7.97 (m, 3H, *o*-C*H*(PPh_2)), 7.50 (m, 7H, *o*/*m*/*p*-C*H*(PPh_2)), 7.39 (d, 1H, C^3-*H*, $^4J_{HH}$ = 2.60 Hz), 6.95 (m, 1H, C^{11}-*H*), 6.83 (td, 1H, C^9-*H*, $^4J_{HH}$ = 1.70 Hz, $^3J_{HH}$ = 7.70 Hz), 6.72 (m, 1H, C^{10}-*H*), 6.63 (dd, 1H, C^8-*H*, $^4J_{HH}$ = 1.30 Hz, $^3J_{HH}$ = 8.10 Hz), 6.46 (dd, 1H, C^5-*H*, $^4J_{HH}$ = 2.60 Hz, $^3J_{PH}$ = 15.9 Hz), 4.43 (d, 1H, C^{13}-H_2, $^2J_{HH}$ = 11.8 Hz), 3.57 (t, 1H, C^{15}-*H*, $^3J_{HH}$ = 11.1 Hz), 3.30 (d, 1H, C^{13}-H_2, $^2J_{HH}$ = 11.8 Hz), 2.56 (s, 3H, C^{14}-H_3), 2.06 (m, 2H, $C^{16\text{-}18}$-H_2), 1.57 (m, 3H, $C^{16\text{-}18}$-H_2), 1.39 (s, 9H, C^2-C(CH_3)$_3$), 1.28 (m, 5H, $C^{16\text{-}18}$-H_2), 1.21 (s, 9H, InO-C(CH_3)$_3$), 1.09 (s, 9H, C^4-C(CH_3)$_3$).

^{31}P{^{1}H} NMR (162 MHz, $CDCl_3$, δ (ppm)): 35.6 (s, P).

^{13}C{^{1}H} NMR (100 MHz, $CDCl_3$, δ (ppm)): 168.1 (d, C^{IV}, $^4J_{PC}$ = 3.30 Hz), 148.2 (d, C^{IV}, $^2J_{PC}$ = 5.70 Hz), 141.9 (d, C^{IV}, $^3J_{PC}$ = 9.10 Hz), 136.4 (d, C^{IV}, $^2J_{PC}$ = 14.8 Hz), 133.7 (d, *o*-*C*H(PPh_2), $^2J_{PC}$ = 9.30 Hz), 133.6 (d, *o*-*C*H(PPh_2), $^2J_{PC}$ = 11.4 Hz), 133.1 (d, *p*-*C*H(PPh_2), $^4J_{PC}$ = 2.60 Hz), 132.6 (d, *p*-*C*H(PPh_2), $^4J_{PC}$ = 2.60 Hz), 131.2 (s, C^{11}-H), 129.2 (d, C^3-H, $^4J_{PC}$ = 2.10 Hz), 128.9 (d, *m*-*C*H(PPh_2), $^3J_{PC}$ = 11.8 Hz), 12.8.8 (d, *m*-*C*H(PPh_2), $^3J_{PC}$ = 12.9 Hz), 128.7 (s, C^9-H), 127.7 (s, C^{IV}), 127.6 (s, C^{IV}), 125.5 (d, C^8-H, $^3J_{PC}$ = 7.60 Hz), 124.9 (d, C^5-H, $^2J_{PC}$ = 13.0 Hz), 121.0 (s, C^{10}-H), 70.0 (s, InO-*C*(CH_3)$_3$), 64.0 (s, C^{15}-H), 55.4 (s, C^{13}-H_2), 41.2 (s, C^{14}-H_3), 35.5 (s, C^4-*C*(CH_3)$_3$), 34.1(s, C^2-*C*(CH_3)$_3$), 34.0 (s, InO-C(*C*H_3)$_3$), 31.6 (s, C^4-C(*C*H_3)$_3$), 30.0 (s, C^2-C(*C*H_3)$_3$), 26.7 (s, $C^{16\text{-}18}$-H_2), 26.3 (s, $C^{16\text{-}18}$-H_2), 26.1 (s, $C^{16\text{-}18}$-H_2), 25.7 (s, $C^{16\text{-}18}$-H_2).

Anal. Calcd for $C_{44}H_{59}ClN_2O_2PIn$: C, 63.73; H, 7.17; N, 3.38. Found: C, 60.85; H, 6.25; N, 3.52.

7.6. References

1 C. Bakewell, T.-P.-A. Cao, N. Long, X. F. Le Goff, A. Auffrant and C. K. Williams, *J. Am. Chem. Soc.*, 2012, **134**, 20577–20580.

2 L. Ding, S. Liang, J. Zhang, C. Ding, Y. Chen and X. Lu, *Inorg. Chem. Commun.*, 2014, **44**, 173–176.

3 Y. Wang, Y. Qin, X. Wang and F. Wang, *Catal. Sci. Technol.*, 2014, **4**, 3964–3972.

4 K. Shen, X. Liu, Y. Cai, L. Lin and X. Feng, *Chem. Eur. J.*, 2009, **15**, 6008–6014.

5 C. A. Busacca, J. C. Lorenz, N. Grinberg, N. Haddad, M. Hrapchak, B. Latli, H. Lee, P. Sabila, A. Saha, M. Sarvestani, S. Shen, R. Varsolona, X. Wei and C. H. Senanayake, *Org. Lett.*, 2005, **7**, 4277–4280.

6 J. D. White and S. Shaw, *Org. Lett.*, 2014, **16**, 3880–3883.

7 M. Braun, R. Fleischer, B. Mai, M.-A. Schneider and S. Lachenicht, *Adv. Synth. Catal.*, 2004, **346**, 474–482.

8 M. Nielsen and K. V. Gothelf, *J. Chem. Soc. Perkin Trans. 1*, 2001, 2440–2444.

9 B. Bildstein, M. Malaun, H. Kopacka, K. Wurst, M. Mitterböck, K.-H. Ongania, G. Opromolla and P. Zanello, *Organometallics*, 1999, **18**, 4325–4336.

10 M. Bochmann, G. Bwembya, K. J. Webb, M. A. Malik, J. R. Walsh and P. O'Brien, in *Inorganic Syntheses*, John Wiley & Sons, Inc., Hoboken, NJ, USA, 2007, pp. 19–24.

11 J. R. Dorgan, J. Janzen, D. M. Knauss, S. B. Hait, B. R. Limoges and M. H. Hutchinson, *J. Polym. Sci. Part B Polym. Phys.*, 2005, **43**, 3100–3111.

12 C. Bakewell, T.-P.-A. Cao, X. F. Le Goff, N. J. Long, A. Auffrant and C. K. Williams, *Organometallics*, 2013, **32**, 1475–1483.

Appendices

A Appendix of Compounds

All numbered compounds synthesised in this thesis

B Crystallographic Data

Summary of crystallographic refinement data and key bond lengths and angles for each structure

C Other

Examples of homonuclear decoupled $^{1}H\{^{1}H\}$ NMR spectra, DOSY NMR spectra and SEC traces.

Appendix A: List of Compounds

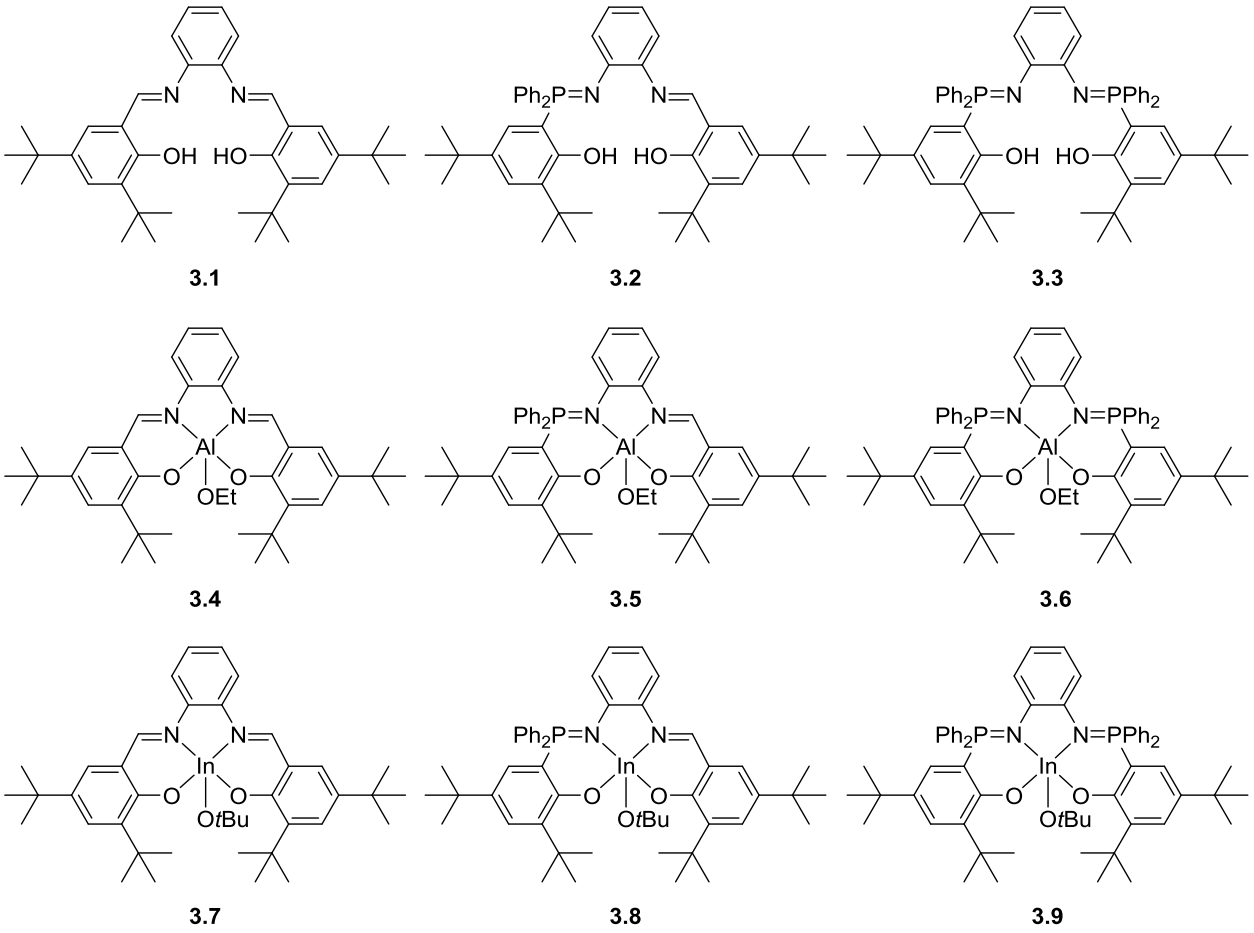

Figure A1. Ligand and initiators **3.1**-**3.9** from Chapter 3.

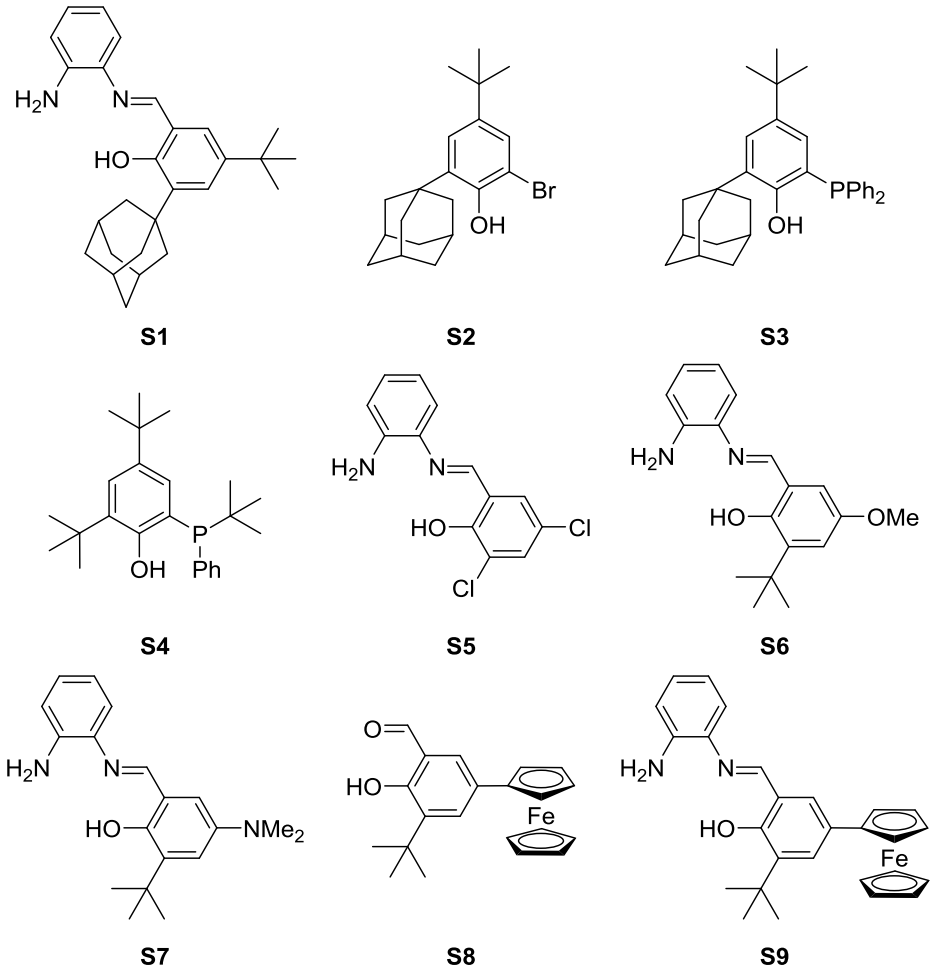

Figure A2. Precursor compounds **S1**-**S9** in Chapter 4.

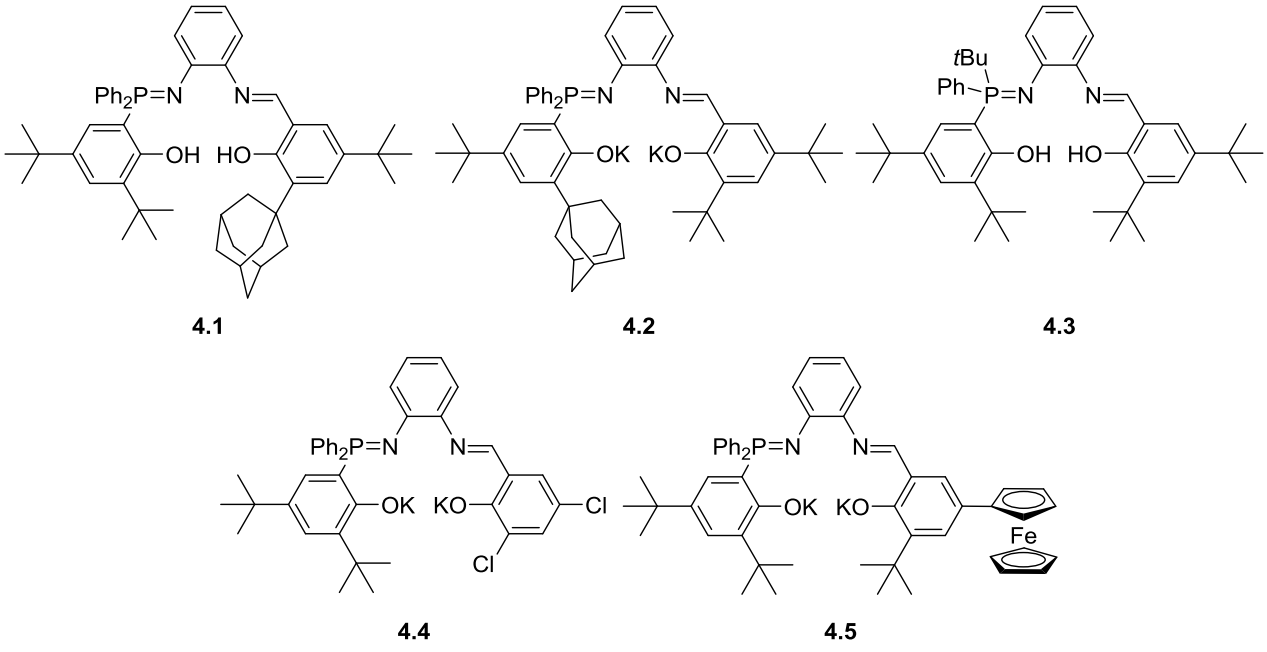

Figure A3. Ligands **4.1**-**4.5** in Chapter 4.

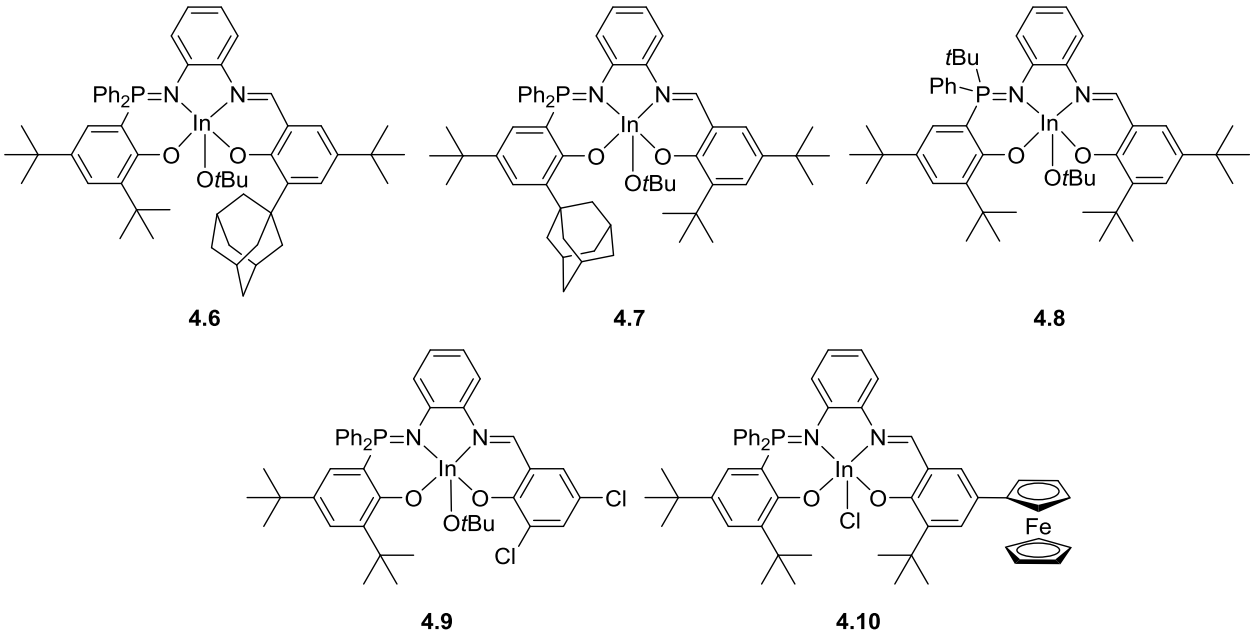

Figure A4. Compounds **4.6**-**4.10** in Chapter 4.

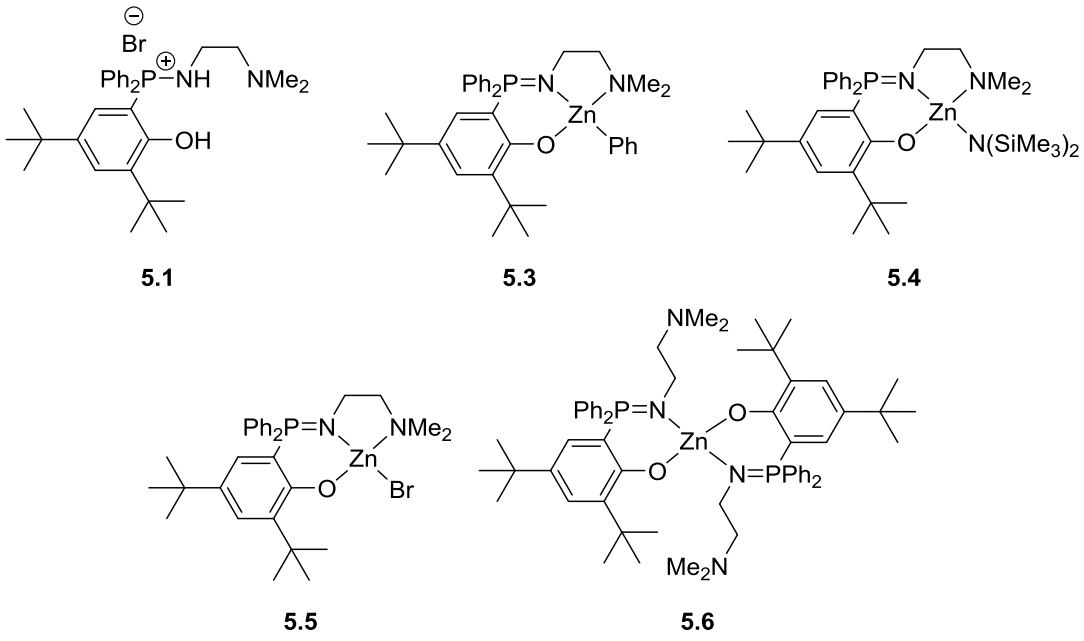

Figure A5. Zinc compounds **5.3**-**5.6** synthesised with ligand **5.1** in Chapter 5.

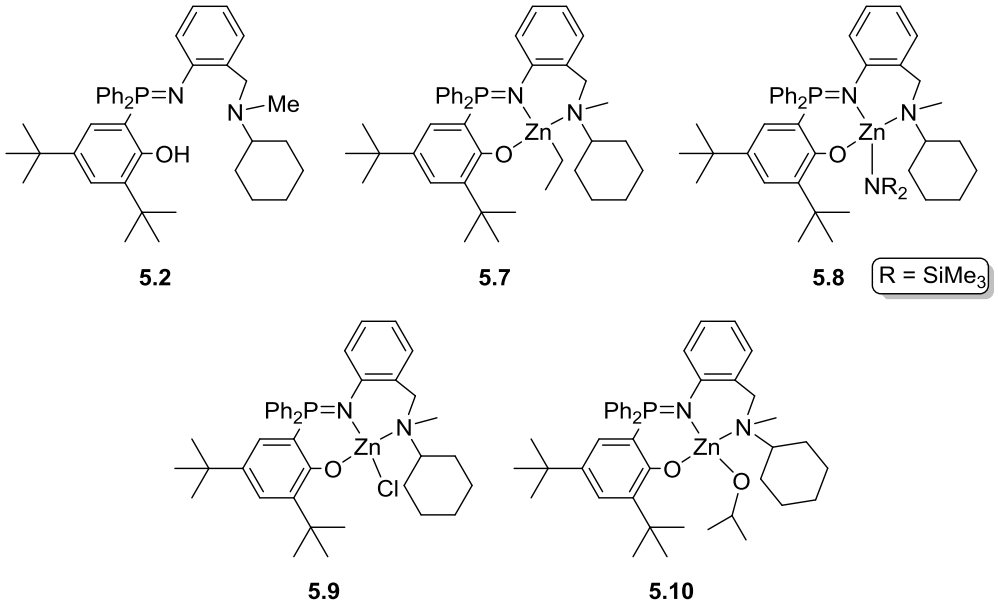

Figure A6. Zinc compound **5.7**-**5.10** synthesised with ligand **5.2** in Chapter 5.

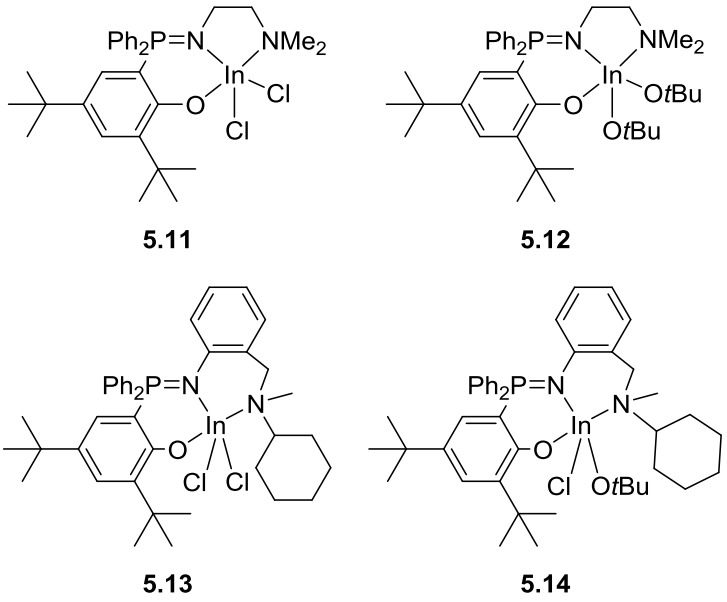

Figure A7. Indium complexes **5.11**-**5.14** in Chapter 5.

Appendix B: Crystallographic Data

Table B1. Summary of compounds with crystallographic data, the location of data collection and original file name.

Compound	Location of data collection	File Name
3.6	Imperial College	CW1616
3.8	Imperial College	CW1628
4.5	Imperial College	CW1619
4.7	Oxford	014CKW17
4.10	Oxford	088CKW17
5.3	Imperial College	CW1601
5.4	Imperial College	CW1612
5.6	Imperial College	CW1610
5.7	Imperial College	CW1607
5.8	Imperial College	CW1618
5.11	Imperial College	CW1702
5.12	Oxford	083CKW17

Table B2. Summary of crystallographic refinement data for initiators **3.6** and **3.8**.

Compound	**3.6**	**3.8**
Chemical Formula	$C_{60}H_{69}AlN_2O_3P_2$ C_4H_8O	$C_{51}H_{64}InN_2O_3P$ C_6H_{14}
Formula weight / g mol^{-1}	1027.19	985.00
Crystal System	Monoclinic	Triclinic
a / Å	12.4445(3)	12.8569(5)
b / Å	16.5166(3)	14.9590(4)
c / Å	28.7880(6)	16.0318(6)
α / °	90	90.275(3)
β / °	91.023(2)	111.373(3)
γ / °	90	108.502(3)
Unit cell volume / Å^3	5916.1(2)	2697.45(17)
No. of formula units per unit cell	4	2
Space group	$P2_1/n$	P^{-1}
Density (calculated) / M_g m^{-3}	1.153	1.213
Diffractometer wavelength / λ	0.71073	0.71073
Temperature / K	173(2)	173(2)
Absorption coefficient / mm^{-1}	0.135	0.510
No. of reflections collected	21081	15673
No. of unique reflections	11963	10655
R_{int}	0.0222	0.0246
Final R_1 values (F > 4σ(F))	0.0524	0.0400
Final wR_2 values (F > 4σ(F))	0.1166	0.0909
Final R_1 values (all data)	0.0738	0.0514
Final wR_2 values (all data)	0.1294	0.0980
Goodness of fit on F^2	1.028	1.050

Table B3. Summary of crystallographic refinement data for compounds **4.5**, **4.7** and **4.10**.

Compound	**4.5**	**4.7**	**4.10**
Chemical Formula	$C_{53}H_{57}FeN_2O_2P$	$C_{57}H_{70}InN_2O_3P$	$C_{117}H_{133}Cl_2Fe_2In_2N_4O_6P_2$
Formula weight / g mol^{-1}	840.82	976.94	2165.45
Crystal System	Monoclinic	Triclinic	Triclinic
a / Å	10.8926(3)	13.6101(4)	9.9304(2)
b / Å	15.5850(4)	15.6270(3)	16.9899(5)
c / Å	27.3760(7)	15.9333(3)	37.4774(10)
α / °	90	61.459(2)	85.875(2)
β / °	92.872(2)	76.774(2)	84.348(2)
γ / °	90	77.842(2)	78.453(2)
Unit cell volume / Å^3	4641.5(2)	2877.59(13)	6156.1(3)
No. of formula units per unit cell	4	2	2
Space group	$P2_1/n$	P^{-1}	P^{-1}
Density (calculated) / M_g m^{-3}	1.203	1.127	1.168
Diffractometer wavelength / λ	0.71073	1.54184	1.54184
Temperature / K	173(2)	150(2)	150(2)
Absorption coefficient / mm^{-1}	0.401	3.844	5.827
No. of reflections collected	16599	67320	74420
No. of unique reflections	9294	11971	25504
R_{int}	0.0246	0.0441	0.0907
Final R_1 values (F > 4σ(F))	0.0487	0.0260	0.0590
Final wR_2 values (F > 4σ(F))	0.1077	0.0677	0.1425
Final R_1 values (all data)	0.0664	0.0291	0.0814
Final wR_2 values (all data)	0.1156	0.0694	0.1571
Goodness of fit on F^2	1.063	1.048	0.999

Table B4. Summary of crystallographic refinement data for compounds **5.3**, **5.4**, **5.6** and **5.7**.

Compound	**5.3**	**5.4**	**5.6**	**5.7**
Chemical Formula	$C_{36}H_{45}N_2OPZn$	$C_{36}H_{58}N_3OPSi_2Zn\ 0.5(C_5H_{14})$	$C_{60}H_{80}N_4O_2P_2Zn$	$C_{42}H_{55}N_2OPZn$
Formula weight / g mol^{-1}	618.08	744.46	1016.59	700.22
Crystal System	Monoclinic	Monoclinic	Orthorhombic	Orthorhombic
a / Å	17.1063(4)	16.5587(4)	14.8310(5)	11.8595(3)
b / Å	9.5633(2)	10.9393(4)	17.3623(8)	31.3899
c / Å	20.8135(4)	23.4243(7)	22.7464(10)	20.7299
α / °	90	90	90	90
β / °	104.562(2)	90.615(3)	90	90
γ / °	90	90	90	90
Unit cell volume / Å^3	3295.55(13)	4242.9(2)	5857.2(4)	7717.0(3)
No. of formula units per unit cell	4	4	4	8
Space group	$P2_1/c$	$P2_1/n$	Pbcn	$Pca2_1$
Density (calculated) / M$_g$ m^{-3}	1.246	1.165	1.153	1.205
Diffractometer wavelength / λ	0.71073	0.71073	0.71073	0.71073
Temperature / K	173(2)	173(2)	173(2)	173(2)
Absorption coefficient / mm^{-1}	0.823	0.704	0.517	0.711
No. of reflections collected	10958	14250	13593	18517
No. of unique reflections	6582	8447	5946	11147
R_{int}	0.0243	0.0284	0.0370	0.0302
Final R_1 values (F > 4σ(F))	0.0371	0.0377	0.0594	0.0431
Final wR_2 values (F > 4σ(F))	0.0871	0.0838	0.1388	0.0821
Final R_1 values (all data)	0.0486	0.0535	0.0903	0.0629
Final wR_2 values (all data)	0.0937	0.0912	0.1601	0.0899
Goodness of fit on F^2	1.037	1.037	1.056	1.101

Table B5. Summary of crystallographic refinement data for compounds **5.8**, **5.11** and **5.12**.

Compound	**5.8**	**5.11**	**5.12**
Chemical Formula	$C_{46}H_{68}N_2OPSi_2Zn$ C_6H_{12}	$C_{30}H_{40}Cl_2InN_2OP$ $0.5(C_6H_{14})$	$C_{38}H_{58}InN_2O_3P$
Formula weight / g mol^{-1}	915.71	740.46	736.65
Crystal System	Orthorhombic	Monoclinic	Monoclinic
a / Å	10.6210(3)	29.9575(15)	40.012(5)
b / Å	21.9837(5)	19.4247(9)	13.1195(8)
c / Å	22.1309(6)	13.3621(5)	23.930(3)
α / °	90	90	90
β / °	90	102.092	133.28(2)
γ / °	90	90	90
Unit cell volume / Å^3	5167.3 92)	7603.1(6)	9146(3)
No. of formula units per unit cell	4	8	8
Space group	$P2_12_12_1$	C2/c	C2/c
Density (calculated) / M_g m^{-3}	1.177	1.294	1.070
Diffractometer wavelength / λ	0.71073	0.71073	1.54184
Temperature / K	173(2)	173(2)	150(2)
Absorption coefficient / mm^{-1}	0.591	0.833	4.688
No. of reflections collected	13167	13747	48566
No. of unique reflections	9010	7581	9532
R_{int}	0.229	0.0196	0.0594
Final R_1 values (F > 4σ(F))	0.0339	0.0451	0.0557
Final wR_2 values (F > 4σ(F))	0.0419	0.1285	0.1315
Final R_1 values (all data)	0.0692	0.0587	0.0611
Final wR_2 values (all data)	0.0732	0.1397	0.1353
Goodness of fit of F^2	1.026	1.068	1.072

Table B6. Key bond lengths and angles of initiator **3.6**.

Bond	Bond Length (Å)	Bond	Bond Length (Å)
Al(1)-O(70)	1.7409(16)	N(8)-C(9)	1.420(3)
Al(1)-O(22)	1.7903(15)	C(14)-N(15)	1.402(3)
Al(1)-O(1)	1.8488(15)	N(15)-P(16)	1.5972(17)
Al(1)-N(8)	1.9502(17)	P(16)-C(17)	1.788(2)
Al(1)-N(15)	2.0344(18)	P(16)-C(43)	1.803(2)
O(1)-C(1)	1.321(2)	P(16)-C(49)	1.808(2)
C(6)-P(7)	1.772(2)	C(22)-O(22)	1.324(2)
P(7)-N(8)	1.6083(17)	O(80)-C(81)	1.353(7)
P(7)-C(37)	1.801(2)	O(80)-C(84)	1.504(8)
P(7)-C(31)	1.807(2)		
Bond	Bond Angle (^{o})	Bond	Bond Angle (^{o})
O(70)-Al(1)-O(22)	118.27(8)	N(8)-P(7)-C(37)	112.19(9)
O(70)-Al(1)-O(1)	95.23(7)	C(6)-P(7)-C(37)	107.05(9)
O(22)-Al(1)-O(1)	94.24(7)	N(8)-P(7)-C(31)	113.56(9)
O(70)-Al(1)-N(8)	123.98(8)	C(6)-P(7)-C(31)	105.29(9)
O(22)-Al(1)-N(8)	116.63(7)	C(37)-P(7)-C(31)	107.39(10)
O(1)-Al(1)-N(8)	91.12(7)	C(9)-N(8)-Al(1)	114.39(13)
O(70)-Al(1)-N(15)	89.38(8)	P(7)-N(8)-Al(1)	121.62(10)
O(22)-Al(1)-N(15)	91.47(7)	C(14)-N(15)-Al(1)	111.60(13)
O(1)-Al(1)-N(15)	169.90(7)	P(16)-N(15)-Al(1)	119.95(10)
N(8)-Al(1)-N(15)	78.86(7)	C(22)-O(22)-Al(1)	137.83(13)
C(1)-O(1)-Al(1)	128.02(13)	C(71)-O(70)-Al(1)	135.0(2)
N(8)-P(7)-C(6)	110.91(9)		

Table B7. Key bond lengths and angles of initiator **3.8**.

Bond	Bond Length (Å)	Bond	Bond Length (Å)
In(1)-O(60)	2.016(2)	P(7)-C(37)	1.809(3)
In(1)-O(22)	2.0766(19)	P(7)-C(31)	1.814(3)
In(1)-O(1)	2.0863(19)	N(8)-C(9)	1.409(3)
In(1)-N(8)	2.192(2)	C(14)-N(15)	1.425(3)
In(1)-N(15)	2.209(2)	N(15)-C(16)	1.289(3)
O(1)-C(1)	1.322(3)	C(22)-O(22)	1.308(3)
C(6)-P(7)	1.789(3)	O(60)-C(61)	1.413(4)
P(7)-N(8)	1.611(2)		
Bond	Bond Angle (^{o})	Bond	Bond Angle (^{o})
O(60)-In(1)-O(22)	114.65(9)	C(6)-P(7)-C(37)	106.82(13)
O(60)-In(1)-O(1)	111.84(9)	N(8)-P(7)-C(31)	111.39(13)
O(22)-In(1)-O(1)	90.04(8)	C(6)-P(7)-C(31)	106.46(13)

O(60)-In(1)-N(8)	97.23(8)	C(37)-P(7)-C(31)	108.92(13)
O(22)-In(1)-N(8)	146.77(9)	C(9)-N(8)-P(7)	124.02(18)
O(1)-In(1)-N(8)	86.35(8)	C(9)-N(8)-In(1)	114.74(17)
O(60)-In(1)-N(15)	109.69(9)	P(7)-N(8)-In(1)	119.43(12)
O(22)-In(1)-N(15)	85.09(8)	C(10)-C(9)-N(8)	125.1(2)
O(1)-In(1)-N(15)	136.17(8)	N(8)-C(9)-C(14)	117.2(2)
N(8)-In(1)-N(15)	75.11(8)	C(13)-C(14)-N(15)	123.6(2)
C(1)-O(1)-In(1)	121.56(17)	C(9)-C(14)-N(15)	116.1(2)
O(1)-C(1)-C(6)	122.5(2)	C(16)-N(15)-C(14)	121.8(2)
O(1)-C(1)-C(2)	119.8(2)	C(16)-N(15)-In(1)	124.43(18)
C(1)-C(6)-P(7)	124.1(2)	C(14)-N(15)-In(1)	113.75(17)
N(8)-P(7)-C(6)	111.96(12)	N(15)-C(16)-C(17)	128.7(3)
N(8)-P(7)-C(37)	111.06(14)		

Table B8. Key bond lengths and angles of compound **4.5**.

Bond	Bond Length (Å)	Bond	Bond Length (Å)
Fe(1)-C(30)	2.029(3)	O(1)-C(1)	1.354(3)
Fe(1)-C(31)	2.031(2)	C(7)-N(8)	1.274(3)
Fe(1)-C(27)	2.036(2)	N(8)-C(9)	1.425(3)
Fe(1)-C(28)	2.037(2)	C(14)-N(15)	1.393(3)
Fe(1)-C(32)	2.038(3)	N(15)-P(16)	1.572(2)
Fe(1)-C(33)	2.039(3)	P(16)-C(17)	1.793(2)
Fe(1)-C(36)	2.040(3)	P(16)-C(43)	1.809(3)
Fe(1)-C(29)	2.042(3)	P(16)-C(37)	1.813(3)
Fe(1)-C(34)	2.042(3)	C(22)-O(22)	1.353(3)
Bond	Bond Angle (^{o})	Bond	Bond Angle (^{o})
C(30)-Fe(1)-C(31)	41.04(10)	C(36)-Fe(1)-C(29)	128.73(17)
C(30)-Fe(1)-C(27)	69.00(10)	C(30)-Fe(1)-C(34)	109.11(11)
C(31)-Fe(1)-C(27)	40.90(10)	C(31)-Fe(1)-C(34)	131.58(15)
C(30)-Fe(1)-C(28)	68.45(11)	C(27)-Fe(1)-C(34)	170.25(19)
C(31)-Fe(1)-C(28)	68.62(11)	C(28)-Fe(1)-C(34)	148.13(19)
C(27)-Fe(1)-C(28)	40.99(9)	C(32)-Fe(1)-C(34)	68.55(8)
C(30)-Fe(1)-C(32)	150.94(19)	C(33)-Fe(1)-C(34)	40.72(6)
C(31)-Fe(1)-C(32)	117.63(13)	C(36)-Fe(1)-C(34)	68.51(7)
C(27)-Fe(1)-C(32)	108.16(12)	C(29)-Fe(1)-C(34)	116.44(15)
C(28)-Fe(1)-C(32)	129.38(18)	O(1)-C(1)-C(6)	119.7(2)
C(30)-Fe(1)-C(33)	118.20(16)	O(1)-C(1)-C(2)	119.2(2)
C(31)-Fe(1)-C(33)	110.02(12)	N(8)-C(7)-C(6)	123.1(2)
C(27)-Fe(1)-C(33)	130.96(18)	C(7)-N(8)-C(9)	117.9(2)
C(28)-Fe(1)-C(33)	169.0(2)	C(10)-C(9)-N(8)	118.4(2)
C(32)-Fe(1)-C(33)	40.76(6)	C(14)-C(9)-N(8)	120.5(2)
C(30)-Fe(1)-C(36)	167.56(18)	N(15)-C(14)-C(9)	117.7(2)

C(31)-Fe(1)-C(36)	149.35(16)	N(15)-C(14)-C(13)	125.4(2)
C(27)-Fe(1)-C(36)	115.46(12)	C(14)-N(15)-P(16)	132.04(17)
C(28)-Fe(1)-C(36)	106.73(12)	N(15)-P(16)-C(17)	106.40(11)
C(32)-Fe(1)-C(36)	40.75(6)	N(15)-P(16)-C(43)	113.00(12)
C(33)-Fe(1)-C(36)	68.56(8)	C(17)-P(16)-C(43)	106.22(12)
C(30)-Fe(1)-C(29)	40.36(11)	N(15)-P(16)-C(37)	117.13(12)
C(31)-Fe(1)-C(29)	68.43(11)	C(17)-P(16)-C(37)	106.01(11)
C(27)-Fe(1)-C(29)	68.77(10)	C(43)-P(16)-C(37)	107.33(12)
C(28)-Fe(1)-C(29)	40.68(10)	C(18)-C(17)-P(16)	117.98(18)
C(32)-Fe(1)-C(29)	167.7(2)	C(22)-C(17)-P(16)	121.58(18)
C(33)-Fe(1)-C(29)	149.9(2)		

Table B9. Key bond lengths and angles for compound **4.7**.

Bond	Bond Length (Å)	Bond	Bond Length (Å)
C(1)-O(1)	1.321(2)	C(54)-O(3)	1.419(2)
C(15)-N(1)	1.290(2)	N(1)-In(1)	2.2225(14)
C(16)-N(1)	1.423(2)	N(2)-P(1)	1.6076(14)
C(21)-N(2)	1.407(2)	N(2)-In(1)	2.1956(14)
C(22)-P(1)	1.8047(18)	O(1)-In(1)	2.0898(12)
C(28)-P(1)	1.8037(18)	O(2)-In(1)	2.0965(12)
C(34)-P(1)	1.7822(18)	O(3)-In(1)	2.0279(12)
C(39)-O(2)	1.328(2)		
Bond	**Bond Angle (°)**	**Bond**	**Bond Angle (°)**
O(1)-C(1)-C(6)	123.15(15)	P(1)-N(2)-In(1)	123.69(8)
O(1)-C(1)-C(2)	119.43(16)	C(1)-O(1)-In(1)	132.67(11)
N(1)-C(15)-C(6)	126.66(16)	C(39)-O(2)-In(1)	131.07(11)
C(17)-C(16)-N(1)	124.56(15)	C(54)-O(3)-In(1)	124.84(11)
C(21)-C(16)-N(1)	114.72(15)	N(2)-P(1)-C(34)	111.99(8)
C(20)-C(21)-N(2)	125.47(15)	N(2)-P(1)-C(28)	112.63(9)
N(2)-C(21)-C(16)	116.06(15)	C(34)-P(1)-C(28)	104.96(9)
C(27)-C(22)-P(1)	124.26(14)	N(2)-P(1)-C(22)	111.06(8)
C(23)-C(22)-P(1)	116.31(14)	C(34)-P(1)-C(22)	106.48(8)
C(29)-C(28)-P(1)	119.10(15)	C(28)-P(1)-C(22)	109.37(8)
C(33)-C(28)-P(1)	121.04(17)	O(3)-In(1)-O(1)	111.99(5)
C(35)-C(34)-P(1)	115.29(13)	O(3)-In(1)-O(2)	109.64(5)
C(39)-C(34)-P(1)	122.14(13)	O(1)-In(1)-O(2)	97.44(5)
O(2)-C(39)-C(34)	122.10(16)	O(3)-In(1)-N(2)	105.40(5)
O(2)-C(39)-C(38)	120.75(15)	O(1)-In(1)-N(2)	137.54(5)
C(15)-N(1)-C(16)	121.38(15)	O(2)-In(1)-N(2)	88.08(5)
C(15)-N(1)-In(1)	126.85(12)	O(3)-In(1)-N(1)	94.98(5)
C(16)-N(1)-In(1)	111.75(10)	O(1)-In(1)-N(1)	84.18(5)
C(21)-N(2)-P(1)	124.19(12)	O(2)-In(1)-N(1)	152.38(5)

C(21)-N(2)-In(1)	111.98(10)	N(2)-In(1)-N(1)	73.05(5)

Table B10. Key bond lengths and angles for compound **4.10**.

Bond	Bond Length (Å)	Bond	Bond Length (Å)
C(1)-O(1)	1.310(6)	C(53)-Fe(1)	2.045(5)
C(6)-P(1)	1.817(4)	C(54)-O(4)	1.325(5)
C(15)-P(1)	1.811(4)	C(55)-P(2)	1.801(5)
C(21)-P(1)	1.811(4)	C(68)-P(2)	1.802(4)
C(27)-N(1)	1.404(6)	C(74)-P(2)	1.821(4)
C(35)-O(2)	1.295(6)	C(80)-N(3)	1.409(6)
C(44)-Fe(1)	2.057(5)	C(85)-N(4)	1.406(5)
C(45)-Fe(1)	2.052(5)	C(86)-N(4)	1.308(6)
C(46)-Fe(1)	2.051(5)	N(1)-P(1)	1.622(4)
C(47)-Fe(1)	2.040(5)	N(1)-In(1)	2.213(3)
C(48)-Fe(1)	2.036(5)	N(2)-In(1)	2.189(3)
C(49)-Fe(1)	2.045(5)	O(1)-In(1)	2.073(3)
C(50)-Fe(1)	2.051(5)	O(2)-In(1)	2.092(3)
C(51)-Fe(1)	2.045(6)	O(3)-In(1)	2.376(3)
C(52)-Fe(1)	2.058(5)	In(1)-Cl(1)	2.4177(11)
Bond	**Bond Angle (°)**	**Bond**	**Bond Angle (°)**
O(1)-C(1)-C(6)	122.2(4)	C(110)-O(3)-In(1)	121.0(3)
O(1)-C(1)-C(2)	119.7(4)	N(1)-P(1)-C(15)	113.9(2)
C(5)-C(6)-P(1)	115.6(3)	N(1)-P(1)-C(21)	110.2(2)
C(1)-C(6)-P(1)	123.4(3)	C(15)-P(1)-C(21)	105.0(2)
C(16)-C(15)-P(1)	121.4(3)	N(1)-P(1)-C(6)	112.64(19)
C(20)-C(15)-P(1)	118.1(3)	C(15)-P(1)-C(6)	102.9(2)
C(26)-C(21)-P(1)	122.0(4)	C(21)-P(1)-C(6)	111.8(2)
C(22)-C(21)-P(1)	117.8(4)	N(3)-P(2)-C(55)	111.3(2)
N(1)-C(27)-C(28)	126.3(4)	N(3)-P(2)-C(68)	110.5(2)
N(1)-C(27)-C(32)	117.7(3)	C(55)-P(2)-C(68)	108.9(2)
N(2)-C(32)-C(27)	116.5(3)	N(3)-P(2)-C(74)	113.95(19)
N(2)-C(33)-C(34)	128.2(4)	C(55)-P(2)-C(74)	105.1(2)
O(2)-C(35)-C(34)	123.2(4)	C(68)-P(2)-C(74)	106.78(19)
O(2)-C(35)-C(36)	118.4(4)	O(1)-In(1)-O(2)	100.10(13)
O(4)-C(54)-C(55)	121.2(4)	O(1)-In(1)-N(2)	160.53(13)
O(4)-C(54)-C(59)	120.3(4)	O(2)-In(1)-N(2)	87.19(14)
C(54)-C(55)-P(2)	120.9(3)	O(1)-In(1)-N(1)	92.43(13)
C(56)-C(55)-P(2)	117.3(3)	O(2)-In(1)-N(1)	160.60(14)
C(27)-N(1)-In(1)	113.1(3)	N(2)-In(1)-N(1)	76.47(14)
P(1)-N(1)-In(1)	118.33(19)	O(1)-In(1)-O(3)	76.49(14)
C(33)-N(2)-C(32)	122.2(3)	O(2)-In(1)-O(3)	81.46(17)
C(33)-N(2)-In(1)	123.8(3)	N(2)-In(1)-O(3)	86.90(13)

C(32)-N(2)-In(1)	114.0(3)	N(1)-In(1)-O(3)	87.22(15)
C(80)-N(3)-P(2)	129.6(3)	O(1)-In(1)-Cl(1)	100.28(10)
C(86)-N(4)-C(85)	121.8(4)	O(2)-In(1)-Cl(1)	95.13(12)
C(1)-O(1)-In(1)	125.6(3)	N(2)-In(1)-Cl(1)	96.98(10)
C(35)-O(2)-In(1)	130.7(3)	N(1)-In(1)-Cl(1)	97.14(10)
C(107)-O(3)-C(110)	107.6(5)	O(3)-In(1)-Cl(1)	174.73(10)
C(107)-O(3)-In(1)	127.2(3)		

Table B11. Key bond lengths and angles for compound **5.3**.

Bond	Bond Length (Å)	Bond	Bond Length (Å)
Zn(1)-O(1)	1.9670(14)	P(7)-N(8)	1.6073(18)
Zn(1)-C(40)	1.975(2)	P(7)-C(26)	1.800(2)
Zn(1)-N(8)	2.0892(17)	P(7)-C(20)	1.810(2)
Zn(1)-N(11)	2.1767(18)	N(8)-C(9)	1.473(3)
Zn(1)-P(7)	2.8870(6)	C(10)-N(11)	1.466(3)
O(1)-C(1)	1.316(2)	N(11)-C(33)	1.472(3)
C(6)-P(7)	1.784(2)	N(11)-C(32)	1.475(3)
Bond	Bond Angle (^{o})	Bond	Bond Angle (^{o})
O(1)-Zn(1)-C(40)	119.79(8)	N(8)-P(7)-Zn(1)	45.08(6)
O(1)-Zn(1)-N(8)	101.34(6)	C(6)-P(7)-Zn(1)	88.87(7)
C(40)-Zn(1)-N(8)	129.94(8)	C(26)-P(7)-Zn(1)	78.99(7)
O(1)-Zn(1)-N(11)	103.67(7)	C(20)-P(7)-Zn(1)	161.28(7)
C(40)-Zn(1)-N(11)	110.07(8)	C(9)-N(8)-P(7)	119.67(14)
N(8)-Zn(1)-N(11)	84.00(7)	C(9)-N(8)-Zn(1)	109.18(13)
O(1)-Zn(1)-P(7)	71.49(4)	P(7)-N(8)-Zn(1)	101.92(8)
C(40)-Zn(1)-P(7)	138.67(7)	N(8)-C(9)-C(10)	109.38(17)
N(8)-Zn(1)-P(7)	33.01(5)	N(11)-C(10)-C(9)	111.80(18)
N(11)-Zn(1)-P(7)	104.31(5)	C(10)-N(11)-C(33)	111.19(18)
C(1)-O(1)-Zn(1)	126.57(13)	C(10)-N(11)-C(32)	110.06(18)
O(1)-C(1)-C(6)	121.29(18)	C(33)-N(11)-C(32)	109.5(2)
O(1)-C(1)-C(2)	121.48(19)	C(10)-N(11)-Zn(1)	100.31(13)
C(5)-C(6)-P(7)	121.86(16)	C(33)-N(11)-Zn(1)	115.67(15)
C(1)-C(6)-P(7)	116.33(15)	C(32)-N(11)-Zn(1)	109.77(14)
N(8)-P(7)-C(6)	114.25(10)	C(21)-C(20)-P(7)	119.20(17)
N(8)-P(7)-C(26)	103.70(9)	C(25)-C(20)-P(7)	121.78(18)
C(6)-P(7)-C(26)	110.17(10)	C(31)-C(26)-P(7)	122.44(17)
N(8)-P(7)-C(20)	116.64(10)	C(27)-C(26)-P(7)	118.44(16)
C(6)-P(7)-C(20)	105.55(9)		
C(26)-P(7)-C(20)	106.21(10)		

Table B12. Key bond lengths and angles for compound **5.4**.

Bond	Bond Length (Å)	Bond	Bond Length (Å)
Zn(1)-N(40)	1.9239(17)	P(7)-C(22)	1.819(2)
Zn(1)-O(1)	1.9895(14)	N(8)-C(9)	1.471(3)
Zn(1)-N(8)	2.0379(17)	C(10)-N(11)	1.474(3)
Zn(1)-N(11)	2.1581(18)	N(11)-C(13)	1.474(3)
O(1)-C(1)	1.310(2)	N(11)-C(12)	1.480(3)
C(6)-P(7)	1.789(2)	N(40)-Si(41)	1.695(2)
P(7)-N(8)	1.6036(17)	N(40)-Si(45)	1.710(2)
P(7)-C(28)	1.800(2)		
Bond	Bond Angle (^{o})	Bond	Bond Angle (^{o})
N(40)-Zn(1)-O(1)	118.03(7)	C(9)-N(8)-P(7)	119.32(14)
N(40)-Zn(1)-N(8)	132.79(8)	C(9)-N(8)-Zn(1)	108.97(13)
O(1)-Zn(1)-N(8)	97.35(6)	P(7)-N(8)-Zn(1)	108.32(9)
N(40)-Zn(1)-N(11)	113.19(7)	N(8)-C(9)-C(10)	108.84(17)
O(1)-Zn(1)-N(11)	103.28(7)	N(11)-C(10)-C(9)	111.05(18)
N(8)-Zn(1)-N(11)	85.07(7)	C(13)-N(11)-C(10)	110.50(19)
C(1)-O(1)-Zn(1)	133.30(13)	C(13)-N(11)-C(12)	108.69(19)
C(1)-O(1)-Zn(1)	133.30(13)	C(10)-N(11)-C(12)	110.01(18)
O(1)-C(1)-C(6)	122.95(19)	C(13)-N(11)-Zn(1)	112.30(14)
O(1)-C(1)-C(2)	120.51(18)	C(10)-N(11)-Zn(1)	101.99(13)
C(5)-C(6)-P(7)	118.54(15)	C(12)-N(11)-Zn(1)	113.22(14)
C(1)-C(6)-P(7)	119.22(15)	C(27)-C(22)-P(7)	121.40(17)
N(8)-P(7)-C(6)	116.28(9)	C(23)-C(22)-P(7)	119.94(16)
N(8)-P(7)-C(28)	105.38(9)	C(29)-C(28)-P(7)	120.98(17)
C(6)-P(7)-C(28)	108.40(10)	C(33)-C(28)-P(7)	119.17(17)
N(8)-P(7)-C(22)	113.46(9)	Si(41)-N(40)-Si(45)	123.57(11)
C(6)-P(7)-C(22)	106.24(9)	Si(41)-N(40)-Zn(1)	122.08(10)
C(28)-P(7)-C(22)	106.61(10)	Si(45)-N(40)-Zn(1)	113.69(10)

Table B13. Key bond lengths and angles for compound **5.6**.

Bond	Bond Length (Å)	Bond	Bond Length (Å)
Zn(1)-O(1)	1.946(2)	P(7)-C(28)	1.821(3)
Zn(1)-N(8)	2.001(2)	N(8)-C(9)	1.484(4)
O(1)-C(1)	1.305(3)	C(10)-N(11)	1.456(4)
C(6)-P(7)	1.783(3)	N(11)-C(13)	1.436(5)
P(7)-N(8)	1.598(3)	N(11)-C(12)	1.459(5)
P(7)-C(22)	1.810(3)		
Bond	Bond Angle (^{o})	Bond	Bond Angle (^{o})
O(1)#1-Zn(1)-O(1)	106.59(11)	C(6)-P(7)-C(28)	105.71(15)

O(1)#1-Zn(1)-N(8)	118.85(10)	C(22)-P(7)-C(28)	104.15(16)
O(1)-Zn(1)-N(8)	97.73(9)	C(9)-N(8)-P(7)	121.4(2)
O(1)#1-Zn(1)-N(8)#1	97.73(9)	C(9)-N(8)-Zn(1)	120.8(2)
O(1)-Zn(1)-N(8)#1	118.85(10)	P(7)-N(8)-Zn(1)	116.17(14)
N(8)-Zn(1)-N(8)#1	117.84(15)	N(8)-C(9)-C(10)	110.6(3)
C(1)-O(1)-Zn(1)	122.09(18)	N(11)-C(10)-C(9)	112.8(3)
O(1)-C(1)-C(6)	121.3(3)	C(13)-N(11)-C(10)	111.3(3)
O(1)-C(1)-C(2)	121.4(3)	C(13)-N(11)-C(12)	109.0(4)
C(5)-C(6)-P(7)	118.8(2)	C(10)-N(11)-C(12)	110.4(3)
C(1)-C(6)-P(7)	119.3(2)	C(27)-C(22)-P(7)	123.3(3)
N(8)-P(7)-C(6)	112.16(14)	C(23)-C(22)-P(7)	118.1(3)
N(8)-P(7)-C(22)	110.41(14)	C(33)-C(28)-P(7)	120.2(3)
C(6)-P(7)-C(22)	109.03(15)	C(29)-C(28)-P(7)	121.0(3)
N(8)-P(7)-C(28)	114.92(15)		

Table B14. Key bond lengths and angles for compound **5.7**.

Bond	Bond Length (Å)	Bond	Bond Length (Å)
Zn(1A)-C(50A)	1.985(6)	P(7A)-C(37A)	1.818(5)
Zn(1A)-O(1A)	1.988(4)	P(7A)-C(31A)	1.824(4)
Zn(1A)-N(8A)	2.058(3)	N(8A)-C(9A)	1.416(6)
Zn(1A)-N(16A)	2.186(4)	C(15A)-N(16A)	1.481(6)
O(1A)-C(1A)	1.314(5)	N(16A)-C(43A)	1.482(6)
C(6A)-P(7A)	1.789(5)	N(16A)-C(17A)	1.507(6)
P(7A)-N(8A)	1.596(4)		
Bond	**Bond Angle (°)**	**Bond**	**Bond Angle (°)**
C(50A)-Zn(1A)-O(1A)	128.1(2)	C(9A)-N(8A)-P(7A)	125.2(3)
C(50A)-Zn(1A)-N(8A)	117.97(19)	C(9A)-N(8A)-Zn(1A)	115.7(3)
O(1A)-Zn(1A)-N(8A)	93.12(15)	P(7A)-N(8A)-Zn(1A)	118.3(2)
C(50A)-Zn(1A)-N(16A)	116.0(2)	C(10A)-C(9A)-N(8A)	123.3(4)
O(1A)-Zn(1A)-N(16A)	100.49(15)	C(14A)-C(9A)-N(8A)	118.4(4)
N(8A)-Zn(1A)-N(16A)	94.23(14)	N(16A)-C(15A)-C(14A)	114.4(4)
C(1A)-O(1A)-Zn(1A)	118.5(3)	C(15A)-N(16A)-C(43A)	110.2(4)
O(1A)-C(1A)-C(6A)	122.1(4)	C(15A)-N(16A)-C(17A)	109.8(4)
O(1A)-C(1A)-C(2A)	121.4(4)	C(43A)-N(16A)-C(17A)	112.8(4)
C(5A)-C(6A)-P(7A)	117.4(3)	C(15A)-N(16A)-Zn(1A)	106.5(3)
C(1A)-C(6A)-P(7A)	120.6(4)	C(43A)-N(16A)-Zn(1A)	108.9(3)
N(8A)-P(7A)-C(6A)	111.8(2)	C(17A)-N(16A)-Zn(1A)	108.4(3)
N(8A)-P(7A)-C(37A)	113.4(2)	N(16A)-C(17A)-C(22A)	111.5(4)
C(6A)-P(7A)-C(37A)	106.7(2)	N(16A)-C(17A)-C(18A)	115.7(4)
N(8A)-P(7A)-C(31A)	110.3(2)	C(36A)-C(31A)-P(7A)	124.3(4)
C(6A)-P(7A)-C(31A)	108.1(2)	C(32A)-C(31A)-P(7A)	116.6(4)
C(37A)-P(7A)-C(31A)	106.2(2)		

Table B15. Key bond lengths and angles for compound **5.8**.

Bond	Bond Length (Å)	Bond	Bond Length (Å)
Zn(1)-N(50)	1.938(2)	P(7)-C(31)	1.801(3)
Zn(1)-O(1)	2.012(2)	N(8)-C(9)	1.431(4)
Zn(1)-N(8)	2.026(3)	C(15)-N(16)	1.498(4)
Zn(1)-N(16)	2.224(3)	N(16)-C(43)	1.481(4)
O(1)-C(1)	1.318(4)	N(16)-C(17)	1.502(4)
C(6)-P(7)	1.786(3)	N(50)-Si(55)	1.706(3)
P(7)-N(8)	1.610(3)	N(50)-Si(51)	1.716(3)
P(7)-C(37)	1.798(3)		
Bond	Bond Angle (°)	Bond	Bond Angle (°)
N(50)-Zn(1)-O(1)	115.03(10)	C(10)-C(9)-N(8)	120.1(3)
N(50)-Zn(1)-N(8)	123.20(11)	N(16)-C(15)-C(14)	114.5(3)
O(1)-Zn(1)-N(8)	97.00(10)	C(43)-N(16)-C(15)	107.5(3)
O(1)-Zn(1)-N(16)	121.34(11)	C(43)-N(16)-C(17)	111.5(3)
N(8)-Zn(1)-N(16)	101.15(10)	C(15)-N(16)-C(17)	111.2(2)
C(1)-O(1)-Zn(1)	94.10(10)	C(43)-N(16)-Zn(1)	105.6(2)
C(5)-C(6)-P(7)	120.9(3)	C(15)-N(16)-Zn(1)	104.4(2)
C(1)-C(6)-P(7)	116.7(2)	C(17)-N(16)-Zn(1)	115.97(18)
N(8)-P(7)-C(6)	116.63(15)	N(16)-C(17)-C(22)	112.1(3)
N(8)-P(7)-C(37)	109.46(14)	N(16)-C(17)-C(18)	114.9(3)
C(6)-P(7)-C(37)	108.30(15)	C(36)-C(31)-P(7)	120.1(3)
N(8)-P(7)-C(31)	107.83(15)	C(32)-C(31)-P(7)	121.0(3)
C(6)-P(7)-C(31)	105.37(16)	C(38)-C(37)-P(7)	121.6(3)
C(37)-P(7)-C(31)	109.00(16)	C(42)-C(37)-P(7)	119.3(3)
C(9)-N(8)-P(7)	120.9(2)	Si(55)-N(50)-Si(51)	122.62(14)
C(9)-N(8)-Zn(1)	119.0(2)	Si(55)-N(50)-Zn(1)	121.53(15)
P(7)-N(8)-Zn(1)	111.81(14)	Si(51)-N(50)-Zn(1)	114.62(14)
C(14)-C(9)-N(8)	119.8(3)		

Table B16. Key bond lengths and angles for compound **5.11**.

Bond	Bond Length (Å)	Bond	Bond Length (Å)
In(1)-O(1)	2.095(3)	P(7)-N(8)	1.610(4)
In(1)-N(8)	2.133(3)	P(7)-C(22)	1.800(4)
In(1)-N(11)	2.355(4)	P(7)-C(28)	1.803(4)
In(1)-Cl(1)	2.4230(10)	N(8)-C(9)	1.475(6)
In(1)-Cl(2)	2.4250(9)	C(10)-N(11)	1.466(6)
O(1)-C(1)	1.327(5)	N(11)-C(13)	1.469(6)
C(6)-P(7)	1.783(4)	N(11)-C(12)	1.477(7)
Bond	Bond Angle (°)	Bond	Bond Angle (°)

O(1)-In(1)-N(8)	89.02(12)	C(6)-P(7)-C(28)	106.8(2)
O(1)-In(1)-N(11)	164.66(12)	C(22)-P(7)-C(28)	106.85(19)
N(8)-In(1)-N(11)	77.63(13)	C(9)-N(8)-P(7)	121.7(3)
O(1)-In(1)-Cl(1)	99.22(8)	C(9)-N(8)-In(1)	115.8(3)
N(8)-In(1)-Cl(1)	113.38(10)	P(7)-N(8)-In(1)	120.92(19)
N(11)-In(1)-Cl(1)	93.07(10)	N(8)-C(9)-C(10)	108.7(4)
O(1)-In(1)-Cl(2)	91.61(8)	N(11)-C(10)-C(9)	112.1(4)
N(8)-In(1)-Cl(2)	129.40(10)	C(10)-N(11)-C(13)	110.5(4)
N(11)-In(1)-Cl(2)	91.11(10)	C(10)-N(11)-C(12)	110.2(4)
Cl(1)-In(1)-Cl(2)	116.40(3)	C(13)-N(11)-C(12)	108.3(4)
C(1)-O(1)-In(1)	132.0(2)	C(10)-N(11)-In(1)	100.0(3)
O(1)-C(1)-C(6)	121.3(4)	C(13)-N(11)-In(1)	114.7(3)
O(1)-C(1)-C(2)	120.7(4)	C(12)-N(11)-In(1)	112.9(3)
C(5)-C(6)-P(7)	118.0(3)	C(27)-C(22)-P(7)	120.8(4)
C(1)-C(6)-P(7)	120.5(3)	C(23)-C(22)-P(7)	120.3(4)
N(8)-P(7)-C(6)	112.13(18)	C(29)-C(28)-P(7)	122.5(3)
N(8)-P(7)-C(22)	114.7(2)	C(33)-C(28)-P(7)	117.8(3)
C(6)-P(7)-C(22)	106.3(2)	C(41)-O(40)-C(44)	109.7(14)
N(8)-P(7)-C(28)	109.6(2)	O(40)-C(41)-C(42)	108.6(11)

Table B17. Key bond lengths and angles for compound **5.12**.

Bond	Bond Length (Å)	Bond	Bond Length (Å)
C(1)-O(1)	1.327(5)	C(31)-O(2)	1.411(5)
C(6)-P(1)	1.781(4)	C(35)-O(3)	1.421(5)
C(15)-P(1)	1.804(5)	N(1)-P(1)	1.596(4)
C(21)-P(1)	1.805(5)	N(1)-In(1)	2.173(4)
C(27)-N(1)	1.483(6)	N(2)-In(1)	2.406(4)
C(28)-N(2)	1.478(6)	O(1)-In(1)	2.174(3)
C(29)-N(2)	1.472(7)	O(2)-In(1)	2.035(3)
C(30)-N(2)	1.483(6)	O(3)-In(1)	2.021(3)
Bond	Bond Angle (^{o})	Bond	Bond Angle (^{o})
O(1)-C(1)-C(6)	119.7(4)	C(29)-N(2)-In(1)	110.8(3)
O(1)-C(1)-C(2)	122.7(4)	C(28)-N(2)-In(1)	104.7(3)
C(5)-C(6)-P(1)	121.0(4)	C(30)-N(2)-In(1)	111.8(3)
C(1)-C(6)-P(1)	117.0(3)	C(1)-O(1)-In(1)	122.9(2)
C(16)-C(15)-P(1)	122.2(4)	C(31)-O(2)-In(1)	132.7(3)
C(20)-C(15)-P(1)	118.2(4)	C(35)-O(3)-In(1)	128.2(3)
C(26)-C(21)-P(1)	122.5(4)	N(1)-P(1)-C(6)	111.9(2)
C(22)-C(21)-P(1)	119.1(4)	N(1)-P(1)-C(15)	111.2(2)
N(1)-C(27)-C(28)	109.1(4)	C(6)-P(1)-C(15)	106.5(2)
N(2)-C(28)-C(27)	111.9(4)	N(1)-P(1)-C(21)	113.4(2)
O(2)-C(31)-C(33)	109.9(4)	C(6)-P(1)-C(21)	107.0(2)

O(2)-C(31)-C(32)	112.3(4)	C(15)-P(1)-C(21)	106.4(2)
O(2)-C(31)-C(34)	105.4(4)	O(3)-In(1)-O(2)	105.75(12)
O(3)-C(35)-C(36)	111.3(4)	O(3)-In(1)-N(1)	135.12(13)
O(3)-C(35)-C(37)	110.6(4)	O(2)-In(1)-N(1)	116.37(14)
O(3)-C(35)-C(38)	106.3(3)	O(3)-In(1)-O(1)	96.76(11)
C(27)-N(1)-P(1)	122.3(3)	O(2)-In(1)-O(1)	106.19(12)
C(27)-N(1)-In(1)	116.8(3)	N(1)-In(1)-O(1)	86.22(12)
P(1)-N(1)-In(1)	119.27(19)	O(3)-In(1)-N(2)	86.69(13)
C(29)-N(2)-C(28)	109.6(4)	O(2)-In(1)-N(2)	94.01(14)
C(29)-N(2)-C(30)	109.3(4)	N(1)-In(1)-N(2)	76.02(13)
C(28)-N(2)-C(30)	110.6(4)	O(1)-In(1)-N(2)	157.61(13)

Appendix C: Other

C1. Homonuclear decoupled $^{1}H\{^{1}H\}$ NMR spectra

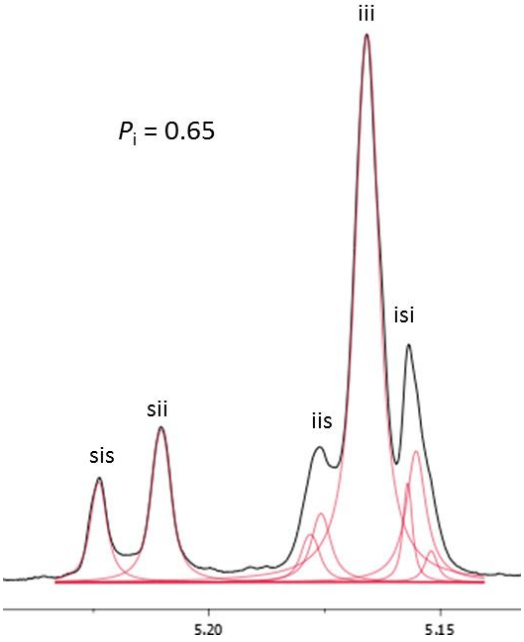

Figure C1. Methine region of the homonuclear decoupled $^{1}H\{^{1}H\}$ NMR spectrum of PLA obtained using aluminium initiator **3.5** ([I]:[LA] 1:100, [LA] = 1 M, Toluene, 353 K; $CDCl_3$, 400 MHz, 298 K).

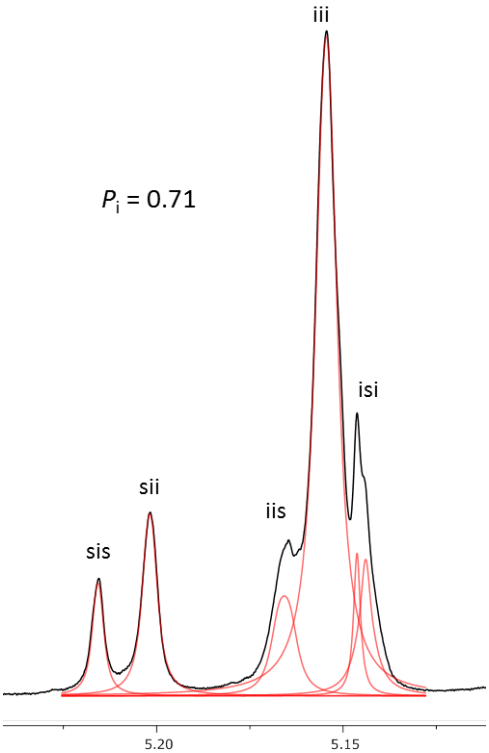

Figure C2. Methine region of the homonuclear decoupled $^{1}H\{^{1}H\}$ NMR spectrum of PLA obtained using indium initiator **3.8** ([I]:[LA] 1:100, [LA] = 1 M, THF, 298 K; $CDCl_3$, 400 MHz, 298 K).

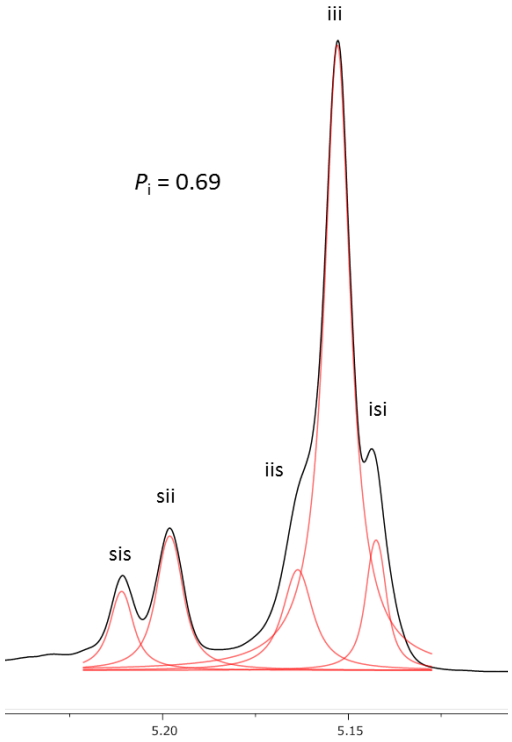

Figure C3. Methine region of the homonuclear decoupled $^{1}H\{^{1}H\}$ NMR spectrum of PLA obtained using zinc initiator **5.10** ([I]:[LA] 1:100, [LA] = 1 M, THF, 298 K; $CDCl_3$, 400 MHz, 298 K).

C2. DOSY NMR

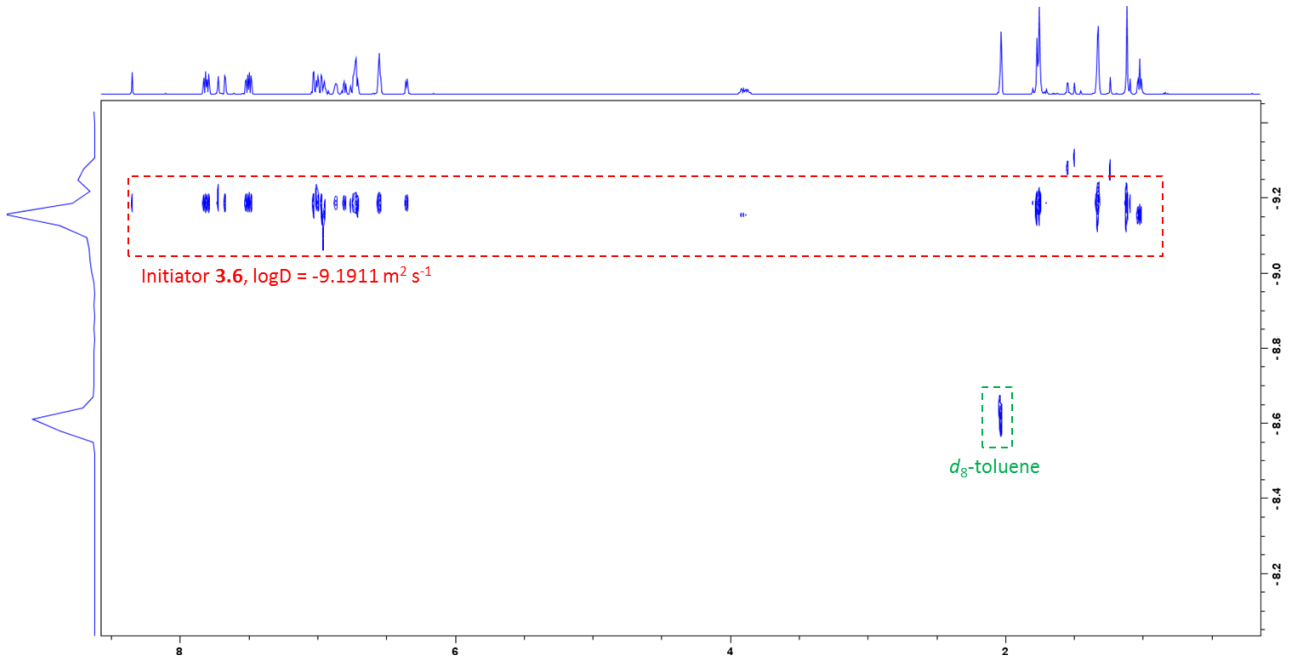

Figure C4. ^{1}H DOSY NMR of aluminium initiator **3.6** in d_8-toluene at 298 K.

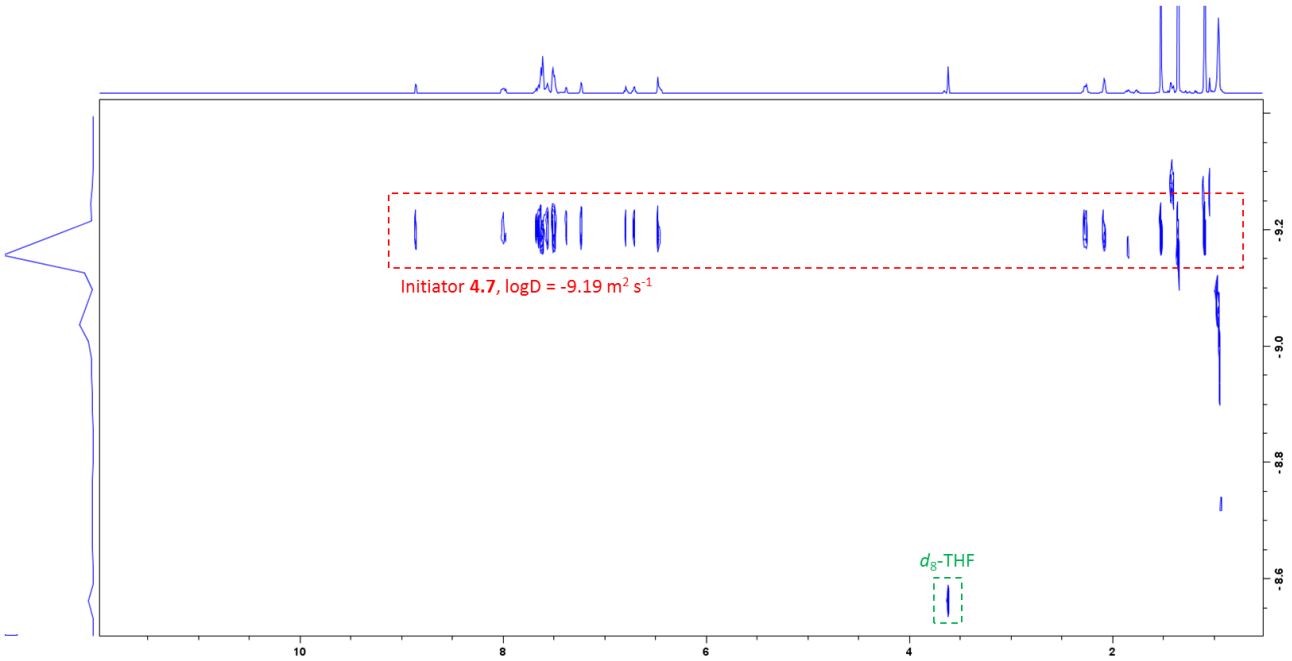

Figure C5. ^{1}H DOSY NMR of indium initiator **4.7** in d_8-THF at 298 K.

C3. SEC Traces

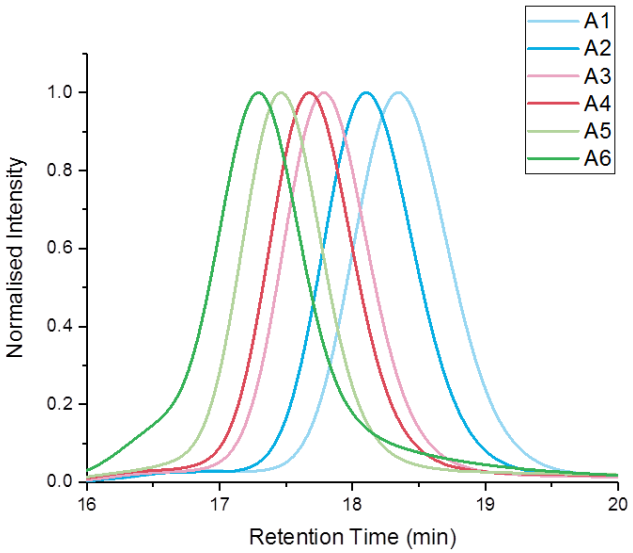

Aliquot	*t* (min)	Conv. (%)	M_n (g mol^{-1})	Đ
1	1440	25	3230	1.04
2	1895	29	4090	1.05
3	2880	38	4880	1.03
4	3360	40	5590	1.02
5	4725	49	6580	1.02
6	10080	77	9110	1.06

Figure C6. Overlay of SEC traces for the polymerisation of *rac*-LA mediated by aluminium initiator **3.4** ([I]:[LA] 1:100, [LA] = 1M, Toluene, 373 K).

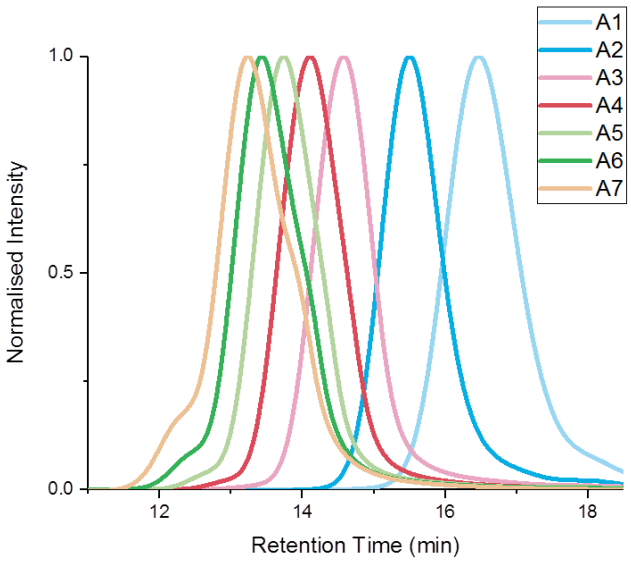

Aliquot	*t* (min)	Conv. (%)	M_n (g mol^{-1})	Đ
1	2.5	18	2650	1.08
2	5	28	4460	1.05
3	10	45	7220	1.06
4	15	58	8960	1.06
5	20	69	11060	1.05
6	30	80	12340	1.04
7	45	91	13410	1.04

Figure C7. Overlay of SEC traces for the polymerisation of *rac*-LA mediated by indium initiator **4.7** ([I]:[LA] 1:100, [LA] = 1M, THF, 298 K).

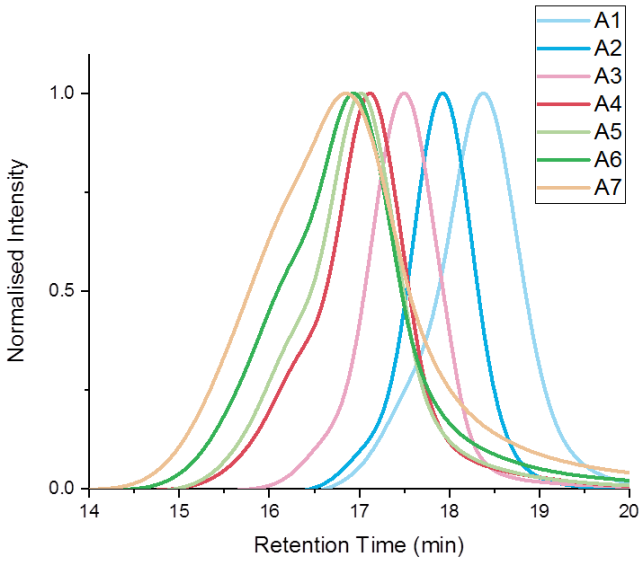

Aliquot	*t* (min)	Conv. (%)	M_n (g mol^{-1})	Đ
1	5	29	3390	1.11
2	10	41	4780	1.15
3	20	62	7000	1.10
4	30	80	9600	1.11
5	45	85	10100	1.13
6	60	90	11000	1.19
7	90	94	11100	1.32

Figure C8. Overlay of SEC traces for the polymerisation of *rac*-LA mediated by zinc initiator **5.8** ([I]:[IPA]:[LA] 1:1:100, [LA] = 1M, THF, 298 K).